Novel Precursors for Polymer-Protein Conjugate Synthesis via Reversible Addition-Fragmentation Chain Transfer Polymerization

Dissertation

zur Erlangung des Doktorgrades
der Fakultät Biologie, Chemie und Geowissenschaften
der Universität Bayreuth

vorgelegt von

Christine Maria Schilli

geboren in Offenburg

Die vorliegende Arbeit wurde unter der Leitung von Herrn Prof. Dr. A.H.E. Müller in der Zeit von April 2000 bis April 2003 an der Universität Bayreuth durchgeführt.

Prüfungsausschuss:

Prof. Dr. A.H.E. Müller (Erstgutachter)
Prof. Dr. F.X. Schmid (Zweitgutachter)
Prof. Dr. H.-W. Schmidt (Vorsitzender)
Prof. Dr. H. Hoffmann
Prof. Dr. P. Strohriegl

Tag der Einreichung: 16.04.2003
Tag des wissenschaftlichen Kolloquiums: 11.07.2003

Vollständiger Abdruck der von der Fakultät für Biologie, Chemie und Geowissenschaften der Universität Bayreuth genehmigten Dissertation zur Erlangung des Grades eines Doktor der Naturwissenschaften (Dr. rer. nat.).

Meiner Familie

Alles Wissen geht aus einem Zweifel hervor
und endet in einem Glauben.

(M. v. Ebner-Eschenbach)

Table of contents

List of abbreviations

A	absorbance
AA	acrylic acid
ACP	4,4'-azo-bis(4-cyanopentanoic acid)
AIBN	2,2'-azobis(isobutyronitrile)
ATRP	atom-transfer radical polymerization
biotinBMCC	1-biotinamido-4-[4'-(maleimidomethyl)cyclohexane-carbox-amido]butane
BM[PEO]$_3$	1,8-bis-maleimidotriethyleneglycol
BSA	bovine serum albumin
c	concentration
C$_I$	chain transfer constant of transfer to initiator
C$_M$	chain transfer constant of transfer to monomer
C$_S$	chain transfer constant of transfer to solvent
cf.	confer
cmc	critical micelle concentration
conv.	conversion
CTA	chain transfer agent
d	diameter
DAA	diacetone acrylamide
DEAD	diethyl azodicarboxylate
DLS	dynamic light scattering
DMF	dimethyl formamide
DMSO	dimethyl sulfoxide
DNA	deoxyribo nucleic acid
DSC	differential scanning calorimetry
DTNB	5,5'-dithiobis-[2-nitrobenzoic acid]
e.g.	for instance
ELP	elastin-like polypeptide
EPR	enhanced permeability and retention
eq.	equivalent
Eq.	equation
ESI	electrospray ionization
ESR	electron spin resonance
et al.	and coworkers
etc.	et cetera

f	initiator efficiency
Fig.	figure
FT	Fourier transform
g_1	field autocorrelation function
g_2	normalized intensity autocorrelation function
GC	gas chromatography
Gly	glycine
GPC	gel permeation chromatography
HABA	4-hydroxyazobenzene-2-carboxylic acid
HPLC	high-performance liquid chromatography
HPMA	N-(2-hydroxypropyl)methacrylamide
I	initiator
i.e.	that is
IgG	immuno-γ-globulin
IR	infrared
K	equilibrium constant
k_{add}	rate constant of addition
k_{app}	apparent rate constant
$k_{-\beta}$	rate constant of fragmentation
k_d	rate constant of decomposition
k_i	rate constant of initiation
k_p	rate constant of propagation
k_t	rate constant of termination
$k_{t,c}$	rate constant of termination by combination
$k_{t,d}$	rate constant of termination by disproportionation
k_{tr}	rate constant of transfer
L	ligand
LCST	lower critical solution temperature
Leu	leucine
M	monomer
M_n	number-average molecular weight
$M_{n,exp}$	experimental number-average molecular weight
$M_{n,theor}$	theoretical number-average molecular weight
M_w	weight-average molecular weight
m	mass
MALDI	matrix-assisted laser desorption ionization
MS	mass spectrometry

MW	molecular weight
NHSM	*N*-hydroxysuccinimide methacrylate
NIPAAm	*N*-isopropylacrylamide
NIR	near infrared
NMP	nitroxide-mediated polymerization
NMR	nuclear magnetic resonance
$\overline{P_n}$	number-average degree of polymerization
$P_n{}^{\bullet}$	polymeric radical
PAGE	polyacrylamide gel electrophoresis
PDI	polydispersity index
PEG	poly(ethylene glycol)
PEO	poly(ethylene oxide)
PEPDTA	1-phenylethyl phenyldithioacetate
Phe	phenylalanine
ppm	parts per million
PSD	post source decay
R	radius
R_h	hydrodynamic radius
R_i	rate of initiation
R_p	rate of propagation
R_t	rate of termination
$R^{\bullet}$	radical
RAFT	reversible addition-fragmentation chain transfer
r.i.	relative intensity
RI	refractive index
rpm	revolutions per minute
r.t.	room temperature
SA	streptavidin
SDS	sodium dodecylsulfate
SFRP	stable free-radical polymerization
SRP	stimuli-responsive polymer
t	time
t_{ind}	induction time
T	temperature
T_c	critical temperature
T_g	glass transition temperature
Tab.	table

TBAB	tetrabutylammonium bromide
TBHP	*tert*-butyl hydroxyperoxide
*t*BuA	*tert*-butyl acrylate
TEM	transmission electron microscopy
THF	tetrahydrofuran
TOF	time of flight
U	non-uniformity
UCST	upper critical solution temperature
UV	ultraviolet
V_e	elution volume
V-70	2,2'-azo-bis(4-methoxy-2,4-dimethyl valeronitrile)
v:v	volume:volume
V	volume
VAZO-88	1,1'-azo-bis(cyclo-hexanecarbonitrile)
vis	visible
VO	2-vinyl-4,4-dimethyl-5-oxazolone
vs.	versus
w	weight fraction
wt.	weight
WTSA	wild-type streptavidin
x	molar fraction
x_p	monomer conversion
z	charge
Z	aggregation number

α	degree of ionization
δ	chemical shift
ε	molar extinction coefficient
λ	wavelength
λ_{max}	wavelength at maximum absorbance
θ	scattering angle

1 Introduction

1.1 Smart polymers and their bioconjugates

1.1.1 Stimuli-responsive polymers

Stimuli-responsive polymers are polymers that respond with large property changes to small physical or chemical changes in their environment. They are usually classified according to the stimuli they respond to as temperature-, pH-, ionic strength-, light-, electric- and magnetic field-sensitive. Some polymers respond to a combination of two or more stimuli.

Introduction of stimuli-responsive polymers into artificial materials or bioactive compounds allows for modulation of their structure that is induced by the respective external stimuli. Consequently, on/off switching of the corresponding functions may be achieved at a molecular level.[1]

Surfaces modified with stimuli-responsive polymers (SRPs) can dynamically change their physico-chemical properties in response to changes in their environmental conditions. These surfaces are frequently referred to as "smart" surfaces. The triggered control of interfacial properties that are imparted from immobilized SRPs at the solid-liquid interface has wide-spread application in the design of biomaterials, regenerable biosensors, and microfluidic bioanalytical devices. Nath et al. have created thermoresponsive surfaces by immobilization of an elastin-like polypeptide (ELP) on a glass surface. The authors succeeded in the reversible addressing of an ELP fusion protein to the surface, which enables a reversible modulation of protein binding at the solid-liquid interface.[2]

Much attention has been devoted to polymer gels whose degree of swelling changes considerably on variation of temperature, solvent, electric field, or pH.[3-6] Such materials could be useful as components of actuators that are able to convert chemical energy into mechanical energy, as absorbents for solvent extraction or as a part of drug delivery systems.[7,8] Kuckling et al. reported the synthesis of double-responsive graft copolymer hydrogels from poly(*N*-isopropylacrylamide), PNIPAAm, and poly(2-vinylpyridine), PVP, with temperature- and pH-dependent swelling properties. The swelling behavior was mostly dominated by PNIPAAm but at high PVP grafting densities, a cooperative effect on pH change was observed. Separation of the temperature- and pH-sensitive component led to a gel that could be swollen by either temperature or pH change.[9] Stile et al. have proposed peptide-modified PNIPAAm-*co*-poly(acrylic acid) hydrogels as model networks for the investigation of cell-material interactions in three dimensions and as potential injectable scaffolds for tissue engineering applications.[10]

1.1.2 Smart polymer-protein conjugates

Stimuli-responsive polymers can be physically mixed with or chemically conjugated to biomolecules to yield polymer-biomolecule systems that respond to biological as well as to physical and chemical stimuli. Conjugation of a synthetic polymer to a biomolecule yields a new, hybrid type of molecule that can synergistically combine the individual properties of the two constituents, leading to new and unusual properties. Based on their similarity with biopolymers, R. Dagani has introduced the expression "smart polymers" for stimuli-responsive polymers as they are able to mimic the non-linear response of biopolymers caused by cooperative interaction between monomers.[11] A.S. Hoffman et al. have synthesized and thoroughly investigated the conjugation of "smart" polymers to proteins. Conjugation was performed both randomly[12-14] and at specific sites of the protein.[15,16] Many other research groups have randomly conjugated smart polymers to proteins, especially for affinity separations and enzyme recovery,[17-19] but the Hoffman group seems to be the only one so far that has synthesized and studied *site-specific* smart polymer bioconjugates.

Random, smart polymer-protein conjugates are mainly used in phase separations for recovery of enzymes from complex solutions or in phase separation immunoassays. For example, thermally induced precipitation of PNIPAAm-protein conjugates from a complex solution will selectively remove only the protein conjugated to PNIPAAm from the solution, leaving the other components in solution.[13,14] Alternatively, if the conjugated protein forms a complex with another biomolecule, e.g. by affinity recognition, the complex will also be selectively precipitated from the solution, and the affinity receptor is detached by eluting with a displacer (Fig. 1.1).[20]

thermoresponsive polymer-ligand conjugate

affinity receptor for ligand

incubate

affinity complex

separate, redissolve and recycle

stimulus-induced precipitation

recover or discard

eluting solution
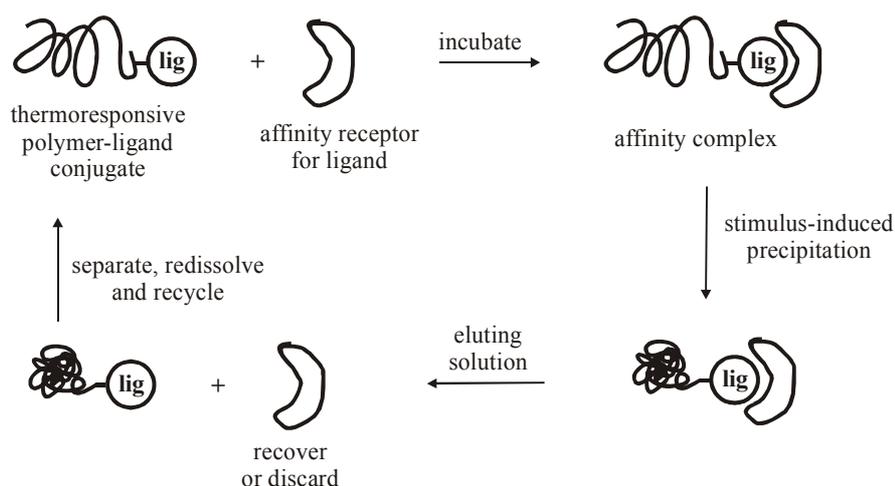
Fig. 1.1. *Stimuli-induced phase separation of a conjugate of a smart polymer and a ligand that is complexed with a recognition protein.[20]*

Conjugation of smart polymers to specific sites on proteins is performed by inserting a reactive amino acid at the selected site, such as cysteine that possesses a reactive thiol group. Such a functionalization of a protein is accomplished by genetically engineering a site-specific mutation into the DNA sequence of the protein and then cloning the mutant in cell culture. The specific site for polymer conjugation may be located far away from the active site to avoid interference with the biological function of the protein or nearby the active site to control the ligand-protein recognition process and the activity of the protein.[21,22]

Site-specific placement of a smart polymer near the active site of a protein may permit sensitive environmental control of the ligand/protein receptor recognition process, which controls all living systems. Small changes in environmental conditions can cause large changes in polymer conformation, leading to reversible "blocking" or "unblocking" of the protein active site and possibly to triggered release of a bound ligand from the protein binding site.[15,16] Hoffman et al. mainly used genetically engineered streptavidin, a tetrameric protein, in their studies of polymer-protein conjugates. Streptavidin is one of the most widely used proteins in affinity separations, analytical assays, and clinical diagnostics due to the high binding affinity of biotin to the four binding pockets of streptavidin. Ding et al. bound biotin to a conjugate composed of PNIPAAm and the streptavidin mutant E116C at temperatures below the lower critical solution temperature, LCST. Raising of the temperature to thermally induce polymer collapse triggered the release of some of the bound biotin molecules. Cycling of the temperature through LCST for several times led to the release of all of the bound biotin (Fig. 1.2).[16] The triggered release of bound ligands may be used to release therapeutics, for localized drug delivery within the body, or to release and recover affinity-bound ligands under eluate-free conditions. Size-selective blocking of biotinylated proteins was possible using a site-specific poly(*N*,*N*-diethylacrylamide)/streptavidin conjugate. Gating was found to be sensitive to the size of the protein, e.g. immuno-γ-globulin, IgG (150 kDa), was unable to bind below and above LCST, protein G (6.2 kDa) was found to bind at all temperatures but bovine serum albumin, BSA (67 kDa), bound only at temperatures above LCST, where the polymer is collapsed. In other words, below LCST, the polymer sterically interferes with the access to the adjacent binding site acting as a "polymer shield", whereas, above LCST, polymer collapse exposes the adjacent site.[23] Fig. 1.2 illustrates the concept of shielding by smart polymers.
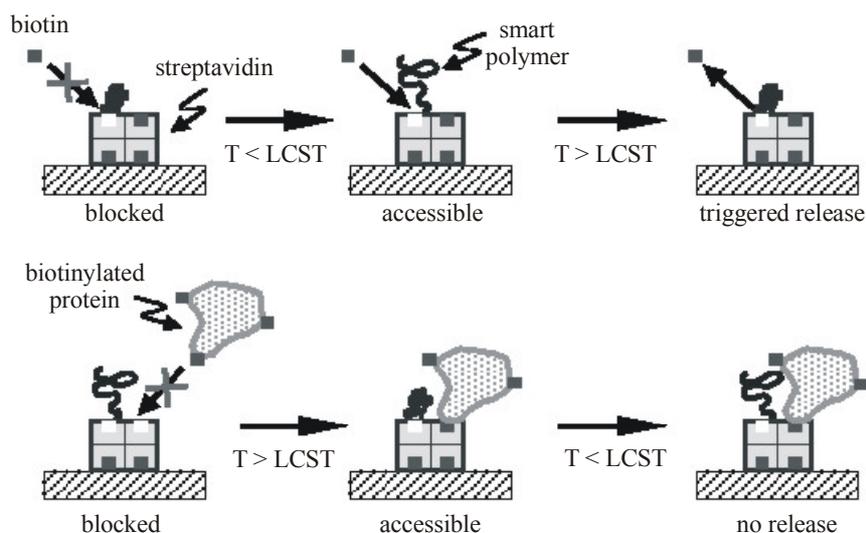
Fig. 1.2.   Different shielding mechanisms; top: triggered release of bound biotin, bottom: blocking of biotinylated protein by expanded polymer at T < LCST and unblocking through polymer collapse at T > LCST.[23]

Other approaches for polymer-protein conjugation use polymers with binding sites for protein functionalities. For example, Uludag et al. have synthesized NIPAAm polymers that contain protein-reactive *N*-acryloxysuccinimide and LCST-altering, hydrophobic alkylmethacrylates to obtain thermoresponsive, protein-conjugating polymers. The thermosensitive polymers were capable of retaining a co-injected therapeutic protein at an application site where tissue regeneration was required and might therefore be applied for drug delivery.[24]

The above-mentioned investigations, along with those of many other researchers, are on the threshold of polymer therapeutics, which will be discussed in the following section.

1.2   Polymer therapeutics in modern medicine

Polymer therapeutics include polymers which are inherently biologically active,[25] polymer-drug conjugates, polymeric micelles,[26] polymer-protein conjugates,[27,28] and polymer-coated liposomes.[29,30] Fig. 1.3 shows an overview of these therapeutic agents.
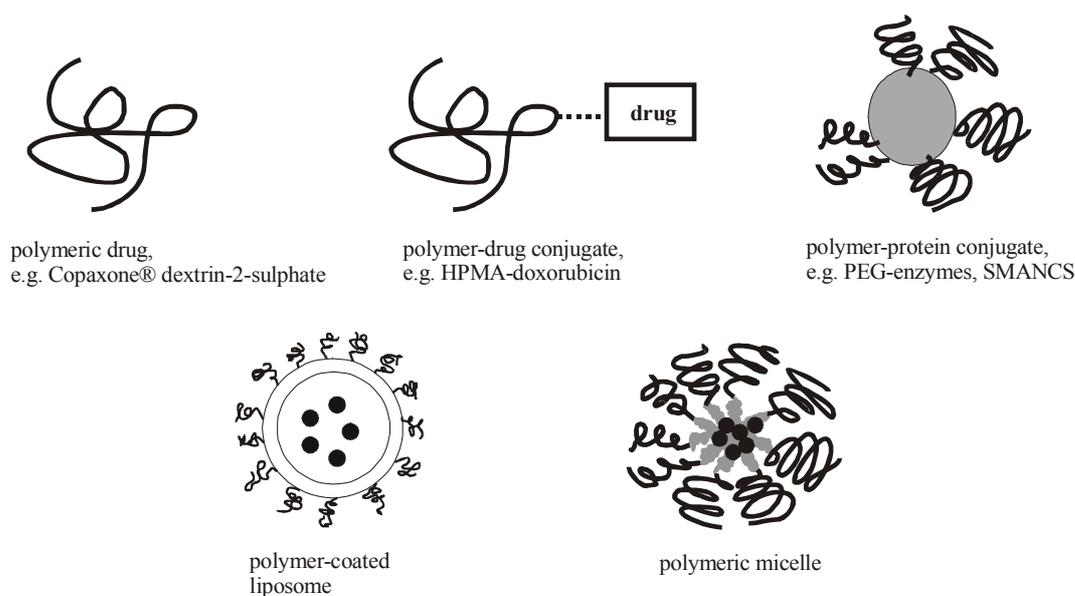
Fig. 1.3.   Overview of different polymer therapeutics.[31]

Polymer-controlled drug delivery has evolved from the need for prolonged and better control of drug administration. Besides, toxic side effects involved with chemotherapy frequently limit the dosage levels. The different means for prolonging the permanence of substances in blood circulation include covalent conjugation of drugs to polymers, drug encapsulation in liposomes, and physical entrapment of drugs in particles, such as micelles or microspheres. The conjugation of anti-tumor agents to polymers yields a new class of anticancer agents that can mediate tumor-selective targeting and reduce toxicity. In conventional drug delivery, the drug concentration in the blood rises on administering, then peaks and declines. Controlled-release devices can maintain the drug in the desired therapeutic range with a single dose and localize delivery of the drug to a particular body compartment.

Most anti-tumor agents are low-molecular weight compounds that penetrate all tissues by passing across the cell membrane, whereas polymer conjugates can only gain entry to the cell by pinocytosis (uptake of material by a cell from the environment by folding inward and pinching off of the plasma membrane[32]). This process involves membrane internalization to form vesicles, which entrap the large polymer drug and deliver it to the cell's interior. The polymer drug circulates for a longer time in the body and accumulates more effectively in tumor tissue as compared to low-molecular weight components. This phenomenon has been termed "enhanced permeability and retention (EPR) effect" by Maeda et al.[33] and has been attributed to tumor vessels that are usually more "leaky" to macromolecules and to the lack of effective tumor lymphatic drainage so that macromolecules leaving the blood vessels are not returned to circulation very quickly. These factors allow conjugate concentration in tumor tissue to reach levels that are 10-

1000 times higher than normally found after administration of the free drug. Fig. 1.4 demonstrates the differences in cellular uptake of free and conjugated drugs.
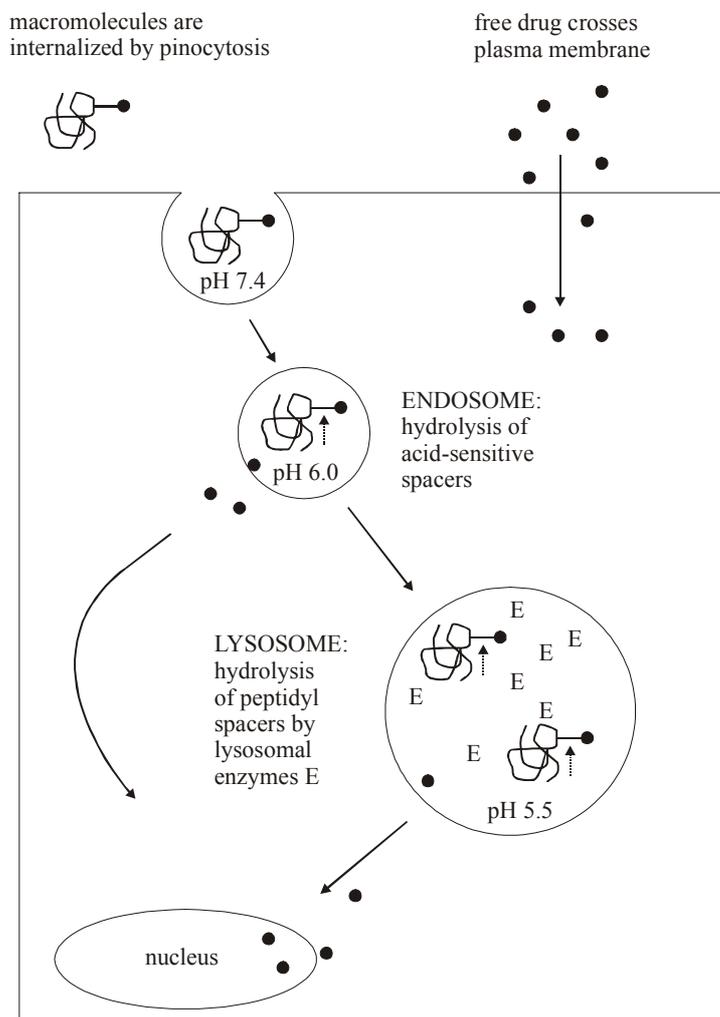
Fig. 1.4.   *Mechanisms of cellular uptake of low-molecular weight anti-tumor agents and polymer-drug conjugates.*[31]

   Molecular weight and stability are the key factors in the optimization of polymer conjugates: polymer backbone as well as polymer-drug linkages must be sufficiently stable and the molecular size must be small enough to ensure elimination from the body by the kidneys, i.e. renal excretion. Thus, polymer-drug conjugate not captured by tumor tissue can largely be removed and the harmful drug is directed away from potential sites of toxicity.

   H. Ringsdorf was the first one to propose a model for polymer-drug conjugates, and he suggested using water-soluble polymers to which the drug could be bound covalently by a linkage that could be degraded at a desired rate in the target site. Furthermore, the inclusion of cell-specific targeting residues would enhance selective delivery further.[26] With the use

of synthetic polymers, potential carriers are at hand that can be tailor-made with all the desired features, such as targeting moieties, peptidyl spacers for enzymatic cleavage, pH-sensitive linkers, etc. Polymer carriers for drug conjugation have to meet some requirements that have to be considered in the design of polymer-drug conjugates, such as biocompatibility, lack of immunogenicity, biological inertia, and functional groups for covalent conjugation to drugs and targeting residues. Even though natural polymers, such as dextran or human serum albumin, are easily available and biocompatible, they exhibit high immunogenicity, which is a major drawback of these compounds.

N-(2-hydroxypropyl)methacrylamide (HPMA) copolymer conjugates with anti-tumor agents have been most extensively studied. HPMA is water-soluble, biocompatible, non-immunogenic and non-toxic at the maximum administrable dose.[34] Generally, the drugs are bound to the polymer backbone using peptidyl spacers designed for cleavage by lysosomal thiol-dependent proteases. These enzymes are elevated in many human tumors.[35] There is also a number of cell-specific targeting groups that has been incorporated into the HPMA copolymer structure, e.g. galactose for targeting the liver. The first synthetic polymer-drug conjugate that was in clinical study is *N*-(2-hydroxypropyl)methacrylamide copolymer-doxorubicin (PK 1), in which the anti-tumor agent doxorubicin is bound to the polymer backbone by a Gly-Phe-Leu-Gly peptidyl side chain. The conjugate displays anti-tumor activity, is five to ten times less toxic than free doxorubicin and shows evidence of tumor-selective targeting.[36]

Beside HPMA copolymers, there are a number of other polymers suitable for drug conjugation. One of the most extensively studied polymers is poly(ethylene glycol), PEG, a linear polyether diol that is biocompatible, soluble in aqueous and organic media, non-toxic and exhibits very low immunogenicity.[37,38] Its polymer backbone is chemically inert, and the terminal hydroxyl groups are available for derivatization. Drug conjugates are usually prepared from monomethoxy-PEG, mPEG, which is generally activated first and then reacted with the target molecule.[39,40]

In recent years, the number of approved polymer-protein drugs as anti-tumor agents has grown and includes PEGylated L-asparaginase (Oncaspar®) for treatment of acute lymphocytic leukaemia in children[28,41] as well as a conjugate of poly(styrene-*co*-maleic anhydride) and the anti-tumor protein neocarzinostatin (SMANCS) for treatment of liver cancer.[27]

Beside the above-discussed polymer-drug and polymer-protein conjugates, polymers also play a vital role in the stabilization of drug-loaded micelles and liposomes. These areas are especially important where polymer-drug conjugation fails, e.g. lack of derivatizable groups in the drug, decrease or loss of activity after conjugation. Self-assembling micellar delivery systems are receiving increasing attention[42-44] and structure-

reactivity relationships of micellar structures formed from PEO as hydrophilic block and poly(L-amino acid) as hydrophobic block carrying doxorubicin are well documented in the literature. For example, poly(ethylene glycol)-*block*-poly(aspartate) doxorubicin conjugates form micelles that accumulate in solid tumors and exhibit anti-tumor activity.[45,46] An EPR effect is also found in the case of polymer micelles and maximizes tumor capture. The micelle may subsequently disassociate to give smaller block copolymer units that can be excreted.

1.3 Block copolymer micelles

One of the most prominent properties of amphiphilic block copolymers is their ability to form micelles in selective solvents. If a block copolymer is dissolved in a solvent that is a good solvent for one block but a poor solvent for the other, the formation of micelles is most likely. Provided that the block ratio is not too asymmetric, it is also possible to obtain inverse micelles from the same block copolymer by choosing appropriate solvents. Polymer micelles have a compact core constituted by collapsed insoluble parts and a diffuse corona composed of soluble chains.

Depending on the ratio of core radius, R_{core}, to corona diameter, d_{corona}, micelles are classified into crew-cut micelles ($R_{core} \gg d_{corona}$) and star micelles ($R_{core} \ll d_{corona}$).[47] Consequently, star micelles are spherical with small cores and expanded coronas,[48] whereas crew-cut micelles possess large cores and short coronal "hair".[49] For star micelles, the radius of the core seems to be independent of the length of the soluble block and scales as $N_B^{3/5}$, where N_B is the number of units in the insoluble block.[47] Beside the rather spherical shapes, there also exist other morphologies of block copolymer aggregates in solution, such as vesicles, wormlike micelles, etc.

Micelle formation requires the presence of two opposing forces, i.e. an attractive force between blocks leading to aggregation and a repulsive force that prevents the unlimited growth of micelles into a distinct macroscopic phase. Micellar growth is further limited by entropic factors due to a constraint in length that induces a negative entropy change owing to stretching of the chains. The micellization process is sufficiently cooperative to yield colloidal particles with narrow size distribution and high aggregation numbers.

The thermodynamic reasons for micelle formation are strong negative energy changes as a result of solvent incompatibility of the core block in conjunction with steric repulsion of the soluble, corona-forming polymeric chains and a combination of intermolecular forces, including hydrophobic interaction, electrostatic interaction, metal complexation, and hydrogen bonding of the constituent block copolymers.[50]

Critical phenomena play an important role in micelle formation; micelles exist only above a certain minimum concentration, i.e. the critical micelle concentration, cmc. The critical micelle concentration is defined as the concentration below which only single chains are present but above which single chains and micellar aggregates coexist. Similarly to a critical concentration for micellization, there is also a critical micelle temperature and, in the case of pH-responsive blocks, a critical micelle pH.[51,52] The block lengths of the copolymers have a considerable impact on the cmc, where the length of the insoluble block affects the cmc much more than that of the soluble block. Theories developed by Nagarajan et al.[53] and Whitmore et al.[54] suggest a scaling relation for aggregation numbers Z that is proportional to $N_A^{\alpha} N_B^{\beta}$, where N_A = length of insoluble block, N_B = length of soluble block, α and β = exponents of scaling relations. Typical exponent values are $\alpha = 0.73$ and $\beta = -0.17$ for polystyrene-*block*-polyisoprene in *n*-heptane or $\alpha = 0.7$ and $\beta = -0.08$ for poly(ethylene oxide)-*block*-poly(propylene oxide) in water.[53] Förster et al. have postulated a universal scaling relation $Z \propto N_A^2 N_B^{-0.8}$ for strongly segregated diblock and triblock copolymer systems that was derived from micellization experiments with polystyrene-*block*-poly(4-vinylpyridine) in toluene.[55]

The micellization process is believed to obey the scheme of "closed association", which describes a dynamic equilibrium between micelles and molecularly dissolved block copolymer (unimers).[56,57] There is also a mechanism of "open association" that comprises a series of equilibria between unimers, dimers, trimers and so on. Micelles formed in selective solvents are dynamic if single block copolymer molecules are exchanged via a thermodynamic equilibrium. However, for a micelle with a glassy core, i.e. with a glass transition temperature of the core-constituting block that is sufficiently high, as is the case for polystyrene, the structure is "kinetically frozen" and may not represent the thermodynamic equilibrium.[58]

Micelles of block copolymers and low-molecular weight surfactants display different characteristics in terms of lability and exchange kinetics. For example, critical micelle concentrations for polymeric micelles are in the micromolar or nanomolar range, whereas those of low-molecular weight surfactants usually lie in the millimolar range.[59,60] Furthermore, polymer micelles display a smaller rate of dissociation as compared to surfactant micelles.

Ionic block copolymers possess hydrophilic blocks of ionic repeating units and hydrophobic blocks of nonionic units. Due to the high degree of incompatibility between the ionic and nonionic blocks, micelles formed from ionic block copolymers display extremely low critical micelle concentrations and high aggregate stabilities. Ionic block copolymers are usually divided into two categories, i.e. block polyelectrolytes and block ionomers, the difference being the polyelectrolyte forming either the micellar corona

(block polyelectrolyte) or the micellar core (block ionomer).[47] Block copolymers containing ionic groups in the corona have a much larger overall size despite their smaller aggregation numbers as compared to non-ionic polymers due to electrostatic repulsion. Non-ionic block copolymer micelles are constituted either of block copolymers containing two different hydrophobic segments or of amphiphilic block copolymers. The requirement for micelle formation in these systems is the use of a selective solvent for one of the blocks.[51]

Micellization conditions usually have to be found by trial and error and are mainly guided by the solubility properties of the individual blocks. Preparation of micelles is usually performed either by addition of a precipitating solvent (mixture) for one block or by direct dissolution in an appropriate solvent (mixture). Changing temperature, pH or ionic strength may result in selective solvent conditions, favoring the formation of micelles. For example, poly(vinyl pyrrolidone)-*block*-poly(ethylene oxide) forms micelles in aqueous solutions on titration from pH 1 to pH 10, and polystyrene-*block*-poly(methacrylic acid) forms micelles upon direct addition to a mixture of dioxane/water 80:20 (v:v) followed by stepwise dialysis to pure aqueous buffer.[61]

Armes et al. have investigated a plethora of micelles formed from ionic and non-ionic block copolymers, some of them displaying response to pH, temperature, and other stimuli. The term "schizophrenic" was coined, describing hydrophilic AB block copolymers that are able to form both conventional and inverse micelles in aqueous media.[62,63] Recently, Armes et al. have reported on the zwitterionic AB diblock copolymer poly(4-vinyl benzoic acid)-*block*-poly(2-(diethylamino)ethyl methacrylate), PVBA-*b*-PDEA, that undergoes spontaneous self-assembly in aqueous solution at 20 °C to form both micelles and inverse micelles simply by switching the solution pH.[62] At pH 2, PVBA-core micelles are found, whereas at pH 10, PDEA-core micelles form. Possible applications of this "schizophrenic" block copolymer are as a pigment dispersant or in the separation and purification of proteins.

Double-responsive behavior of block copolymer micelles has been reported by Laschewsky et al. who synthesized water-soluble block copolymers from *N*-isopropylacrylamide, NIPAAm, and the zwitterionic monomer 2-[*N*-(3-methacryl-amidopropyl)-*N,N*-dimethyl]ammoniopropane sulfonate, SPP. Double-thermoresponsive behavior is found due to the lower critical solution temperature (LCST) of PNIPAAm and the upper critical solution temperature (UCST) of PSPP displayed in aqueous media. The colloidal aggregates can switch reversibly with temperature, and the micellar domains are formed at low and high temperature from the block that is collapsed under the given conditions, i.e. PSPP at low temperatures and PNIPAAm at high temperatures.[64] The varying polarity of the micellar core – rather polar at low temperature with PSPP as core

and unpolar at high temperature with PNIPAAm as core – enables the solubilization of compounds simply by varying the temperature.

Possible applications of polymer micelles are manifold and range from biotechnology to nanoscience. Antonietti et al. used polymer micelles as "nanoreactors" to produce highly dispersed metal or semiconductor particles.[65,66] Spatz et al. performed a controlled mineralization of gold nanoparticles in micelles composed of polystyrene-*block*-poly(2-vinylpyridine).[67] Micelles that show a pH-dependent behavior suggest applications as sensors or pH-driven chemical or drug delivery systems. Polymer micelles as drug carriers were first envisioned by Ringsdorf et al.[68] The application as drug delivery systems arises from the micellar size that is typical of that of a virus, thereby avoiding filtration by the kidneys and reticuloendothelial system uptake (reticuloendothelial system = group of cells having the ability to take up and sequester inert particles and vital dyes[69]). Besides, polymer micelles used as carriers of tumor therapeutics circulate in the blood for a long period of time and eventually pass through the capillaries that are disrupted near tumor growth.[70]

1.4 Synthesis of functionalized polymers via controlled radical polymerization

Preparation of well-defined, functional polymers is a major concern in the development of polymer-protein and polymer-drug conjugates. Most of the polymers used so far for the synthesis of polymer therapeutics have relatively broad molecular weight distributions and compositions are not uniform. Especially in the light of a detailed investigation of the biodistribution of these conjugates, it is desirable to have well-defined polymers that allow for a detailed correlation of structure, molecular weight and solution properties with the biological profile. Very narrow molecular weight distributions ensure well-defined compositions and distinct retention times of the conjugates in the body.

The solution to this problem seems to be controlled/living polymerizations that yield polymers with low polydispersities and defined molecular weights. These polymerizations include anionic polymerization, atom-transfer radical polymerization (ATRP), and reversible addition-fragmentation chain transfer (RAFT) polymerization.

Anionic polymerization requires the use of rather stringent reaction conditions, being very sensitive to impurities. Besides, a large number of monomers cannot be polymerized due to interaction with the reactive initiators (metal amides, alkoxides, or organometallic compounds). For example, anionic polymerization fails for monomers containing active hydrogen atoms, such as primary and secondary acrylamides, acrylic acid, etc. In order to

polymerize these monomers, protecting groups have to be introduced which necessitates deprotection of the functional groups after polymerization. Furthermore, polymerization of polar monomers in polar solvents is complicated by side reactions due to interaction of functional groups with the carbanion center.[71,72]

Atom-transfer radical polymerization generally uses transition metal ions complexed to nitrogen-containing ligands as catalysts. Even though requiring less severe polymerization conditions than anionic polymerization, ATRP suffers two major drawbacks. One is contamination of the polymers by the transition metal catalyst and the second is complexation of certain monomer functionalities by the metal ions. For the latter reason, polymerization of carboxyl-, amine-, or hydroxyl-containing monomers is only possible if the functionality is protected.[73,74] One exception to this rule has been the successful synthesis of *N*-(2-hydroxypropyl)methacrylamide (HPMA) copolymers via ATRP in DMSO as solvent, leading to quite narrowly distributed molecular weights but displaying some difficulties in choice of monomer/solvent ratio due to possible competitive chelation of the transition metal ion by solvent.[75]

For the design of polymer-protein or polymer-drug conjugates from well-defined functional polymers, a polymerization technique is needed that does not require expensive reactors or other costly equipment but can be performed with means that are available in a standard, even non-polymeric, laboratory. No complicated purification of reactants should be necessary and protecting group chemistry should be evitable. The method of choice seems to be RAFT polymerization that can be applied to virtually all kinds of monomers without protection of functional groups using common solvents and initiators at temperatures ranging from 25 °C to 100 °C. For example, acrylic acid, that cannot be polymerized in a non-protected form via anionic or atom-transfer polymerization, can be RAFT polymerized without modification. The use of dithiocarbonyl compounds RS(C=S)Z as chain transfer agents results in end-functionalized polymers that can be further derivatized. The dithiocarbonyl-derived –S(C=S)Z chain ends are especially attractive for conjugation to proteins since hydrolysis yields thiol-terminated polymers that react selectively with thiol-reactive functionalities, such as cysteine residues, in the protein. If required, the R group of the chain transfer agent can be chosen in such a way that it contains a derivatizable functionality which is introduced to the other chain end in the RAFT process, giving rise to two functional groups at both ends of the polymer chain that may be modified further. Such a telomeric polymer might be interesting for attaching a protein to one end and a targeting moiety to the other, which transports the protein to the desired site in the body. Additionally, RAFT polymerization offers the possibility of synthesizing a vast range of different polymer architectures, including block, graft and star copolymers.[76-79]

References

(1)   Hoffman, A. S.; Stayton, P. S.; Bulmus, V.; Chen, G.; Chen, J.; Cheung, C.; Chilkoti, A.; Ding, Z.; Dong, L.; Fong, R.; Lackey, C. A.; Long, C. J.; Miura, M.; Morris, J. E.; Murthy, N.; Nabeshima, Y.; Park, T. G.; Press, O. W.; Shimoboji, T.; Shoemaker, S.; Yang, H. J.; Monji, N.; Nowinski, R. C.; Cole, C. A.; Priest, J. H.; Harris, J. M.; Nakamae, K.; Nishino, T.; Miyata, T. *J. Biomed. Mater. Res.* **2000**, *52*, 577-586.

(2)   Nath, N.; Chilkoti, A. *Adv. Mater.* **2002**, *14*, 1243-1247.

(3)   Freitas, R. F. S.; Cussler, E. L. *Chem. Eng. Sci.* **1987**, *42*, 97.

(4)   Tanaka, T.; Fillmore, D. J.; Sun, T.; Nishio, I.; Swislow, G.; Shah, A. *Phys. Rev. Lett.* **1980**, *45*, 1636.

(5)   Osada, Y.; Kishi, R.; Hasebe, M. *J. Polym. Sci., Part C: Polym. Lett.* **1987**, *25*, 481.

(6)   Brannon, L.; Peppas, N. A. *Chem. Eng. Sci.* **1991**, *46*, 715.

(7)   Osada, Y. *Adv. Polym. Sci.* **1987**, *82*, 1.

(8)   Lim, Y. H.; Kim, D.; Lee, D. S. *J. Appl. Polym. Sci.* **1997**, *64*, 2647-2655.

(9)   Kuckling, D.; Wohlrab, S. *Polymer* **2001**, *43*, 1533-1536.

(10)   Stile, R. A.; Healy, K. E. *Biomacromolecules* **2001**, *2*, 185-194.

(11)   Dagani, R. *Chem. Eng. News* **1995**, *9*, 30-33.

(12)   Cole, C.-A.; Schreiner, S. M.; Priest, J. H.; Monji, N.; Hoffman, A. S. *ACS Symp. Ser.* **1987**, *350 (Reversible Polym. Gels Relat. Syst.)*, 245-254.

(13)   Chen, G.; Hoffman, A. S. *Bioconjugate Chem.* **1993**, *4*, 509-514.

(14)   Ding, Z.; Chen, G.; Hoffman, A. S. *J. Biomed. Mater. Res.* **1998**, *39*, 498-505.

(15)   Bulmus, V.; Ding, Z.; Long, C. J.; Stayton, P. S.; Hoffman, A. S. *Bioconjugate Chem.* **2000**, *11*, 78-83.

(16)   Ding, Z.; Long, C. J.; Hayashi, Y.; Bulmus, E. V.; Hoffman, A. S.; Stayton, P. S. *Bioconjugate Chem.* **1999**, *10*, 395-400.

(17)   Galaev, I. Y.; Mattiasson, B. *Biotechnol. Bioeng.* **1993**, *41*, 1101-1106.

(18)   Nguyen, A. L.; Luong, J. H. T. *Biotechnol. Bioeng.* **1989**, *34*, 1186-1190.

(19)   Gupta, M. N.; Mattiasson, B. *Highly Selective Separations in Biotechnology*; Blackie Academic & Professional: London, 1994.

(20)   Chen, J. P.; Hoffman, A. S. *Biomaterials* **1990**, *11*, 631-634.

(21)   Chilkoti, A.; Chen, G.; Stayton, P. S.; Hoffman, A. S. *Bioconjugate Chem.* **1994**, *5*, 504-507.

(22)   Stayton, P. S.; Shimoboji, T.; Long, C.; Chilkoti, A.; Chen, G.; Harris, J. M.; Hoffman, A. S. *Nature* **1995**, *378*, 472-474.

(23)   Ding, Z.; Fong, R. B.; Long, C. J.; Stayton, P. S.; Hoffman, A. S. *Nature* **2001**, *411*, 59-62.

(24)   Uludag, H.; Norrie, B.; Kousinioris, N.; Gao, T. *Biotechnol. Bioeng.* **2001**, *73*, 510-521.

(25)   Seymour, L. *J. Bioact. Compat. Polym.* **1991**, *6*, 178-216.

(26)   Ringsdorf, H. *J. Polym. Sci. Polymer Symp.* **1975**, *51*, 135-153.

(27)   Maeda, H. *Adv. Drug Delivery Rev.* **2001**, *46*, 169-185.

(28)   Nucci, M. L.; Shorr, R.; Abuchowski, A. *Adv. Drug Delivery Rev.* **1991**, *6*, 133-151.

(29)   Gregoriadis, G. *Liposome Technology*; CRC Press: Boca Raton, FL, 1992.

(30)   Scheule, R. K.; Cheng, S. H. *Liposome delivery systems*; BIOS Scientific Publishers Inc.: Oxford, 1996.

(31)   Duncan, R.; Dimitrijevic, S.; Evagorou, E. G. *S.T.P. Pharma Sciences* **1996**, *6*, 237-263.

(32)   www.nlm.nih.gov/medlineplus/mplusdictionary.html. Merriam-Webster.

(33)   Maeda, H.; Matsumura, Y. *CRC Crit. Rev. Ther. Drug Carrier Sys.* **1989**, *6*, 193-210.

(34)   Rihova, B.; Kopecek, J.; Ulbrich, K.; Chytry, V. *Makromol. Chem. (Suppl.)* **1985**, *9*, 13-24.

(35)   Duncan, R. *Pharmaceutical Science & Technology Today* **1999**, *2*, 441-449.

(36)   Seymour, L. W. *Brit. J. Cancer* **1994**, *70*, 636-641.

(37)   Powell, G. M. In *Handbook of Water Soluble Gums and Resins*; Davidson, R. L., Ed.; McGraw-Hill: New York, 1980; Vol. 18, pp 1-31.

(38)   Dreborg, S.; Akerblom, E. B. *Crit. Rev. Ther. Drug Carrier Syst.* **1990**, *6*, 315-365.

(39)   Zalipsky, S. *Bioconjugate Chem.* **1995**, *6*, 150-165.

(40)   Herman, S.; Hooftman, G.; Schacht, E. *J. Bioact. Compat. Polym.* **1995**, *10*, 145-187.

(41)   Fuertges, F.; Abuchowski, A. *J. Control. Release* **1990**, *11*, 139-148.

(42)   Yokoyama, M.; Okano, T.; Sakurai, Y.; Kataoka, K. *J. Control. Release* **1994**, *32*, 269-277.

(43)   Kabanov, A. V.; Alakhov, V. Y. *J. Control. Release* **1994**, *28*, 15-35.

(44)   Calibrese, P.; Chabner, B. A. In *The Pharmacological Basis of Therapeutics*; Hardman, J. G.; Limbird, L. E., Eds.; McGraw-Hill: New York, 1996; pp 1225-1288.

(45)   Kwon, G. S.; Kataoka, K. *Adv. Drug Delivery Rev.* **1995**, *16*, 295-309.

(46)   Kataoka, K.; Kwon, G. S.; Yokoyama, M.; Okano, T.; Sakurai, Y. *J. Control. Release* **1993**, *24*, 119-132.

(47) Moffitt, M.; Khougaz, K.; Eisenberg, A. *Acc. Chem. Res.* **1996**, *29*, 95-102.

(48) Halperin, A. *Macromolecules* **1989**, *22*, 3806.

(49) Nagarajan, R.; Ganesh, C. *Macromolecules* **1989**, *22*, 4312.

(50) Tuzar, Z.; Kratochvil, P. In *Surface and colloid science*; Matijevic, E., Ed.; Plenum Press: New York, 1993; Vol. 15, p 1.

(51) Astafieva, I.; Zhong, X. F.; Eisenberg, A. *Macromolecules* **1993**, *26*, 7339-7352.

(52) Lee, A. S.; Bütün, V.; Vamvakaki, M.; Armes, S. P.; Pople, J. A.; Gast, A. P. *Macromolecules* **2002**, *35*, 8540-8551.

(53) Nagarajan, R.; Ganesh, K. *J. Phys. Chem.* **1989**, *90*, 5843.

(54) Whitmore, M. D.; Noolandi, J. *Macromolecules* **1985**, *18*, 657.

(55) Förster, S.; Zisensis, M.; Wenz, E.; Antonietti, M. *J. Chem. Phys.* **1996**, *104*, 9956-9970.

(56) Elias, H.-G. In *Light Scattering from Polymer Solutions*; Huglin, M. B., Ed.; Academic Press: London, 1972; pp 397-457.

(57) Elias, H.-G. *J. Macromol. Sci.* **1973**, *A7*, 601.

(58) Tuzar, Z. *Solvents and Self-Organization of Polymers*; Kluwer: Dordrecht, 1996; Vol. E 327.

(59) Wilhelm, M.; Zhao, C. L.; Wang, Y.; Xu, R.; Winnik, M. A. *Macromolecules* **1991**, *24*, 1033.

(60) Quintana, J. R.; Villacampa, M.; Katime, I. A. *Macromolecules* **1993**, *26*, 606.

(61) Webber, S. E. *J. Phys. Chem. B* **1998**, *102*, 2618-2626.

(62) Liu, S.; Armes, S. P. *Angew. Chem. Int. Ed.* **2002**, *41*, 1413-1416.

(63) Liu, S.; Billingham, N. C.; Armes, S. P. *Angew. Chem., Int. Ed.* **2001**, *40*, 2328-2331.

(64) Arotcarena, M.; Heise, B.; Ishaya, S.; Laschewsky, A. *J. Am. Chem. Soc.* **2002**, *124*, 3787-3793.

(65) Antonietti, M.; Wenz, E.; Bronstein, L. M.; Seregina, M. V. *Adv. Mater.* **1995**, *7*, 1000.

(66) Antonietti, M.; Förster, S.; Hartmann, J.; Oesteich, S. *Macromolecules* **1996**, *29*, 3800.

(67) Spatz, J. P.; Mössmer, S.; Möller, M. *Chem. Eur. J.* **1996**, *2*, 1552-1555.

(68) Bader, H.; Ringsdorf, H.; Schmidt, B. *Angew. Makromol. Chem.* **1984**, *123/124*, 457-485.

(69) www.ndif.org/t-a.html. Nephrogenic Diabetes Insipidus (NDI) Foundation.

(70) Harada, A.; Kataoka, K. *Adv. Drug Delivery Rev.* **1995**, *16*, 295.

(71)   Young, R. N.; Quirk, R. P.; Fetters, L. J.; Luston, J.; Vass, F. *Anionic Polymerization*; Springer-Verlag: Berlin, Heidelberg, New York, Toronto, 1984; Vol. 56.

(72)   Hsieh, H. L.; Quirk, R. P. *Anionic Polymerization*; Marcel Dekker, Inc.: New York, Basel, Hong Kong, 1996.

(73)   Wang, J. S.; Matyjaszewski, K. *Macromolecules* **1995**, *28*, 7901-7910.

(74)   Matyjaszewski, K.; Xia, J. *Chem. Rev.* **2001**, *101*, 2921-2990.

(75)   Godwin, A.; Hartenstein, M.; Müller, A. H. E.; Brocchini, S. *Angew. Chem. Int. Ed.* **2001**, *40*, 594.

(76)   Le, T. P.; Moad, G.; Rizzardo, E.; Thang, S. H. In *WO 98/01478*; E.I. Du Pont De Nemours and Co., USA; Le, Tam Phuong; Moad, Graeme; Rizzardo, Ezio; Thang, San Hoa: Australia, 1998.

(77)   Chiefari, J.; Mayadunne, R. T. A.; Moad, G.; Rizzardo, E.; Thang, S. H. In *WO 99/31144*; E.I. DuPont de Nemours and Company: Australia, 1999.

(78)   Chong, Y. K.; Le, T. P. T.; Moad, G.; Rizzardo, E.; Thang, S. H. *Macromolecules* **1999**, *32*, 2071-2074.

(79)   Rizzardo, E.;   Chiefari, J.; Mayadunne, R. T. A. In *Controlled/Living Radical Polymerization - Progress in ATRP, NMP, and RAFT, ACS Symposium Series*; Matyjaszewski, K., Ed.; American Chemical Society: Washington, DC, 2000; Vol. 768, pp 278-295.

2 Motivation

The purpose of the present work was to create new routes for the synthesis of polymer-peptide / polymer-protein conjugates and eventually polymer-drug conjugates. As a means to achieve this, reversible addition-fragmentation chain transfer (RAFT) polymerization was employed, which is a novel, controlled radical polymerization technique that does not require protection group chemistry on functional monomers like other controlled polymerization methods and can be applied to virtually any radically polymerizable monomer. RAFT polymerization generally leads to well-defined polymers with narrow molecular weight distributions and chain end functionalization. The functionalized polymeric chain end can subsequently be modified for attachment of model compounds and proteins.

As the RAFT process tolerates virtually any monomer functionality, a great variety of polymers can be synthesized in a well-controlled manner.

Since RAFT is a relatively new polymerization method, it was of interest to perform this polymerization on a variety of monomers that are suited for the synthesis of bioconjugates and also to investigate the kinetic characteristics of the process as not many details were known at that point. Useful polymers include active esters, such as poly(*N*-hydroxysuccinimide methacrylate), or the stimuli-responsive poly(*N*-isopropylacrylamide) and poly(acrylic acid).

By the use of thiocarbonylthio compounds as chain transfer agents, these functionalities are incorporated into the polymeric structure. The thus obtained dithiocarbonyl-terminated polymers can be hydrolyzed to obtain thiol-terminated polymers. Thiol-terminated polymers provide ideal conjugation sites for the thiol groups of peptides and proteins that are relatively rare so that selective binding can be achieved.

Beside synthesizing endgroup-functionalized polymers, a variety of active ester monomers can be (co)polymerized to have binding sites for primary amino groups.

Characterization of the functionalized homopolymers and block copolymers in terms of endgroup functionality, solution behavior, and molecular weight (distribution) provides new insights into their potential use as drug carriers or as components of bioconjugates.

As an approach to the synthesis of bioconjugates, the conjugation of active ester polymers to model peptides and of stimuli-responsive polymers to thiol-functionalized proteins can be probed. The protein streptavidin was chosen for the synthesis of polymer-protein conjugates as this system had been investigated thoroughly and it is possible to

genetically engineer thiol groups at the desired sites. Characterization of the protein-polymer conjugates provides some new insights into the features of these conjugates, especially in terms of their ability to block/unblock binding of ligands to the protein's active site.

The synthesis of stimuli-responsive polymers, such as thermoresponsive poly(*N*-isopropylacrylamide) or pH-responsive poly(acrylic acid), and their incorporation into block copolymers with subsequent conjugation to proteins enables modulation of structure and binding properties by pH and/or temperature.

3   Fundamentals of controlled radical polymerization

Controlled polymerization has become of vital importance since Szwarc[1,2] reported the "living" nature of the anionic polymerization of styrene and diene monomers in 1956. Living polymerization is defined as a polymerization that undergoes neither irreversible termination nor irreversible chain transfer. A plot of molecular weight versus conversion is therefore linear, and the first-order time-conversion plot results in a straight line in the absence of termination. If initiation and equilibration between active species are fast with respect to propagation, the polymer chains all grow at the same rate, thereby decreasing the polydispersity. Consequently, the molecular weight of the polymers produced in a living polymerization process is governed by the stoichiometry of the reaction and the degree of monomer conversion. The living nature of the propagating chains is the basis of the synthesis of block, graft, star, and hyperbranched copolymers.

Until recently, ionic polymerizations were the only "living" techniques available that controlled efficiently the architecture and structure of vinyl polymers. Due to the incompatibility of the propagating ionic polymer chains with a great number of functional groups and some monomer classes along with the rather drastic reaction conditions that require extremely pure solvents, complete absence of oxygen and mostly very low temperatures, more convenient polymerization methods were desired.[3] The answer to this problem was the control over radical polymerization which tolerates a much greater number of functional groups and offers moderate reaction conditions, such as a convenient temperature range and the tolerance of impurities. In a first attempt to control the radical polymerization of styrenes and methyl methacrylates, in 1955, Ferington and Tobolsky used dithiuram disulfides as initiators.[4] However, due to the high transfer constants involved, retardation of polymerization was observed. Considering the nature of ionic polymerizations, in order to establish a living radical polymerization process, it was reasonable to assume that initiation should be fast providing a constant concentration of growing chains and that the living process involves equilibration between propagating free radicals and dormant species. As these equilibria are shifted towards the dormant species, the concentration of free radicals decreases substantially and thereby suppresses any transfer and termination steps. Therefore, these polymerizations are usually denoted as controlled/living polymerizations rather than as true living polymerizations because termination and transfer cannot be avoided completely.

3.1 Conventional radical polymerization

3.1.1 Mechanism

Radical chain polymerization may be considered as a process comprising three steps: initiation, propagation and termination.[5] The initiation reaction is the attack of the monomer by a primary radical originating from the initiator. This is generally achieved by homolytic cleavage of the initiator molecule to yield a pair of radicals:

$$I \xrightarrow{k_d} 2R^\bullet$$
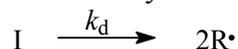
In the initiation step, radicals are usually generated by thermal decomposition of a particular species, such as an azo or peroxy compound (e.g. 1,1'-azobis(isobutyronitrile) AIBN and *tert*-butyl hydroxyperoxide TBHP). Alternatively, radicals can also be formed electrochemically or photochemically. The initiation process continues with the initiating species adding to a monomer molecule, yielding a propagating polymer chain.

In the propagation step, the polymer chain reacts with the unsaturated group in the monomer via radical addition to the double bond.

Once the propagating chain is established, the polymer chain continues to react with monomer until some sort of termination occurs. There are two main termination events: (i) disproportionation occurs when a hydrogen atom is transferred from one propagating chain to another, yielding two dead polymer chains.
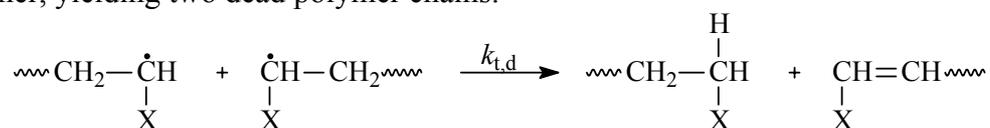
(ii) Combination occurs when two propagating polymer chains combine to form one dead polymer chain.
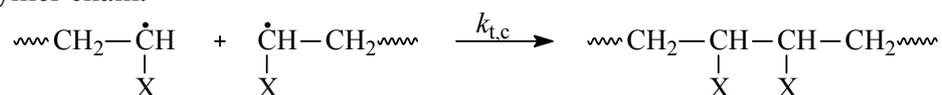
3.1.2 Kinetics

The afore-mentioned steps can be translated into a kinetic scheme and a rate equation. Based on the assumption that the dissociation of the initiator is the rate-determining step in the initiation, the rate of initiation is given by:

$$R_i = 2 f k_d [I] \hspace{4cm} \text{Eq. 3.1}$$

where f is the efficiency of the initiation process, k_d is the rate constant of initiator decomposition and [I] is the initiator concentration. The overall rate of monomer consumption may be considered as the sum of the rate of initiation R_i and the rate of propagation R_p, i.e.

$$-\frac{d[M]}{dt} = R_i + R_p$$

Eq. 3.2

However, if the number of monomers consumed in the initiation step is much less than the number of monomers consumed in the propagation steps, which is the case for a process producing high-molecular weight polymers, then the equation simplifies to:

$$-\frac{d[M]}{dt} = R_p$$

Eq. 3.3

As the rate constant of propagation is principally independent of the chain length, R_p may be expressed as follows:

$$R_p = k_p \, [M][P_n^\bullet]$$

Eq. 3.4

where k_p is the rate constant of propagation, $[M]$ and $[P_n^\bullet]$ are the concentrations of monomer and propagating radical chains, respectively. Based on the assumption that the number of radicals during the polymerization remains constant (steady-state approximation), the following relation between the rate of initiation R_i and the rate of termination R_t is obtained:

$$R_i = R_t$$

Eq. 3.5

Since termination processes are always bimolecular radical processes, the rate of termination is expressed as:

$$R_t = 2 \, k_t \, [P_n^\bullet]^2$$

Eq. 3.6

where k_t is the rate constant of termination. The value of k_t is composed of a disproportionation and a combination term. Inserting Eq. 3.6 into Eq. 3.1 and considering Eq. 3.5 yields Eq. 3.7:

$$[P_n^\bullet] = \left(\frac{f k_d [I]}{k_t} \right)^{1/2}$$

Eq. 3.7

Eq. 3.7 can be substituted by Eq. 3.4, yielding the rate equation for free radical polymerization:

$$R_p = k_p [M] \left(\frac{f k_d [I]}{k_t} \right)^{1/2}$$

Eq. 3.8

Another side reaction of free radical polymerization is chain transfer. It occurs when the radical at the chain end is transferred to another species, resulting in the formation of dead polymer chains and a small radical. It is usually facilitated by the addition of a chain transfer agent, such as a halide or thiol. In the chain transfer process, an atom is transferred from the transfer agent to the growing polymer chain, thereby terminating its growth and giving rise to a new, shorter radical species. As a result, a lower-molecular weight polymer

is formed. An example of a chain transfer reaction is the chain transfer of a propagating styrene radical to carbon tetrachloride:
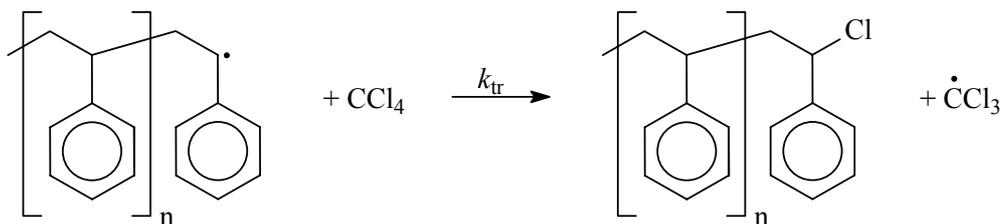
Chain transfer can be problematic in some systems since the propagating species might transfer quickly to initiator, monomer, polymer or solvent.

Chain transfer kinetics can be described by the Mayo equation:[6]

$$\frac{1}{\overline{P_n}} = \frac{1}{\left(\overline{P_n}\right)_0} + C_M + C_S \frac{[S]}{[M]} + C_I \frac{[I]}{[M]}$$

Eq. 3.9

where $\overline{P_n}$ and $\left(\overline{P_n}\right)_0$ is the number-average degree of polymerization with and without chain transfer, respectively. $C_M = k_{tr,M}/k_p$ is the chain transfer constant of transfer to monomer, C_S is the chain transfer constant of transfer to solvent, C_I is the chain transfer constant of transfer to initiator, [M] is the monomer concentration, [S] is the chain transfer agent concentration, and [I] is the initiator concentration.[5]

In most cases, transfer to monomer and to initiator can be neglected, which simplifies Eq. 3.9 to Eq. 3.10:

$$\frac{1}{\overline{P_n}} = \frac{1}{\left(\overline{P_n}\right)_0} + C_S \frac{[S]}{[M]}$$

Eq. 3.10

Degenerative chain transfer takes place when the polymer acts as a transfer agent itself, with chain transfer agent and chain transfer product having the same chemical structure. One example of such a transfer reaction is polymerization mediated by a polymeric iodide:

$$\sim\sim CH_2-I \ + \ H_2\dot{C}\sim\sim \ \rightleftharpoons \ \sim\sim\dot{C}H_2 \ + \ I-CH_2\sim\sim$$
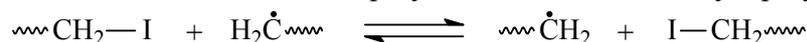
Under controlled conditions, degenerative transfer may be used for polymerization in a living manner. One example is reversible addition-fragmentation chain transfer (RAFT) polymerization, which will be discussed below.

3.2   Controlled/living polymerization

The definition of the terms "controlled" and "living" has been the subject of much controversy and a uniform terminology has not yet been agreed on.[7] One definition of a living polymerization has been proposed by Webster:[8]

(a) the polymerization proceeds to complete conversion with further monomer addition leading to continuing polymerization

(b) the number-average molecular weight is directly proportional to conversion

(c) the number of polymer chains in the system remains constant throughout the polymerization process

(d) the molecular weight can be controlled via the reaction stoichiometry

(e) polymers with chain end functionality are obtained quantitatively

An ideal living polymerization process is characterized by the following reaction steps:

initiation:

$$R^\bullet + M \quad \xrightarrow{k_i} \quad P_1^\bullet$$

propagation:

$$P_i^\bullet + M \quad \xrightarrow{k_p} \quad P_{i+1}^\bullet$$
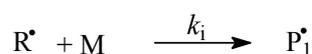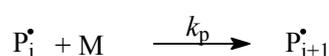
A polymerization is termed living if there are no irreversible transfer and termination reactions throughout the polymerization.[1,9] Considering a controlled living polymerization process, there is a fast initiation step and $k_i \gg k_p$. The equilibration between different active centers will be faster than the polymerization process itself. This means that the number of active centers is always constant:

$$[P^\bullet] = \sum_i [P_i^\bullet] = const. \qquad\qquad \text{Eq. 3.11}$$

In this case, only the propagation reaction has to be taken into account. The polymerization rate R_p follows a pseudo-first order time law, where k_{app} can be defined as the "apparent" rate constant:

$$R_p = -\frac{d[M]}{dt} = k_p[P^\bullet][M] = k_{app}[M] \qquad\qquad \text{Eq. 3.12}$$

Integration of Equation 3.12 results in:

$$\ln\frac{[M]_0}{[M]_t} = k_p[P^\bullet]t = k_{app}t \qquad\qquad \text{Eq. 3.13}$$

In the absence of termination reactions, the first-order time-conversion plot is a straight line with slope $k_{app} = k_p[P^\bullet]$.

In living polymerizations, the number-average polymerization degree P_n increases linearly with monomer conversion x_p:

$$P_n = \frac{concentration\ of\ reacted\ monomers}{concentration\ of\ polymer\ chains} = \frac{[M]_0 \cdot x_p}{[P]} \qquad\qquad \text{Eq. 3.14}$$

where [P] is the total concentration of polymer chains (including those resulting from termination). A non-linearity of the relationship between number-average polymerization degree and monomer conversion is indicative of either a slow initiation or the occurrence of transfer reactions since the concentration of polymer chains increases with monomer conversion in both cases. The termination of polymer chains cannot be deduced from such a plot as only the concentration of active chains decreases, whereas the total concentration of all chains remains constant. If the number-average polymerization degree is found to be greater than the one calculated from Eq. 3.14, either initiator termination (initiator efficiency $f = [P^{\bullet}]/[I]_0 < 1$) or termination via recombination occurs.

In the case of living polymerization with fast initiation, the expected molecular-weight distribution should be identical with a Poisson distribution,[10] and the non-uniformity U or polydispersity index PDI, respectively, are given by:

$$U = PDI - 1 = \frac{M_w}{M_n} - 1 = \frac{P_{n-1}}{P_n^2} \approx \frac{1}{P_n} << 1 \qquad \text{Eq. 3.15}$$

Therefore, using living polymerization, it is basically possible to produce polymers with very narrow molecular-weight distributions. If, however, broad molecular-weight distributions should be observed in a controlled/living process, this might be ascribed to impurities of the reactants, slow initiation, co-existence of different active species or depolymerization.

In the last decade, three methods of controlled free radical polymerization have gained importance in the synthesis of well-defined polymers with controlled molecular weights and narrow molecular weight distributions. These recent methods include stable free-radical polymerization (SFRP) - best represented by nitroxide-mediated polymerization (NMP) – atom-transfer radical polymerization (ATRP), and reversible addition-fragmentation chain transfer (RAFT) polymerization.

In nitroxide-mediated polymerization (NMP), nitroxides and N-alkoxyamines are used to deactivate the growing radical reversibly, thus reducing the overall concentration of the propagating radical chain end.[11-18] In the absence of other reactions resulting in the initiation of new polymer chains the probability of irreversible termination reactions is very low so that a high degree of control over the polymerization is obtained. Nevertheless, it has to be noted that NMP is successful for making homopolymers and block copolymers based on styrene and its derivatives, but fails mostly in other systems. The only exception known so far is the successful polymerization of acrylates in the presence of phosphonate-derivatized nitroxyl radicals that has been reported by Tordo et al.[16,19,20]
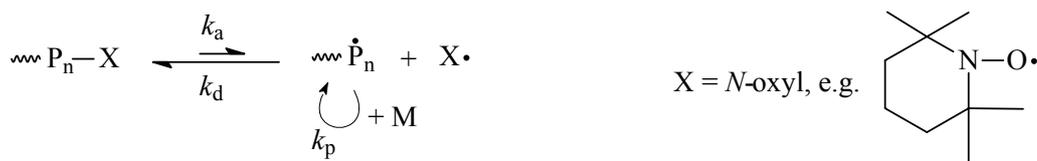
Fig. 3.1.   *Mechanism of nitroxide-mediated polymerization (NMP).*

Atom-transfer radical polymerization (ATRP) makes use of a reversible transfer to a halogen atom between growing polymer chains and a redox-active transition metal catalyst.[21-30] In the key reaction step, macromolecular alkyl halides are activated by reduction to free radicals and the transition metal complexes are oxidized by coordinating the halogen atoms. A number of monomer classes have been polymerized successfully by ATRP, including styrenes, acrylates, methacrylates, and vinyl pyridine. The major drawbacks of the ATRP process are its incompatibility with a variety of monomers, such as acidic or highly polar monomers, due to interaction with the catalyst, and subsequent removal of the transition metal catalyst after polymerization.

X = halide, pseudohalide

Mt = Cu, Fe, Ru, Ni, Pd

m = valency of metal ion

L = ligand
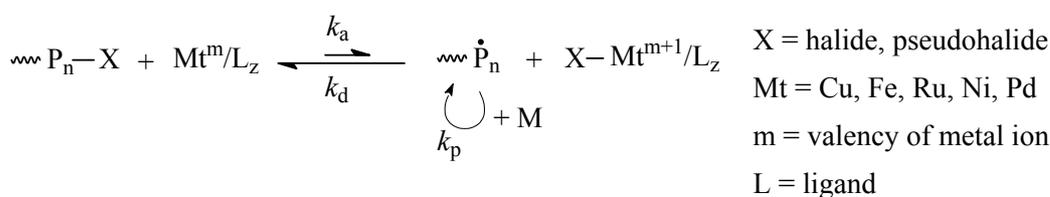
Fig. 3.2.   *Mechanism of atom-transfer radical polymerization (ATRP).*

Reversible addition-fragmentation chain transfer (RAFT) polymerization will be dealt with in the following section.

3.3   RAFT polymerization

Although the synthetic potential of the RAFT process is well documented, its mechanistic and kinetic understanding is still the subject of lively debate in the scientific community. Recently, the mechanism and kinetics of RAFT polymerization have been investigated by various research groups in order to determine rate coefficients and other kinetic parameters.[31-34] Despite the combined effort to elucidate the specifics of the RAFT process, there is some disagreement between different studies concerning kinetic and mechanistic details. It has to be noted, though, that even well-established controlled radical polymerization techniques, such as nitroxide-mediated or atom-transfer radical polymerization, are still being the subject of ongoing research in terms of their mechanism and kinetics.[18,25,35]

3.3.1   Mechanism

From a conceptual point of view, the "iniferter" (*ini*tiator – trans*fer* – *ter*minator) technique introduced by Otsu in 1982[36-38] is a predecessor to the controlled radical polymerization method known as reversible addition-fragmentation chain transfer (RAFT) polymerization.[39-41] In the iniferter case, disulfides R-S-S-R or *N,N*-diethyldithiocarbamoyl $Et_2N(C=S)SR$ compounds were proposed as photochemical initiators where cleavage occurs at the C-S bond to yield a carbon-based radical and the mediating thio radical (Fig. 3.3).

$$Et_2N-\underset{\underset{S}{\|}}{C}-SR \quad \xrightarrow{h\nu} \quad Et_2N-\underset{\underset{S}{\|}}{C}-S^{\bullet} \;+\; R^{\bullet}$$

$$Et_2N-\underset{\underset{S}{\|}}{C}-S^{\bullet} \;+\; n M \quad \longrightarrow \quad Et_2N-\underset{\underset{S}{\|}}{C}-S-(M)_{n-1}-M^{\bullet}$$
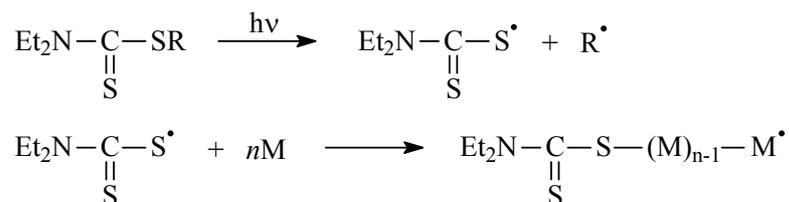
Fig. 3.3.   Decomposition of dithiocarbamoyl compounds used in the iniferter technique.

Albeit the linear increase of molecular weight with conversion observed with this method, it fails to produce polymers with controlled molecular weights and low polydispersities as the thio radical can also initiate polymerization. With the introduction of a variety of (thiocarbonyl)sulfanyl derivatives of common structure Z-C(=S)-SR by Rizzardo et al., chain transfer agents became available that can be fragmented in a controlled manner in the presence of initiating species. The key to the living character of RAFT polymerization is the very high transfer constant associated with the thiocarbonylthio group and, consequently, the fast equilibration between active and dormant polymer chains. One of the major accomplishments of the RAFT method as compared to the iniferter technique is the use of dithiocarbamates that have the nonbonded electron pair of nitrogen incorporated into an aromatic system resulting in highly effective chain transfer agents in styrene and (meth)acrylate ester polymerization. In contrast, simple *N,N*-dialkyl dithiocarbamates are ineffective in RAFT polymerization.[42] Besides these dithiocarbamates, a great variety of dithioesters, trithiocarbonates, xanthates and similar compounds have been found to be effective chain transfer agents (cf. Fig. 3.4.).[43-45]

$$\underset{\text{thiocarbonylthio compound}}{Z-\overset{\overset{\textstyle S}{\|}}{C}-SR}$$

$$\underset{\text{dithioester}}{R'-\overset{\overset{\textstyle S}{\|}}{C}-SR} \qquad \underset{\text{trithiocarbonate}}{R'S-\overset{\overset{\textstyle S}{\|}}{C}-SR}$$

$$\underset{\text{xanthate}}{R'O-\overset{\overset{\textstyle S}{\|}}{C}-SR} \qquad \underset{\text{dithiocarbamate}}{R'R''N-\overset{\overset{\textstyle S}{\|}}{C}-SR}$$
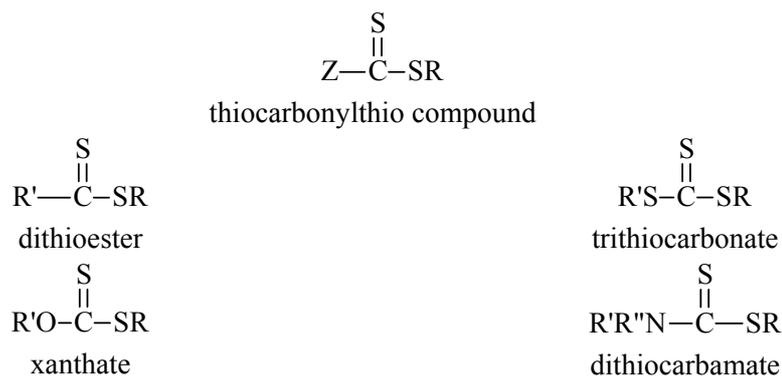
Fig. 3.4. *General structures of chain transfer agents used in RAFT polymerization.*

The experimental conditions employed in RAFT polymerization are those used for conventional free radical polymerizations. The polymerization can be performed in bulk, solution, emulsion or suspension. Common initiators, such as azo or peroxy compounds, are used and there are no particular limitations on solvent and reaction temperature. One of the major advantages of the RAFT process over other controlled/living radical polymerization processes is its compatibility with a wide range of monomers including functional monomers containing acid, acid salt, hydroxyl or amino groups.

The mechanism of the RAFT process is believed to involve a series of reversible addition-fragmentation steps. Addition of a propagating radical $P_n^\bullet$ to a thiocarbonylthio compound gives an adduct radical which fragments into a polymeric thiocarbonylthio compound and a new radical $R^\bullet$ (Fig. 3.5.). The radical $R^\bullet$ then reinitiates polymerization to give a new propagating radical $P_m^\bullet$. Subsequent addition-fragmentation steps set up an equilibrium between the propagating radicals $P_n^\bullet$ and $P_m^\bullet$ and the dormant polymeric thiocarbonylthio compounds by way of an intermediate radical. Equilibration of the growing chains gives rise to a narrow molecular weight distribution. Throughout the polymerization and at its end, the majority of the polymer chains are end capped by a thiocarbonylthio group.
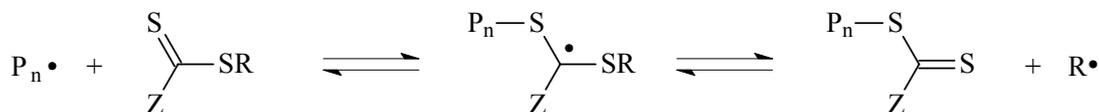
Fig. 3.5. *Simplified mechanism of the RAFT process (addition-fragmentation step).*

Evidence for this mechanism was found by direct ESR observation of the intermediate radical[46] and by end group analysis of the polymer products by NMR and UV-vis spectroscopy[41] as well as by MALDI-TOF mass spectrometry.[47-49]

3.3.2   Kinetics

Despite the growing number of publications in the area of RAFT polymerization, detailed kinetic data for RAFT systems are still rare but their investigation is one of the major subjects of recent research. Early estimates for some of the coefficients involved have been made by Fukuda et al.[32,34] and Monteiro et al.[50] Some research groups have investigated controlled/living processes using simulation,[51,52] with the most comprehensive studies performed by Fischer and Souaille,[53] Barner-Kowollik et al.,[33,54] and Vana et al.[55,56]

The overall mechanism of RAFT polymerization can be divided into five major steps: (1) initiation, (2) propagation, (3) chain transfer, (4) reinitiation, (5) chain equilibration, and (6) termination (Fig. 3.6).
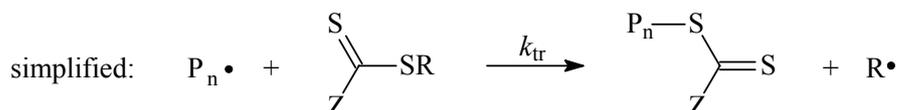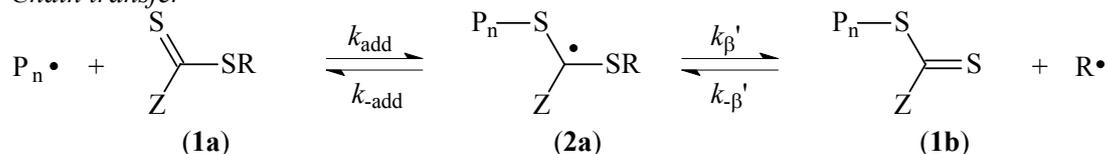
(1) Initiation

$$\text{initiator} \xrightarrow{\;k_d\;} 2\,\text{I}\bullet$$

$$\text{I}\bullet + \text{monomer (M)} \xrightarrow{\;k_i\;} P_1\bullet$$

(2) Propagation

$$P_n\bullet + \text{monomer (M)} \xrightarrow{\;k_p\;} P_{n+1}^\bullet$$

(3) Chain transfer

(1a)   **(2a)**   **(1b)**

$$\text{simplified:}\quad P_n\bullet + \text{(CS}_2\text{SR)} \xrightarrow{\;k_{tr}\;} P_n\text{—S(C=S)Z} + R\bullet$$

(4) Reinitiation

$$R\bullet + \text{monomer (M)} \xrightarrow{\;k_i'\;} P_1\bullet$$

(5) Chain equilibration (degenerative transfer)

(2b)

(6) Termination

$$P_n\bullet + P_m\bullet \xrightarrow{\;\langle k_t\rangle\;} P_{n+m} \;(\text{or}\; P_n + P_m)$$
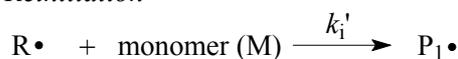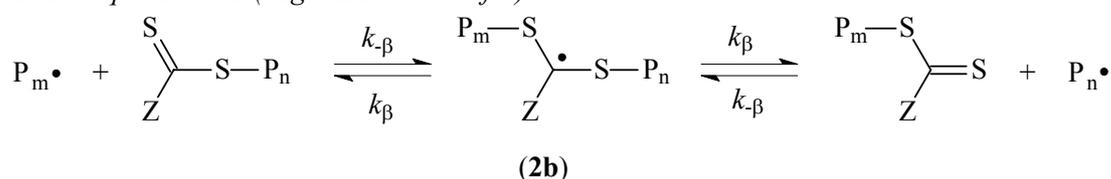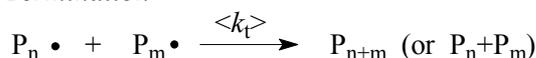
Fig. 3.6.   *Major steps of the RAFT process.*

The decomposition of the initiator I proceeds with the effective rate coefficient $k_d = k_d^* \cdot f$, where k_d^* is the rate coefficient for initiator composition and f is the initiator efficiency. The reaction of an initiator-derived radical I$^\bullet$ with monomer is described by the rate coefficient of initiation k_i (step (1) in Fig. 3.6). The rate of addition of propagating radicals P$_n^\bullet$ to chain transfer agent is given by the rate coefficient of addition k_{add}, where the reverse reaction is described by the coefficient k_{-add} ((2) in Fig. 3.6). This RAFT preequilibrium can be considered as a transfer reaction in which the leaving group R is released as initiating free radical. The corresponding chain transfer coefficient k_{tr} is a composite of the rate coefficients governing the pre-equilibrium (simplified (2) in Fig. 3.6). Reinitiation of polymerization by the chain transfer agent leaving group R$^\bullet$ proceeds with the rate coefficient of initiation k_i' and propagation of the polymeric radicals is described by the rate coefficient of propagation k_p (step (3) in Fig. 3.6). The equilibrium between growing and dormant polymeric chains ((4) in Fig. 3.6) is the core of the RAFT process and is described by the equilibrium constant K, representing the quotient of the rate coefficient of addition $k_ß$ and the rate coefficient of fragmentation $k_{-ß}$:

$$K = \frac{k_\beta}{k_{-\beta}}$$

Eq. 3.16

In the addition step, k_β controls the bimolecular reaction between free polymeric radicals and polymeric chain transfer agent, which leads to the formation of macroRAFT radical (**2b**); $k_{-\beta}$ describes the inverse average lifetime of the intermediate macroRAFT radical.[55]

Bimolecular termination between growing chains to form "dead" polymer is described by the mean rate coefficient of termination $\langle k_t \rangle$ (step (5) in Fig. 3.6). Among the termination reactions not considered in the above mechanism are termination between free polymeric radicals and initiator-derived radicals I$^\bullet$ or initial chain transfer agent-derived radicals R$^\bullet$. These can usually be neglected.

The rate of polymerization R_p is similar to conventional free-radical polymerization:

$$R_p = k_p [M][P_n^\bullet]$$

Eq. 3.17

The variation of [P$_n^\bullet$] with time is quite different from that in free-radical polymerization and can be described as follows, assuming that [**2b**] << [**1b**]:

$$\frac{d[P_n^\bullet]}{dt} = 2f[I]_0 k_d e^{-k_d t} - k_t [P_n^\bullet]^2 - k_{add}[\textbf{1a}][P_n^\bullet] + k_{-add}[\textbf{2a}]$$

Eq. 3.18

where [**1a**] and [**2a**] are the concentrations of chain transfer agent and intermediate radical, respectively (cf. Fig. 3.6).

The polymer chains that are able to propagate are divided among dormant CTA-capped chains, propagating chains P$_n^\bullet$, and intermediate radicals, leading to a reduced

concentration of propagating radicals and therefore to less termination reactions compared to free-radical polymerization.[57]

For the estimation of the chain transfer constants, the Mayo equation can only be used if consumption of chain transfer agent and monomer can be neglected. This is only the case for less active chain transfer agents in low-conversion polymerizations. The direct application of the Mayo method underestimates the transfer constant for more active chain transfer agents. For reversible chain transfer, the rate of consumption of chain transfer agent depends on two transfer constants, $C_{tr} = k_{tr}/k_p$ and $C_{-tr} = k_{-tr}/k_i'$, which describe the reactivity of the propagating radical $P_n{}^\bullet$ and expelled radical $R^\bullet$, respectively:

$$-\frac{d[CTA]}{d[M]} \approx C_{tr} \frac{[CTA]}{[M] + C_{tr}[CTA] + C_{-tr}[macroCTA]}$$

<div align="right">Eq. 3.19</div>

Under the assumption that the adduct radical (**2a**) (Fig. 3.6) undergoes no reactions other than fragmentation, the rate constants for chain transfer are:[58]

$$k_{tr} = k_{add} \frac{k_\beta}{k_{-add} + k_\beta}$$

<div align="right">Eq. 3.20</div>

and

$$k_{-tr} = k_{-\beta} \frac{k_{-add}}{k_{-add} + k_\beta}$$

<div align="right">Eq. 3.21</div>

If the rate of the reverse reaction between $R^\bullet$ and macroCTA is negligible and the chains are long, Eq. 3.17 simplifies to that of conventional chain transfer:[59]

$$-\frac{d[CTA]}{d[M]} \approx C_{tr} \frac{[CTA]}{[M]}$$

$$C_{tr} = \frac{k_{tr}}{k_p} \approx \frac{[M]d[CTA]}{[CTA]d[M]} = \frac{d\ln[CTA]}{d\ln[M]}$$

<div align="right">Eq. 3.22</div>

As can be seen from Eq. 3.20, the slope of the plot of ln[M] versus ln[CTA] yields the transfer constant. If the rate of reactions of $R^\bullet$ with macroCTA is not negligible, the apparent transfer constant obtained from the plot is lower than the actual transfer constant. The transfer constants of various thiocarbonylthio compounds have been reported to extend over more than five orders of magnitude (< 0.01 to > 1000) depending on the R and Z groups of the CTA and the respective monomer.[60]

3.3.3   Influence of chain transfer agent structure

Different RAFT agents are required for monomers with different properties. Methyl methacrylate, for example, gives rise to radicals that are very good leaving groups and can only be polymerized effectively when the chain transfer agent has an at least equally good

leaving group. Furthermore, the thiocarbonyl group has to be activated toward radical addition. If the thiocarbonyl is not active enough, extensive propagation may occur before transfer. In the case of a highly active monomer such as vinyl acetate, the thiocarbonyl group can also be too active to radical addition and the intermediate radical formed will be too stable so that no chains will be available for propagation. In this case, the thiocarbonyl compound has to be deactivated toward radical addition.[61]

The selection of the transfer agent is crucial for the synthesis of low-polydispersity products. It does not only depend on the chain transfer constant but also on the structure of the transfer agent. The R moiety should be a good homolytic leaving group, and the formed $R^{\bullet}$ radical should be able to reinitiate the polymerization. Its leaving group ability is determined by both steric and stability factors. The R group can be either of alkyl or aryl nature. The most frequently used R groups in the RAFT polymerization of styrenes and (meth)acrylates are benzyl ($-CR'''_2Ph$) and cyanoalkyl ($-CR'''_2CN$) moieties. The capability of $R^{\bullet}$ as a leaving group is also determined by the nature of the propagating species formed in the course of polymerization. In order to avoid retardation, the R''' substituents should be chosen in a way that $R^{\bullet}$ easily adds to monomer. The ability of $R^{\bullet}$ to reinitiate polymerization will also depend on the nature of the monomers used in RAFT polymerization. It has been shown that the most effective R groups in RAFT polymerization of styrene and methacrylates are cyanoalkyl and benzyl derivatives, whereas benzyl derivatives are less effective in vinyl acetate polymerization due to the slow initiation which might result in retardation of the polymerization. For this reason, cyanoalkyl derivatives and their corresponding esters ($-CR'''_2CO_2alkyl$) are the R moieties of choice in vinyl acetate polymerization.[61]

The Z group should activate the C=S double bond toward radical addition in order to ensure a higher transfer constant. The Z moiety usually includes alkyl, aryl, or heterocyclic groups. In polymerization of (meth)acrylates and styrenes, dithiocarbamate chain transfer agents with conjugating or electron-withdrawing groups at the nitrogen atom are much more effective than dithiocarbamates with simple alkyl substituents. Consequently, the preferred Z groups are aromatic azacycles, such as pyrroles or imidazoles, or cyclic amides, such as lactams, imides or phthalimides. The reason for the higher effectiveness of the above-mentioned chain transfer agents seems to be correlated with the higher activity of the C=S double bond towards radical addition. This, in turn, is attributed to the conjugating or electron-withdrawing substituents that bestow greater double bond character upon the C=S double bond. In carbamates and amides, the N-CO link has partial double bond character as a result of the delocalisation of the non-bonded nitrogen lone pair with the p electrons of the carbonyl group.[62] As a result, the oxygen of the carbonyl group has a partial negative charge. Since sulfur has a higher electron affinity than oxygen, this effect

would be expected to be more pronounced in dithiocarbamates. If the nitrogen lone pair participates in an alternate π-system (e.g. the aromatic pyrrole ring), the lone pair will be less available for delocalization into the thiocarbonyl bond resulting in a greater double bond character for the C=S double bond and hence a greater reactivity of the chain transfer agent towards radicals (see Fig. 3.7.).
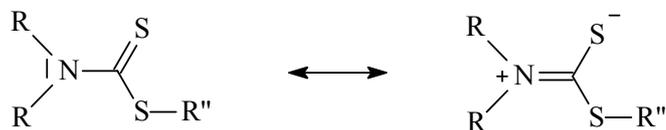
Fig. 3.7.   Effect of nitrogen substituents R on double bond character of C=S bond in dithiocarbamates.

Similar considerations apply in the case of xanthate esters. The effectiveness of xanthate ester chain transfer agents in providing low polydispersity polymers in acrylate polymerization increases in the series where R' is $-OEt < -OC_6H_5 < OC_6F_5$.

For the right choice of chain transfer agent, it has to be considered that the transfer constants of both xanthates and dithiocarbamates are strongly dependent on the type of monomer used. Dithiocarbamate and xanthate derivatives possess relatively low transfer constants in the polymerization of styrene and methacrylates. Nevertheless, in polymerization of vinyl acetate, vinyl butyrate, vinyl chloride and similar vinyl monomers, dithiocarbamates and xanthates show higher transfer constants, enabling the synthesis of polymers with narrow molecular-weight distributions.[61]

Tab. 3.1 summarizes the most effective CTA moieties used in the RAFT polymerization of different monomer classes.

Tab. 3.1. *Overview of effective chain transfer agent moieties used for the RAFT polymerization of different monomer classes.*[61]

$$Z-\overset{\overset{\displaystyle S}{\|}}{C}-SR$$

monomer	Z	R
styrene	pyrrole, imidazole, lactams, imides, phthalimides	benzyl, 1-phenylethyl, 2-phenylethyl, 2-(alkoxycarbonyl)prop-2-yl, 2-cyanoprop-2-yl, 2-cyanobut-2-yl, 1-cyanocyclohexyl
methacrylates	phenyl, methylthio, pyrrole, imidazole, lactams, imides, phthalimides, OR' (R' = Et < C_6H_5 < C_6F_5)	2-phenylpropyl, 2-cyanoprop-2-yl, 2-cyanobut-2-yl, 1-cyanocyclohexyl
vinyl acetate[*]	*N*-aryl, *N*-alkyl, alkoxy	2-(alkoxycarbonyl)prop-2-yl, cyanomethyl, 2-cyanoprop-2-yl, 2-cyanobut-2-yl, 1-cyanocyclohexyl
acrylates/ acrylic acid	phenyl, pyrrole, methylthio, lactams	benzyl, 2-cyanoprop-2-yl
acrylamides	phenyl	2-phenylpropyl

[*]complete inhibition with dithioesters, trithiocarbonates and aromatic dithiocarbamates

References

(1)   Szwarc, M. *Nature* **1956**, *178*, 1168.

(2)   Szwarc, M.; Levy, M.; Milkovich, R. *J. Am. Chem. Soc.* **1958**, *78*, 2656.

(3)   Quirk, R. P.; Kinning, D. J.; Fetters, L. J. **1989**, *7*.

(4)   Ferington, T. E.; Tobolsky, A. V. *J. Am. Chem. Soc.* **1955**, *77*, 4510-4512.

(5)   Odian, G. *Principles of Polymerization*, 3rd ed.; John Wiley & Sons, Inc.: New York, 1991.

(6)   Mayo, F. R.; Gregg, R. A.; Matheson, M. S. *J. Am. Chem. Soc.* **1951**, *73*, 1691.

(7)   Darling, T. R.; Davis, T. P.; Fryd, M.; Gridnev, A. A.; Haddleton, D. M.; Ittel, S. D.; Jr., R. R. M.; Moad, G.; Rizzardo, E. *J. Polym. Sci., Part A: Polym. Chem.* **2000**, *38*, 1709-1752.

(8)   Webster, O. *Science* **1991**, *251*, 887.

(9)   Matyjaszewski, K.; Müller, A. H. E. *Polym. Prepr. (Am. Chem. Soc., Div. Polym. Chem.)* **1997**, *38*, 6.

(10)   Flory, P. J. *J. Am. Chem. Soc.* **1940**, *62*, 1561.

(11)   Georges, M. K.;   Veregin, R. P. N.;   Kazmaier, P. M.; Hamer, G. K. *Macromolecules* **1993**, *26*, 2987-2988.

(12)   Hawker, C. J. *J. Am. Chem. Soc.* **1994**, *116*, 11185-11186.

(13)   Puts, R. D.; Sogah, D. Y. *J. Am. Chem. Soc.* **1996**, *29*, 3323 - 3325.

(14)   Veregin, R. P. N.; Odell, P. G.; Michalak, L. M.; Georges, M. K. *Macromolecules* **1996**, *29*, 2746-2754.

(15)   Burguière, C.; Dourges, M.-A.; Charleux, B.; Vairon, J.-P. *Macromolecules* **1999**, *32*, 3883 - 3890.

(16)   Benoit, D.; Grimaldi, S.; Robin, S.; Finet, J.-P.; Tordo, P.; Gnanou, Y. *J. Am. Chem. Soc.* **2000**, *122*, 5929 - 5939.

(17)   Harth, E.; Hawker, C. J.; Fan, W.; Waymouth, R. M. *Macromolecules* **2001**, *34*, 3856-3862.

(18)   Hawker, C. J.; Bosman, A. W.; Harth, E. *Chem. Rev.* **2001**, *101*, 3661-3688.

(19)   Benoit, D.; Grimaldi, S.; Finet, J. P.; Tordo, P.; Fontanille, M.; Gnanou, Y. *Polym. Prepr. (Am. Chem. Soc., Div. Polym. Chem.)* **1997**, *38*, 729-730.

(20)   Benoit, D.; Grimaldi, S.; Finet, J. P.; Tordo, P.; Fontanille, M.; Gnanou, Y. In *Controlled Radical Polymerization, ACS Symposium Series*; Matyjaszewski, K., Ed.; American Chemical Society: Washington D.C., 1998; Vol. 685, pp 225-235.

(21)   Kato, M.; Kamigaito, M.; Sawamoto, M.; Higashimura, T. *Macromolecules* **1995**, *28*, 1721 - 1723.

(22)   Wang, J. S.; Matyjaszewski, K. *Macromolecules* **1995**, *28*, 7901-7910.

(23)   Wang, J. S.; Matyjaszewski, K. *J. Am. Chem. Soc.* **1995**, *117*, 5614-5615.

(24)   Xia, J.; Matyjaszewski, K. *Macromolecules* **1997**, *30*, 7679-7700.

(25)   Matyjaszewski, K.; Xia, J. *Chem. Rev.* **2001**, *101*, 2921-2990.

(26)   Coessens, V.; Pintauer, T.; Matyjaszewski, K. *Prog. Polym. Sci.* **2001**, *26*, 337-377.

(27)   Matyjaszewski, K. *Macromol. Symp.* **2000**, *161*, 1-9.

(28)   Ando, T.; Kato, M.; Kamigaito, M.; Sawamoto, M. *Macromolecules* **1996**, *29*, 1070-1072.

(29)   Kotani, Y.; Kato, M.; Kamigaito, M.; Sawamoto, M. *Macromolecules* **1996**, *29*, 6979-6982.

(30)   Takahashi, H.; Ando, T.; Kamigaito, M.; Sawamoto, M. *Macromolecules* **1999**, *32*, 3820-3823.

(31)   Monteiro, M. J.; Hodgson, M.; Brouwer, H. D. *J. Polym. Sci. Part A: Polym. Chem.* **2000**, *38*, 3864-3874.

(32)   Goto, A.; Sato, K.; Tsujii, Y.; Fukuda, T.; Moad, G.; Rizzardo, E.; Thang, S. H. *Macromolecules* **2001**, *34*, 402-408.

(33)   Barner-Kowollik, C.; Quinn, J. F.; Morsley, D. R.; Davis, T. P. *J. Polym. Sci., Part A: Polym. Chem.* **2001**, *39*, 1353-1365.

(34)   Kwak, Y.; Goto, A.; Tsujii, Y.; Murata, Y.; Komatsu, K.; Fukuda, T. *Macromolecules* **2002**, *35*, 3026 -3029.

(35)   Fischer, H. *Chem. Rev.* **2001**, *101*, 3581 - 3610.

(36)   Otsu, T.; Yoshida, M. *Makromol. Chem. Rapid Commun.* **1982**, *3*, 127-132.

(37)   Otsu, T. *J. Polym. Sci.: A Polym. Chem.* **2000**, *38*, 2121-2136.

(38)   Otsu, T.; Matsumoto, A. *Adv. Polym. Sci.* **1998**, *136*, 75-137.

(39)   Rizzardo, E.; Moad, G.; Thang, S. H.: Australia, 1998.

(40)   Le, T. P.; Moad, G.; Rizzardo, E.; Thang, S. H. In *WO 98/01478*; E.I. Du Pont De Nemours and Co., USA; Le, Tam Phuong; Moad, Graeme; Rizzardo, Ezio; Thang, San Hoa: Australia, 1998.

(41)   Chiefari, J.; Chong, Y. K.; Ercole, F.; Krstina, J.; Jeffery, J.; Le, T. P. T.; Mayadunne, R. T. A.; Meijs, G. F.; Moad, C. L.; Moad, G.; Rizzardo, E.; Thang, S. H. *Macromolecules* **1998**, *31*, 5559-5562.

(42)   Mayadunne, R. T. A.; Rizzardo, E.; Chiefari, J.; Chong, Y. K.; Moad, G.; Thang, S. H. *Macromolecules* **1999**, *32*, 6977-6980.

(43)   Thang, S. H.; Chong, B. Y. K.; Mayadunne, R. T. A. *Tetrahedr. Lett.* **1999**, *40*, 2435-2438.

(44)   Laus, M.; Papa, R.; Sparnacci, K.; Alberti, A.; Benaglia, M.; Macciantelli, D. *Macromolecules* **2001**, *34*, 7269-7275.

(45) Donovan, M. S.; Lowe, A. B.; Sumerlin, B. S.; McCormick, C. L. *Macromolecules* **2002**, *35*, 4123-4132.

(46) Hawthorne, D. G.; Moad, G.; Rizzardo, E.; Thang, S. H. *Macromolecules* **1999**, *32*, 5457-5459.

(47) Ganachaud, F.; Monteiro, M. J.; Gilbert, R. G.; Dourges, M.-A.; Thang, S. H.; Rizzardo, E. *Macromolecules* **2000**, *33*, 6738-6745.

(48) Destarac, M.; Charmot, D.; Franck, X.; Zard, S. Z. *Macromol. Rapid. Commun.* **2000**, *21*, 1035-1039.

(49) Schilli, C.; Lanzendörfer, M. G.; Müller, A. H. E. *Macromolecules* **2002**, *35*, 6819-6827.

(50) Monteiro, M. J.; Brouwer, H. d. *Macromolecules* **2001**, *34(3)*, 349-352.

(51) Moad, G.; Anderson, A. G.; Ercole, F.; Johnson, C. H. J.; Krstina, J.; Moad, C. L.; Rizzardo, E.; Spurling, T. H.; Thang, S. H. In *Controlled Radical Polymerization, ACS Symposium Series*; Matyjaszewski, K., Ed.; American Chemical Society: Washington D.C., 1998; Vol. 685, pp 332-360.

(52) Shipp, D. A.; Matyjaszewski, K. *Polym. Prepr. (Am. Chem. Soc., Div. Polym. Chem.)* **1999**, *40(2)*, 450-451.

(53) Souaille, M.; Fischer, H. *Macromolecules* **2000**, *33*, 7378-7394.

(54) Barner-Kowollik, C.; Quinn, J. F.; Nguyen, T. L. U.; Heuts, J. P. A.; Davis, T. P. *Macromolecules* **2001**, *34*, 7849-7857.

(55) Vana, P.; Quinn, J. F.; Davis, T. P.; Barner-Kowollik, C. *Aust. J. Chem.* **2002**, *55*, 425-431.

(56) Vana, P.; Davis, T. P.; Barner-Kowollik, C. *Macromol. Theory Simul.* **2002**, *11*, 823-835.

(57) Favier, A.; Charreyre, M.-T.; Chaumont, P.; Pichot, C. *Macromolecules* **2002**, *35*, 8271-8280.

(58) Moad, C. L.; Moad, G.; Rizzardo, E.; Thang, S. H. *Macromolecules* **1996**, *29*, 7717-7726.

(59) Chong, B. Y. K.; Krstina, J.; Le, T. P. T.; Moad, G.; Postma, A.; Rizzardo, E.; Thang, S. H. *Macromolecules* **2003**, *in press*.

(60) Quinn, J. F. *Ph.D. thesis*; The University of New South Wales: Sydney, 2002.

(61) Chiefari, J.; Mayadunne, R. T. A.; Moad, G.; Rizzardo, E.; Thang, S. H. In *WO 99/31144*; E.I. DuPont de Nemours and Company: Australia, 1999.

(62) Deslongchamps, P. *Stereoelectronic effects in organic chemistry*, 1st ed.; Pergamon Press: New York, 1983; Vol. 1.

4 Synthesis of homopolymers and block copolymers

4.1 Synthesis of the chain transfer agents

The synthesis of chain transfer agents is one of the fundamental steps in the application of the reversible addition-fragmentation chain transfer (RAFT) process. Hardly any RAFT agents are available commercially so that different synthetic routes were developed. Very often, the synthesis of the chain transfer agents is a multi-step process involving a number of side reactions so that a couple of purification steps are required, which can decrease the final yields considerably.

The main techniques for the synthesis of chain transfer agents (CTAs) employed in the present work are outlined below.

4.1.1 Substitution of halides with a dithiocarboxylic acid salt

This process involves the nucleophilic substitution of a dithiocarboxylic acid salt (**3**) with an alkyl or aryl halide (**4**) to give dithioesters (**5**). Generally, the dithiocarboxylic acid salt (**3**) is obtained by addition of carbon disulfide (**2**) to a nucleophile (**1**), such as a Grignard reagent or a pyrrole anion. Fig. 4.1 shows the general synthetic scheme.
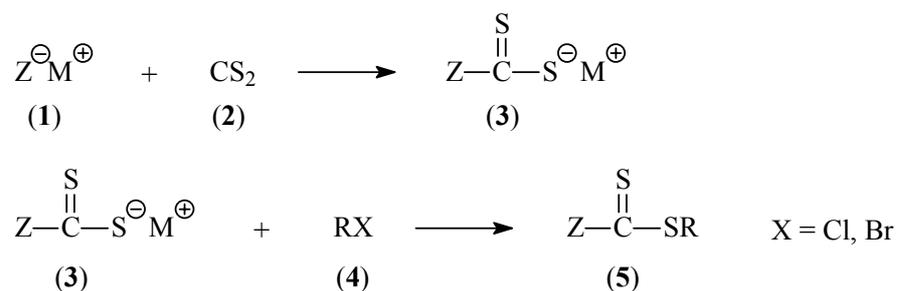

Fig. 4.1.   General scheme for the synthesis of dithiocarbonyl compounds from halides.

The substitution with halide can be done in situ.[1,2] An example of the synthetic procedure is shown in Fig. 4.2.
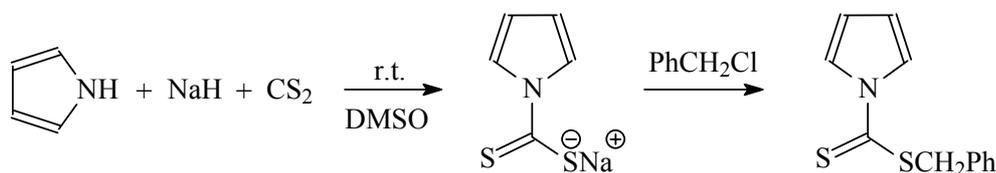

Fig. 4.2.   Synthesis of benzyl 1-pyrrolecarbodithioate from pyrrole and carbon disulfide.

In the present work, the chain transfer agents benzyl/cumyl 1-pyrrolecarbodithioate[3,4] and 1-cyanoethyl 2-pyrrolidone-1-carbodithioate[3,5,6] have been synthesized according to this procedure (Tab. 4.1):

Tab. 4.1.   Structures of the chain transfer agents synthesized by substitution of halides.

benzyl 1-pyrrole-carbodithioate	cumyl 1-pyrrole-carbodithioate	1-cyanoethyl 2-pyrrolidone-1-carbodithioate
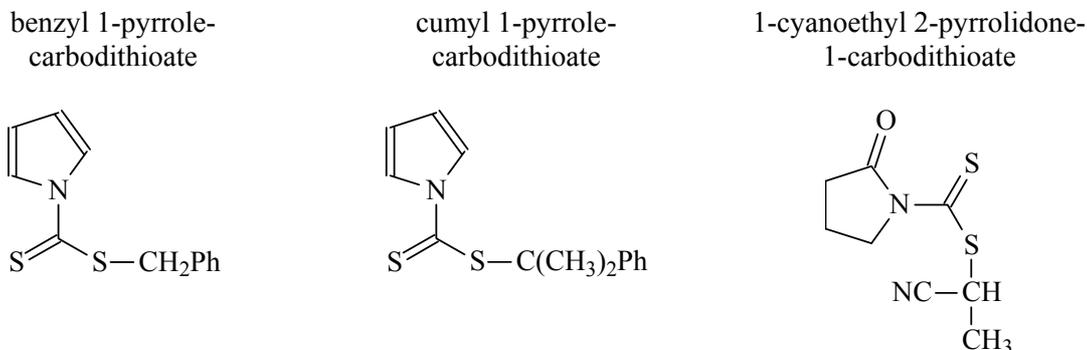
Cumyl 1-pyrrolecarbodithioate has been synthesized for the first time because of its superiority over benzyl 1-pyrrolecarbodithioate in certain polymerizations, which is manifested in lower polydispersities and better control of molecular weights.

4.1.2   Reaction of bis(thiocarbonyl) disulfides with azo compounds

This method is especially useful when the desired R group of the dithio compound $Z(C=S)SR$ can be introduced as an initiator fragment from a commercially available azo initiator, e.g. 2,2'-azo-bis-isobutyronitrile (AIBN) yields cyanoisopropyl-1-benzylcarbodithioate (see Fig. 4.4). Bis(thiocarbonyl) disulfides are generated by oxidation of the corresponding dithiocarboxylic acid with iodine, hydrogen peroxide, $K_3Fe(CN)_6$ or similar oxidants.[7-10]

Usually, a solution of the appropriate bis(thiocarbonyl) disulfide (**2**) is heated along with 1.5 eq of the azo compound (**1**) under inert atmosphere. A reaction time of four to five half lives of the azo compound is employed.[11] Radicals formed from decomposition of the azo compound (**1**) react with disulfide (**2**) to form the desired dithioester (**3**) and a (thiocarbonyl)sulfanyl radical (**4**), the latter being consumed most likely by reaction with another free radical to form again a dithioester (**3**) (see Fig. 4.3). It may also couple with another (thiocarbonyl)sulfanyl radical (**4**) to reform the initial bis(thiocarbonyl)disulfide compound (**2**). Possible side reactions are the combination of the azo compound-derived radical R$^\bullet$ with itself or its disproportionation.

$$R-N=N-R \xrightarrow{\Delta} 2\,R^{\bullet}$$
$$(1)$$

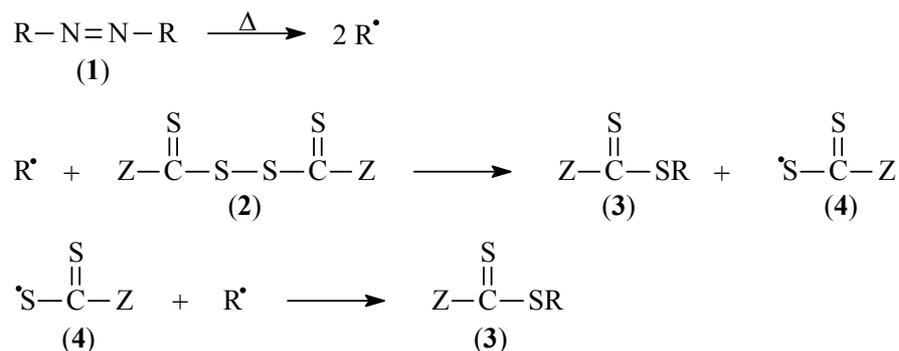$$R^{\bullet} \;+\; \underset{(2)}{Z-\overset{\displaystyle S}{\overset{\|}{C}}-S-S-\overset{\displaystyle S}{\overset{\|}{C}}-Z} \;\longrightarrow\; \underset{(3)}{Z-\overset{\displaystyle S}{\overset{\|}{C}}-SR} \;+\; \underset{(4)}{^{\bullet}S-\overset{\displaystyle S}{\overset{\|}{C}}-Z}$$

$$\underset{(4)}{^{\bullet}S-\overset{\displaystyle S}{\overset{\|}{C}}-Z} \;+\; R^{\bullet} \;\longrightarrow\; \underset{(3)}{Z-\overset{\displaystyle S}{\overset{\|}{C}}-SR}$$

Fig. 4.3.   *Suggested mechanism for formation of dithiocarbonyl compounds from azo compounds.[11]*

The RAFT agent cyanoisopropyl-1-benzylcarbodithioate[11,12] was synthesized following this method (see Fig. 4.4).

$$Ph-\overset{\displaystyle S}{\overset{\|}{C}}-SH \;\xrightarrow{[Ox]}\; Ph-\overset{\displaystyle S}{\overset{\|}{C}}-S-S-\overset{\displaystyle S}{\overset{\|}{C}}-Ph$$

$$Ph-\overset{\displaystyle S}{\overset{\|}{C}}-S-S-\overset{\displaystyle S}{\overset{\|}{C}}-Ph \;+\; NC-\overset{\displaystyle CH_3}{\underset{\displaystyle CH_3}{C}}-N=N-\overset{\displaystyle CH_3}{\underset{\displaystyle CH_3}{C}}-CN \;\xrightarrow[-\,N_2]{EtOAc,\,\Delta}\; 2\; Ph-\overset{\displaystyle S}{\overset{\|}{C}}-S-\overset{\displaystyle CH_3}{\underset{\displaystyle CH_3}{C}}-CN$$
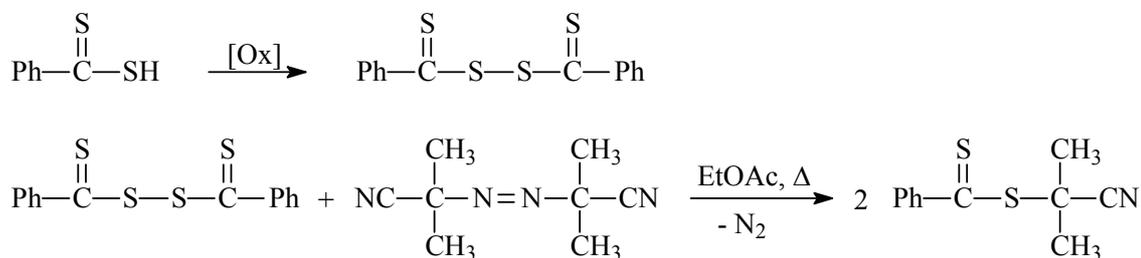
Fig. 4.4.   *Synthesis of cyanoisopropyl-1-benzylcarbodithioate from AIBN.*

4.1.3   Addition of dithiocarboxylic acids to unsaturated compounds

Dithiocarboxylic acids Z(C=S)SH are able to react both as nucleophiles and electrophiles depending on the nature of the reactant. In the presence of a nucleophilic olefin, such as styrene, dithiocarboxylic acid reacts in an electrophilic manner. Addition takes place at the most substituted olefinic carbon atom following Markovnikov's rule. The resulting dithioesters possess good homolytic leaving groups. The chain transfer agent 1-phenylethyl phenyldithioacetate (**5**)[13] was prepared using this technique (cf. Fig. 4.5). Dithiocarboxylic acid (**3**) is obtained by reaction of the corresponding Grignard reagent with carbon disulfide and subsequent hydrolysis of the adduct (**2**). Electrophilic addition of dithiobenzoic acid (**3**) to styrene (**4**) yields the chain transfer agent (**5**).

Fig. 4.5. Synthesis of 1-phenylethyl phenyldithioacetate from styrene.

4.1.4 Other methods of chain transfer agent synthesis

Recent techniques for the synthesis of dithiocarboxylic esters involve the use of phosphorus pentasulfide P_4S_{10}[14] or sodium tetrathiophosphate Na_3PS_4.[15] The reaction of carboxylic acids (**1**) with thiols or alcohols (**2**) in the presence of P_4S_{10} as catalyst and reagent gives the corresponding dithiocarboxylic esters (**3**) in high yields (Fig. 4.6).[14]

Fig. 4.6. Synthesis of dithiocarboxylic esters with phosphorus pentasulfide.

In a similar approach, Dureault et al. generated dithiocarboxylic esters in situ from reaction between sodium tetrathiophosphate Na_3PS_4 and carboxylic acid containing compounds that were used immediately for RAFT polymerization simply by adding monomer and free radical initiator.[15]

Favier et al. used the commercially available carboxymethyl dithiobenzoate (**1**), which was derivatized with thiols/thiolates (**2**) in a thioacylation procedure under alkaline conditions to obtain new dithioesters (**3**) for RAFT (Fig. 4.7).[16]

Fig. 4.7. Thioacylation of carboxymethyl dithiobenzoate for the synthesis of new dithioesters.

Tab. 4.2 and Tab. 4.3 summarize the chain transfer agents and initiators, respectively, used in this work along with the abbreviations employed in the text.

Tab. 4.2. *Chain transfer agent structures and abbreviations used in this work.*

chain transfer agent	abbreviation	structure
benzyl 1-pyrrole-carbodithioate	benzyl CTA	
cumyl 1-pyrrole-carbodithioate	cumyl CTA	
1-phenylethyl phenyldithioacetate	PEPDTA	
1-cyanoethyl 2-pyrrolidone-1-carbodithioate	pyrrolidone CTA	
cyanoisopropyl 1-benzylcarbodithioate	cyanoisopropyl CTA	
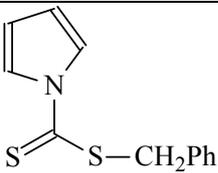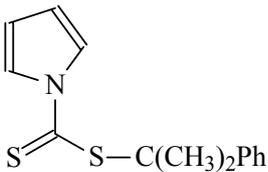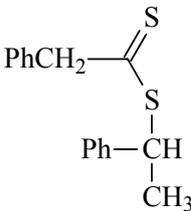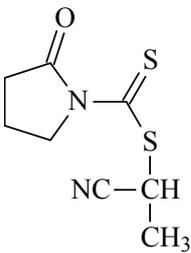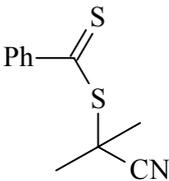
Tab. 4.3.   Initiators used in this work.

full name (abbreviation)	structure	10 h half-life decomposition temperature
2,2'-azo-bis-isobutyronitrile (AIBN)	$NC-\underset{\underset{CH_3}{\vert}}{\overset{\overset{CH_3}{\vert}}{C}}-N=N-\underset{\underset{CH_3}{\vert}}{\overset{\overset{CH_3}{\vert}}{C}}-CN$	65 °C (toluene)
1,1'-azo-bis(cyclo-hexanecarbonitrile) (VAZO-88)		88 °C (toluene)
2,2'-azo-bis(4-methoxy-2,4-dimethyl valeronitrile) (V-70)	$H_3C-\underset{\underset{CH_3}{\vert}}{\overset{\overset{OCH_3}{\vert}}{C}}-CH_2-\underset{\underset{CN}{\vert}}{\overset{\overset{CH_3}{\vert}}{C}}-N=N-\underset{\underset{CN}{\vert}}{\overset{\overset{CH_3}{\vert}}{C}}-CH_2-\underset{\underset{CH_3}{\vert}}{\overset{\overset{OCH_3}{\vert}}{C}}-CH_3$	30 °C (toluene)
4,4'-azo-bis(4-cyanopentanoic acid) (ACP)	$HOOCCH_2CH_2-\underset{\underset{CN}{\vert}}{\overset{\overset{CH_3}{\vert}}{C}}-N=N-\underset{\underset{CN}{\vert}}{\overset{\overset{CH_3}{\vert}}{C}}-CH_2CH_2COOH$	69 °C (water)
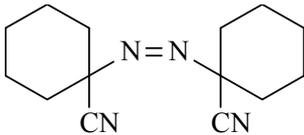
4.2   Poly(acrylamide)s

The free radical polymerization of acrylamides is characterized by propagating radicals of low steric bulk and high reactivity. Therefore, a wide range of chain transfer agents can be employed in the RAFT polymerization of these monomers.[3]

4.2.1   Poly(*N*-isopropylacrylamide)

N-Isopropylacrylamide   (NIPAAm)   has   been   polymerized   via   free-radical polymerization in organic solutions and redox polymerization in aqueous media.[17] Ionic polymerization and ATRP suffer from the drawback that the active amide hydrogen interferes with initiator or transition metal catalyst, respectively. Anionic polymerization has been reported for the protected monomer, e.g. trimethyl-silyl protected[18] or *N*-methoxymethyl-substituted NIPAAm.[19]

PNIPAAm exhibits a macromolecular transition from a hydrophilic to a hydrophobic structure that occurs abruptly at the so-called lower critical solution temperature (LCST).[17] This behaviour has made the polymer especially interesting for biomedical applications, e.g. for the controlled release of drugs triggered by environmental temperature change.[20,21]

4.2.1.1 *Polymerization kinetics using in-situ FT-NIR spectroscopy*

The principles of RAFT polymerization were applied to the polymerization of *N*-isopropylacrylamide (NIPAAm), which was carried out in the presence of the dithiocarbamates benzyl 1-pyrrolecarbodithioate (benzyl CTA) and cumyl 1-pyrrolecarbodithioate (cumyl CTA), respectively, as chain transfer agents in 1,4-dioxane at 60 °C.

The course of the polymerization was followed by in-situ Fourier-transform near-infrared (in-situ FT-NIR) spectroscopy. In addition, samples were withdrawn at different time intervals in order to determine the molecular weights and the development of the molecular weight distribution with conversion. FT-NIR allows the continuous determination of monomer conversion in controlled radical polymerization.[22,23] The determination of the monomer conversion can be more reliable with FT-NIR spectroscopy than with gravimetry. With a gravimetric determination of the conversion by precipitation, soluble oligomeric fractions will not be taken into account. Even GC determination of the residual monomer was not reliable as the conversions determined for the same sample varied considerably due to sublimation of the monomer and evaporation of the internal standard (*n*-decane).

In the FT-NIR measurements, spectra of the reaction mixture were recorded every 30 s. The spectra cover the range from 4500 to 7500 cm^{-1}. The variation of the intensity of the bands with time was followed. For the evaluation of the FT-NIR results, monomer bands were chosen that do not considerably overlap other bands, e.g. of the solvent or polymer.

For *N*-isopropylacrylamide, the vinylic stretching overtone was found at 6157 cm^{-1} and used to determine conversion. Other signals (5989 cm^{-1} and approx. 5930 cm^{-1}) were too close to the solvent cutoff and thus were not used. In the range of combination vibrations, additional peaks were determined and assigned as monomer signals (4727, 4644, 4597, 4500 cm^{-1}). An absorption at 6727 cm^{-1} increasing during the polymerization was attributed to the formation of poly(*N*-isopropylacrylamide). The signal intensities were converted into conversions by evaluating the intensities for zero monomer conversion and for total conversion. Fig. 4.8 shows the evolution of the FT-NIR bands with time for the RAFT polymerization of NIPAAm.

The time-conversion plots obtained from FT-NIR spectroscopy show long induction periods for both polymerization processes (Fig. 4.9 and Fig. 4.10). After the induction period, the first-order time-conversion plots (Fig. 4.10) show slowly decreasing slopes, indicating a slow decrease of the active radical concentration.
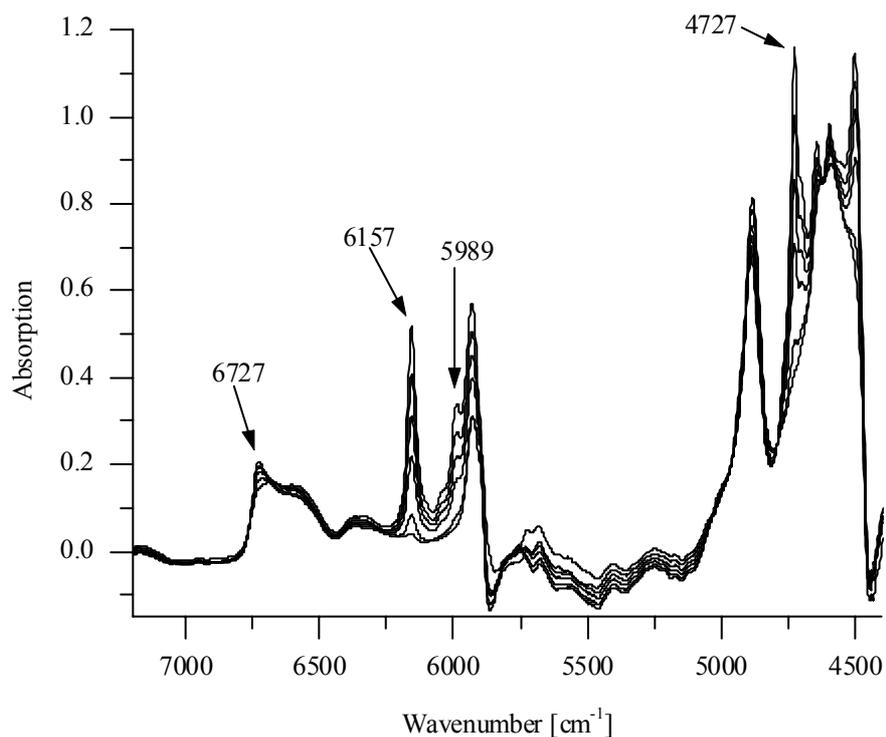
Fig. 4.8. *Evolution of various vibration overtone bands (after 2, 255, 283, 323, 551, and 1519 min, respectively) in the RAFT polymerization of NIPAAm in dioxane using benzyl 1-pyrrolecarbo-dithioate as chain transfer agent.*
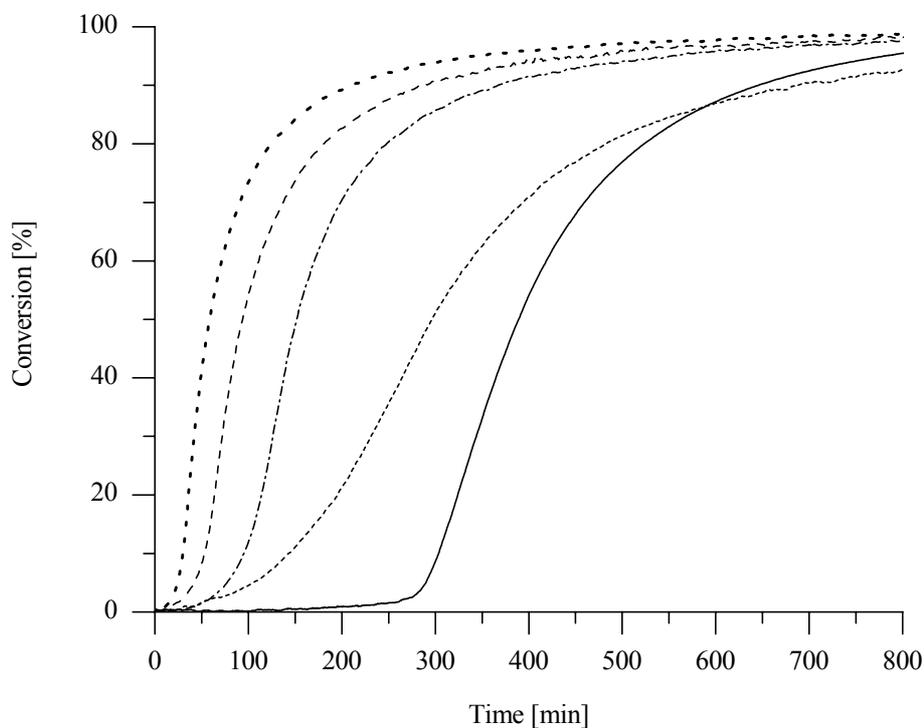

Fig. 4.9. *Time-conversion plot during the initial 500 min for the RAFT polymerization of NIPAAm in dioxane at 60 °C with (┄┄) benzyl CTA with $[CTA]_0 = 3.92 \cdot 10^{-2}$ mol/L, (┄┄) $1.96 \cdot 10^{-2}$ mol/L, (┅┅) $9.80 \cdot 10^{-3}$ mol/L, and (┄┄) $4.90 \cdot 10^{-3}$ mol/L, (——) cumyl CTA with $[CTA]_0 = 1.96 \cdot 10^{-2}$ mol/L.*
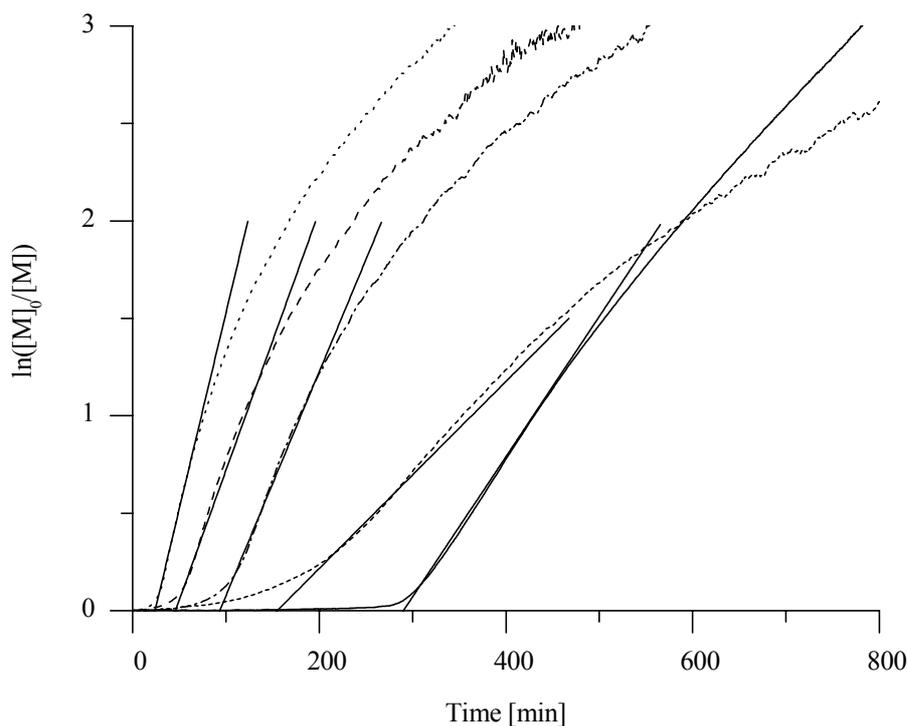
Fig. 4.10. *First-order time-conversion plots for the RAFT polymerizations with benzyl and cumyl CTA, symbols see Fig. 4.9; straight lines represent tangents fitted to the curves at the inflection points in order to determine* k_{app}.

For the quantitative determination of the induction periods, a tangent was fitted to the steep part of the curves. The values of the induction periods were obtained from the point of intersection of this tangent with the time axis. The induction periods amount to ca. 280 min for the NIPAAm/cumyl CTA system and to ca. 88 min for the NIPAAm/benzyl CTA system at a CTA concentration of $1.96 \cdot 10^{-2}$ mol/L.

A polymerization series conducted at different benzyl CTA concentrations shows that the observed induction periods increase with increasing CTA concentration. Furthermore, the apparent rate constants, k_{app}, for the polymerization were determined as the slopes of the first-order time-conversion plots at the inflection point (Tab. 4.4):

$$\frac{d \ln([M]_0 / [M]_t)}{dt} = k_p [P_n^\bullet] = k_{app} \qquad \text{Eq. 4.1}$$

The increasing induction periods are accompanied with a decrease of the apparent rate constants, which show a practically linear dependence on the RAFT agent concentration. Thus, induction and retardation seem to be correlated.

Tab. 4.4. *Induction times, t_{ind}, apparent rate constants, k_{app}, number-average molecular weights and polydispersity indices at full monomer conversion for the RAFT polymerizations of NIPAAm.[a] For abbreviations see Tab. 4.2.*

| CTA	$[CTA]_0$ [mmol/L]	t_{ind} [min]	$10^4 \cdot k_{app}$ [s^{-1}]	$M_{n,theor}$ [g/mol]	$M_{n,exp}$[b] [g/mol]	M_w/M_n[c]
	39.2	133	0.81	5300	3900	1.28
benzyl	19.6	88	1.9	10300	6400	1.37
	9.8	44	2.2	20300	16800	1.25
	4.9	23	3.4	40400	38800	1.21
cumyl	19.6	280	1.2	10300	15200	1.09[b]

[a] At 60 °C in dioxane. $[NIPAAm]_0 = 1.742$ mol/L and $[AIBN]_0 = 6.90$ mmol/L.
[b] Determined by MALDI-TOF MS.
[c] Determined by GPC using calibration with PNIPAAm samples.

For the sake of clarity, the main steps of the RAFT mechanism discussed in chapter 3 are summarized below (Fig. 4.11):

Chain transfer

Chain equilibration (degenerative transfer)

(2b)
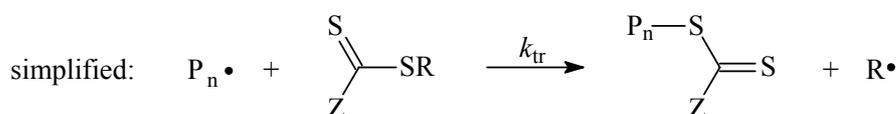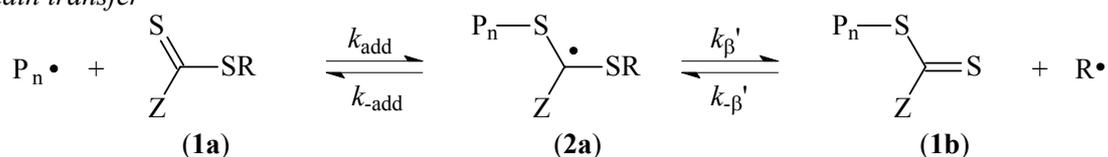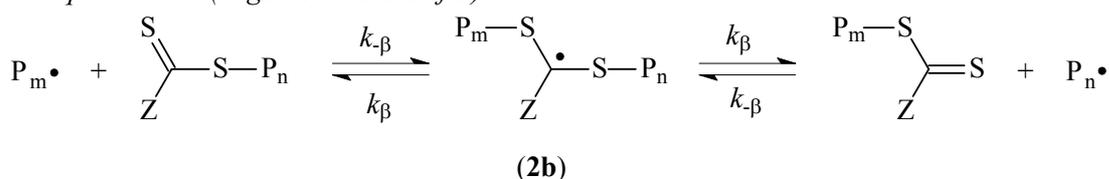
Fig. 4.11. *Main steps of the RAFT mechanism.*

The reasons for the induction periods or retardation observed with some chain transfer agents are not clearly understood but a number of possible explanations have been suggested (for numbering cf. Fig. 4.11):[24]

    a) slow fragmentation of the adduct **2a** formed from the initial RAFT agent **1a**,

    b) slow fragmentation of the adduct **2b** formed from the polymeric RAFT agent **1b**,

    c) slow reinitiation by the expelled radical R$^\bullet$,

    d) tendency of the expelled radical R$^\bullet$ to add to RAFT agent **1a** rather than to monomer,

e) specificity for the propagating radical $P_n^\bullet$ to add to the RAFT agent rather than monomer (i.e. transfer constant too high).

Monteiro et al.[25] suggested termination by addition of a propagating polymer chain to the adduct (**2b**) formed from the polymeric RAFT agent as a reason for retardation (Fig. 4.12). The formation of a three-arm star chain (**1c**) has been confirmed by Fukuda et al. in an experiment that mimics RAFT polymerization without chain growth. The authors activated polystyrene bromide by a CuBr/Me$_6$TREN complex to give a polystyryl radical that added to the polymeric RAFT agent polystyrene-dithiobenzoate to form an intermediate radical species similar to **2b**, which in turn would be attacked by another polystyryl radical to form a three-arm star (**1c**).[26]
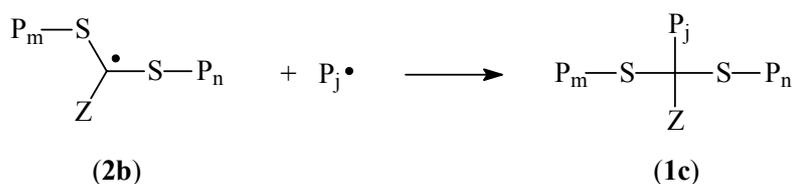

(2b)   **(1c)**

Fig. 4.12.   Additional intermediate radical termination mechanism used to explain retardation.

Barner-Kowollik et al.[27] have reported an induction period for the RAFT polymerization of styrene with cumyl dithiobenzoate as chain transfer agent. They tentatively explained this observation by the formation of di-cumyl radicals, Ph-$\dot{C}$(S-cumyl)$_2$. Intermediate radicals (**2**) have recently been observed experimentally using ESR spectroscopy.[28] In the present case, the induction periods might also be ascribed to the formation of di-benzyl or di-cumyl RAFT radicals (**2c**), respectively, via the reaction of excess CTA (**1a**) with benzyl or cumyl radicals R$^\bullet$, respectively (Fig. 4.13).

(1a)   **(2c)**
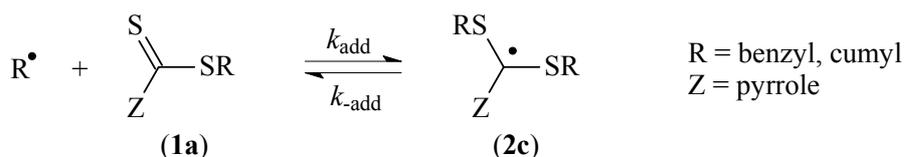
*Fig. 4.13.   Tentative explanation of the induction period by formation of stable intermediate radicals **2c**.*

This reaction will reduce the extent of reinitiation occurring until equilibrium is reached, resulting in an induction period. The observed induction periods agree well with simulations of Barner-Kowollik et al.[27] The longer induction period with the cumyl CTA would imply a higher stability of the di-cumyl radicals as compared to the di-benzyl radicals. However, di-cumyl radicals are expected to fragment more easily than di-benzyl radicals. Therefore, another explanation has to be envisaged. In a recent paper by M. Donovan et al.[29], similar induction periods are observed in the polymerization of *N,N*-dimethylacrylamide with cumyl and benzyl dithiobenzoate, respectively. As in the present

work, the cumyl CTA shows a longer induction period as compared to the benzyl CTA of the same concentration. The authors ascribed this result to the different stabilities of the cumyl and benzyl radicals. Considering the radical stability, the bulky cumyl radical adds slower to NIPAAm monomer than the primary benzyl radical. Thus, the benzyl radical is expected to be a better initiating species.

4.2.1.2   UV and MALDI-TOF MS analysis of the polymers

The formation of the dithiocarbamate endgroups of the resultant polymers is proven by both UV spectroscopy and MALDI-TOF mass spectrometry. The UV spectrum (Fig. 4.14) shows a perceptible band with a maximum at $\lambda = 296$ nm in chloroform, which is ascribed to the pyrrolecarbodithioate moiety.

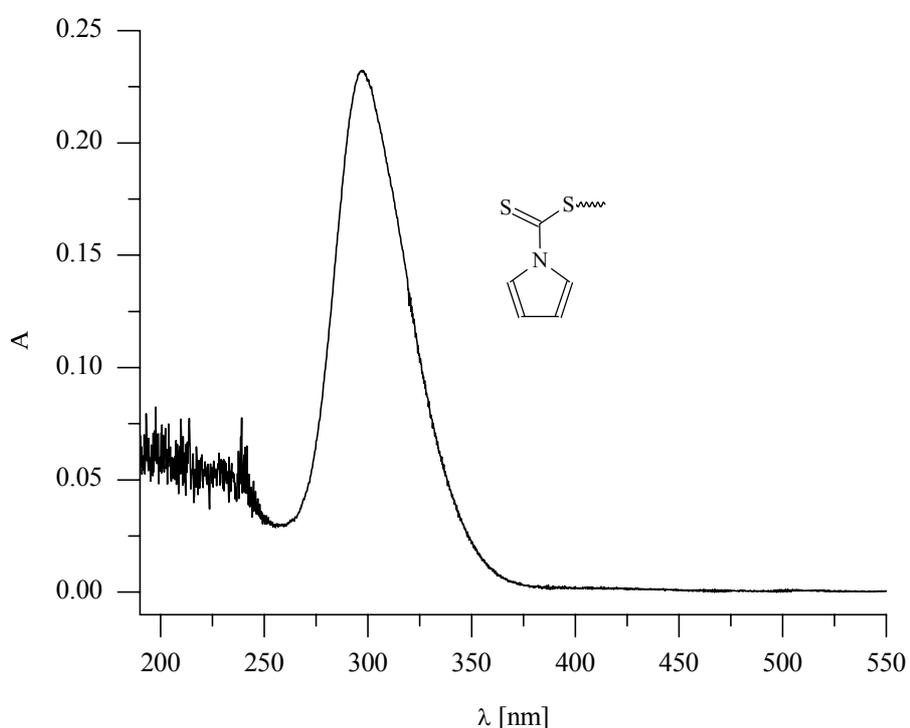*Fig. 4.14.*   *UV spectrum of dithiocarbamate-terminated PNIPAAm in CHCl₃.*

MALDI-TOF mass spectra of the obtained RAFT polymers can indicate to which degree the polymerization is living and give information on the nature of the endgroups. In RAFT polymerizations using cumyl (cum) dithiocarbamate (dit) as CTA, the products shown in Tab. 4.5 can be expected in principle (Fig. 4.16b for structures):

Tab. 4.5.   Masses of expected reaction products in the mass range of 1900-2000 g/mol.

	structure	X		monoisotopic mass
(i) CTA derived products:				
living	cum-M_X-dit	15	$C_{104}H_{180}N_{16}O_{15}S_2K^+$	1996.28
disproportionation + transfer	cum-M_X-H	15	$C_{105}H_{188}N_{16}O_{16}K^+$	1968.39
disproportionation	cum-M_X-doub	15	$C_{105}H_{186}N_{16}O_{16}K^+$	1966.38
combination	cum-M_X-cum	15	$C_{108}H_{187}N_{15}O_{15}K^+$	1973.39
(ii) initiator derived products:				
living	in-M_X-dit	15	$C_{99}H_{175}N_{17}O_{15}S_2K^+$	1945.26
disproportionation + transfer	in-M_X-H	15	$C_{100}H_{183}N_{17}O_{16}K^+$	1917.37
disproportionation	in-M_X-doub	15	$C_{100}H_{181}N_{17}O_{16}K^+$	1915.35
combination	in-M_X-in	16	$C_{104}H_{188}N_{18}O_{16}K^+$	1984.40
(iii) mixed combination products:				
combination	in-M_X-cum	16	$C_{104}H_{188}N_{18}O_{16}K^+$	1922.36

In the literature, only two references on the MALDI-TOF characterization of RAFT polymers exist. Destarac et al.[30] report the MALDI-TOF mass spectrum of poly(vinyl acetate) obtained by RAFT polymerization in bulk using AIBN as initiator and *S*-malonyl *N,N*-diphenyldithiocarbamate as chain transfer agent. They observed initiator-derived and hydrogen-terminated polymers. The formation of the latter was ascribed to transfer reactions since no olefinic endgroups were found. Ganachaud et al.[31] discuss the MALDI-TOF spectrum of PNIPAAm obtained by RAFT polymerization in benzene with AIBN as initiator and benzyl dithiobenzoate as chain transfer agent. They report products resulting from termination by either disproportionation or transfer to monomer. However, they found only olefinic endgroups, but no hydrogen-terminated chains, as one would expect for the disproportionation or transfer products.

Fig. 4.15 and Fig. 4.16 show the MALDI-TOF mass spectra of PNIPAAm obtained with benzyl CTA and cumyl CTA, respectively. Samples were cast from THF solution, dithranol was used as a matrix, and sodium or potassium trifluoroacetate was added for ion formation.
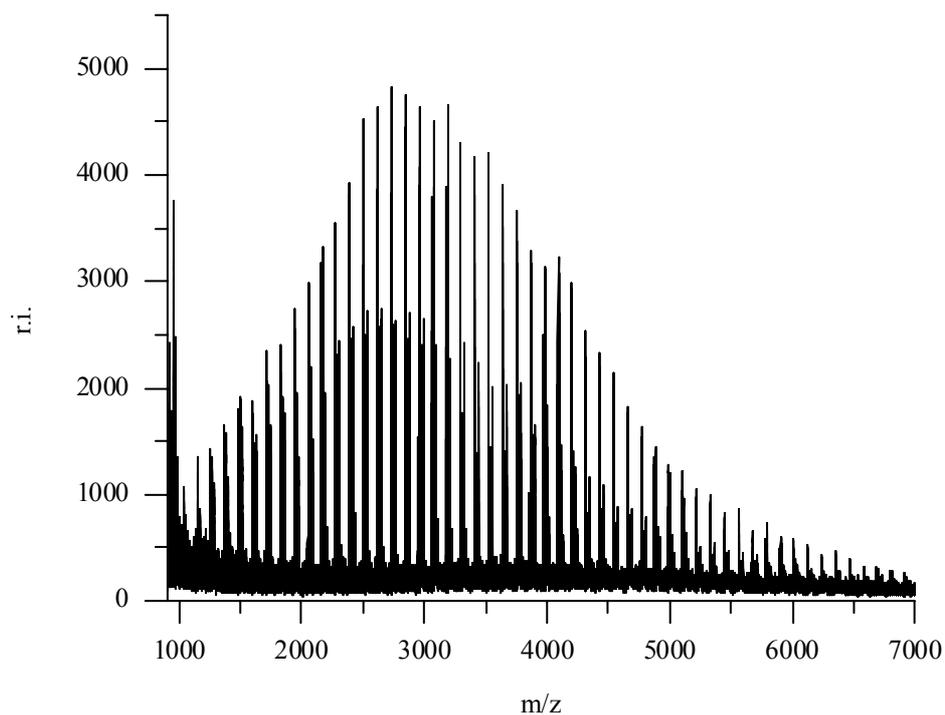
Fig. 4.15a. *MALDI-TOF mass spectrum of PNIPAAm with benzyl CTA (sample taken at 41 % conversion).*
Complete spectrum of K^+ ionized sample.

Fig. 4.15b. *MALDI-TOF mass spectrum of PNIPAAm with benzyl CTA (sample taken at 41 % conversion).*
Determination of the chain-end structures.

Fig. 4.16a.   MALDI-TOF mass spectrum of PNIPAAm with cumyl CTA (sample taken at 13 % conversion). Complete spectrum of K+ ionized sample.

In both spectra, the expected signals (isotopic patterns) of the polymer with transfer agent endgroups are observed (benz-M_x-dit and cum-M_x-dit, respectively). Besides these signals, signals ascribed to hydrogen- and double bond-terminated products (benz-M_x-doub/benz-M_x-H and cum-M_x-doub/cum-M_x-H, respectively) for both samples are found. On first sight, these might be ascribed to products of disproportionation and transfer (see below). In the case of the cumyl chain transfer agent (Fig. 4.16b), initiator-derived polymers (in-M_x-dit, in-M_x-doub, in-M_x-H, in-M_x-in) were observed due to a very good signal-to-noise ratio and due to the low monomer conversion (13 %) of the sample. The intensity of the corresponding initiator-derived polymer signals is very low so that a good resolution is necessary, which might explain why these products have not been detected before.[31]
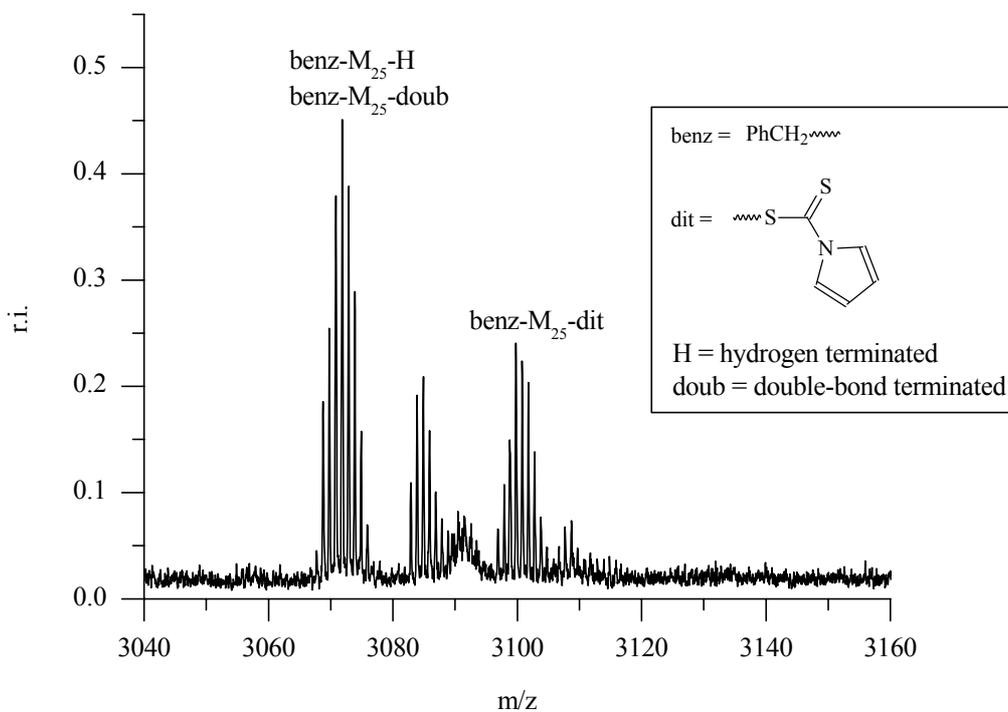
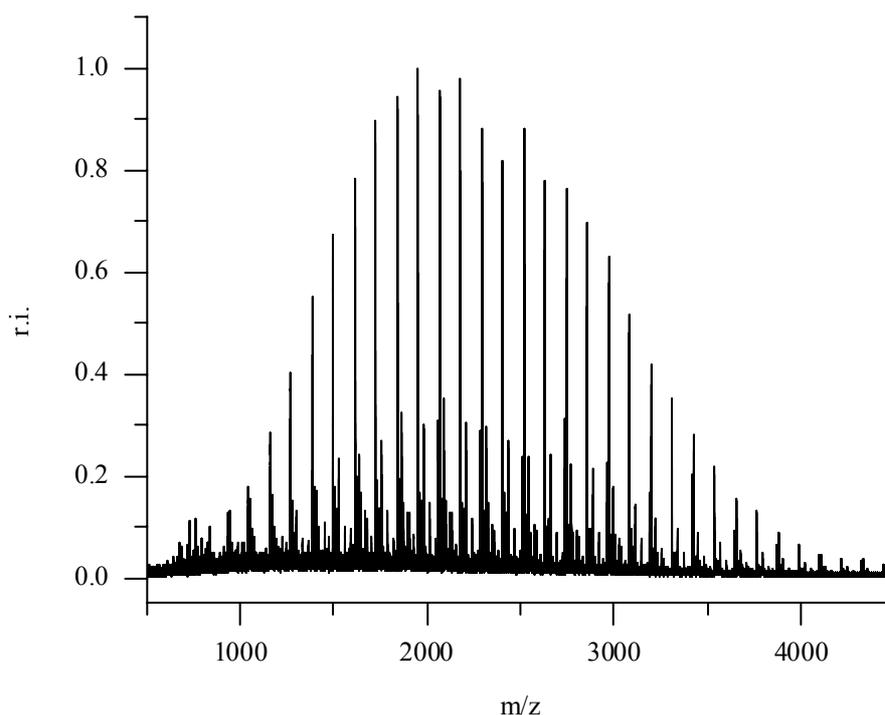*Fig. 4.16b.* *MALDI-TOF mass spectrum of PNIPAAm with cumyl CTA (sample taken at 13 % conversion). Determination of the chain-end structures. Experimental (top) and simulated (bottom) data.*

In the MALDI-TOF spectra of the two different polymer samples, there are peaks that cannot be ascribed to the expected chain-end structures. The K^+ ionized MALDI spectrum of the polymer obtained with cumyl CTA, for example (Fig. 4.16b), reveals two series of signals with good isotopic resolution (1980.10 g/mol, 2003.97 g/mol) and another rather noisy signal (1987-1990 g/mol) that cannot be ascribed to any of the possible structures expected from the synthesis. One of the signals (1980.10 g/mol) fits the CTA-derived main product (cum-M_x-dit) as Na^+ adduct. However, closer inspection of the Na^+ ionized MALDI spectra shows the same series of signals as in the K^+ ionized samples shifted by the Na^+ to K^+ mass difference of 16 g/mol. This seems to identify this signal as a K^+ adduct of a chain with unknown endgroup structure. The signal at about 1987 g/mol is probably

the result of a fragmentation in the flight tube. If the other two signals are also the result of a fragmentation under MALDI conditions, they must have formed in the ion source during ionization rather than during the flight time because of their good resolution. The occurrence of fragmentation during ionization in the MALDI-TOF analysis of dithiocarbamate-terminated polymers has already been reported by Beyou et al.[32] They prepared dithiocarbamate-terminated polystyrene via substitution of nitroxide moieties by dithiocarbamate moieties in polystyrene obtained by nitroxide-mediated free radical polymerization.

The MALDI-TOF spectra show that the peaks ascribed to disproportionation/transfer products have the highest intensity of all signals. This is a quite unexpected result as a combination of growing radicals is expected for poly(N-isopropylacrylamide) rather than disproportionation. Moreover, kinetics indicate only little termination and transfer. This becomes evident from the linear first-order time-conversion plot, especially at low monomer conversion (Fig. 4.10), and from the plot of M_n versus conversion (Fig. 4.20 and Fig. 4.21). Therefore, the question arises whether these signals are due to fragmentation of the polymer during the MALDI-TOF measurement. Furthermore, the relative intensities of double bond terminated structures (cum-M_x-doub) to hydrogen terminated ones (cum-M_x-H) is not 1:1 but 1:(2.5±1), which was confirmed by a simulation of the corresponding overlapping isotopic patterns (Fig. 4.16c).
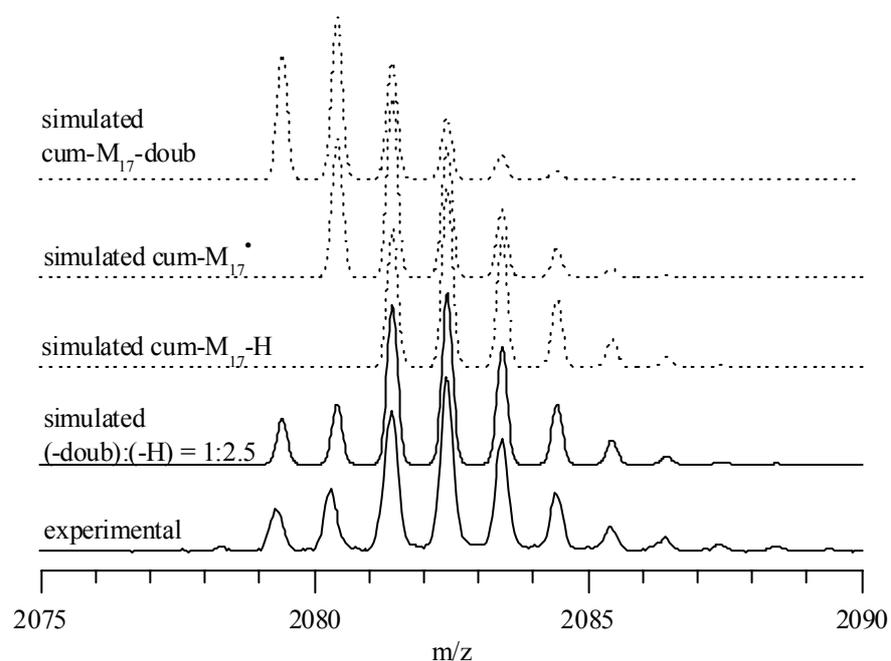

Fig. 4.16c.   *MALDI-TOF mass spectrum of PNIPAAm with cumyl CTA (sample taken at 13 % conversion). Simulation of signal overlap of assumed disproportionation/transfer signals.*

The higher amount of cum-M_x-H chains might result from the cum-M_x radicals abstracting protons from the matrix during desorption. One possibility to prove this assumption is to perform a fragmentation analysis of the CTA-derived polymeric chains cum-M_x-dit·K^+ in the MALDI experiment. For this purpose, a Post Source Decay (PSD) analysis[33] was performed. This method is used for controlled fragmentation in the field-free region of the mass spectrometer. It occurs on the 10 μs time scale and yields fragment ions in the mass spectrum from the reflection detector only. MALDI-PSD is very useful for the determination of peptide sequences or end-group identification in polymers.[34,35] With the aid of a suitable precursor ion selector in the field-free region of the linear flight path and a scanning reflectron voltage, a PSD product ion spectrum can be obtained. PSD analysis of the PNIPAAm obtained with cumyl CTA showed that cum-M_x-dit·K^+ ions readily fragment under loss of the dit endgroup and formation of the corresponding cum-M_x-doub or cum-M_x-H chains but also into other fragments (Fig. 4.16d), which corroborates the aforementioned conclusions. This result does not exclude the formation of cum-M_x-doub by the synthetic process but strongly indicates that the corresponding peaks stem from fragmentation during ionization.

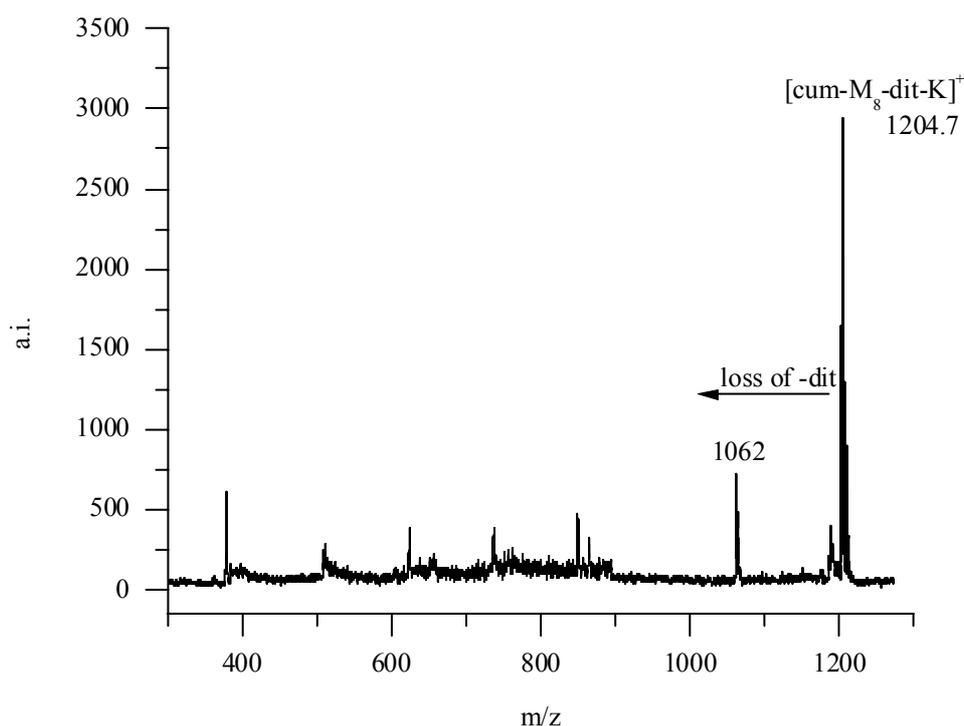Fig. 4.16d.   *MALDI-TOF mass spectrum of PNIPAAm with cumyl CTA (sample taken at 13 % conversion). Post Source Decay MALDI-TOF mass spectrum of PNIPAAm with the composition cum-M_8-dit. The most intense fragment peak corresponds to the loss of the dit residue.*

Another indication of the fragmentation occurring during ionization is found in the MALDI-TOF spectrum of the hydrolyzed polymer (see Fig. 4.17). For this purpose, the

dithio endgroups of the obtained polymer samples were hydrolyzed to yield the corresponding thiol-terminated polymers under basic conditions using a mixture of MeOH/ aq. 28 % NaOH (2:1). The reaction mixture was acidified with 88 % formic acid, MeOH was evaporated and the residue was freeze-dried. The solid obtained was directly subjected to MALDI-TOF analysis. As can be seen from the figure, the spectrum of the hydrolyzed sample shows no hydrogen- and double bond-terminated structures. Only the thiol structure and a small peak ascribed to residual unhydrolyzed dithiocarbamate can be found. This proves that the hydrogen and olefinic endgroups do not result from the polymerization procedure but from fragmentation of the dithio moiety during ionization.
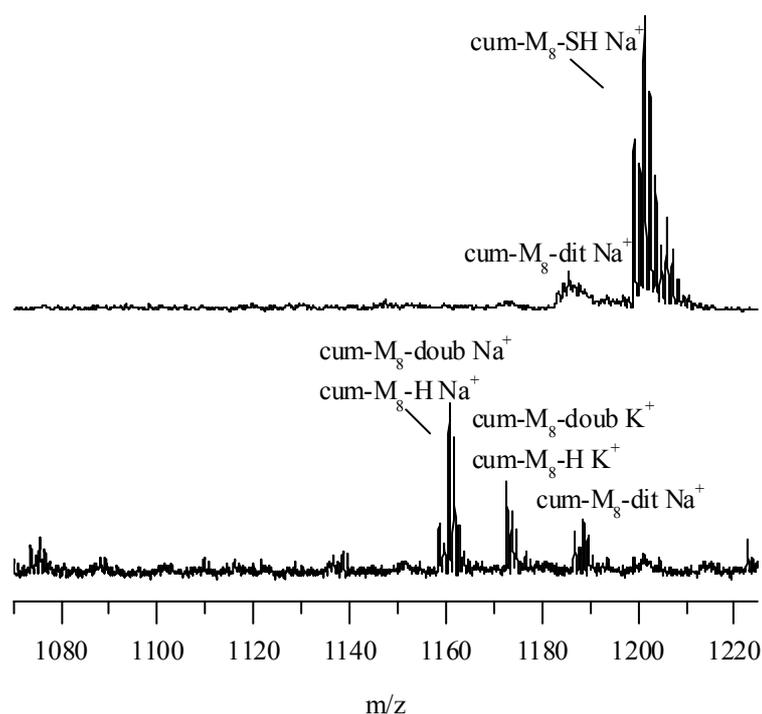

Fig. 4.17. *MALDI-TOF mass spectra of hydrolyzed PNIPAAm (top) and unhydrolyzed sample (bottom) for comparison.*

Since the spectrum of the dithioester moiety (λ_{max} = 296 nm, cf. Fig. 4.14) overlaps with the laser frequency (337 nm) for the MALDI process, this observation is not surprising. These findings suggest that the signals attributed to disproportionation/transfer by other authors[30,31] may also result from fragmentation. As an alternative, electrospray ionization mass spectrometry (ESI MS) might be applied to avoid fragmentation. However, this technique suffers some drawbacks with respect to MALDI-TOF MS; for example, the mass range limits its application to low-molecular weight polymers and multiple ionization is often encountered, which complicates spectrum interpretation and evaluation of molecular weight data.[36]

4.2.1.3   GPC analysis of the polymers

The GPC characterization of poly(*N*-isopropylacrylamide) in THF involves various problems[37,38] due to irreversible chain aggregation after complete drying of the polymer samples.[31] Nevertheless, in the present work, good results have been obtained by the addition of 0.25 wt.-% tetrabutylammonium bromide (TBAB) to the THF solution and using PSS SDVgel columns, whereas with pure THF no analyzable results could be obtained.

Fig. 4.18 and Fig. 4.19 show the GPC traces of PNIPAAm at different monomer conversions for the polymerization with benzyl CTA and cumyl CTA, respectively.

$$\begin{array}{l}
\text{- - - - 97 min, } x_p=0.108 \\
\text{——— 120 min, } x_p=0.247 \\
\text{-------- 139 min, } x_p=0.410 \\
\text{-------- 186 min, } x_p=0.659 \\
\text{——— 315 min, } x_p=0.868 \\
\text{- - - - 485 min, } x_p=0.938 \\
\text{-------- 2000 min, } x_p=0.999
\end{array}$$

V_e [mL]

Fig. 4.18.   GPC traces (RI detector) of PNIPAAm at different monomer conversions x_P in THF with 0.25 % TBAB for the polymerization with a benzyl CTA concentration of 19.6 mmol/L.

For conversions higher than 90 %, a high-molecular weight shoulder is observed. This is usually observed for RAFT polymers[31] at high monomer conversions, which is most likely due to combination of the growing chains.
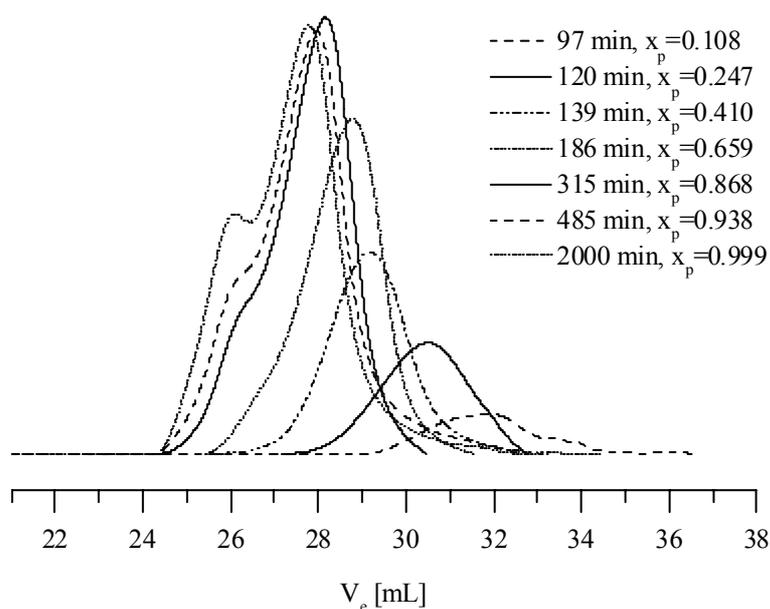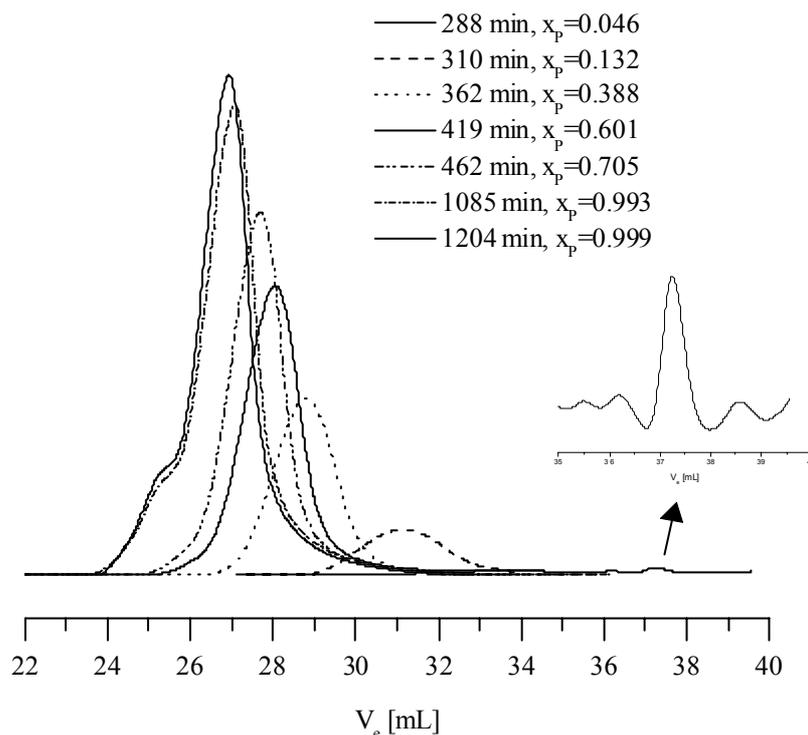
Fig. 4.19.   *GPC traces (RI detector) of PNIPAAm at different monomer conversions x_P in THF with 0.25 % TBAB for the polymerization with cumyl CTA.*

Fig. 4.20 and Fig. 4.21 show the dependences of M_n (determined by MALDI-TOF MS) and PDI on conversion for benzyl CTA and for cumyl CTA, respectively, as chain transfer agent.

The straight lines in Fig. 4.20 represent the dependence of the calculated number-average molecular weight on conversion,

$$M_{n,theor} = \frac{[M]_0}{[CTA]_0} \cdot x_p \cdot M_{monomer} + M_{CTA}$$
         Eq. 4.2

where x_p denotes monomer conversion, $[M]_0$ and $[CTA]_0$ are the initial concentrations of monomer and chain transfer agent, respectively. It has to be noted that Eq. 4.2 applies only under reaction conditions where the number of initiator-derived chains is less than 10 % with respect to total chains and when added chain transfer agent is completely reacted. Otherwise, the number of initiator-derived chains has to be taken into account (expressed by an additional term $2 \cdot f \cdot ([I]_0 - [I]_t)$ in the denominator, where f = initiator efficiency).[16] The linearity of the plots indicates the absence of irreversible transfer reactions. The slight increase at high conversions is ascribed to combination reactions of the living polymer chains.
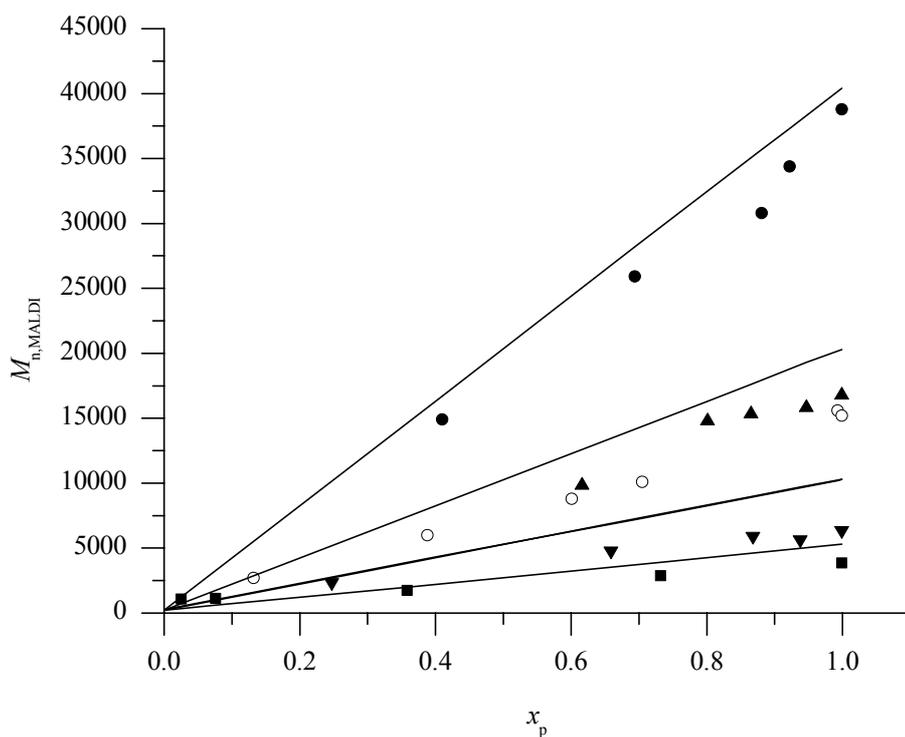
Fig. 4.20. Dependence of M$_{n,MALDI}$ *on monomer conversion for benzyl and cumyl CTA. (■) benzyl CTA with [CTA]$_0$ = 3.92·10^{-2} mol/L, (▼) 1.96·10^{-2} mol/L, (▲) 9.80·10^{-3} mol/L, (●) and 4.90·10^{-3} mol/L, (○) cumyl CTA with with [CTA]$_0$ = 1.96·10^{-2} mol/L, (—)* M$_{n,theor}$.

Fig. 4.21. Dependence of PDI (from GPC with PNIPAAm calibration) on conversion for benzyl and cumyl CTA. Symbols see Fig. 4.20; (·····) lines to guide the eye.

The agreement of the experimental M_n values with the calculated ones is better for benzyl CTA as chain transfer agent than for cumyl CTA (see Tab. 4.4). This may be explained by the higher impurity (approx. 5 %, as determined by ^{1}H-NMR spectroscopy) of the cumyl RAFT a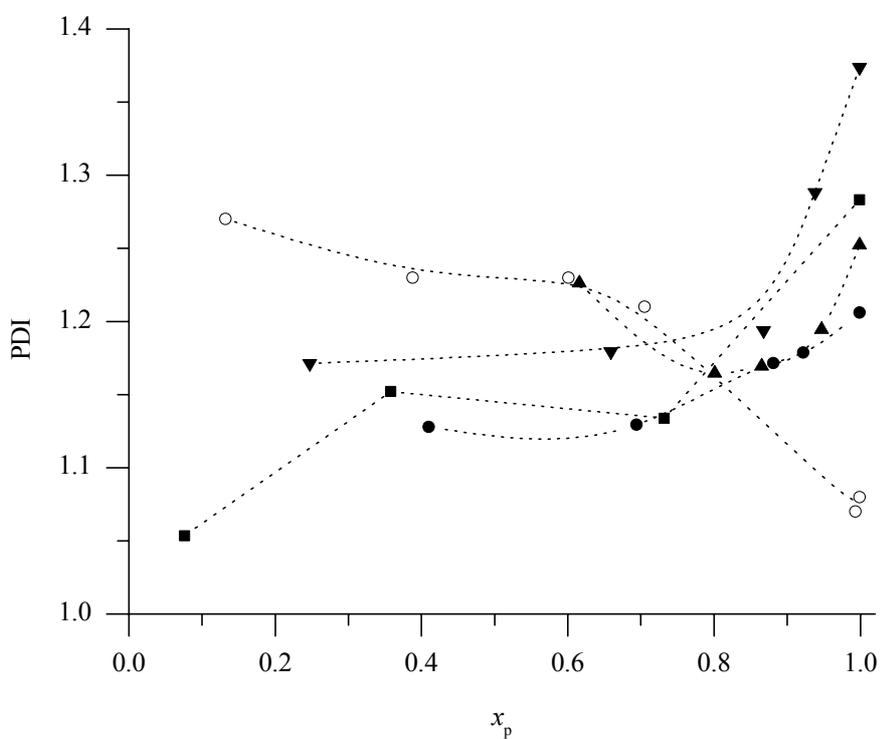gent. For the polymerizations with benzyl CTA, the polydispersity indices generally decrease with increasing conversion (Fig. 4.21) except at high conversion, due to combination of growing chains at high conversion, which is typical for controlled polymerizations with exchange between active and dormant species.[39] In the case of cumyl CTA, polydispersities decrease constantly with conversion. This may result from the absence of termination even at high conversions, making the transfer agent more effective with increasing conversion.

GPC evaluation of the molecular weights using polystyrene standards for calibration gives significantly higher molecular weights than those obtained from MALDI-TOF analysis (Fig. 4.22).
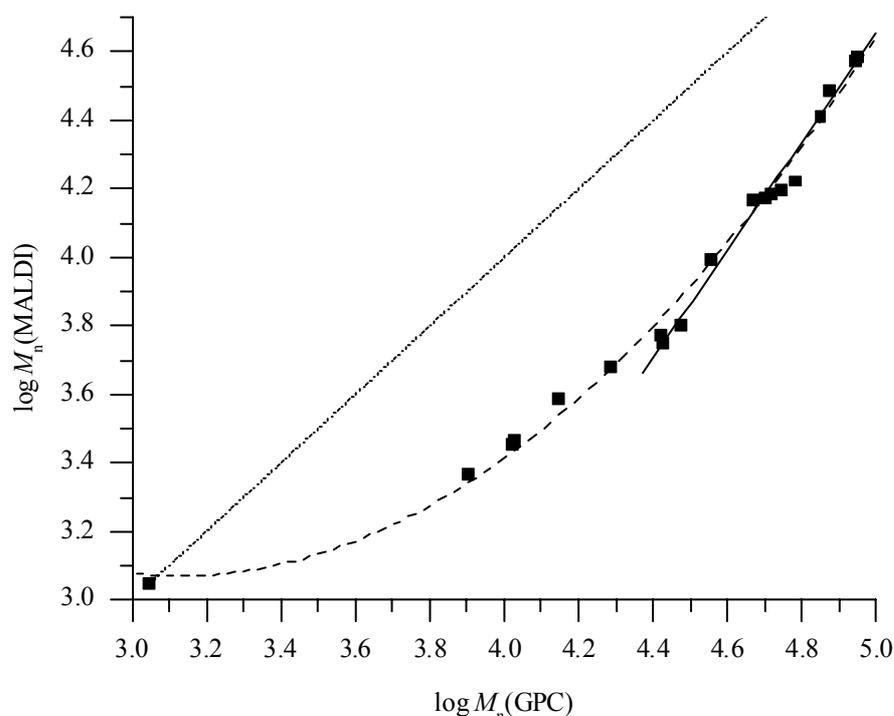
Fig. 4.22.   Bilogarithmic plot of M_n(MALDI) versus M_n(GPC) for the polymerization with benzyl CTA, (—) linear fit of data points for log M_n(MALDI) > 3.8, (---) second-order polynomial fit of all data points, (⋯) line expected for M_n(MALDI) = M_n(GPC).

The difference between M_n(MALDI) and M_n(GPC) is much more pronounced than the one reported for PNIPAAm by Ganachaud et al.[31] who used THF GPC to determine the molecular weights. The maximum deviation with a ratio of M_n(GPC)/M_n(MALDI) ≈ 4 is observed at M_n(GPC) ≈ 25,000 g/mol. A linear fit of the bilogarithmic plot of M_n(MALDI)

vs. M_n(GPC) for the PNIPAAm samples obtained with benzyl CTA (Fig. 4.22) results in the relation

$$\log M_n(\text{MALDI}) = -3.23(\pm 0.32) + 1.577(\pm 0.069)\cdot \log M_n(\text{GPC}) \qquad \text{Eq. 4.3}$$

The linear relationship between $\log M_n$(MALDI) and $\log M_n$(GPC) is based on the linearity of the Mark-Houwink relation which typically holds true for $M_n \geq 10^4$ g/mol. The fit was therefore only applied to $\log M_n$(MALDI) > 3.8; corresponding to M_n(GPC) > 4.4. If all values are considered, a second-order polynomial approximates the values:

$$\log M_n(\text{MALDI}) = 7.44 - 2.80\log M_n(\text{GPC}) + 0.448[\log M_n(\text{GPC})]^2 \qquad \text{Eq. 4.4}$$

For the polymerization with cumyl CTA, slightly higher M_n(MALDI) values are obtained as compared to the polymerization with benzyl CTA. Most of these samples had molecular weights M_n(GPC) below 25,000 g/mol so that they were not considered in the linear fit.

Fig. 4.23 shows the GPC calibration curve for polystyrene and for PNIPAAm samples with M_n determined by MALDI-TOF mass spectrometry.
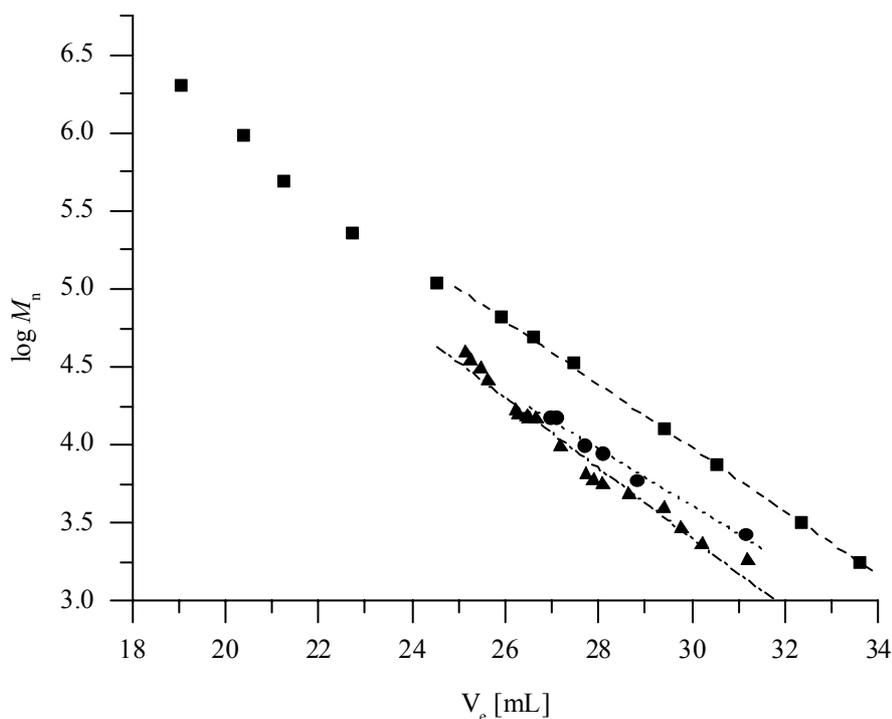
Fig. 4.23. *GPC calibration curves for polystyrene standards (■) and PNIPAAm samples with (●) cumyl and (▲) benzyl CTA, respectively.*

From the figure, it is evident that the determination of molecular weights of PNIPAAm using polystyrene calibration yields incorrect M_n values. For the same elution volume, polystyrene shows higher molecular weights compared to PNIPAAm. This means that PNIPAAm samples having the same molecular weight as polystyrene elute at much lower elution volumes. From the M_n values obtained by MALDI-TOF mass spectrometry and the

known elution volumes, a new calibration curve can be established for PNIPAAm. The calibration curves shown in Fig. 4.23 can be regarded as linear in the given molecular weight range (10^3-$3 \cdot 10^6$ g/mol).

4.2.1.4 Determination of degree of polymerization

The presence of dithiocarbamate endgroups introduced by the RAFT process allows determination of the degree of polymerization of the PNIPAAm samples using either UV or NMR spectroscopy. Generally, thiocarbonylthio compounds of structures (aryl)C(=S)S- and (alkyl)C(=S)S- are UV-active, and the chain transfer agent benzyl-1-pyrrolecarbodithioate shows a distinct absorption at $\lambda_{max} = 296$ nm in chloroform. The molar extinction coefficient of the dithiocarbamate was determined as $\varepsilon_{max} = 29,710$ cm^2/mmol. For deduction of the degree of polymerization, it was assumed that the molar extinction coefficient is not considerably changed by incorporation of the dithiocarbamate moiety into the polymer as compared to free chain transfer agent. For UV measurements, a certain amount of polymer was dissolved in chloroform and the solution was diluted to a specific degree until absorption was below 1.0 in order to ensure the linearity of Lambert-Beer's law. From the absorption at λ_{max}, the apparent concentration of chain transfer agent was calculated according to Eq. 4.5.

$$c_{app} = \frac{A}{\varepsilon \cdot l}$$

Eq. 4.5

where c_{app} = apparent, molar CTA concentration, A = absorbance, and l = path length of absorbing solution.

From the ratio of the known concentration of the polymer solution to the apparent concentration of dithiocarbamate, the degree of polymerization was deduced (see Tab. 4.6).

In the ^{1}H-NMR spectra of low-molecular weight PNIPAAm ($M_n < 15,000$ g/mol), the signals in the aromatic region are characteristic of the chain transfer agent's pyrrole and phenylic protons. Fig. 4.24 shows a typical ^{1}H-NMR spectrum of PNIPAAm. For determination of the degree of polymerization, the signals of pyrrole methine (**h+i**) ($\delta = 7.6$ ppm and 6.2 ppm) and isopropyl methine protons (**c**) ($\delta = 3.9$ ppm) were used. As the pyrrole-CH signal (**h**) in the downfield part of the spectrum is partially overlapped by the phenylic and amine protons (**e+f**), only the pyrrole-CH signal (**i**) at higher field ($\delta = 6.2$ ppm) was considered for integration.
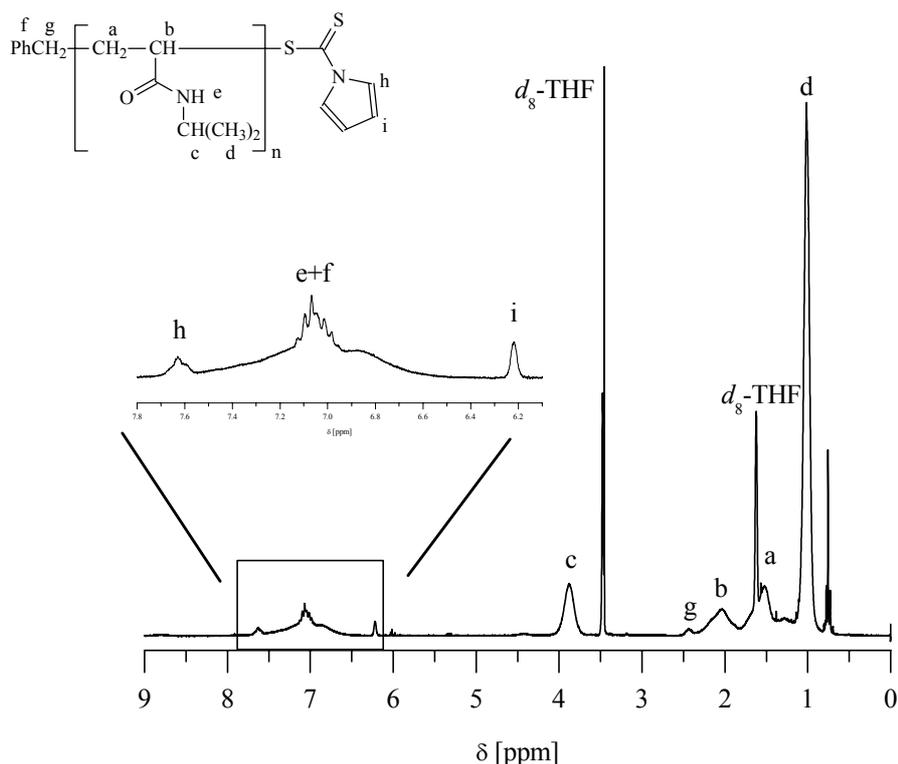
Fig. 4.24. *NMR spectrum of dithiocarbamate-terminated PNIPAAm in* d$_8$-THF, *synthesized with benzyl CTA as chain transfer agent.*

Tab. 4.6 compares the molecular weights obtained by different characterization methods, i.e. by UV, GPC, ^{1}H-NMR, and MALDI-TOF analysis.

Tab. 4.6. *Comparison of molecular weight data of PNIPAAm samples obtained by UV, GPC, NMR, and MALDI-TOF analysis.*

entry	conv. [%]	$M_{n,theor}$	$M_{n,GPC}$[a]	$M_{n,MALDI}$	$M_{n,UV}$	$M_{n,NMR}$
1	33	1000	2900	1340	1900	1700
2	80	2100	6100	1870	4500	3300
3	97	2500	6300	1910	4600	3400
4	99	2550	6400	1920	5100	3500

[a] polystyrene calibration

It is evident that agreement between the different values is quite well in the low-molecular weight region (entry 1). However, the molecular weights determined at high monomer conversions are much too high compared to the MALDI-TOF values. Molecular weight determination by GPC is problematic due to the lack of suitable calibration standards for PNIPAAm, as has been discussed in section 4.2.1.3. Both NMR and UV spectroscopy seem to underestimate the number of dithiocarbamate moieties at high conversions. This is ascribed to an actual absence of dithiocarbamate groups at some

polymeric chain ends as, with high conversions, there is also termination by combination of growing radicals, i.e. these polymers do not bear any dithiocarbamate moieties. In UV spectroscopy, another difficulty might be the dependence of the molar extinction coefficient of dithiocarbamate on polymer molecular weight. In the molecular weight calculations, the coefficient was assumed to be constant. $M_{n,NMR}$ values are smaller than $M_{n,UV}$ values so that this reasoning seems to be right. This is supported by UV measurements performed on other polymers with different chain transfer agents that indicate a dependence of the extinction coefficient on the molecular weight of incorporated polymer as well as on the respective chain transfer agent structure. In the case of cyanoisopropyl CTA terminated polymer chains, $M_{n,UV}$ values were one order of magnitude higher than the expected values, while pyrrolidone CTA yielded reliable data, and cumyl and benzyl CTA led to some deviations with molecular weights in the range of 2,000-20,000 g/mol.

As can be seen from Tab. 4.6, $M_{n,NMR}$ values are between $M_{n,UV}$ and $M_{n,MALDI}$ values. One reason might be the absence of transfer agent endgroups in some of the polymer chains, as mentioned above, or the discrimination of high-molecular weight fractions by MALDI-TOF. The good agreement between theoretical and MALDI molecular weights favors the first explanation.

4.2.2   Poly(diacetone acrylamide)

The polymerization of diacetone acrylamide (DAA, N-(1,1-dimethyl-3-oxobutyl)acrylamide) has been described under free-radical and ionic conditions.[40-42] The polymer possesses the reactivity of an activated double bond, an N-substituted amide and a methyl ketone.[40] PDAA forms imines on reaction of primary amino groups with its keto function, thus enabling the synthesis of polymer-protein conjugates if primary amino groups are present in the protein. Diacetone acrylamide is water-soluble, but its polymer is insoluble in water.

The RAFT polymerization of diacetone acrylamide (DAA, structure see Fig. 4.25) has not been reported in the literature to date. In the present work, the monomer was polymerized for the first time using pyrrolidone CTA as chain transfer agent.
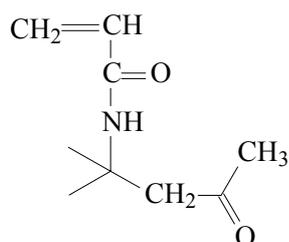
$$CH_2{=}CH$$
$$|$$
$$C{=}O$$
$$|$$
$$NH$$

CH₃

CH₂

O

Fig. 4.25.   Structure of diacetone acrylamide (DAA).

Two different initiators, namely AIBN and ACP, were employed but no significant influence was found on molecular weights and polydispersities even though ACP gives rise to faster polymerizations (70 % conversion after 2 h compared to the same conversion after 4 h with AIBN). Polymerizations were conducted in methanol. The results are summarized in Tab. 4.7.

Tab. 4.7.   Results of the RAFT polymerization of diacetone acrylamide using pyrrolidone CTA as chain transfer agent and AIBN or ACP, respectively, as initiator in methanol at 65 °C. For abbreviations see Tab. 4.2 and Tab. 4.3.

entry	monomer (mol/L)	CTA (mmol/L)	initiator (mmol/L)	time (min)	conv. (%)	$M_{n,GPC}$	$M_{n,theor}$	PDI
1	1.18	21.27	AIBN	120	49	4000	4800	1.29
			(3.57)	240	71	5900	6900	1.23
2	1.20	21.69	ACP	120	70	5600	6800	1.23
			(4.15)	240	89	6600	8500	1.21

Agreement between number-average molecular weights determined by GPC in THF using polystyrene calibration and calculated values is quite good. The observed polydispersities of 1.2-1.3 indicate that the polymerization proceeds in a controlled manner. The ^{1}H-NMR spectra show the expected polymer signals. Absence of free chain transfer agent in the NMR spectra of the mother liquors of the polymers precipitated from the polymerization mixture indicates complete consumption of transfer agent, which confirms the controlled nature of the polymerization. Fig. 4.26 shows the GPC elution curves of the polymer samples from Tab. 4.7.
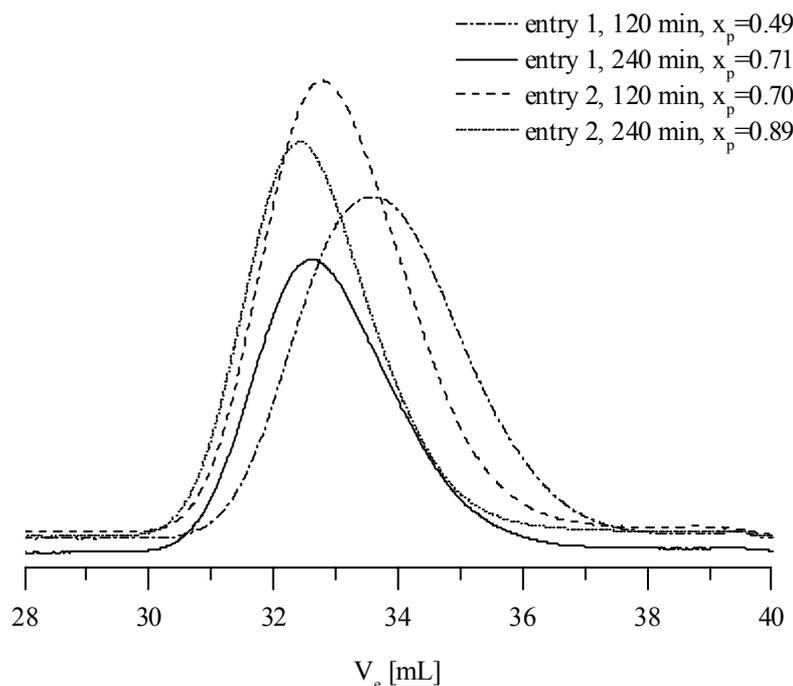
Fig. 4.26. *GPC traces (RI detector) of poly(diacetone acrylamide) using THF as an eluent and polystyrene calibration.*

Monomodal molecular weight distributions are obtained in all cases. Even in the case of high conversion (89 %, entry 2), there is no high-molecular weight shoulder detectable, which would indicate some termination of growing chains by combination. These results, along with the NMR data, indicate a controlled RAFT polymerization of diacetone acrylamide.

4.2.3   Poly(2-vinyl-4,4-dimethyl-5-oxazolone)

The monomer 2-vinyl-4,4-dimethyl-5-oxazolone (VO, structure see Fig. 4.27) can be regarded as a protected acrylamide which is obtained upon hydrolysis of the monomer or reaction with amines. The oxazolone is quite reactive towards compounds containing active hydrogen atoms, such as alcohols and water, so that drying and purification of solvents is vital for the success of the polymerization. The electrophilic azlactone ring is especially interesting as a site for polymer modification by nucleophilic attack of functional molecules, such as alcohols, amines, and thiols. Azlactone ring opening is particularly facile with primary amines.[43] Free-radical polymerization of the monomer has been reported to produce high-molecular weight azlactone-functional polymers.[44-46] Polymerizations proceed to high conversions (> 95 %) when run at 65 °C in bulk or benzene solution using AIBN as initiator.[44]
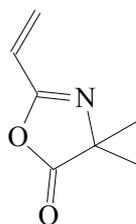
Fig. 4.27. *Structure of 2-vinyl-4,4-dimethyl-5-oxazolone (VO).*

Although having been polymerized in a free-radical manner, 2-vinyl-4,4-dimethyl-5-oxazolone had not been polymerized by the RAFT process before.

The RAFT polymerization of VO was performed in benzene at 65 °C using cyanoisopropyl CTA and pyrrolidone CTA as chain transfer agents with AIBN as initiator. The results are summarized in Tab. 4.8.

Tab. 4.8. *Results of the RAFT polymerization of 2-vinyl-4,4-dimethyl-5-oxazolone in benzene at 65 °C with cyanoisopropyl CTA and pyrrolidone CTA as chain transfer agents. For abbreviations see Tab. 4.2 and Tab. 4.3.*

entry	monomer (mol/L)	CTA (mmol/L)	initiator (mmol/L)	time (min)	conv. (%)	$M_{n,GPC}$	$M_{n,theor}$	PDI
1		cyanoisopropyl (159.0)	14.63	240	19	800	800	1.10
				360	35	1200	1300	1.09
				480	53	1700	1900	1.08
	3.52			960	64	2200	2200	1.09
2		cyanoisopropyl (45.4)	7.35	960	82	9100	9100	1.06
3		pyrrolidone (200.0)	13.84	4140	99	2300	2600	1.46

Tab. 4.8 shows that cyanoisopropyl CTA gives rise to very narrow molecular weight distributions, whereas the use of pyrrolidone CTA under similar conditions results in relatively high polydispersities.

Fig. 4.28 shows the plot of M_n (THF GPC using polystyrene calibration) and PDI, respectively, versus conversion for the RAFT polymerization of the vinyl oxazolone monomer using cyanoisopropyl CTA as chain transfer agent (entry 1 in Tab. 4.8). The agreement between experimental and calculated molecular weights (shown as solid line in the plot) is excellent, especially at high conversions, as well as the obtained polydispersities which are equal or smaller than 1.10.
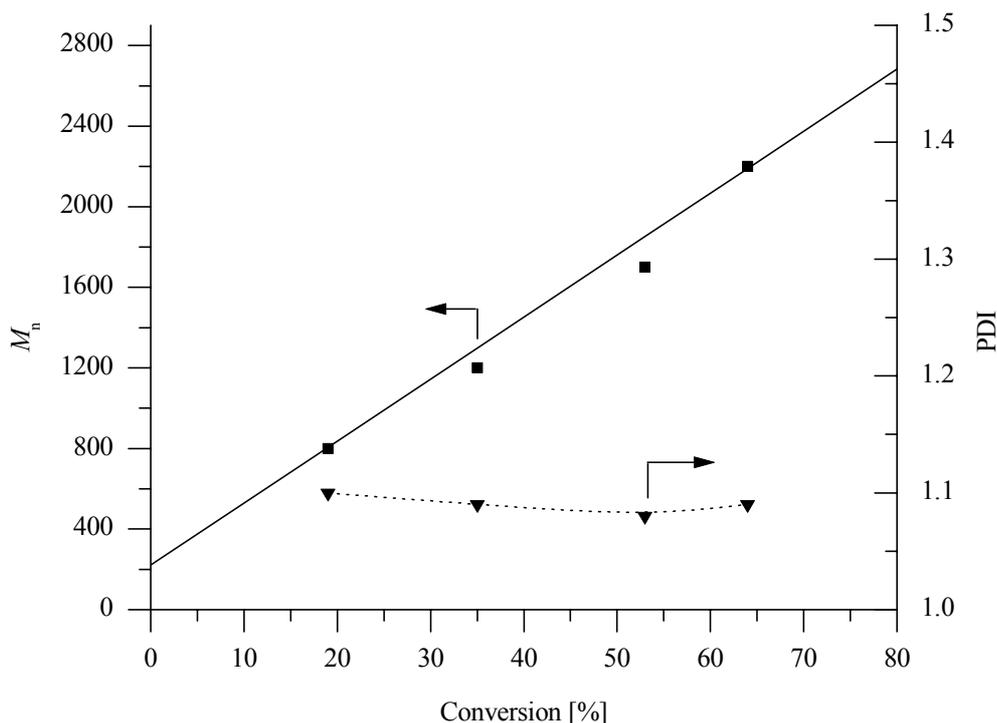
Fig. 4.28.   *Plot of* M$_n$*(■) and PDI(▼) versus conversion for the RAFT polymerization of vinyl oxazolone using cyanoisopropyl CTA (entry 1 in Tab. 4.8); the solid line represents the calculated molecular weights.*

Entry 2 in Tab. 4.8 shows that a controlled polymerization is even possible at relatively low chain transfer agent concentration.

With the chain transfer agent pyrrolidone CTA, a broad molecular weight distribution was obtained (entry 3 in Tab. 4.8). This result might be attributed to the pyrrolidone moiety which is less reactive towards radicals in the RAFT process as compared to the phenyl substituent in cyanoisopropyl CTA. This is due to the lone pair of nitrogen of pyrrolidone that delocalizes into the thiocarbonyl bond, resulting in a decreased double bond character of the C=S bond (cf. chapter 3.3.3)[3,47]

Number-average molecular weights were also determined by MALDI-TOF measurement in the linear mode. The results are compared with those of GPC and theoretical values in Tab. 4.9.

Tab. 4.9.   *Comparison of number-average molecular weights of poly(2-vinyl-4,4-dimethyl-5-oxazolone) obtained using GPC, MALDI-TOF, and calculated values.*

entry	time (min)	conv. (%)	$M_{n,theor}$	$M_{n,GPC}$	$M_{n,MALDI}$
1	480	53	1900	1700	1900
	960	64	2200	2200	2600
2	960	82	9100	9100	8600
3	4140	99	2600	2300	2500

Agreement between M_n values obtained by different methods is quite well. Polystyrene-calibrated THF GPC gives values that tend to be a bit smaller than the MALDI-TOF values but both GPC and MALDI-TOF values are in good agreement with the calculated molecular weights.

4.3 Poly(acrylate)s

The free radical polymerization of acrylates involves propagating radicals of relatively low steric bulk and high reactivity. These features facilitate both the addition of propagating radicals to the C=S double bond and fragmentation of the R group in the RAFT agent, tolerating a greater number of Z and R substituents.[3]

4.3.1 Poly(*tert*-butyl acrylate)

The monomer *tert*-butyl acrylate (*t*BuA) has been polymerized by anionic,[48,49] nitroxide-mediated,[50] and metallocene-mediated[51] polymerization as well as by ATRP, the latter yielding polymers of moderately narrow molecular weight distribution.[52,53] The monomer has also been polymerized by the RAFT process using xanthates as chain transfer agents, namely *O*-ethyl-*S*-(2-cyano-isoprop-2-yl)xanthate[3,47] and *O*-pentafluorophenyl-*S*-benzyl xanthate,[3] which led to polymers with polydispersities of 1.77 and 1.40, respectively.

Due to its relatively reactive *tert*-butyl group, poly(*tert*-butyl acrylate) can also be modified chemically, e.g. by hydrolysis to poly(acrylic acid).

In the following paragraph, it is shown that *tert*-butyl acrylate can be RAFT polymerized in a controlled manner using chain transfer agents other than xanthates, namely dithiocarbamates. The polymerization was further improved in terms of polydispersity by adjusting the substituents of the transfer agent.

The RAFT polymerization of *tert*-butyl acrylate was performed in ethyl acetate at 60 °C using benzyl CTA and cumyl CTA, respectively, as chain transfer agent with AIBN as initiator. The results are shown in Tab. 4.10.

Tab. 4.10. *Experimental conditions and results of the RAFT polymerization of* t*BuA;* M$_{n,GPC}$ *obtained using poly(*tert-*butyl acrylate) calibration. For abbreviations see Tab. 4.2.*

entry	monomer (mol/L)	CTA (mmol/L)	initiator (mmol/L)	time (min)	conv. (%)	$M_{n,theor}$	$M_{n,GPC}$	PDI
1	3.572	benzyl (24.29)	6.99	60	26	5100	4700	1.32
				120	58	11200	11600	1.19
				250	60	11500	14100	1.19
				1410	96	18300	25600	1.26
				5760	99	18900	26900	1.34
2	3.546	cumyl (15.92)	6.41	60	1	600	-	-
				120	5	1700	-	-
				250	52	15100	20100	1.18
				1410	89	25700	44400	1.28
				5760	99	28500	50500	1.29

Fig. 4.29 shows the first-order time conversion plot for the polymerizations. Obviously, in contrast to RAFT polymerization of NIPAAm with the same transfer agents, there is no induction period, accounting for a higher reactivity of the *tert*-butyl acrylate monomer toward the chain transfer agents. Polymerization with benzyl CTA is faster than that with cumyl CTA.
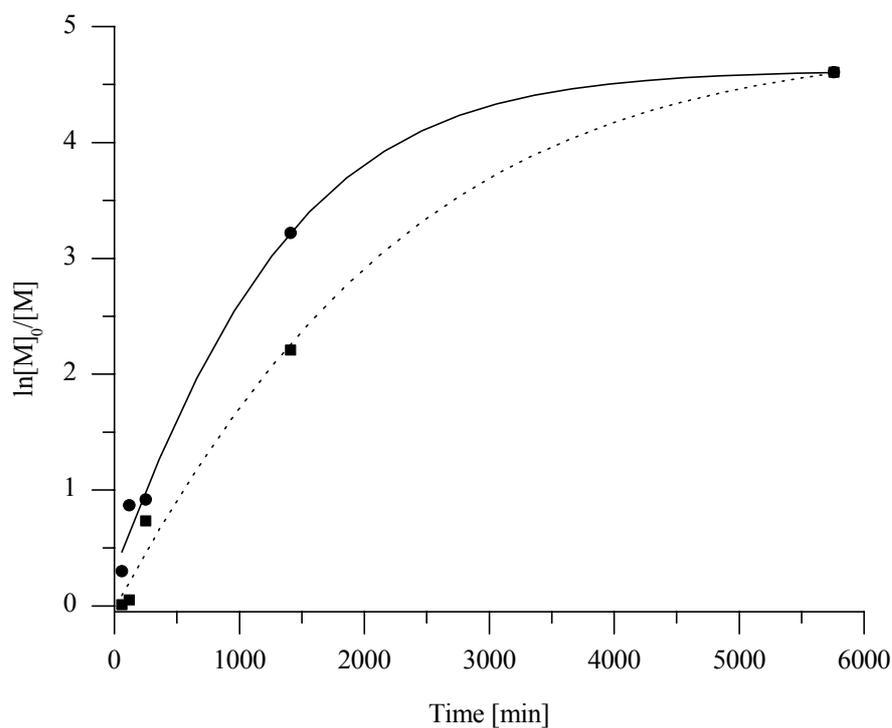

Fig. 4.29. *First-order time-conversion plot for the RAFT polymerization of* tert-*butyl acrylate using benzyl (●) and cumyl CTA (■), respectively.*

GPC of the polymer samples was performed in THF using poly(*tert*-butyl acrylate) standards for calibration. Fig. 4.30 shows the GPC traces of poly(*tert*-butyl acrylate) at different monomer conversions for the polymerization with benzyl CTA. From the figure, it can be seen that the molecular weight distributions become bimodal only at conversions higher than ca. 90 %, i.e. a high-molecular weight shoulder is detected. This is commonly observed for RAFT polymers at high monomer conversions, which is most likely due to combination of the growing chains.[31]
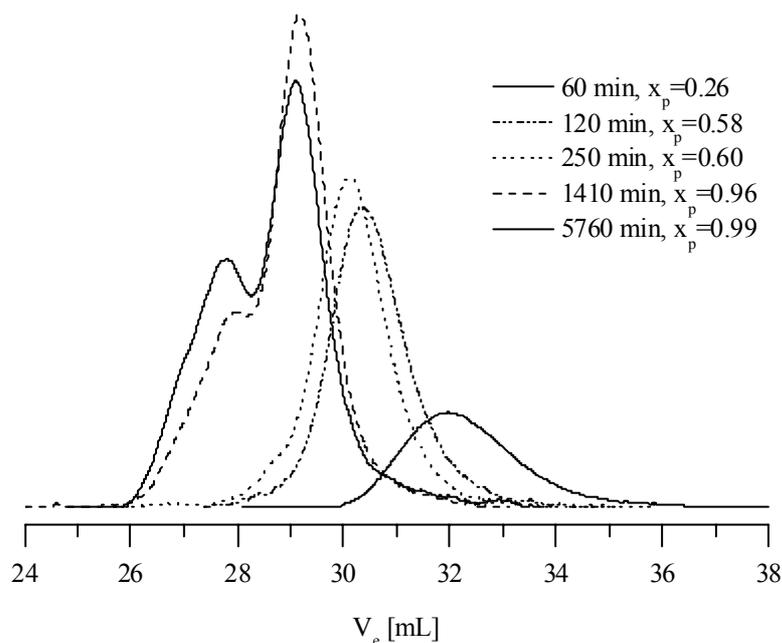

*Fig. 4.30.   GPC traces (RI detector) of poly(*tert-*butyl acrylate) at different monomer conversions x_P in THF with benzyl CTA as chain transfer agent.*

Fig. 4.31 shows the plot of M_n/PDI versus conversion for the polymerization of *tert*-butyl acrylate. It is obvious that high conversions (greater than 80 %) lead to relatively broad molecular weight distributions, and an increasing discrepancy between calculated and experimental molecular weights is observed with increasing conversion. This is due to a less controlled polymerization with increasing molecular weight. Regarding the polymerization rate, the RAFT polymerization with benzyl CTA seems to be faster in the initial state than with cumyl CTA. This can be ascribed to the higher reactivity of the benzyl radical because of its lower stability as compared to the cumyl radical. In general, the polymerization with cumyl CTA seems less controlled presumably because the ratio of RAFT agent to monomer is considerably smaller than that in the benzyl CTA controlled polymerization. This is reflected in the molecular weights that are almost twice as high as expected in the case of cumyl CTA.
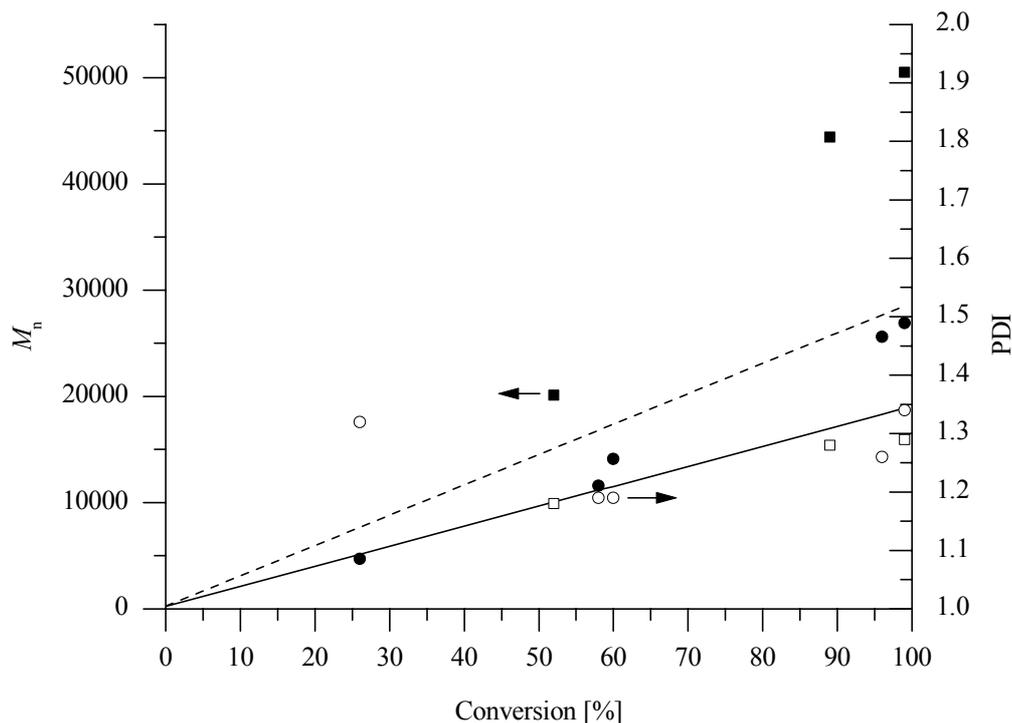
Fig. 4.31. *Plot of* M_n *(filled symbols) and PDI (open symbols) versus conversion for the RAFT polymerization of* tert-*butyl acrylate using benzyl CTA (—●—) and cumyl CTA (·····■·····), respectively, as chain transfer agent. The straight lines represent the theoretical molecular weights.*

4.3.2   Poly(acrylic acid)

Polymerization of acrylic acid (AA) in organic solvents is generally extremely slow. In contrast to that, the control of acrylic acid polymerization in aqueous or alcoholic media is especially challenging due to its very high propagation rate constant in these solvents and rapid gel formation.[54] Unlike other living polymerization techniques, RAFT polymerization of acrylic acid has the unique advantage that the monomer can be polymerized without protection of the carboxylic acid. In ATRP, for example, the acid functionality forms complexes with the transition metal catalyst, rendering the system ineffective for polymerization. In this case, a protected acrylic acid, such as *tert*-butyl acrylate, has to be used for polymerization followed by hydrolysis to poly(acrylic acid). Synthesis of poly(acrylic acid) via the RAFT process has been first described by Rizzardo et al. using AIBN as initiator, DMF as solvent, and 1-phenylethyl dithiobenzoate as CTA as well as with methanol as solvent using cyanoisopropyl-1-benzylcarbodithioate as RAFT agent, which lead to quite low-polydispersity products.[12,55] Low-molecular weight PAA ($\leq$ 5,100 g/mol) was prepared using xanthates, such as *O*-ethyl-*S*-(1-methoxycarbonyl-

ethyl)xanthate, as CTAs in RAFT polymerization at 70 °C in aqueous medium with polydispersities as low as 1.23.[56] Ladavière et al. succeeded in the RAFT polymerization of acrylic acid in ethanol using different xanthates, dithioates and trithiocarbonates with the lowest polydispersity obtained being 1.3 for $M_n \leq 4,100$ g/mol.[54] Controlled polymerization of acrylic acid has also been achieved under ^{60}Co irradiation in the presence of dibenzyl trithiocarbonate with very narrow molecular weight distributions (PDI ≥ 1.11).[57]

The acid functionalities in poly(acrylic acid) can be reversibly protonated and deprotonated. Besides, the activity of the carboxylic acid groups is dependent on ionic strength which, in turn, influences condensation of counter ions. Consequently, poly(acrylic acid) shows response to both pH and ionic strength.

4.3.2.1 RAFT polymerization

As acrylic acid is a quite active monomer in terms of radical polymerization, chain transfer agents with moderate activities can be used. As already mentioned above, acrylic acid has been polymerized by Rizzardo et al. using cyanoisopropyl-1-benzylcarbodithioate as chain transfer agent and methanol as solvent.[12] In the present work, the RAFT polymerization of acrylic acid was conducted in a mixture of methanol/water (4:1) in order to increase solvent polarity and thereby accelerate the polymerization with respect to RAFT polymerization in pure methanol. Pyrrolidone CTA was used as chain transfer agent. The experimental conditions and results are shown in Tab. 4.11.

Tab. 4.11. *Experimental conditions and results of RAFT polymerization of acrylic acid in MeOH/H$_2$O (4:1) at 90 °C using pyrrolidone CTA and VAZO-88 as initiator; [M]=5.84 M, [I]=0.66 mM. For abbreviations see Tab. 4.2 and Tab. 4.3.*

entry	CTA (mmol/L)	time (min)	conv. (%)	$M_{n,theor}$	$M_{n,GPC}$	$M_{n,MALDI}$	PDI
1	0.89	30	68	319,400[a]	38200	-	3.12
2	41.41	60	18	2000	1800	2500	1.48
3	42.64	180	80	8100	7900	6600	1.19

[a] CTA and initiator concentration considered for calculation, see Eq. 4.6

The pyrrolidone moiety of the chain transfer agent shows a moderate reactivity as for activating the C=S double bond towards radical addition. Under these conditions, best results are obtained at medium to high conversions (cf. Tab. 4.11). From entry 1 in Tab. 4.11, it can be seen that low chain transfer agent concentrations aiming at high theoretical molecular weights result in an uncontrolled polymerization of acrylic acid. Theoretical molecular weight in this case was calculated under consideration of the initiator concentration using Eq. 4.6:

$$M_{n,theor} = \frac{[M]_0}{[CTA]_0 + f[I]_0(1 - e^{-k_d t})} \cdot x_p \cdot M_{monomer} + M_{CTA} \qquad \text{Eq. 4.6}$$

where $[M]_0$, $[CTA]_0$, and $[I]_0$ are the initial concentrations of monomer, CTA, and initiator, respectively, x_p denotes monomer conversion, f is the initiator efficiency and k_d the rate constant for initiator decomposition. The initiator efficiency was assumed to be $f \approx 0.5$ and the decomposition rate constant was approximated as $k_d \approx 10^{-5}$ s^{-1}. However, the result is not much influenced by the additional term in the denominator of Eq. 4.6 ($M_{n,theor}$ is 321,500 g/mol without and 319,400 g/mol with consideration of the initiator concentration).

Samples taken at low conversions show high polydispersities, indicating an incomplete equilibration between dormant and active polymer chains.

In summary, the rate of polymerization was increased by the use of the very polar water/methanol mixture as a solvent instead of pure methanol. Despite the increased rate, the RAFT polymerizations proceeded in a controlled manner. Polydispersities of poly(acrylic acid) could be improved with respect to previous works by using pyrrolidone CTA as a chain transfer agent.

4.3.2.2   GPC and MALDI-TOF MS characterization

GPC was performed on the methylated poly(acrylic acid) samples using THF as an eluent.

The molecular weights of the non-methylated polymers from entries 2+3 in Tab. 4.11 were also determined by MALDI-TOF mass spectrometry in the linear mode; the molecular weight of the polymer from entry 1 is too high to be detected in the mass spectrometer. MALDI-TOF values should reflect the true molecular weights of the polymers. Measurement of poly(acrylic acid) samples with MALDI-TOF mass spectrometry is complicated by the high ionization potential of the carboxylic acid groups. Samples were cast from ethanol solution, and sinapinic acid was used as a matrix. Resolution in both the linear and reflector mode was relatively low. Peak distances were determined to be 72 g/mol as expected for the acrylic acid repeating unit, and major peaks could be assigned to the commonly found chain end structures, i.e. dithiocarbamate-terminated as well as hydrogen- and double-bond terminated chain ends (Fig. 4.32).
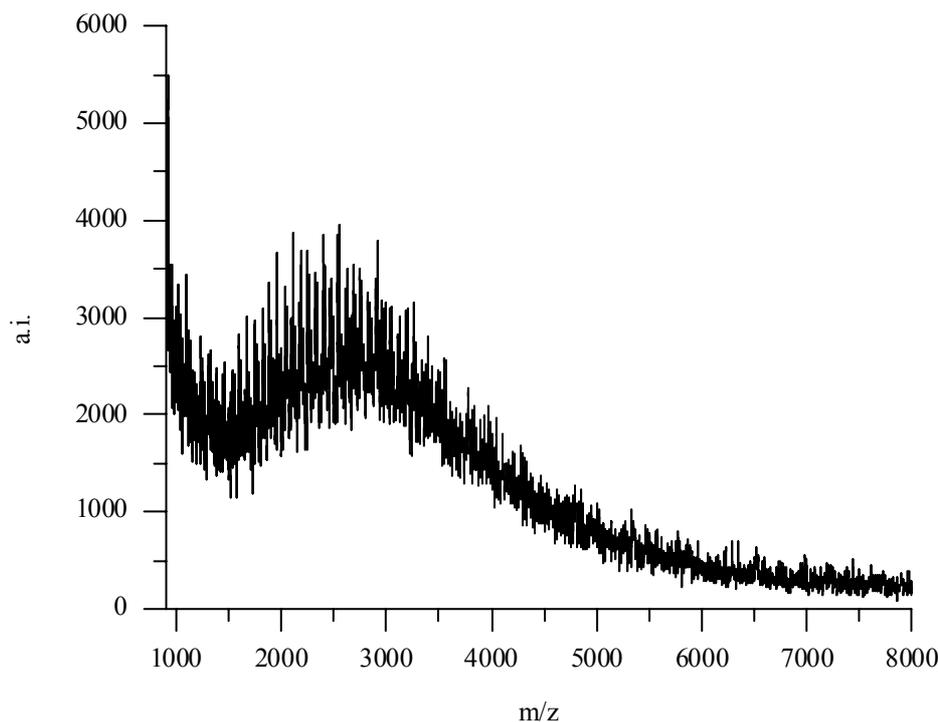
Fig. 4.32.   MALDI-TOF mass spectrum of poly(acrylic acid) (entry 2 in Tab. 4.11), recorded in the linear mode.

Comparison of the calculated and experimentally determined molecular weights shows that the MALDI-TOF values are relatively close to the theoretical values and to those determined by GPC. Polydispersities obtained by MALDI are generally lower than the true ones due to discrimination of high-molecular weight fractions. The relatively low resolution of the MALDI-TOF spectra that requires a baseline correction gives rise to some errors in determination of M_n and PDI. Thus, the values obtained should only be considered as an approximation. Nevertheless, they confirm the order of magnitude of the GPC and theoretical M_n values.

4.4   Poly(methacrylate)s

The free radical polymerization of methacrylates requires relatively bulky propagating radicals with moderate reactivity. It has been demonstrated that efficient RAFT polymerization of these monomers requires chain transfer agents with bulky R substituents, i.e. stabilized R$^\bullet$ radicals, and radical-stabilizing Z substituents that increase the rate of addition of radicals to the C=S double bond.[3]

4.4.1   Poly(*N*-hydroxysuccinimide methacrylate)

The active ester monomer *N*-hydroxysuccinimide methacrylate (NHSM, structure see Fig. 4.33) was successfully polymerized by RAFT for the first time. The monomer is more hydrolytically stable than other commonly used active esters.[58] As an active ester, it reacts readily with amines and alcohols[59] and has been used for drug attachment.[60]
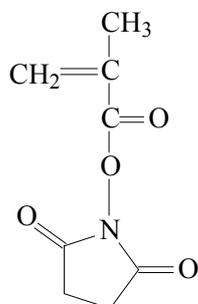

Fig. 4.33.   Structure of N-*hydroxysuccinimide methacrylate (NHSM).*

4.4.1.1   RAFT polymerization

Polymerization in THF and acetone is limited by premature precipitation during polymerization[60] so that these solvents cannot be used for RAFT polymerization. Nevertheless, both monomer and polymer are soluble in DMF and DMSO.[59,61] DMF as a solvent is problematic in ATRP due to possible competitive complexation of metal ions[62] but it is not expected to influence the performance of RAFT polymerization.

The RAFT polymerization of *N*-hydroxysuccinimide methacrylate was carried out using four different chain transfer agents at different polymerization temperatures and DMF as a solvent. The experimental conditions and results are summarized in Tab. 4.12.

Tab. 4.12.   Experimental conditions and results of RAFT polymerization of N-*hydroxysuccinimide methacrylate in DMF at 60 °C and 30 °C (entry 4), respectively. For abbreviations see Tab. 4.2 and Tab. 4.3.*

entry	monomer (mol/L)	CTA (mmol/L)	initiator (mmol/L)	time (min)	conv. (%)	$M_{n,theor}$ ($\cdot 10^{-3}$)	$M_{n,GPC}$[a] ($\cdot 10^{-3}$)	PDI
1	1.373	benzyl	AIBN	600	74	2.6	41.3	2.34
		(78.0)	(10.0)	960	89	3.1	43.5	2.11
2	1.376	cumyl	AIBN	600	60	2.3	22.4	1.78
		(74.8)	(10.0)	960	83	3.1	24.1	1.71
3	1.360	cyanoisopropyl	AIBN	600	70	2.7	24.2	1.47
		(70.3)	(5.08)	960	81	3.1	24.5	1.52
4	1.367	PEPDTA	V-70	600	58	2.2	31.3	1.95
		(77.0)	(12.16)	960	63	2.3	36.2	2.06

[a] polystyrene calibration

As can be seen from Tab. 4.12, no satisfactory results are obtained regarding polydispersities and control of molecular weight. NHSM is a rather active monomer in controlled radical polymerization and reactive radicals are produced upon initiation. Therefore, a chain transfer agent containing an equally active leaving group has to be used to ensure effective polymerization. The RAFT agent cyanoisopropyl CTA fulfills this requirement as it consists of a reactive cyanoisopropyl leaving group. It is one of the most reactive chain transfer agents known at present. Nevertheless, the obtained polymers showed polydispersities around 1.5 and their molecular weights (polystyrene calibration) were much higher than predicted (entry 3 in Tab. 4.12). Residual unreacted chain transfer agent was detected in the ^{1}H-NMR spectra of the mother liquors of the polymers precipitated from the polymerization mixture. The same findings were made for polymerizations using the RAFT agents PEPDTA, cumyl CTA, and benzyl CTA. This observation suggests an incomplete consumption of chain transfer agent, leading to a less controlled polymerization process.

The chain transfer agent PEPDTA decomposes at ambient temperature,[13] and the RAFT polymerization was conducted at 30 ºC using the low-temperature initiator V-70. For the success of RAFT polymerization at room temperature, the structure of the Z group has to be adjusted in a way that the stability of the intermediate RAFT radical is decreased, i.e. the RAFT equilibrium is shifted to increase the concentration of propagating polymer chains. In the case of alkyl acrylates, this was achieved by changing the Z group from phenyl to benzyl as the radical in the RAFT intermediate is in a relatively unstable disulfur alkyl position as compared to the disulfur benzylic position in the phenyl analogue.[13] This increases the rate of fragmentation and results in a faster establishment of the RAFT equilibrium. It was assumed that a lower polymerization temperature combined with the use of PEPDTA might cause an overcompensation of the polymerization rate constant k_p by the chain transfer constant k_{tr}, leading to a controlled polymerization. This was not the case, though. Possible reasons could be side reaction of the dithiocarbamate with the active ester or a very high polymerization rate even at low temperature and in the presence of a rather reactive chain transfer agent.

Among the chain transfer agents used, cyanoisopropyl CTA showed the best results with respect to polydispersity and agreement between theoretical and experimental molecular weights. This underlines the assumption that a highly reactive chain transfer agent is needed for the polymerization of *N*-hydroxysuccinimide methacrylate.

4.4.1.2   GPC and MALDI-TOF MS characterization

MALDI-TOF mass spectrometry of the polymer was performed in order to elucidate the chain end structure of the samples. Due to the insolubility of high-molecular weight

fractions in DMSO, the measurements were performed on the solid polymer samples with dihydroxybenzoic acid (DHB) as a matrix; DMSO solutions of the polymers gave only signals in the low-molecular weight region and low peak resolution. Only in the case of PNHSM obtained with benzyl CTA and cumyl CTA, MALDI-TOF MS gave reliable results and well resolved peaks. Molecular weight determination by MALDI measurement in the linear mode gave lower molecular weights than those obtained by GPC in DMF/LiBr using polystyrene calibration but MALDI values were quite close to the calculated molecular weights. Only for the polymers prepared with benzyl CTA, coherent information on molecular weights and polydispersities could be deduced. Tab. 4.13 summarizes the information deduced from MALDI and GPC measurements.

Tab. 4.13.   *Comparison between* M_n *values obtained from MALDI and from GPC.*

entry	time (min)	conv. (%)	$M_{n,theor}$	$M_{n,GPC}$	$M_{n,MALDI}$	PDI [a]
1	600	89	3100	43500	4200	2.11
(benzyl CTA)	960	74	2600	41300	3500	2.34

[a] determined by GPC

These findings suggest that the molecular weights obtained with GPC are much higher than the true ones. $M_{n,GPC}$ values are more than ten times higher than $M_{n,MALDI}$ values, and it is hard to evaluate the reliability of the MALDI results. Difficulties in the preparation of the samples suggest that an interpretation is not straightforward. Besides, only two polymer samples out of eight could be characterized in the linear mode. The fact that the samples were measured in the solid state might be responsible for the discrimination of high-molecular weight fractions due to their lower ionization probability.

Another peculiarity is found in the mass spectra that were recorded on the solid polymer samples in the reflector mode. In the case of PNHSM obtained with benzyl CTA, the distances between the peaks of the repeating units are not equal to 183 g/mol, as would have been expected for the NHSM repeating unit, but they are equal to 44 g/mol (see Fig. 4.34). This might also be attributed to sample preparation.

When the PNHSM samples are cast from DMSO solution, the expected distances are found for both polymers obtained with benzyl and with cumyl CTA. Nevertheless, a severe mass discrimination of high-molecular weight fractions is observed. A closer look at the different peaks shows that only double-bond and hydrogen-terminated polymers can be found, containing the aromatic end of the chain transfer agent at the other end (see Fig. 4.35), which accounts for fragmentation during ionization as was observed for PNIPAAm. No initiator-derived chains were detected, which indicates that polymerization

is successfully initiated by the chain transfer agent. These findings would be another indication that GPC evaluation leads to wrong conclusions.
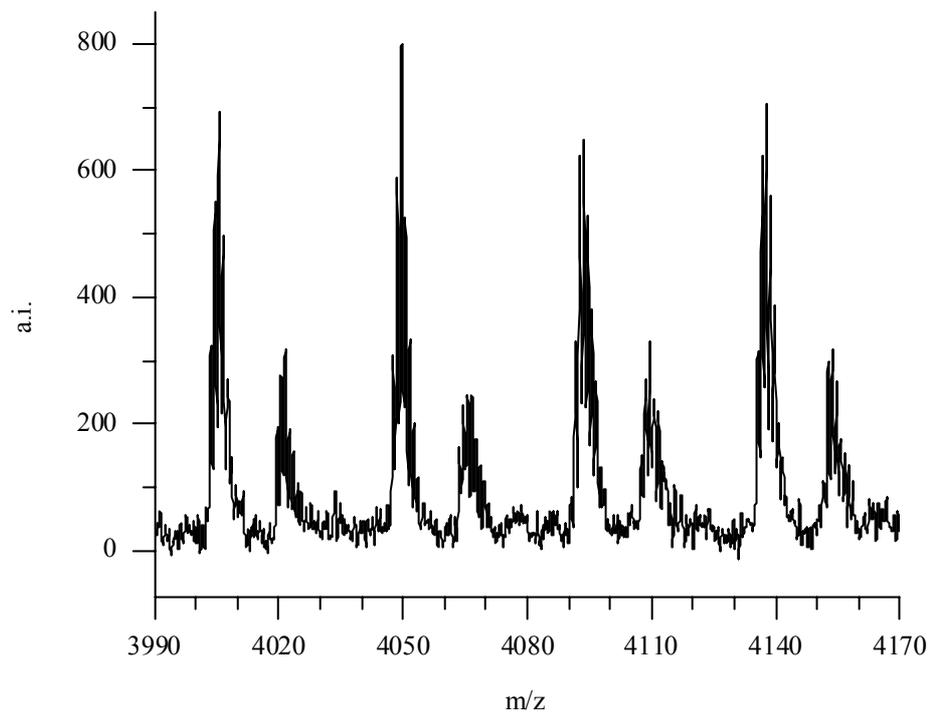

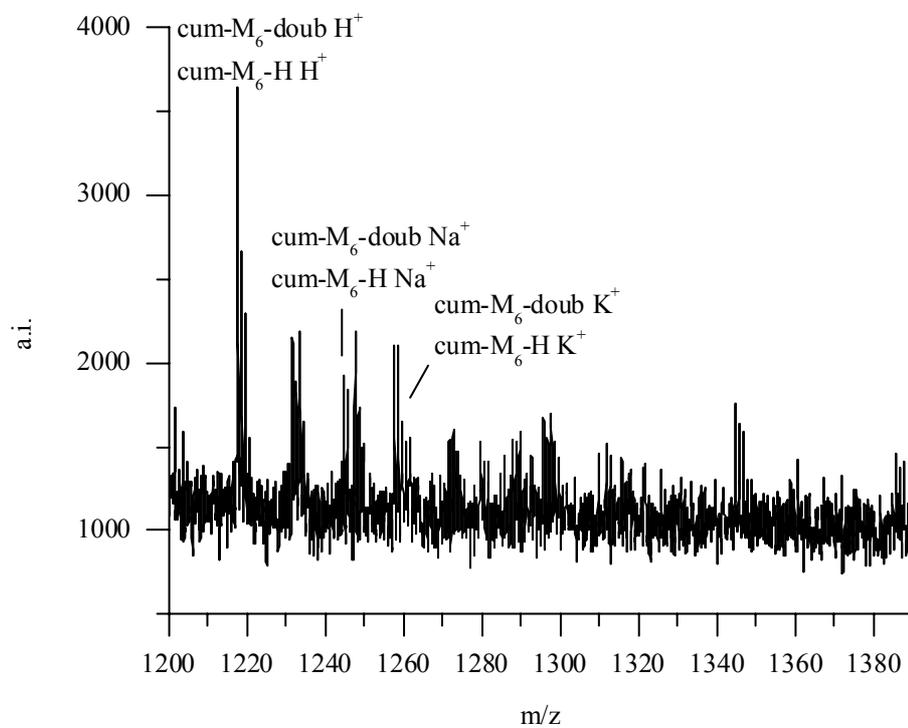*Fig. 4.34.   MALDI-TOF mass spectrum of PNHSM synthesized with benzyl CTA, solid sample.*

Fig. 4.35.   MALDI-TOF mass spectrum of PNHSM obtained with cumyl CTA, sample cast from DMSO.

As already mentioned above, GPC on the samples was performed in DMF/LiBr. Fig. 4.36 shows the GPC traces for PNHSM obtained with PEPDTA as chain transfer agent (entry 4 in Tab. 4.12). For all polymer samples, only monomodal molecular weight distributions were found. Thus, again, there is no indication that the RAFT polymerization of the monomer is uncontrolled.
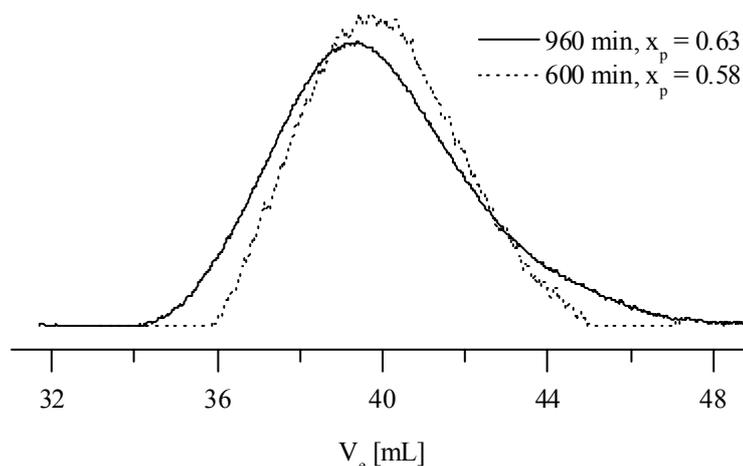

Fig. 4.36.   *GPC traces (RI detector) of PNHSM obtained with PEPDTA in DMF/LiBr.*

4.5   **Block copolymers**

4.5.1   Poly(*N*-isopropylacrylamide)-*block*-poly(acrylic acid)

The block copolymer PNIPAAm-*b*-PAA was synthesized by RAFT for the first time. The block copolymerization was performed using poly(acrylic acid) as a macromolecular chain transfer agent. Poly(acrylic acid), obtained from RAFT polymerization with pyrrolidone CTA as chain transfer agent (see section 4.3.2.1), was purified by precipitating its methanol solution into ethyl acetate in order to remove residual monomer and avoid formation of gradient copolymers in the subsequent block copolymerization with NIPAAm. RAFT polymerizations were carried out in methanol as solvent using AIBN as initiator at 60 °C. The obtained polydispersities were quite low. Tab. 4.14 summarizes the results obtained for block copolymers of PAA block length m=110 and variable PNIPAAm block lengths n.

Tab. 4.14.   *Experimental conditions and results of the block copolymerization of PAA with PNIPAAm using PAA as macromolecular chain transfer agent (*M_n *= 7900 g/mol and PDI = 1.19) with AIBN as initiator and methanol as solvent at 60 °C; [M] = 1.50 M; GPC in DMF/LiBr with PMMA calibration.*

entry	CTA[a] (mmol/L)	initiator (mmol/L)	time (min)	conv. (%)	$M_{n,theor}$	$M_{n,GPC}$	$M_{n,MALDI}$	PDI
1	14.78	7.0	600	64	15100	$2.28 \cdot 10^5$ $(2.37 \cdot 10^{6*})$	13600	1.11
2			960	82	17200	$2.66 \cdot 10^5$ $(2.75 \cdot 10^{6*})$	14000	1.09
3	9.40	7.0	960	48	16500	$2.22 \cdot 10^5$	16300	1.06
4	12.99	4.6	600	75	17700	$8.57 \cdot 10^4$	14300	1.15
5	6.49	4.6	600	65	24900	$2.92 \cdot 10^5$	23400	1.03

[a] GPC using DMF + 0.05 M LiBr as eluent and universal calibration

MALDI-TOF mass spectrometry for determination of number-average molecular weights leads not only to singly charged but also to doubly or even multiply charged molecules due to the ease of ionization of the acrylic acid blocks. In general, two major peaks were found in the MALDI-TOF spectra, which were attributed to single- and double-charged polymers.

Both DMF and aqueous GPC were used to determine molecular weights and polydispersities of the block copolymers from entry 1+2 in Tab. 4.14. In all cases, the molecular weights determined by GPC are about one order of magnitude higher than the theoretical and MALDI values. Universal calibration yields even higher values (entry 1+2 in Tab. 4.14) This was attributed to the formation of aggregates in solution and will be discussed along with further details on aqueous GPC in chapter 5.

4.5.2   Poly(*N*-isopropylacrylamide)-*block*-poly(2-vinyl-4,4-dimethyl-5-oxazolone)

To date, no literature reports on the synthesis of the active ester containing PNIPAAm-*b*-PVO block copolymer are known, neither by controlled nor by free radical polymerization. Block copolymer synthesis was performed using PVO as a macromolecular chain transfer agent and AIBN as initiator in benzene at 65 °C. PVO was synthesized by RAFT polymerization with cyanoisopropyl CTA as chain transfer agent (see section 4.2.3). Tab. 4.15 summarizes the results obtained for the block copolymerizations.

Tab. 4.15.   *Experimental conditions and results for the block copolymerization of PNIPAAm with PVO using PVO as macromolecular chain transfer agent (M_n = 2200 g/mol and PDI = 1.09) with AIBN as initiator and benzene as solvent at 65 °C; [M] = 2.24 M, [CTA] = 18.2 mM, [I] = 1.94 M.*

entry	time (min)	conv. (%)	$M_{n, theor}$	$M_{n,GPC}$	PDI
1	960	26	5800	5800	1.22
2	1320	32	6600	6200	1.14

Agreement between the number-average molecular weights obtained from GPC and the calculated ones is very good. Nevertheless, polymerization seems to be fairly slow since the conversion is quite low, even after 22 h (entry 2 in Tab. 4.15). This clearly shows that incorporation of the highly reactive chain transfer agent cyanoisopropyl CTA into the polymer PVO, i.e. formation of a macromolecular chain transfer agent, leads to a considerable decrease of its reactivity.

GPC measurements were performed in THF as an eluent. The GPC traces show some tailing in the low-molecular weight region (Fig. 4.37).
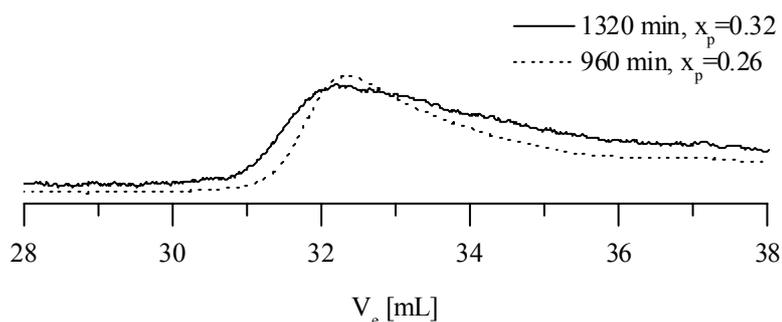

Fig. 4.37.   *GPC traces (RI detector) of PNIPAAm-b-PVO in THF.*

Tailing is attributed to interaction of the rather polar polymer with the column material (SDV gel), leading to partial adsorption on the column and a broadening of the elution profile. The PNIPAAm homopolymer adsorbs completely on the columns if measurement is performed without addition of salt to the eluent (cf. section 4.2.1). Thus, the relatively high polydispersities might be related to interaction with the column material, which implies that the true polydispersities are somewhat lower.

References

(1)   Houben-Weyl. *Schwefel-, Selen-, Tellur-Verbindungen*; Georg Thieme Verlag: Stuttgart, 1955; Vol. 9.

(2)   Houben-Weyl. In *Methoden der Organischen Chemie*; Kraatz, U., Ed.; Georg Thieme Verlag: Stuttgart, 1983; Vol. E4.

(3)   Chiefari, J.; Mayadunne, R. T. A.; Moad, G.; Rizzardo, E.; Thang, S. H. In *WO 99/31144*; E.I. DuPont de Nemours and Company: Australia, 1999.

(4)   Schilli, C.; Lanzendörfer, M. G.; Müller, A. H. E. *Macromolecules* **2002**, *35*, 6819-6827.

(5)   Takeshima, T.; Ikeda, M.; Yokoyama, M.; Fukada, N.; Muraoka, M. *J. Chem. Soc., Perkin Trans. 1* **1979**, 692-695.

(6)   Thang, S. H. *personal communication*.

(7)   Oddo, B.; Carlo, A. *Gazz. Chim. Ital.* **1938**, *68*, 204-208.

(8)   Ramadas, K.; Srinivasan, N. *Synth. Commun.* **1995**, *25*, 227-234.

(9)   Rizzardo, E.; Moad, G.; Thang, S. H. In *WO 99/05099*: Australia, 1998.

(10)   Mitsukami, Y.; Donovan, M. S.; Lowe, A. B.; McCormick, C. L. *Macromolecules* **2001**, *34(7)*, 2248-2256.

(11)   Thang, S. H.; Chong, B. Y. K.; Mayadunne, R. T. A. *Tetrahedr. Lett.* **1999**, *40*, 2435-2438.

(12)   Le, T. P.; Moad, G.; Rizzardo, E.; Thang, S. H. In *WO 98/01478*; E.I. Du Pont De Nemours and Co., USA; Le, Tam Phuong; Moad, Graeme; Rizzardo, Ezio; Thang, San Hoa: Australia, 1998.

(13)   Quinn, J. F.; Rizzardo, E.; Davis, T. P. *Chem. Commun.* **2001**, 1044-1045.

(14)   Sudalai, A.; Kanagasabapathy, S.; Benicewicz, B. C. *Organic Letters* **2000**, *2*, 3213-3216.

(15)   Dureault, A.; Destarac, M.; Leising, F.; Guerrero-Santos, R.; Gnanou, Y.; Taton, D. *Polym. Prepr. (Am. Chem. Soc., Div. Polym. Chem.)* **2002**, *43*, 120-121.

(16)   Favier, A.; Charreyre, M.-T.; Chaumont, P.; Pichot, C. *Macromolecules* **2002**, *35*, 8271-8280.

(17)   Schild, H. G. *Prog. Polym. Sci.* **1992**, *17*, 163-249.

(18)   Kitayama, T.; Shibuya, W.; Katsukawa, K.-I. *Polymer Journal (Tokyo, Japan)* **2002**, *34*, 405-409.

(19)   Ishizone, T.; Ito, M. *J. Polym. Sci., Part A: Polym. Chem.* **2002**, *40*, 4328-4332.

(20)   Lim, Y. H.; Kim, D.; Lee, D. S. *J. Appl. Polym. Sci.* **1997**, *64*, 2647-2655.

(21) Stauch, O.; Uhlmann, T.; Froehlich, M.; Thomann, R.; El-Badry, M.; Kim, Y.-K.; Schubert, R. *Biomacromolecules* **2002**, *3*, 324-332.

(22) Schilli, C.; Müller, A. H. E. *Abstract, SML'01 International Symposium on Free Radical Polymerization: Kinetics and Mechanism, Il Ciocco, Italy* **2001**.

(23) Lanzendörfer, M.; Schmalz, H.; Abetz, V.; Müller, A. H. E. *Polym. Prepr. (Am. Chem. Soc., Div. Polym. Chem.)* **2001**, *42*, 329-330.

(24) Moad, G.; Chiefari, J.; Chong, Y. K.; Krstina, J.; Mayadunne, R. T. A.; Postma, A.; Rizzardo, E.; Thang, S. H. *Polym. Int.* **2000**, *49*, 993-1001.

(25) Monteiro, M. J.; Brouwer, H. d. *Macromolecules* **2001**, *34(3)*, 349-352.

(26) Kwak, Y.; Goto, A.; Tsujii, Y.; Murata, Y.; Komatsu, K.; Fukuda, T. *Macromolecules* **2002**, *35*, 3026 -3029.

(27) Barner-Kowollik, C.; Quinn, J. F.; Morsley, D. R.; Davis, T. P. *J. Polym. Sci., Part A: Polym. Chem.* **2001**, *39*, 1353-1365.

(28) Calitz, F. M.; Tonge, M. P.; Sanderson, R. D. *5th Annual UNESCO School and Conference on Macromolecules & Materials Science, Stellenbosch, South Africa* **2002**.

(29) Donovan, M. S.; Lowe, A. B.; Sumerlin, B. S.; McCormick, C. L. *Macromolecules* **2002**, *35*, 4123-4132.

(30) Destarac, M.; Charmot, D.; Franck, X.; Zard, S. Z. *Macromol. Rapid. Commun.* **2000**, *21*, 1035-1039.

(31) Ganachaud, F.; Monteiro, M. J.; Gilbert, R. G.; Dourges, M.-A.; Thang, S. H.; Rizzardo, E. *Macromolecules* **2000**, *33*, 6738-6745.

(32) Beyou, E.; Chaumont, P.; Chauvin, F.; Devaux, C.; Zydowicz, N. *Macromolecules* **1998**, *31*, 6828-6835.

(33) Kaufmann, R.; Spengler, B.; Lutzenkirchen, F. *Rapid Commun. Mass Spectrom.* **1993**, *7*, 902-910.

(34) Montaudo, G. *Mass Spectrometry of Polymers*; CRC Press: Boca Raton, 2002.

(35) Garozzo, D.; Nasello, V.; Spina, E.; Sturiale, L. *Rapid Commun. Mass Spectrom.* **1997**, *11*, 1561-1566.

(36) Nielen, M. W. F. *Mass Spectrom. Rev.* **1999**, *18*, 309-344.

(37) Cole, C.-A.; Schreiner, S. M.; Monji, N. *Polym. Prepr. (Am. Chem. Soc., Div. Polym. Chem.)* **1986**, *27(1)*, 237-238.

(38) Yang, H. J.; Cole, C.-A.; Monji, N.; Hoffman, A. S. *J. Polym. Sci., Part A: Polym. Chem.* **1990**, *28*, 219-226.

(39)   Litvinenko, G. I.; Simon, P. F. W.; Müller, A. H. E. *Macromolecules* **1999**, *32*, 2410-2419.

(40)   Coleman, L. E.; Bork, J. F.; Wyman, D. P.; Hoke, D. I. *J. Polym. Sci., Part A* **1965**, *3*, 1601-1607.

(41)   Marans, N. S.; Ehrig, R. J. *J. Polym. Sci., Part A-1* **1966**, *4*, 2330-2335.

(42)   Jochsberger, T.; Indictor, N.; Gudulludglu, N.; Shahani, C. J.; Baer, N. S.; Indictor, N. *J. Polym. Sci., Polym. Chem. Ed.* **1978**, *16*, 309-311.

(43)   Guichard, B.; Noel, C.; Reyx, D.; Thomas, M.; Chevalier, S.; Senet, J.-P. *Macromol. Chem. Phys.* **1998**, *199*, 1657-1674.

(44)   Taylor, L. D.; Chiklis, C. K.; Platt, T. E. *J. Polym. Sci., Part B: Polym. Lett.* **1971**, *9*, 187-190.

(45)   Muthiah, J.; Mathias, L. J. *J. Polym. Sci., Part A: Polym. Chem.* **1991**, *29*, 29-37.

(46)   Muthiah, J.; Mathias, L. J. *Polym. Prepr. (Am. Chem. Soc., Div. Polym. Chem.)* **1990**, *31*, 480-481.

(47)   Rizzardo, E.; Chiefari, J.; Mayadunne, R. T. A. In *Controlled/Living Radical Polymerization - Progress in ATRP, NMP, and RAFT, ACS Symposium Series*; Matyjaszewski, K., Ed.; American Chemical Society: Washington, DC, 2000; Vol. 768, pp 278-295.

(48)   Ishizone, T.; Yoshimura, K.; Hirao, A.; Nakahama, S. *Macromolecules* **1998**, *31*, 8706.

(49)   Ishizone, T.; Yoshimura, K.; Yanasc, E.; Nakahama, S. *Macromolecules* **1999**, *3*, 955.

(50)   Goto, A.; Fukuda, T. *Macromolecules* **1970**, *3*.

(51)   Deng, H.; Soga, K. *Macromolecules* **1996**, *29*, 1847.

(52)   Cheng, G.; Simon, P. F. W.; Hartenstein, M.; Müller, A. H. E. *Macromol. Rapid Commun.* **2000**, *21*, 846-852.

(53)   Davis, K. A.; Matyjaszewski, K. *Macromolecules* **2000**, *33*, 4039-4047.

(54)   Ladaviere, C.; Doerr, N.; Claverie, J. P. *Macromolecules* **2001**, *34*, 5370-5372.

(55)   Chiefari, J.; Chong, Y. K.; Ercole, F.; Krstina, J.; Jeffery, J.; Le, T. P. T.; Mayadunne, R. T. A.; Meijs, G. F.; Moad, C. L.; Moad, G.; Rizzardo, E.; Thang, S. H. *Macromolecules* **1998**, *31*, 5559-5562.

(56)   Taton, D.; Wilczewska, A.-Z.; Destarac, M. *Macromolecular Rapid Communications* **2001**, *22*, 1497-1503.

(57)   Hong, C.-Y.; You, Y.-Z.; Bai, R.-K.; Pan, C.-Y.; Borjihan, G. *J. Polym. Sci., Part A: Polym. Chem.* **2001**, *39*, 3934-3939.

(58)   Hermanson, G. T. *Bioconjugate Techniques*; Academic Press Inc.: San Diego, 1996.

(59)   Batz, H.-G.; Franzmann, G.; Ringsdorf, H. *Angew. Chem.* **1972**, *84*, 1189-1190.

(60)   Godwin, A.; Hartenstein, M.; Müller, A. H. E.; Brocchini, S. *Angew. Chem. Int. Ed.* **2001**, *40*, 594.

(61)   Ferruti, P.; Bettelli, A.; Fere, A. *Polymer* **1972**, *13*, 462-464.

(62)   Beers, K. L.; Boo, S.; Gaynor, S. G.; Matyjaszewski, K. *Macromolecules* **1999**, *32*, 5772-5776.

5   Properties of homopolymers and block copolymers

5.1   Poly(*N*-isopropylacrylamide)

5.1.1   LCST measurements

Poly(*N*-isopropylacrylamide), PNIPAAm, shows l̲ower c̲ritical s̲olution t̲emperature (LCST) behaviour in aqueous solutions and a sharp phase transition is observed at 32 °C in water.[1-3] The temperature-dependent solubility in aqueous solutions is based on the presence of both hydrophilic and hydrophobic groups. At low temperatures, the hydrophilic interactions dominate and, due to the structure of water, a decreased entropy upon mixing is observed that is overcompensated by the exothermic enthalpy of hydrogen bonds formed between hydrophilic groups of the polymer and water molecules.[4] As the temperature is increased, the free energy change upon mixing becomes positive at one stage, resulting in phase separation. The phase-separation process consists of two steps. First, breaking of intermolecular hydrogen bonds between water and amide groups of the polymer takes place, and free amide groups are formed. The second step consists of an increase in intramolecular hydrogen bonding, which induces a coil-globule transition.[5,6]

PNIPAAm samples of different degrees of polymerization were prepared to investigate the influence of polymer molecular weight on the LCST value. In order to determine LCST, cloud point measurements were performed. For this purpose, the UV-vis transmission of 0.25 wt.-% aqueous polymer solutions was recorded at a wavelength of 500 nm while heating at a rate of 0.5 K/min. Cloud point measurement is a common method for determination of the LCST, and different wavelengths of observation can be found in the literature. The wavelength of the measurement determines the minimum size of detectable precipitated particles. For binary aqueous solutions of PNIPAAm, there is no particular advantage to any wavelength. Only in the presence of additives, such as organic solvents, salts, or surfactants, the observed LCST may be a function of the wavelength and it is difficult to assign an LCST based on cloud point measurements.[2] In the present work, distilled and deionized water was used to dissolve the polymer samples so that the cloud points are independent of wavelength.

Fig. 5.1 shows the plot of cloud point versus the inverse molecular weight of the PNIPAAm samples. It can be seen that the cloud point decreases virtually linearly with increasing reciprocal molecular weight and approaches 32 °C for $M_n \geq 20{,}000$ g/mol. This result seems reasonable as the hydrophobic endgroups lower the LCST due to an increase of overall hydrophobicity and a collapse of the intramolecular hydrogen bonds at lower temperature. This effect becomes less and less important the higher the molecular weight

of the polymer, i.e. the smaller the molar fraction of the hydrophobic endgroups in the polymer.
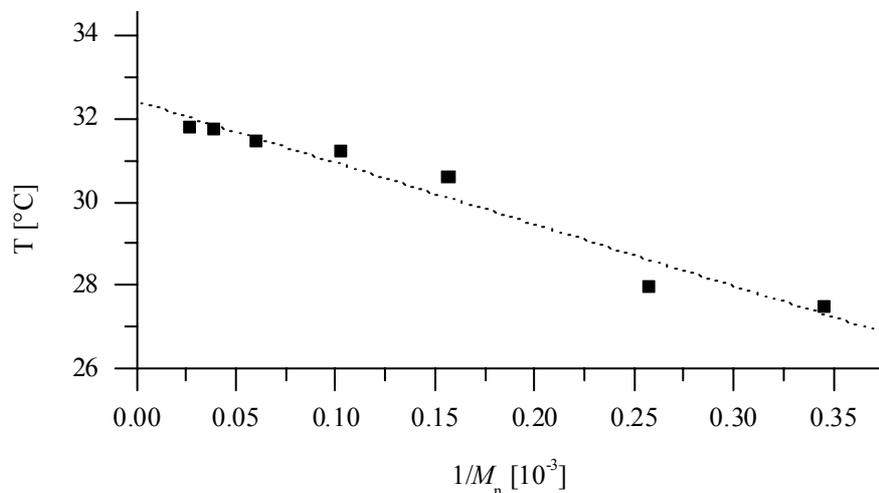

Fig. 5.1.   Dependence of cloud point on inverse molecular weight of PNIPAAm samples.

Fujishige et al.[7] have shown that PNIPAAm samples with molecular weights ranging from 50,000 to 8,400,000 g/mol display the same cloud point. The measurements performed on the RAFT polymers indicate that the cloud point increases with increasing molecular weight. These findings do not necessarily contradict the results obtained by Fujishige as the molecular weights of the RAFT polymers are much lower ($\leq$ 40,000 g/mol) and the samples contain hydrophobic endgroups introduced by the chain transfer agents. Nakahama et al. have reported a similar dependence of LCST on endgroup structure for poly(*N,N*-diethylacrylamide) that agrees well with the result obtained herein.[8]

5.2   Poly(2-vinyl-4,4-dimethyl-5-oxazolone)

Poly(2-vinyl-4,4-dimethyl-5-oxazolone), PVO, undergoes azlactone ring opening in the presence of moisture, which yields the corresponding poly(*N*-carboxy-isopropylidene acrylamide) (structure see Fig. 5.3). In the present work, azlactone ring opening was proven by MALDI-TOF (Fig. 5.2) and IR spectroscopy (Fig. 5.3).

Tab. 5.1 summarizes the masses of the expected MALDI signals for PVO. Samples were cast from THF solution, and dihydroxybenzoic acid (DHB) was used as a matrix.
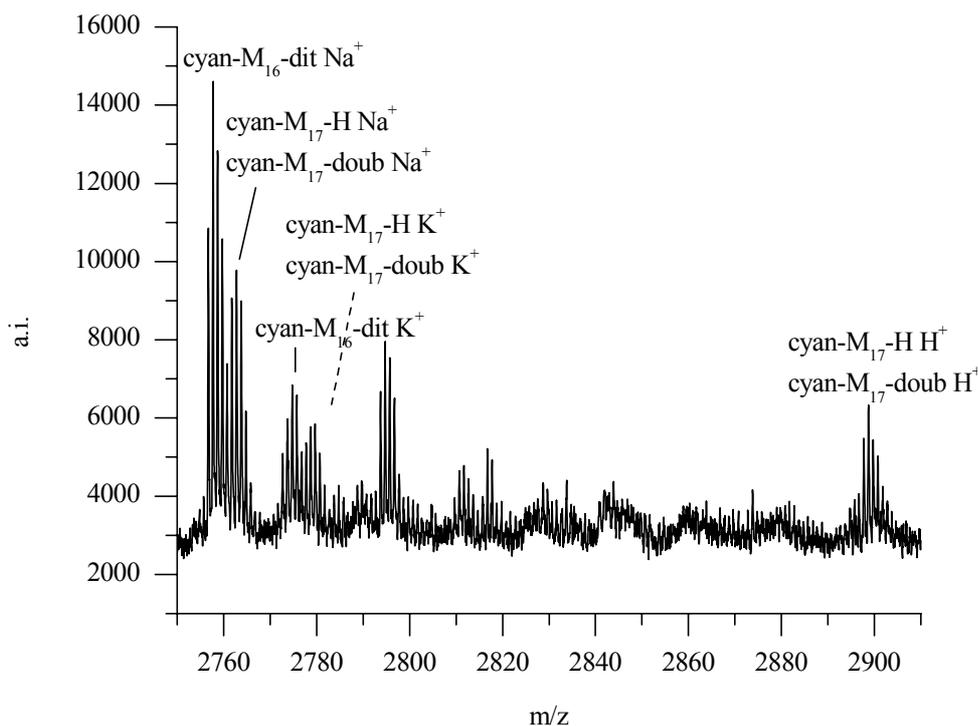
Fig. 5.2.   *MALDI-TOF mass spectrum of hydrolyzed poly(vinyloxazolone); sample cast from THF (cf. Tab. 5.1 for structure assignments).*

Tab. 5.1.   *Masses of expected MALDI signals in the mass range of 2700-2900 g/mol.*

	structure	X		monoisotopic mass
(i) unhydrolyzed PVO				
living	cyan-M_X-dit	19	$C_{144}H_{182}N_{20}O_{38}S_2Na^+$	2886.23
fragmentation (protonation)	cyan-M_X-H	20	$C_{144}H_{187}N_{21}O_{40}Na^+$	2873.31
fragmentation (deprotonation)	cyan-M_X-doub	20	$C_{144}H_{185}N_{21}O_{40}Na^+$	2871.30
(ii) hydrolyzed PVO				
living	cyan-M_X-dit	16	$C_{123}H_{187}N_{17}O_{48}S_2Na^+$	2757.21
fragmentation (protonation)	cyan-M_X-H	17	$C_{123}H_{194}N_{18}O_{51}Na^+$	2762.30
fragmentation (deprotonation)	cyan-M_X-doub	17	$C_{123}H_{192}N_{18}O_{51}Na^+$	2760.29
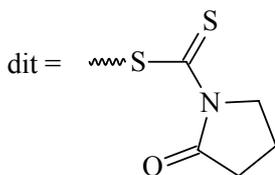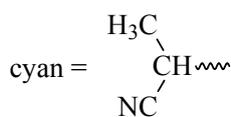
H = hydrogen terminated
doub = double-bond terminated

The MALDI-TOF mass spectrum of a polymer sample stored in air (Fig. 5.2) shows only signals of the hydrolyzed polymer and signals of hydrogen- and double-bond terminated hydrolyzed polymer. The latter two signals are observed with most of the RAFT polymers owing to fragmentation of the thiocarbonylthio moiety during ionization (see chapter 4.2). Care has also to be taken when choosing a matrix for MALDI-TOF analysis. An aprotic matrix was used in order to avoid ring opening by matrix protons.

IR spectroscopy also clearly reveals hydrolysis of the polymer sample stored in air (Fig. 5.3). This is most evident in the strong H···OH band, representing intermolecular hydrogen bonding between the carboxyl groups.
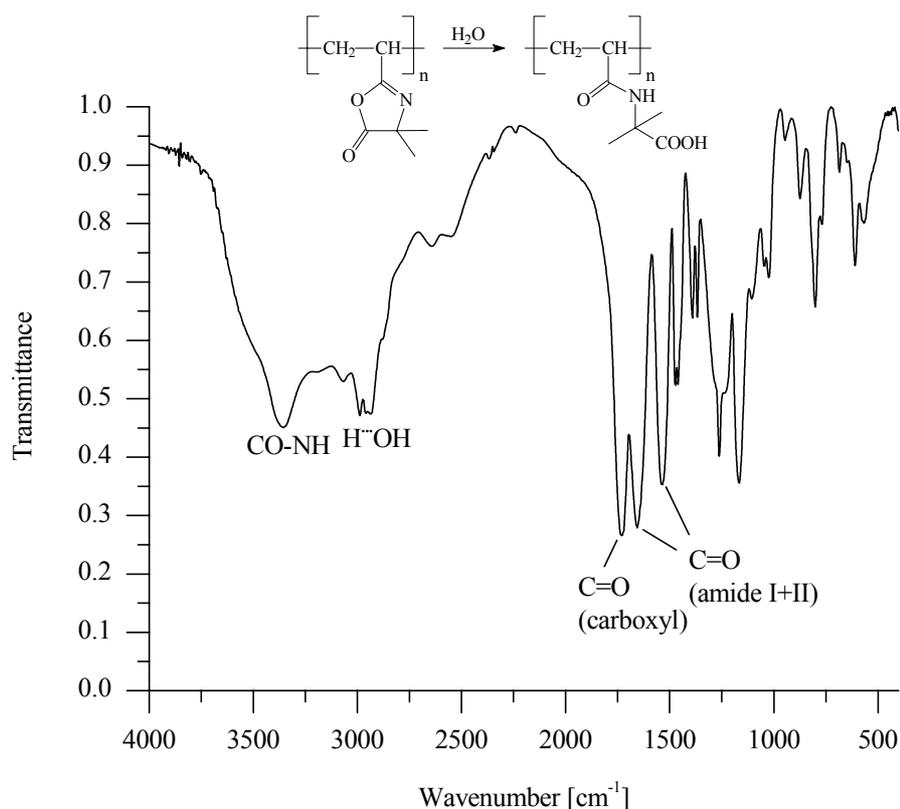
Fig. 5.3.   *FT-IR spectrum of PVO (KBr pellet).*

PVO is a very reactive polymer due to its azlactone ring that reacts readily not only with water but also with other compounds containing active hydrogen atoms, such as alcohols or amines. The synthesis of polymer-peptide conjugates via ring-opening addition of primary amines is demonstrated in chapter 6.

5.3   Poly(*N*-isopropylacrylamide)-*block*-poly(acrylic acid)

The synthesis of block copolymers consisting of poly(acrylic acid) and poly(*N*-isopropylacrylamide), PNIPAAm-*b*-PAA, is of interest for a variety of reasons. First of all, poly(acrylic acid) is a polymer that responds to changes in pH and ionic strength with changes in its properties, e.g. at pH ≤ 4 precipitation occurs in aqueous solutions due to protonation of the carboxylate groups, which renders the polymer sparsely soluble in water. The thermoresponsive behavior of PNIPAAm has already been discussed in section 5.1.1. The combination of pH-responsive PAA and temperature-responsive PNIPAAm creates systems that respond to combined external stimuli. Conjugation of drugs or proteins to PNIPAAm-*b*-PAA generates thermo- and pH-responsive entities that can be addressed through external stimuli.

More importantly, PNIPAAm-*b*-PAA block copolymers may form micelles or other aggregates depending on solvent, temperature, pH, and block lengths (cf. Fig. 5.4).
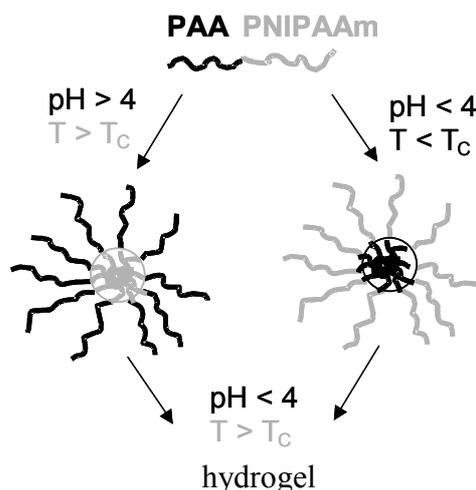
Fig. 5.4.   *Possible modes of aggregate formation for PNIPAAm-b-PAA in aqueous solution in dependence of pH and temperature.*

Polymeric micelles have recently emerged as novel promising carriers for the targeting of poorly water-soluble drugs, and they are considerably more stable than surfactant micelles. Polymeric micelles can solubilize substantial amounts of hydrophobic compounds in their inner core.[9] They have distinct advantages over other carriers, such as small size, high solubility, simple sterilization by filtration, and controlled release of drugs. Due to their hydrophilic shell and small size, they exhibit prolonged circulation times *in vivo*, circumvent host defenses and are able to accumulate in tumor tissues. Polymeric micelles are often compared to naturally occurring carriers, such as viruses or lipoproteins, as they all have a similar core-shell structure that allows their content to be protected while

it is transported to the target cell. While lipoproteins as carriers may also be recognized by healthy cells[10] and viral carriers should not be used for repeated application since they are likely to elicit an immune response,[11] polymeric micelles do not suffer these drawbacks and therefore seem to be one of the most advantageous carriers for the delivery of water-insoluble drugs.

Temperature- or pH-sensitive micelles could eventually be used to confer bioadhesive properties; pH-sensitive micelles might be applied in the drug delivery to tumors, inflamed tissues or endosomal compartments, where a pH lower than in normal tissue is found.[9]

In the following, the characteristics of PNIPAAm-*b*-PAA block copolymers with a fixed AA block length of 110 units and a varying NIPAAm block length of n units is discussed, and polymers will be abbreviated as $(NIPAAm)_n$-*b*-$(AA)_{110}$.

5.3.1   Behavior of PNIPAAm-*b*-PAA in solution

Gel permeation chromatography with DMF as eluent, using universal calibration, was used to evaluate the molecular weights of the block copolymers. The obtained M_n values were about two orders of magnitude higher than the calculated ones (cf. chapter 4). Therefore, it was assumed that some sort of micelle formation takes place. This is not quite expected as DMF should be a good solvent for both the PNIPAAm and the PAA block. In order to prove this assumption, aqueous GPC of the polymer samples was recorded at 25 °C and 60 °C. At 25 °C, only one peak is observed, whereas two peaks were found at 60 °C, namely one in the high-molecular weight region and one at the same elution volume as the peak observed at 25 °C (Fig. 5.5).
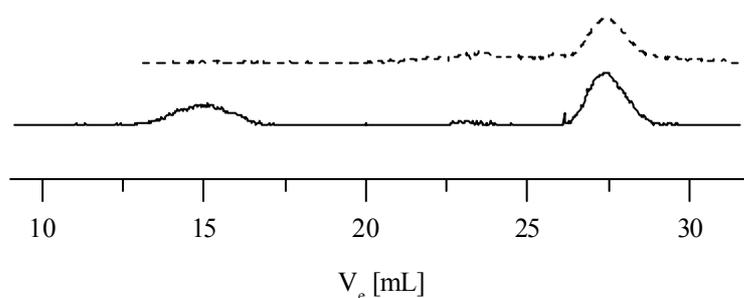

$$V_e \text{ [mL]}$$

Fig. 5.5.   *GPC traces (RI detector) of $(NIPAAm)_{50}$-b-$(AA)_{110}$ at 25 °C (top) and 60 °C (bottom) in water + 0.05 M NaN_3.*

This observation strongly indicates the formation of micelles at 60 °C, which is above the LCST of PNIPAAm. At this temperature, PNIPAAm is insoluble in aqueous solution, and it is assumed that it forms the core of the block copolymer micelle with PAA forming the corona. Micelle formation at elevated temperature was also confirmed by dynamic light

scattering (see section 5.3.3.2). Thus, the peak at lower elution volume in Fig. 5.5 corresponds to micelles.

5.3.2 Temperature-sweep NMR

Due to the high molecular weights of the polymer samples (cf. chapter 4) observed with DMF GPC at 80 °C, ^{1}H-NMR spectroscopy was conducted under the same conditions, namely using d_7-DMF + 0.05 M LiBr as a solvent, in a temperature-sweep experiment varying temperature from 25 °C to 125 °C. The results (Fig. 5.6) indicate aggregation of the block copolymers: The methine proton of the acrylic acid block disappears at temperatures around 328 K and then reappears above 358 K. Thus, in the mid-temperature range, the PAA block is shielded but it is deshielded again at high temperatures.
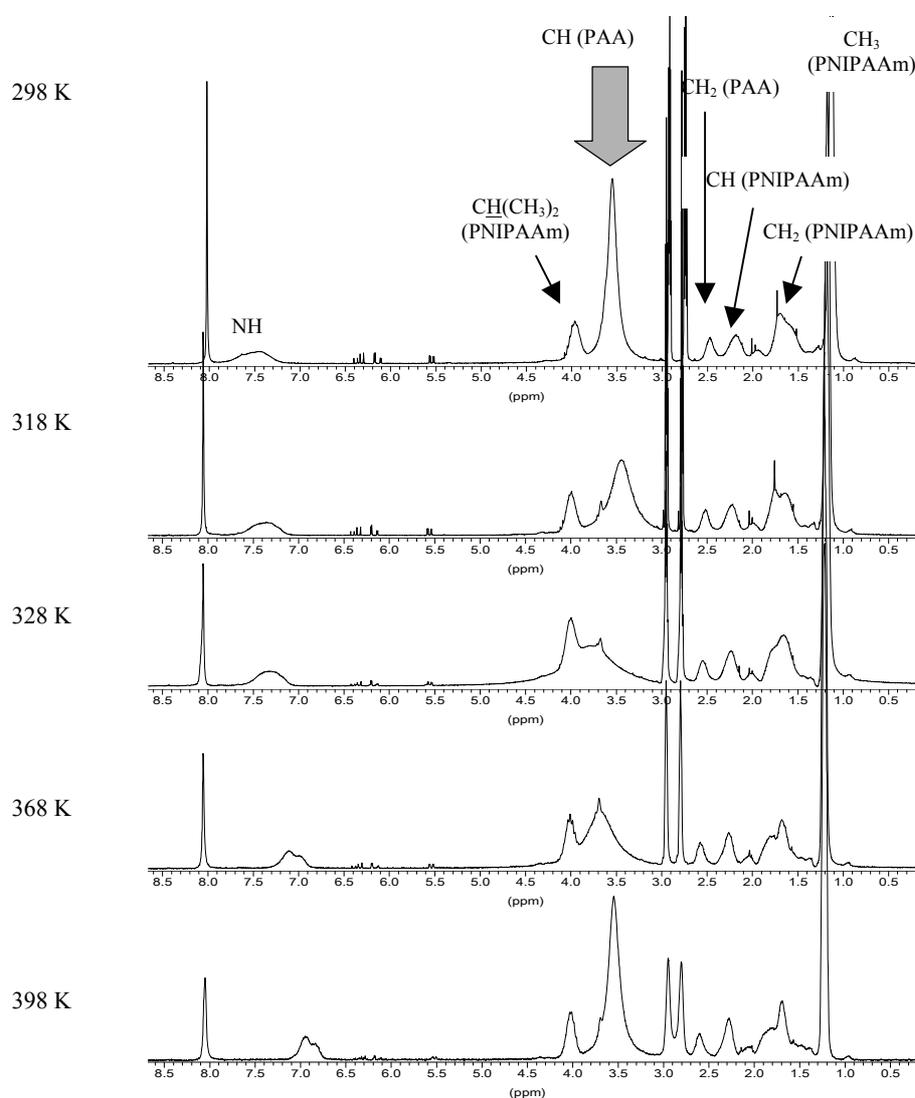
Fig. 5.6. *^{1}H-NMR spectra of (NIPAAm)$_{50}$-b-(AA)$_{110}$ in* d$_7$*-DMF + 0.05 M LiBr at different temperatures.*

At low temperatures, hydrogen bonds between PNIPAAm and PAA prevail and the block copolymer is dissolved molecularly. The degree of hydrogen bonding decreases with increasing temperature. The disappearance of the acrylic acid proton signals at elevated temperature may be attributed to the formation of micelles with PAA forming the core and PNIPAAm forming the corona. At temperatures above 358 K, thermal motion leads to disaggregation of the micelles, which is manifested in the reappearance of the acrylic acid signals.

The upfield shift of the NH proton with temperature from 7.5 to 7.0 ppm is not unusual as the degree of hydrogen bonding decreases with increasing temperature.

5.3.3   Investigation of micelle structure
5.3.3.1   Turbidimetry measurements

The combination of pH-responsive poly(acrylic acid), PAA, and thermoresponsive poly(*N*-isopropylacrylamide), PNIPAAm, in a block copolymer leads to a system that responds to both pH and temperature. The solubility of the PAA block in aqueous solutions depends on the pH value of the medium. The lower the pH value, the more carboxylate groups of the PAA blocks are protonated and the less soluble this block gets in aqueous media. At high pH values, virtually all carboxylate groups are deprotonated, and the PAA segment is readily soluble in water. From the PNIPAAm point of view, its LCST is altered through the attachment of acrylic acid chains and it is expected to be raised if the acrylic acid block is hydrophilic and lowered if the acrylic acid block is hydrophobic. In some cases, LCST behavior can even be lost if the length of the acrylic acid block is too large.[12]

The influence of different pH values on the cloud point, T_c, was investigated on 0.2 wt.-% buffered aqueous solutions with pH values ranging from 7 to 4.5. For pH values 5.0-7.0, 0.1 M phosphate buffer and for pH 4.5-5.0, 0.1 M citrate buffer was used. No influence of the type of buffer (phosphate or citrate buffer) on the appearance of the turbidimetric curves was found so that small differences in ionic strength owing to the different buffer systems can be neglected.

Fig. 5.7 shows the turbidimetric curves of PNIPAAm-*b*-PAA at different pH values. From the figure, it becomes obvious that the transmission decreases only slightly at pH values 5.0-7.0 when the temperature is raised above the LCST of PNIPAAm. This suggests the presence of micelles with PNIPAAm forming the micellar core at $T > T_c$ and PAA forming the corona. Dynamic light scattering confirms these findings (see following section). Transmission decreases to 0 % at pH 4.5 when the temperature is raised above T_c, indicating the formation of a gel or larger aggregates due to increasing insolubility of the protonated PAA corona. Consequently, the formation of this type of micelles is dependent on both pH and temperature. Such a doubly-responsive behavior in aqueous media has also

been described by Armes et al. and by Laschewsky et al. for the system poly(2-diethylaminoethyl methacrylate)-*block*-poly(propylene oxide) and poly(2-[*N*-(3-methacryl-amidopropyl)-*N*,*N*-dimethyl]ammoniopropane sulfonate)-*block*-poly(*N*-isopropylacryl-amide), respectively,[13,14]
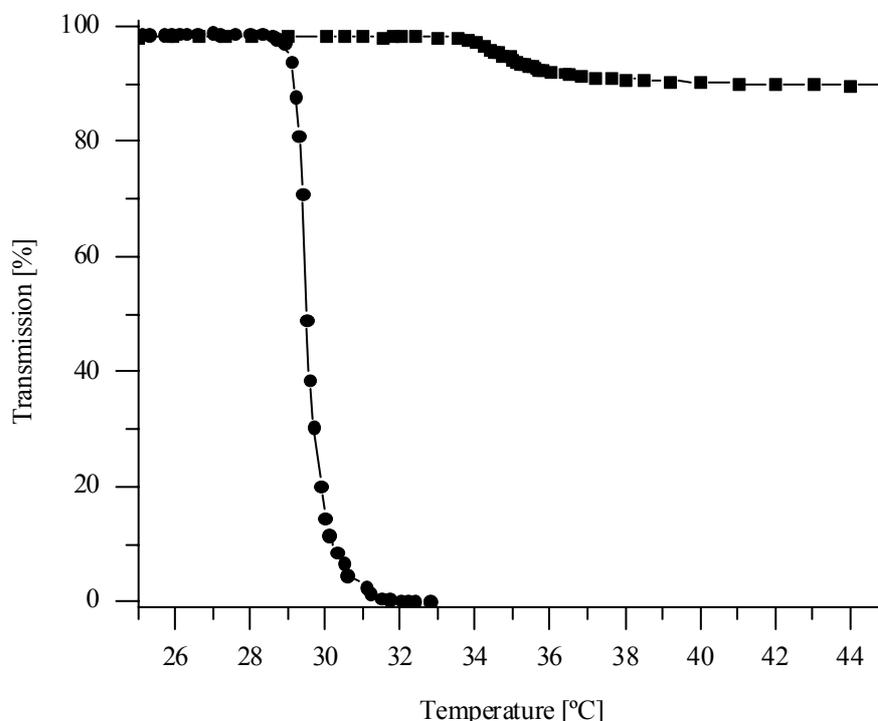

Fig. 5.7.   *Turbidimetry of buffered aqueous solutions of (NIPAAm)$_{50}$-b-(AA)$_{110}$; (●) pH 4.5, (■) pH 5-7.*

Fig. 5.7 also shows that the LCST of PNIPAAm is raised to ca. 35 °C at pH 5-7, whereas it is slightly lowered at pH 4.5 and amounts to ca. 29 °C. This is due to acrylic acid segments that are hydrophilic at pH 5-7 and thereby increase the LCST with respect to the value of 32 °C for the pure homopolymer, but the acrylic acid segments are relatively hydrophobic at pH 4.5 due to protonation of the carboxylate groups, which decreases the LCST.

5.3.3.2   *Dynamic light scattering*

Dynamic light scattering, DLS, was performed on buffered aqueous solutions of PNIPAAm-*b*-PAA of pH 5.6 at different temperatures. At 20 °C $\leq T \leq$ 35 °C, three peaks are found in the distribution function (Fig. 5.8a), which are believed to correspond to unimers, aggregates, and larger aggregates. Aggregate formation was confirmed by Raman and IR spectroscopy (see subsequent section).
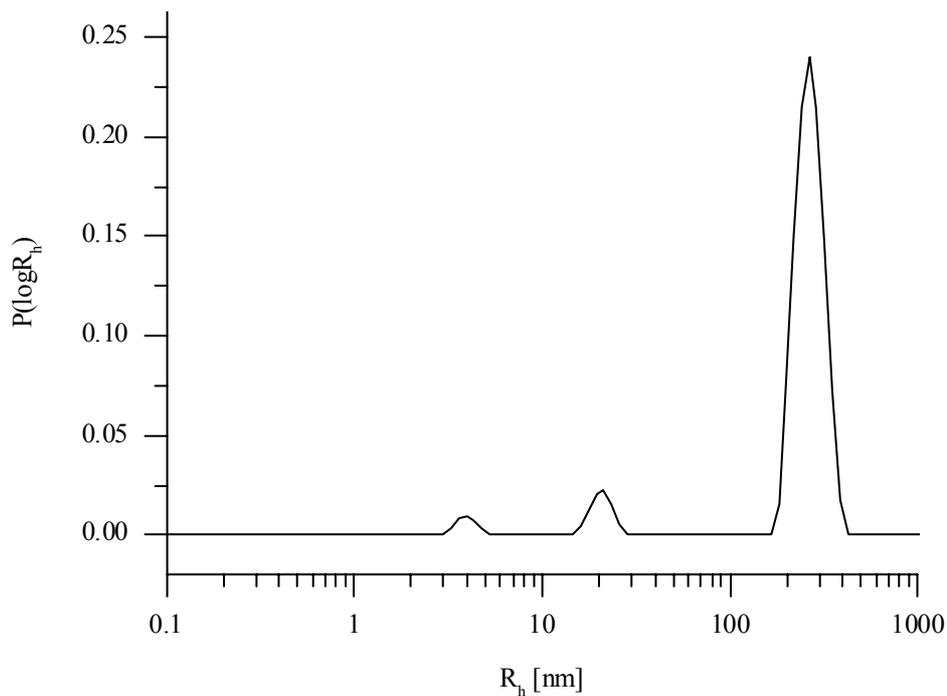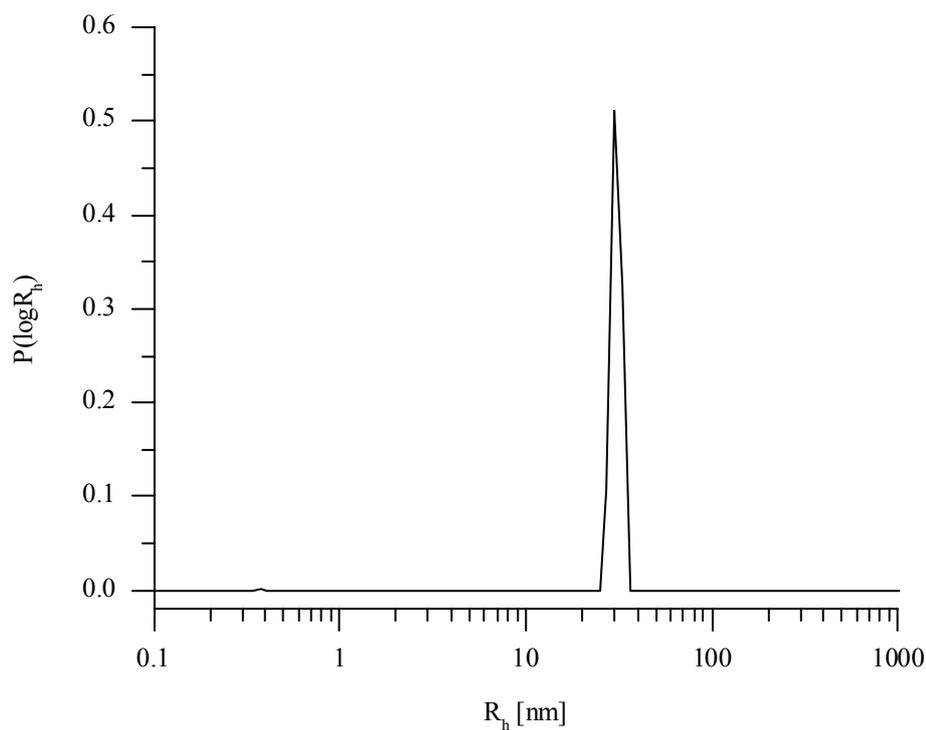
Fig. 5.8a.   *Hydrodynamic radii distribution of $(NIPAAm)_{74}$-b-$(AA)_{110}$ in 0.1 M phosphate buffer pH 5.6 (CONTIN analysis of the field correlation function $g_2(t)$-1); $\theta = 30°$, 20 °C $\leq$ T $\leq$ 35 °C.*

Fig. 5.8b.   *Hydrodynamic radii distribution of $(NIPAAm)_{74}$-b-$(AA)_{110}$ in 0.1 M phosphate buffer pH 5.6 (CONTIN analysis of the field correlation function $g_2(t)$-1); $\theta = 30°$, T = 50 °C.*

At $T \geq 42 °C$, which is above the LCST of PNIPAAm, results indicate the coexistence of micelles and unimers. Micelles with hydrophobic PNIPAAm constituting the micellar core and PAA forming the corona are most likely. A slight decrease in micellar size from 42 °C to 50 °C is observed, which is attributed to shrinking of the expanded PNIPAAm core upon heating to higher temperatures. At 50 °C, only micelles are found (Fig. 5.8b).

5.3.3.3   *Raman and IR spectroscopy*

DLS suggests the formation of aggregates at room temperature as the hydrodynamic radii of the particles are smaller than those of the micelles observed at higher temperature but too large for unimers. In the literature, hydrogen-bonded interpolymer complexes between poly(acrylic acid) and poly(acrylamide) derivatives have been reported, where acrylamide acts as a strong hydrogen acceptor and acrylic acid provides hydrogen for binding.[15,16] Taking into consideration these findings, it can be assumed that intermolecular hydrogen bonding takes place between PAA and PNIPAAm. In order to prove hydrogen bonding between amide and carboxylic acid, Shibanuma et al. applied FT-IR spectroscopy using the ATR (attenuated total reflectance) technique that allows for measurement in aqueous solutions.[6,16] In this work, Raman spectroscopy was considered as a substitute for the ATR technique. One of the advantages of Raman spectroscopy is that water can be used as a solvent, which is almost impossible in IR spectroscopy due to the strong absorption of water, requiring the use of special techniques, such as ATR. Raman spectroscopy is usually best suited for the characterization of non-polar or only slightly polar bonds. The strong and characteristic IR bands of polar groups, such as C=O or O-H, are usually reduced in the Raman spectra so that relatively weak carbonyl stretching bands are expected.[17]

Fig. 5.9 shows the Raman spectrum obtained for a 2 wt.-% solution of PNIPAAm-*b*-PAA in citrate buffer pH 5.6 along with that of a 2 wt.-% aqueous PNIPAAm solution for comparison. In order to eliminate buffer signals, pure 0.1 M citrate buffer was recorded and the spectrum was subtracted from the Raman spectrum of the block copolymer.

The carbonyl and amide stretching bands in the Raman spectrum appear at a somewhat lower wavenumber as compared to IR spectroscopy. The respective stretching bands are relatively weak, as was expected for a polar group in Raman spectroscopy. Comparing the spectrum of the homopolymer PNIPAAm with the block copolymer PNIPAAm-*b*-PAA, the bands at 1556 and 1613 cm^{-1} in the PNIPAAm spectrum were attributed to amide stretching, which is found at 1556 and 1616 cm^{-1} in the block copolymer spectrum. The band at 1682 cm^{-1} arises from carbonyl stretching of the acrylic acid carboxyl groups in PNIPAAm-*b*-PAA. On comparison of the stretching bands in the PNIPAAm and PNIPAAm-*b*-PAA spectra, it is evident that the stretching bands in the block copolymer

spectrum are broadened with respect to the PNIPAAm spectrum. This is an indication for some complexation or hydrogen bonding taking place between the two blocks. Such a broadening of stretching bands due to cooperative H···O interactions has also been observed by other authors.[18]
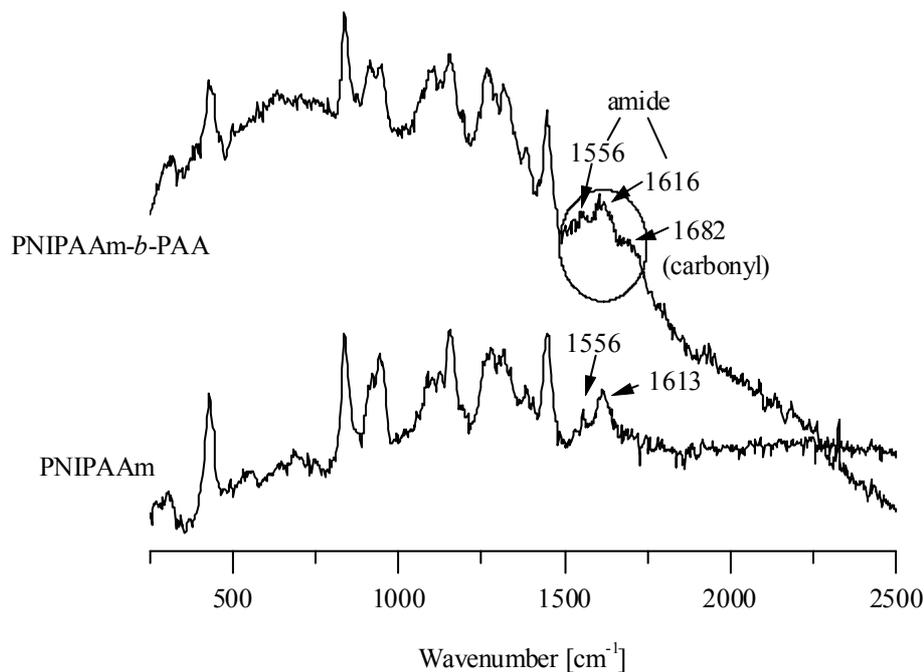

Fig. 5.9.   *Raman spectra of aqueous solutions of (NIPAAm)$_{137}$-b-(AA)$_{110}$ and PNIPAAm.*

In order to exclude that broadening in the Raman spectra has an origin other than hydrogen bonding, IR spectroscopy was used on block copolymer samples that were cast on calcium fluoride plates from 2 wt.-% aqueous phosphate-buffered solutions. Fig. 5.10 shows an exemplary IR spectrum with those of the homopolymers for comparison. On comparison of the different spectra, a splitting of the amide stretching band in PNIPAAm-*b*-PAA is evident and the band is shifted to lower wavenumbers, whereas the split carbonyl stretching band of the block copolymer is shifted to higher wavenumbers with respect to the homopolymer spectra. These observations agree with those reported in the literature for hydrogen bonding between acrylic acid and acrylamides.[16] The carbonyl stretching band in the PAA homopolymer spectrum is already somewhat split due to partial hydrogen bonds between the carboxylic acid groups. This also agrees with results reported in the literature.[16]
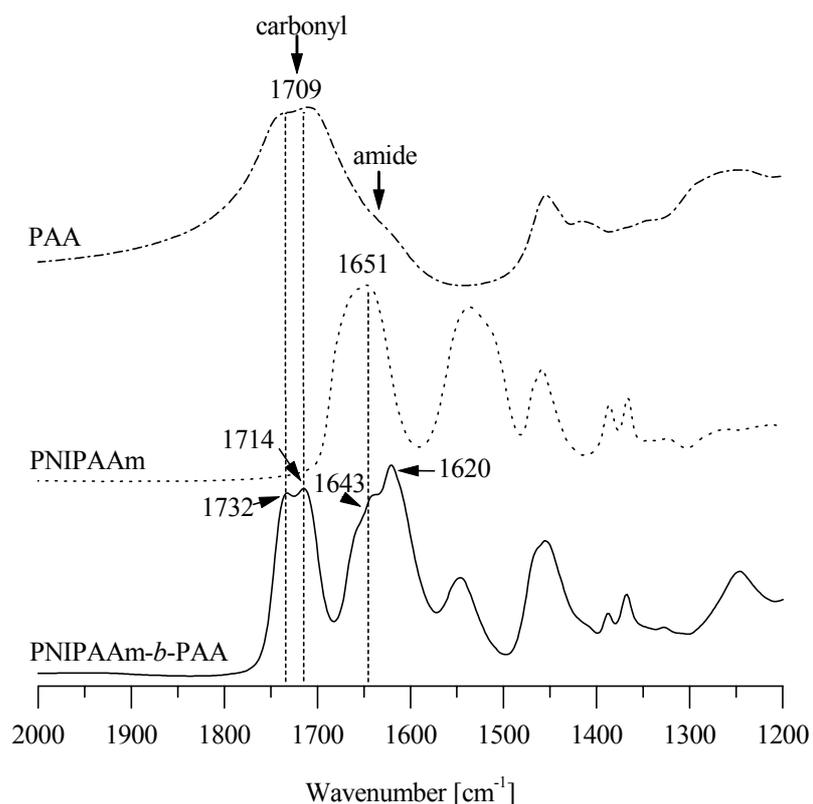
Fig. 5.10. *IR spectrum of (NIPAAm)*$_{137}$*-b-(AA)*$_{110}$ *with spectra of the homopolymers PNIPAAm and PAA for comparison.*

In conclusion, interpolymer hydrogen bonding in PNIPAAm-*b*-PAA leads to the formation of aggregates at room temperature. Micelles are formed at temperatures above ca. 40 °C with PNIPAAm forming the micellar core and PAA constituting the corona.

5.3.3.4 *Cryogenic transmission electron microscopy*

Dynamic light scattering as well as Raman and IR spectroscopy indicate aggregate formation of PNIPAAm-*b*-PAA in buffered aqueous solutions. In order to further investigate the structures in solution, cryogenic transmission electron microscopy (cryoTEM) measurements were performed on PNIPAAm-*b*-PAA solutions of pH 4.5 and pH 5.6 at 20 °C and 45 °C. These temperatures were chosen to study the solutions below and above the LCST of PNIPAAm. Sample preparation is described in the experimental section (chapter 7).

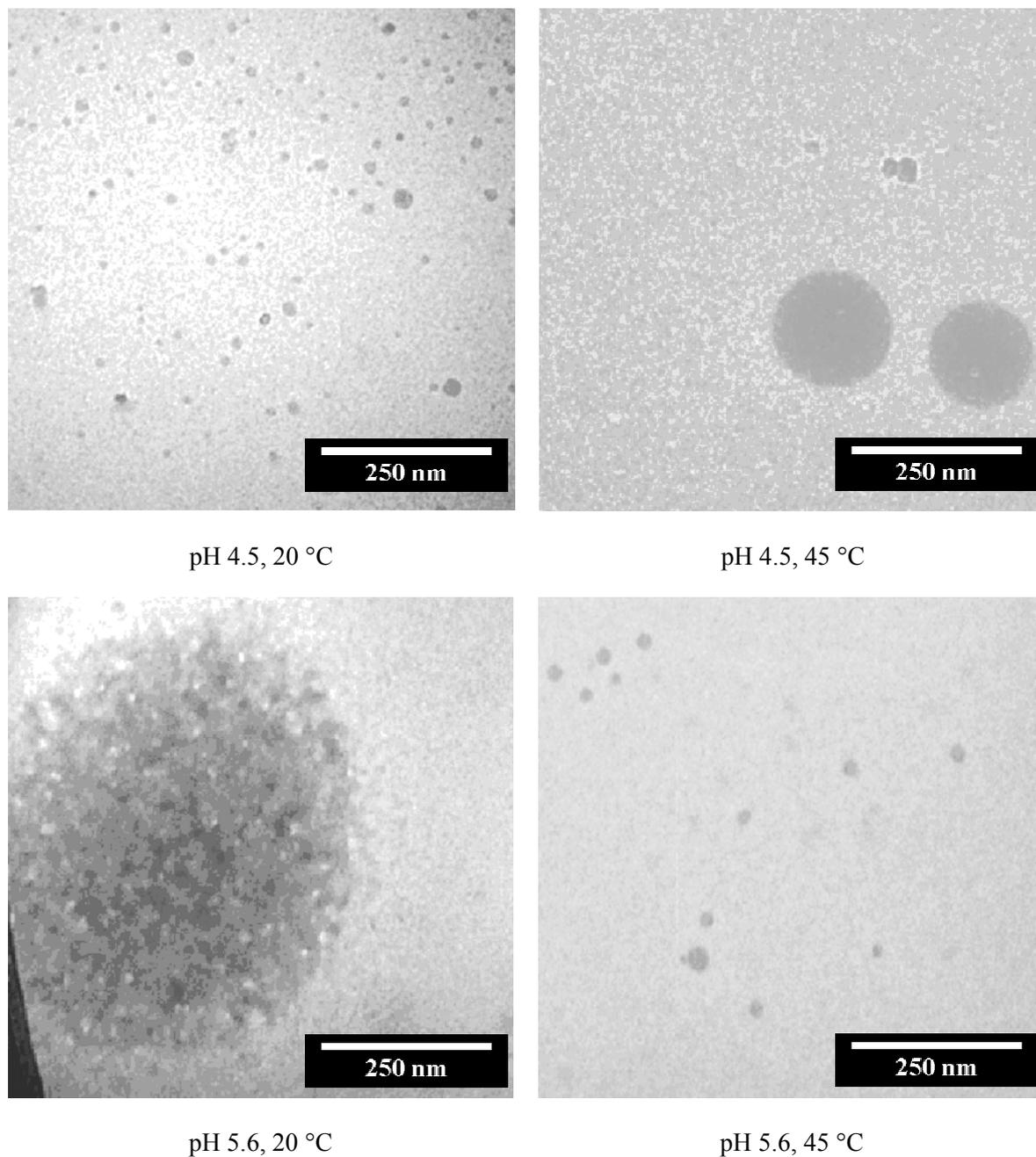Fig. 5.11 shows the cryoTEM images at different pH values and temperatures.

pH 4.5, 20 °C   pH 4.5, 45 °C

pH 5.6, 20 °C   pH 5.6, 45 °C

Fig. 5.11.   CryoTEM images for (NIPAAm)$_{74}$-b-(AA)$_{110}$ cast from buffered aqueous solutions of pH 4.5 or pH 5.6, respectively, at temperatures below and above LCST of PNIPAAm.

The transmission electron micrograph at pH 4.5 and 20 °C shows particles of diameters in the range of 10-30 nm. Due to poor electron scattering from the particles, resulting in a low contrast, the existence of small block copolymer particles cannot be excluded. At pH 4.5 and 45 °C, the formation of large particles is seen in the micrographs (the smaller species above are ice crystals). These have been assigned to aggregates and their diameters are about 130 nm. It is obvious that no hydrogel formation takes place as it was anticipated

due to the insolubility of both PNIPAAm and PAA at high temperature and low pH values, respectively. Hydrogel formation may require a higher concentration than that of 2 wt.-%, which was used for the block copolymer solutions.

The transmission electron micrograph at pH 5.6 and 20 °C shows large aggregates and barely visible, smaller particles, confirming the DLS results that indicated particles of three different sizes. The smallest particles observed in the DLS studies are invisible due to lack of sufficient contrast in the images. At pH 5.6 and 45 °C, aggregates of diameters in the range of 10-30 nm are observed. This is in good agreement with DLS measurements, where a coexistence of micelles and unimers was found. Again, small particles, i.e. unimers, are not detected due to the low contrast.

5.3.4   Tensiometry

The results of dynamic light scattering and cryogenic transmission electron microscopy indicate that PNIPAAm-b-PAA forms aggregates in (buffered) aqueous solutions at room temperature. In order to determine the critical aggregate concentration (cac), surface tension was measured at different concentrations on buffered aqueous block copolymer solutions at different pH values. Block copolymers $(NIPAAm)_n$-b-$(AA)_m$ of varying PNIPAAm block length (n = 57, 74, 137) were used with a constant PAA block length of m = 110. Tab. 5.12 summarizes the molecular characteristics of the used block copolymers and the abbreviations used throughout the text.

Tab. 5.12.   *Molecular characteristics of the $(NIPAAm)_n$-b-$(AA)_{110}$ blocks used for tensiometric measurements.*

entry	M_n [a)] [g/mol]	n	abbrev.
1	23,400	137	n137
2	16,300	74	n74
3	14,300	57	n57

[a)] determined by MALDI-TOF

Fig. 5.13 shows the plots of surface tension σ versus log c for $(NIPAAm)_{74}$-b-$(AA)_{110}$ at different pH values. The figure shows two different curves around the critical aggregate concentration (cac). The left curve (c < cac) is approximated by a tangent fitted to the steepest part, and the right curve (c > cac) is approximated by a straight line. The point of intersection of the two fittings is the critical aggregate concentration (cac).
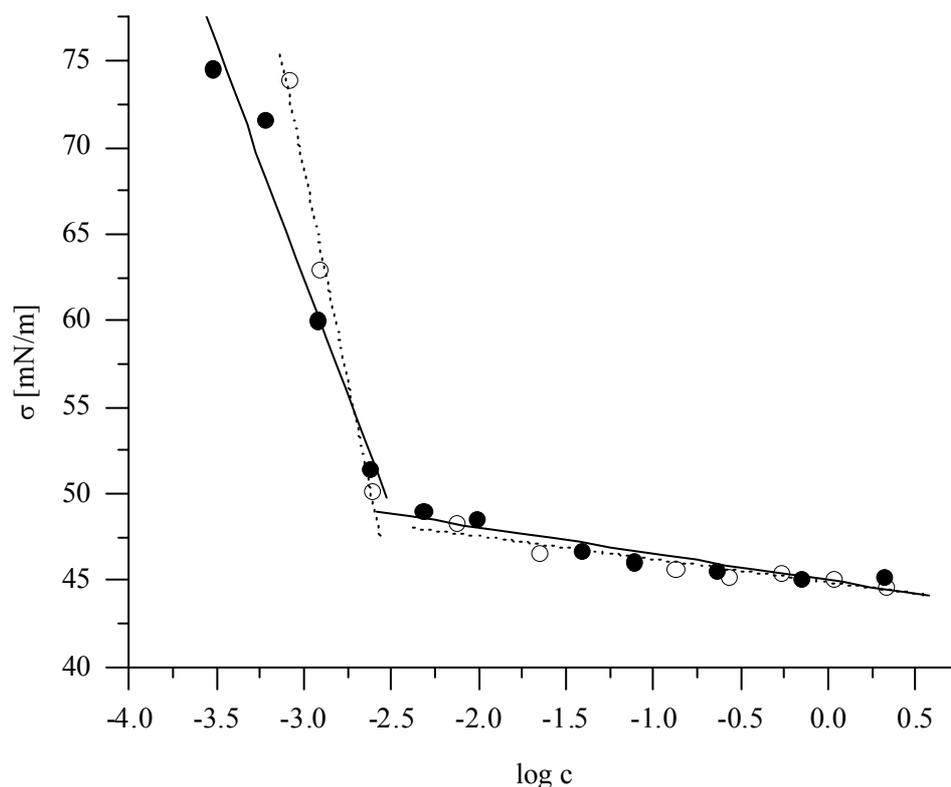
Fig. 5.13. Plot of surface tension versus log c for $(NIPAAm)_{74}$-b-$(AA)_{110}$ at (●) pH 4.5 and (○) pH 5.6.

Tab. 5.2 shows the cac values for the block copolymers.

Tab. 5.2. *Critical aggregate concentration, cac, for $(NIPAAm)_n$-b-$(AA)_{110}$ block copolymers in 0.1 M citrate buffer at pH 4.5 and pH 5.6, respectively.*

sample	pH	log c	cac [mg/mL]·10^3	cac [mol/L]·10^7
n137	5.6	-2.54	2.88	1.23
	4.5	-2.52	3.02	1.29
n74	5.6	-2.58	2.63	1.61
	4.5	-2.49	3.24	1.99
n57	5.6	-2.24	5.75	4.02
	4.5	-2.00	10.0	6.99

The critical aggregate concentration increases with decreasing pH and is highest for the block copolymer with the shortest PNIPAAm segment (n57). Consequently, formation of aggregates via hydrogen bonding interactions is more favored in the block copolymers with a low PNIPAAm fraction. This is in part the result of pH-dependent ionization of carboxylic acid groups of the PAA segments, which will be discussed further in the next section.

5.3.5   Potentiometric titrations

The PNIPAAm-*b*-PAA block copolymers readily dissolve in water under alkaline conditions. The pH of the aqueous solutions influences the conformation of PAA due to ionization and repulsion between the carboxylate groups.

Potentiometric titrations were performed using 0.1 M aqueous NaCl solutions under alkaline conditions and titrating with 0.01 M HCl. The addition of salt was necessary to stabilize the block copolymer solutions. An experiment without NaCl led to large variations in the measured pH on titration with acid, even after a sufficient equilibration time. Evaluation of the titration curves allows for determination of the molar fraction of acrylic acid in the block copolymers, the degree of neutralization, and the apparent dissociation constant.

Fig. 5.14 shows the titration curves for block copolymers (NIPAAm)$_n$-*b*-(AA)$_{110}$ with n = 57, 74, and 137.
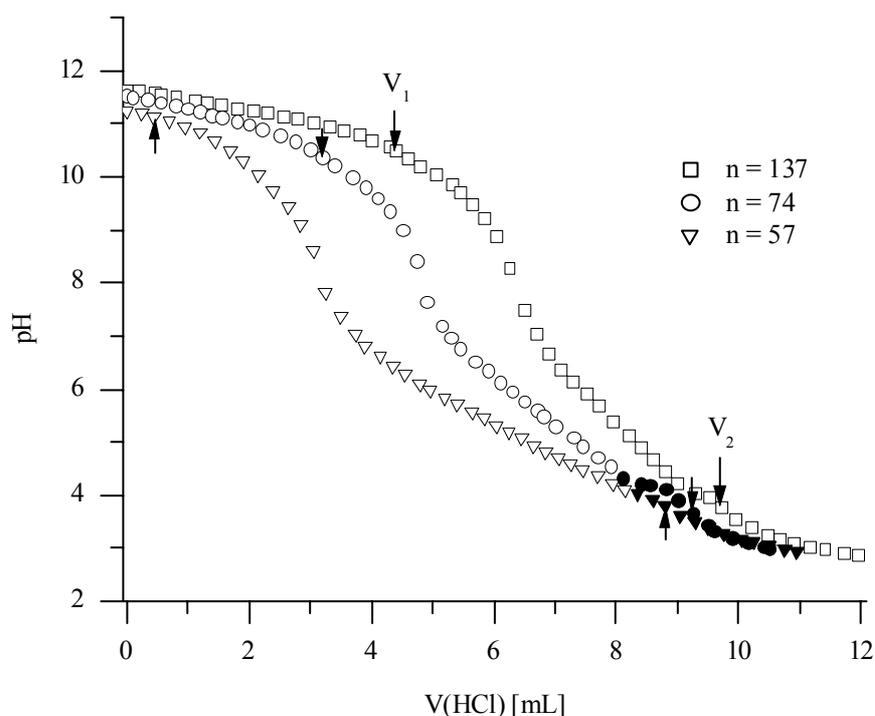
Fig. 5.14.   *Titration curves for (NIPAAm)$_n$-b-(AA)$_{110}$ with n = 57, 74, and 137; filled symbols indicate precipitation of polymer.*

The titration process can be divided into three steps: first, excess NaOH is neutralized until volume V_1, followed by neutralization of acrylic acid until V_2, and finally, further decrease of pH is attributable to the increasing concentration of HCl. The volumes V_1 and V_2 were determined from the first derivatives of the titration curves. The block copolymers with high content of acrylic acid (PNIPAAm block length n = 57 and 74) precipitate at pH values around 4 due to increasing insolubility of protonated acrylic acid and the relatively

short PNIPAAm block length that is not sufficient to keep the block copolymers in solution.

The molar fraction of acrylic acid units, x_{AA}, in the block copolymer is calculated according to Eq. 5.1:

$$x_{AA} = \frac{w_{AA}}{w_{AA} + (1 - w_{AA})\dfrac{M_{AA}}{M_{NIPAAm}}} \qquad \text{Eq. 5.1}$$

where M_{AA} and M_{NIPAAm} are the molecular weights of acrylic acid and NIPAAm monomers, respectively, and w_{AA} is the weight fraction of acrylic acid. The latter is given by Eq. 5.2:

$$w_{AA} = \frac{m_{AA}}{m_P} \qquad \text{Eq. 5.2}$$

where m_P = total weight of block copolymer and m_{AA} = weight of acrylic acid. This is calculated according to Eq. 5.3:

$$m_{AA} = c(HCl) \cdot (V_2 - V_1) \cdot M_{AA} \qquad \text{Eq. 5.3}$$

V_1 and V_2 are depicted in Fig. 5.14, $(V_2\text{-}V_1)$ corresponds to the volume of HCl needed to fully protonate acrylic acid, and $M_{AA} = 72$ g/mol.

The degree of ionization, α, is calculated from the ratio of the effective concentration of added HCl, $c(HCl)$, to the monomeric concentration of polymer chains, $c(M)$ (Eq. 5.4).

$$\alpha = \frac{c(HCl)}{c(M)} = \frac{c(HCl) \cdot (V - V_1) \cdot M_{AA}}{m_{AA}} \qquad \text{Eq. 5.4}$$

where V = volume of added HCl at any point during titration between V_1 and V_2.

Fig. 5.15 shows the plot of pH versus degree of ionization α.

The pH value of a weak polyacid is given by Eq. 5.5[19,20]:

$$pH = pK_{a,app} + \log\left(\frac{\alpha}{1 - \alpha}\right) \qquad \text{Eq. 5.5}$$

where $pK_{a,app}$ is the negative logarithm of the effective, α-dependent dissociation constant $K_{a,app}$. Eq. 5.5 can be transformed into Eq. 5.6, which is used to calculate the apparent $pK_{a,app}$ for a given α value:

$$pK_{a,app} = pH + \log\left(\frac{1 - \alpha}{\alpha}\right) \qquad \text{Eq. 5.6}$$

As is seen from Eq. 5.6, $pK_{a,app}$ equals pH at $\alpha = 0.5$. The $pK_{a,app}$ values at $\alpha = 0.5$ can be read from Fig. 5.15 and are included in Tab. 5.3.
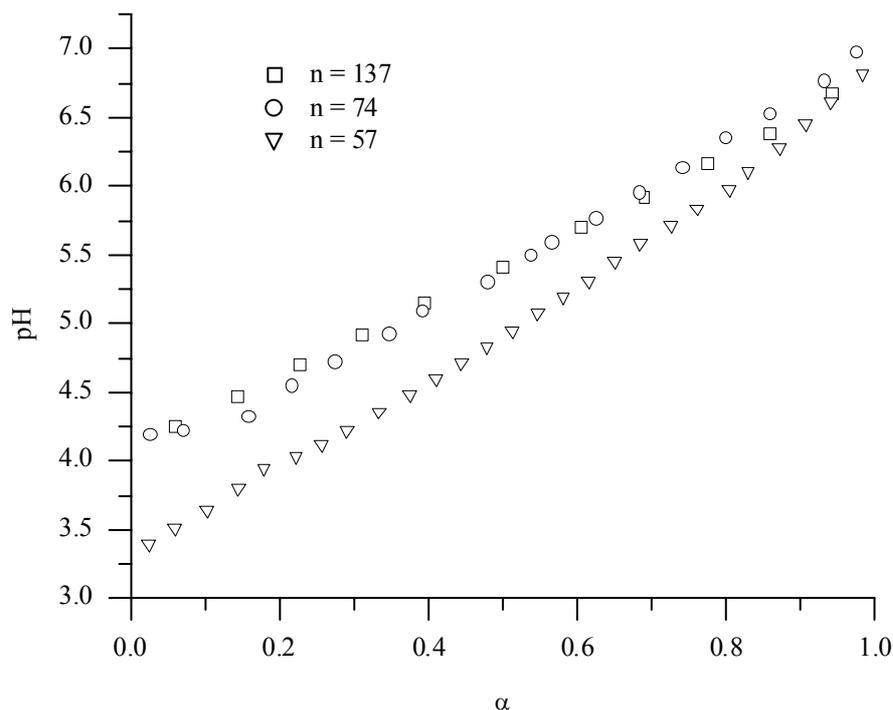
Fig. 5.15. *Plot of pH versus degree of ionization, α, for (NIPAAm)$_n$-b-(AA)$_{110}$.*

Tab. 5.3 summarizes the results derived from potentiometric titration of different PNIPAAm-*b*-PAA block copolymers and compares the experimental molar fractions of acrylic acid with those deduced from MALDI-TOF mass spectrometry.

Tab. 5.3. *Results obtained from potentiometric titrations of aqueous solutions of (NIPAAm)$_n$-b-(AA)$_{110}$.*

n	V_1 [mL]	V_2 [mL]	$x_{AA,titr}$	$x_{AA,MALDI}$	p$K_{a,app}$
57	0.45	8.83	0.59	0.65	4.89
74	3.22	9.27	0.51	0.59	5.40
137	4.40	9.71	0.42	0.44	5.41

Molar fractions of acrylic acid obtained by titration ($x_{AA,titr}$) and MALDI-TOF analysis ($x_{AA,MALDI}$) agree relatively well with each other and confirm the molecular weights determined by MALDI. The pK_a values at $\alpha = 0.5$ increase with decreasing molar fraction of acrylic acid, i.e. from PNIPAAm block lengths n = 57 to n = 137 (Tab. 5.3). This means that the ionization of carboxylic acid groups in block copolymers with high NIPAAm fraction (e.g. n = 137) proceeds at higher pH values as compared to copolymers of relatively low NIPAAm fraction (n = 57). The result can be explained in terms of formation of hydrophobic domains between several acrylic acid segments, rendering the carboxylic acid groups less accessible for ionization. In other words, acrylic acid is a stronger acid in block copolymers with low NIPAAm fractions.

5.3.6   Differential scanning calorimetry (DSC)

In order to investigate the mixing behavior of the two blocks in the solid phase, differential scanning calorimetry (DSC) was performed on the block copolymer and homopolymer samples. Fig. 5.16 shows the DSC traces for the homopolymers PNIPAAm and PAA as well as for PNIPAAm-*b*-PAA with block lengths of 110 and 50 repeating units for PAA and PNIPAAm, respectively.
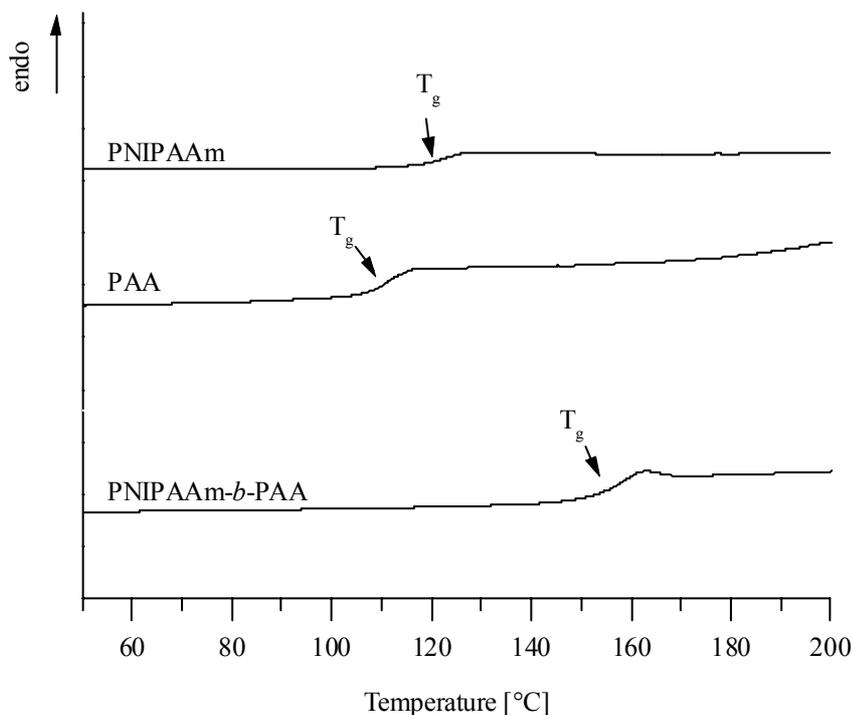

Fig. 5.16.   DSC heating curves for homopolymers and block copolymer (NIPAAm)₅₀-b-(AA)₁₁₀ at a heating rate of 10 K/min, second heating curves are displayed.

The glass transition temperature, T_g, of the homopolymer PNIPAAm was determined as 124 °C (literature value 130 °C[21]) and that of the homopolymer PAA was 112 °C (literature value 106 °C[22]).

For phase-separated block copolymers, two different T_gs are expected, whereas non-phase-separated block copolymers display a single T_g that is between the two homopolymer T_g values. In the present case, only one T_g value for the block copolymer is observed but it is much higher than those of the homopolymers and amounts to 156 °C for (NIPAAm)$_{50}$-*b*-(AA)$_{110}$. This is attributed to the additional amount of PAA carboxyl groups forming hydrogen bonds with PNIPAAm amide groups, which increases the T_g values. These findings are consistent with observations reported in the literature, where random copolymers of NIPAAm and AA showed a considerable increase of T_g with an increasing molar fraction of acrylic acid in the copolymer.[4] Furthermore, the difference

between onset and endset of the glass transition process, ΔT_g, increases with increasing number of molecular interactions. ΔT_g reflects the number of relaxation processes associated with glass transition. If the system contains microenvironments that are caused by dipole-dipole interactions or hydrogen bonding, it should undergo relaxation processes with different relaxation times, leading to a broadening of glass transition. Therefore, in a system that is characterized by strong hydrogen interactions between the components, ΔT_g higher than that of pure polymer is expected.[23] Indeed, while ΔT_g is 15.5 °C for PNIPAAm and 13.8 °C for PAA, the block copolymer shows a ΔT_g value of 23.0 °C, again a strong indication for hydrogen bonding, which has also been confirmed by Raman and IR spectroscopy (see section 5.1.3.3) The "overshoot" in the DSC trace (a small hump is found for the block copolymer) is caused by enthalpy relaxation of the glassy polymer.[24]

5.4 Poly(*N*-isopropylacrylamide)-*block*-poly(2-vinyl-4,4-dimethyl-5-oxazolone)

Block copolymers consisting of poly(*N*-isopropylacrylamide) and poly(2-vinyl-4,4-dimethyl-5-oxazolone), PNIPAAm-*b*-PVO, represent thermoresponsive systems with active ester blocks. These are especially attractive for conjugation to peptides, proteins or drugs via primary amino groups that react readily with the reactive azlactone ring of PVO (see chapter 6). Beside imparting thermoresponsive properties on the entire block copolymer, PNIPAAm also solubilizes the active ester blocks or rather the molecules conjugated to them, which is an important issue in drug delivery where hydrophobic targets have to be solubilized. At the same time, the LCST of the block copolymer system depends on the polarity of the second block, e.g. attachment of hydrophilic functionalities raises the LCST and hydrophobic moieties lower it.

In the course of this work, it was shown that the block copolymerization of PNIPAAm and PVO using the RAFT technique leads to well-defined block copolymers with narrow molecular weight distributions and a distinct number of active ester blocks. These new block copolymers enable attachment of a precise number of target molecules, such as drugs, and ensures distinct retention times of drug-conjugates in the body. If large molecules, such as proteins, are used for conjugation, only one molecule per copolymer chain may be attached due to steric constraints.

In view of the LCST behavior of PNIPAAm, it was of interest to investigate its LCST in the block copolymer. Cloud point measurements were performed on 0.25 wt.-% aqueous solutions of PNIPAAm-*b*-PVO with a PNIPAAm block length n of 32 or 39 repeating

units, respectively, and a constant PVO block length of 16 repeating units. These will be abbreviated as $(NIPAAm)_n$-b-$(VO)_{16}$ in the following. Fig. 5.17 shows the results of the turbidimetry experiments. The cloud point curves of the two block copolymers are identical, which confirms the expectations as the PNIPAAm block lengths are not very much different from each other. It is evident that the LCST of PNIPAAm-b-PVO is higher than that of the PNIPAAm homopolymer (32 °C) and it amounts to ca. 40 °C. This can be explained by the hydrophilicity introduced by the PVO block that increases the LCST.[2]
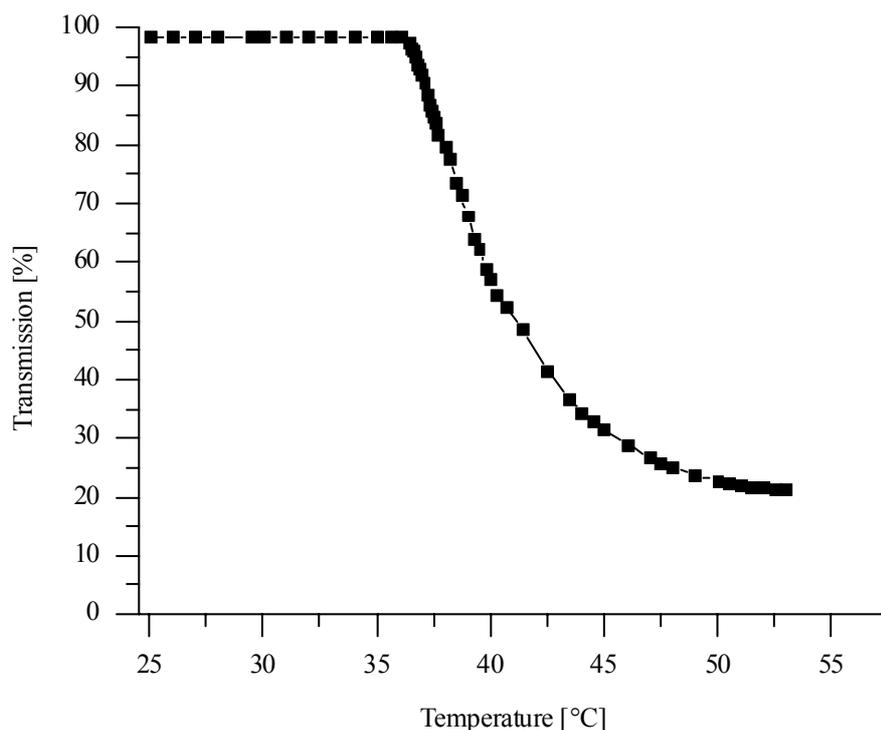
Fig. 5.17.   Turbidimetry of 0.25 wt.-% aqueous solutions of (NIPAAm)$_{39}$-b-(VO)$_{16}$.

It should be noted that the hydrogen-active azlactone ring of PVO is readily opened in the presence of water (cf. chapter 4). Therefore, the observed LCST behavior is rather that of the hydrolysis product PNIPAAm-b-poly(N-carboxy-isopropylidene acrylamide) than that of PNIPAAm-b-PVO.

In order to evaluate mixing behavior in the dry block copolymers, DSC measurements were performed on PNIPAAm-b-PVO samples. Fig. 5.18 represents the DSC curves for the PNIPAAm and PVO homopolymers as well as that of $(NIPAAm)_{39}$-b-$(VO)_{16}$.
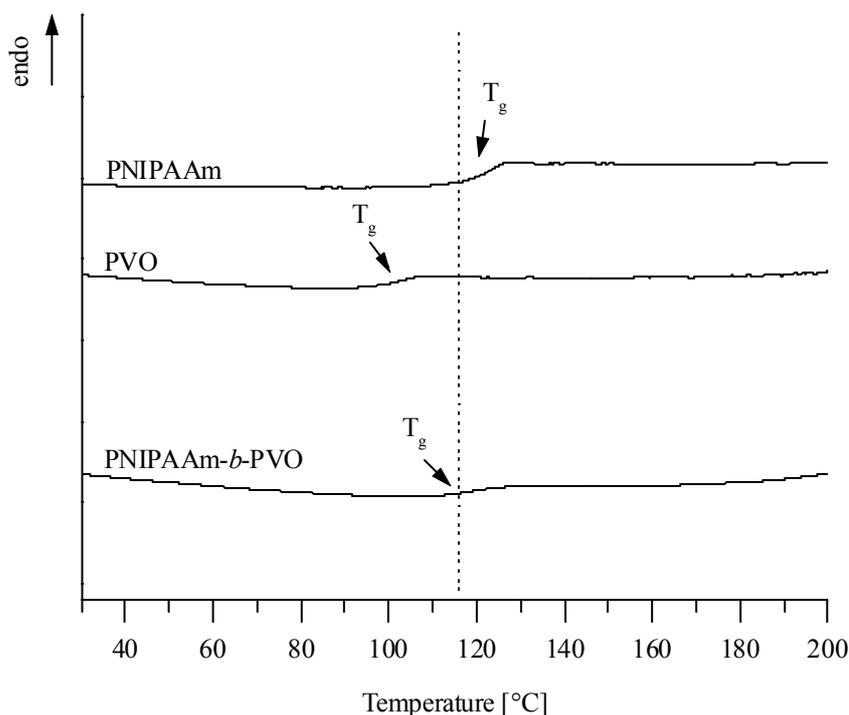
Fig. 5.18. DSC curves of PNIPAAm and PVO homopolymers as well as of (NIPAAm)$_{39}$-b-(VO)$_{16}$ block copolymer at a heating rate of 10 K/min, second heating curves are displayed; the dotted line is a guide for the eye and indicates the glass transition temperature of the block copolymer.

The T_g value of the homopolymer PNIPAAm was determined as 124 °C (literature 130 °C[21]) and that of PVO as 103 °C. For PVO, literature values vary from 92 °C[25] over 96 °C[26] to 108 °C[27]. No explanation is given in the literature, but the different values might result from partial hydrolysis of the azlactone ring. In fact, the T_g value of hydrolyzed PVO, i.e. poly(*N*-carboxy-isopropylidene acrylamide), was found to be about 6 °C higher than that of the unhydrolyzed polymer.

The T_g value of 116 °C for the PNIPAAm-*b*-PVO block copolymer is between the T_g values of the homopolymers, indicating mixing of the blocks in the solid phase. For non-phase-separated AB block copolymers the resulting mixed T_g ($T_{g,mixed}$) is calculated from the T_g of the homopolymers under consideration of the weight fractions using the empirical Fox equation (Eq. 5.7):[28]

$$\frac{1}{T_{g,mixed}} = \frac{w_A}{T_{g,A}} + \frac{w_B}{T_{g,B}}$$

Eq. 5.7

where w_A and w_B are the weight fractions of block A and B, respectively, and $T_{g,A}$ and $T_{g,B}$ are the corresponding glass transition temperatures of the homopolymers. For (NIPAAm)$_{32}$-*b*-(VO)$_{16}$, the weight fractions are $w_{PNIPAAm} = 0.62$ and $w_{PVO} = 0.38$, which yields a mixed T_g of 115 °C, while (NIPAAm)$_{39}$-*b*-(VO)$_{16}$ gives rise to $w_{PNIPAAm} = 0.66$ and $w_{PVO} = 0.34$ so that $T_{g,mixed} = 116$ °C, which is exactly the value obtained by DSC.

References

(1)   Wang, X.; Wu, C. *Macromolecules* **1999**, *32*, 4299-4301.

(2)   Schild, H. G. *Prog. Polym. Sci.* **1992**, *17*, 163-249.

(3)   Hsu, S.-H.; Yu, T.-L. *Macromol. Rapid Commun.* **2000**, *21*, 476-480.

(4)   Kuckling, D.; Adler, H.-J. P.; Arndt, K.-F. *Macromol. Chem. Phys.* **2000**, *201*, 273-280.

(5)   Ptitsyn, O. B.; Kron, A. K.; Eizner, Y. Y. *J. Polym. Sci., Part C: Polym. Lett.* **1968**, 3509-3517.

(6)   Ramon, O.; Kesselman, E.; Berkovici, R.; Cohen, Y.; Paz, Y. *J. Polym. Sci., Part B: Polym. Phys.* **2001**, *39*, 1665-1677.

(7)   Fujishige, S.; Kubota, K.; Ando, I. *J. Phys. Chem.* **1989**, *93*, 3311-3313.

(8)   Kobayashi, M.; Okuyama, S.; Ishizone, T.; Nakahama, S. *Macromolecules* **1999**, *32*, 6466-6477.

(9)   Jones, M.-C.; Leroux, J.-C. *Eur. J. Pharm. Biopharm.* **1999**.

(10)   Firestone, R. A. *Bioconjugate Chem.* **1994**, *5*, 105-113.

(11)   Scheule, R. K.; Cheng, S. H. *Liposome delivery systems*; BIOS Scientific Publishers Inc.: Oxford, 1996.

(12)   Bulmus, V.; Ding, Z.; Long, C. J.; Stayton, P. S.; Hoffman, A. S. *Bioconjugate Chem.* **2000**, *11*, 78-83.

(13)   Liu, S.; Billingham, N. C.; Armes, S. P. *Angew. Chem., Int. Ed.* **2001**, *40*, 2328-2331.

(14)   Arotcarena, M.; Heise, B.; Ishaya, S.; Laschewsky, A. *J. Am. Chem. Soc.* **2002**, *124*, 3787-3793.

(15)   Wang, Y.; Morawetz, H. *Macromolecules* **1989**, *22*, 164-167.

(16)   Shibanuma, T.; Aoki, T.; Sanui, K.; Ogata, N.; Kikuchi, A.; Sakurai, Y.; Okano, T. *Macromolecules* **2000**, *33*, 444-450.

(17)   Hesse, M.; Meier, H.; Zeeh, B. *Spektroskopische Methoden in der organischen Chemie*, 5th ed.; Georg Thieme Verlag: Stuttgart, 1995.

(18)   Blatchford, M. A.; Raveendran, P.; Wallen, S. L. *J. Am. Chem. Soc.* **2002**, *124*, 14818-14819.

(19)   Alexandrowicz, Z.; Katchalsky, A. *J. Polym. Sci., Part A: Polym. Chem.* **1963**, *A1*, 3231.

(20)   Tripathy, S. K.; Kumar, J.; Nalwa, H. S. *Handbook of Polyelectrolytes and Their Applications: 2 Polyelectrolytes, Their Characterization and Polyelectrolyte Solutions*; American Scientific Publishers: Stevenson Ranch, 2002; Vol. 2.

(21)   Brandrup, J.; Immergut, E. H. *Polymer Handbook*; John Wiley & Sons: New York, 1989.

(22)   Lechner, M. D.; Gehrke, K.; Nordmeier, E. H. *Makromolekulare Chemie*; Birkhäuser Verlag: Basel, 1993.

(23)   Rocco, A. M.; Bielschowsky, C. E.; Pereira, R. P. *Polymer* **2003**, *44*, 361-368.

(24)   Zhang, J.; Roberts, C. J.; Shakesheff, K. M.; Davies, M. C.; Tendler, S. J. B. *Macromolecules* **2003**, *36*, 1215-1221.

(25)   Taylor, L. D.; Chiklis, C. K.; Platt, T. E. *J. Polym. Sci., Part B: Polym. Lett.* **1971**, *9*, 187-190.

(26)   Muthiah, J.; Mathias, L. J. *J. Polym. Sci., Part A: Polym. Chem.* **1991**, *29*, 29-37.

(27)   Guichard, B.; Noel, C.; Reyx, D.; Thomas, M.; Chevalier, S.; Senet, J.-P. *Macromol. Chem. Phys.* **1998**, *199*, 1657-1674.

(28)   Fox, T. G. *Bull. Am. Phys. Soc.* **1956**, *1*, 123.

6   Novel route to polymer-protein conjugates

6.1   Bioconjugates

Bioconjugation involves the linking of two or more molecules to form a new complex having the combined properties of its constituting components. Natural or synthetic compounds with their individual activities can be chemically combined to create novel substances possessing unique characteristics. For example, a protein able to bind selectively to a target molecule within a complex mixture may be linked to another molecule capable of being detected to form a traceable conjugate. The detection component provides visibility for the targeting component, producing a complex that can be localized, followed through various processes, or used for measurement.

The ability to chemically attach one molecule to another has caused the naissance of billion-dollar industries serving research, diagnostics, and therapeutic markets. A significant portion of all biological assays, including clinical testing, is now done using unique conjugates that have the ability to interact with particular analytes in solutions, cells, or tissues. Cross-linking and modifying agents can be applied to alter the native state and function of peptides and proteins, lipids, oligonucleotides and also polymers.

In recent years, the conjugation of biomolecules with polymers has gained importance because of the various applications involved with these compounds, ranging from biotechnology to medicine. The development of bioconjugates to polymers was pioneered by Ringsdorf et al. who investigated model reactions for creating polymer-drug conjugates as early as 1972.[1] The basic idea was to attach therapeutics, e.g. the anti-cancer drug doxorubicin, to water-soluble polymers while retaining their biological activity. This was accomplished primarily by synthesis of water-soluble copolymers with short active ester blocks, such as *N*-hydroxysuccinimide methacrylate,[1,2] that serve as binding sites for the drug. Alternatively, the biocompatible *N*-(2-hydroxypropyl)methacrylamide HPMA copolymer was used for conjugate synthesis with a reactive precursor as a second block to which an aliphatic amino group may be bound by an aminolysis reaction.[3] To date, the polymer-drug conjugates most extensively studied for improvement of cancer chemotherapy are monomethoxy poly(ethylene glycol) (mPEG) covalently linked to proteins.[4]

Another area of bioconjugates that has grown lately uses stimuli-responsive polymers that respond with large property changes to small physical or chemical changes, such as pH, ionic strength, temperature, or light. These "smart" polymer-engineered protein conjugates[5-7] are used for affinity separations of molecules and cells, clinical diagnostics and immunoassays, biosensors, cell culture processes, triggered drug release and many

more.[8] Phase-separation immunoassays comprise the selective isolation and assay of an analyte from a complex mixture using a conjugate that phase-separates upon temperature change.[9] Immobilized biocatalysts consist of enzyme-polymer conjugates and experience drastic changes in polymer conformation that affect enzyme activity and substrate access.[6] Affinity precipitations use conjugates of smart polymers with ligands that are specific for the target protein. After complex formation of the conjugate with the target, phase separation of the complex is triggered and the target protein can be isolated.[10] While the potential of thermosensitive polymers, such as PNIPAAm, has been explored thoroughly, great possibilities have lately been attributed to pH-sensitive polymers, especially in the area of gene delivery and gene therapy research, not only due to their membrane permeation-enhancing function but also because their charges can be switched on and off. For example, transport of naked DNA into the cell is a difficult process because of the negative charges and the large size of the DNA molecules. Positively charged polymers balance out this charge and condense DNA to nanoparticles of ca. 100 nm size.[11,12] Deprotonation releases free DNA and the polymer. Very recently, the groups of A.S. Hoffman and P.S. Stayton have demonstrated the potential of pH-responsive polymers for the delivery of therapeutics and vaccines.[13]

Although polymer-protein conjugates have been known for almost three decades, only with the emergence of controlled/living polymerizations that tolerate a large number of functionalities and do not require such stringent conditions as anionic polymerization, defined polymers could be synthesized with means that are available in a standard, non-polymeric laboratory. These polymers allow for a detailed investigation concerning the correlation of structure, molecular weight and solution properties with the biological profile. Very narrow molecular weight distributions ensure well-defined compositions and distinct retention times of the conjugates in the body.

6.1.1   Functional targets

The prerequisite for site-specific conjugation and a fixed number of conjugating molecules is the presence of reactive functionalities that react selectively with either the cross-linking agent or directly with the respective functional groups of the target molecule. Consequently, conjugation techniques are dependent on the availability and compatibility of functional groups in the reactants. Knowledge of the basic mechanisms by which the reactive groups couple to target functional groups provides the means to design intelligently a conjugation strategy.

Functional targets in proteins and peptides comprise the functional groups introduced by the constituting amino acids. The most important amino acids for conjugation purposes are the ones containing ionizable groups. These are aspartic acid, glutamic acid, lysine,

arginine, cysteine, histidine, and tyrosine. Carboxylate groups, for example, can be derivatized using amide bond forming agents, active esters, or reactive carbonyl intermediates. The amine-containing groups in lysine, arginine, and histidine are typically exposed on the protein surface and can be derivatized readily, where alkylation and acylation are the most important reactions. Cysteine is the only amino acid that contains a sulfhydryl group. The moiety is usually protonated and ionization occurs only at high pH (pK_a 8.8-9.1). The most important reaction of cysteine groups in proteins is formation of disulfide cross-links with another cysteine molecule. The formed cysteine disulfides (cystine residues) often represent key points in the stabilization of protein structure and conformation. Cysteine/cystine groups are relatively hydrophobic and can usually be found within the protein core, thus rendering the complete reduction of disulfides in large proteins difficult unless a denaturing agent is used to open up the inner structure and make these groups accessible. Derivatization of the sulfhydryls of cysteine is one of the most important reactions for conjugation to proteins. Reactions of cysteine sulfhydryls or cystine disulfides, respectively, include alkylation, acylation, oxidation reactions etc.

Nucleophilic addition is a valuable reaction for conjugation. The nucleophilicity of amino acid functionalities relative to the major groups encountered in biological molecules decreases in the order $R-S^- > R-NH_2 > R-COO^- = Ph-O^-$. Thus, the strongest nucleophile in proteins is the sulfhydryl group of cysteine, particularly in the ionized thiolate form. Most reactive groups used for conjugation couple in greater yield as the pH of the reaction is raised closer to the pK_a of the ionizable target. Nevertheless, an increase of pH beyond pK_a may sometimes be detrimental, as many reactive groups will hydrolyze at high pH values. According to the theoretical pK_a values for the ionizable groups of amino acids, nucleophilic substitution involving primary amines or sulfhydryl groups on proteins should not be efficient below pH $\approx$ 8.5. In practice, however, reactions proceed in high yields at pH values that are not much higher than 7 as changes in pK_a are experienced by the residues due to microenvironmental effects within the three-dimensional protein structure. Changes in pK_a make it virtually impossible to select exclusively certain functionalities for conjugation simply by modulation of the reaction conditions. Consequently, in order to site-direct a conjugation reaction, the proper choice of chemical reactions and reactive groups is much more critical than changes in pH.[14]

6.1.2 Streptavidin and avidin

Streptavidin was used for both covalent and non-covalent attachment to stimuli-responsive polymers. In the following, a brief description of the protein's characteristics is given.

Streptavidin is a tetrameric protein that is isolated from *Streptomyces avidinii* and possesses a high affinity to biotin (vitamin H). Its interaction is among the strongest non-covalent affinities known ($K_a \approx 10^{15}$ L/mol).[15] The binding occurs between biotin and a pocket within each of the four subunits of the protein (Fig. 6.1). It is insensitive to pH changes in the range of 2 to 13.[15]
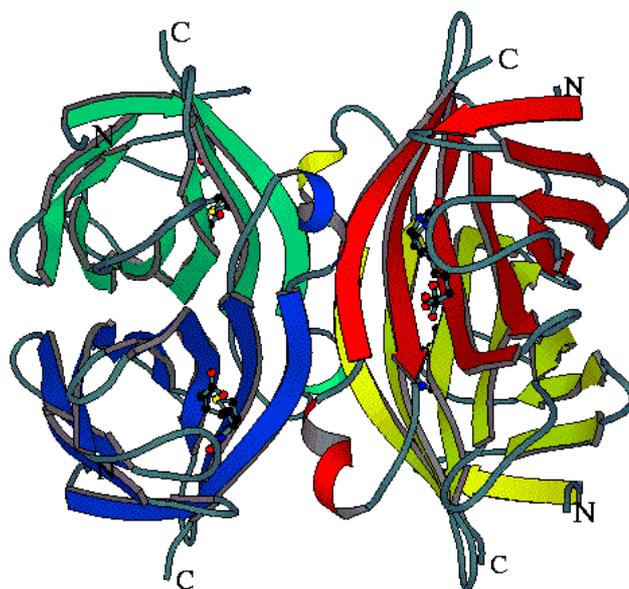

Fig. 6.1.   Simplified structure of streptavidin; different-colored sections indicate protein subunits, molecules drawn within represent biotin molecules located in binding pockets.

With a D_{222} symmetry,[16,17] streptavidin is a tetramer consisting of two tightly associated dimers. Biotin sits in an eight-stranded antiparallel β barrel pocket, with its ureido ring facing the bottom of the pocket, and interacts with residues of streptavidin through a hydrogen bond network and van der Waals interactions.[18] In addition, the interaction between W-120 (tryptophan in position 120) and the neighboring biotin increases the thermal stability of the streptavidin tetramer.[19] The binding loop of streptavidin composed of residues 45 to 52 enhances biotin binding by changing to a closed loop conformation from an open loop conformation.[20] The hydrogen bond network is the main source of the high affinity. Water bridges contribute significantly to the stability of the biotin-streptavidin complex. The high affinity recognition of biotin and biotinylated molecules has made streptavidin one of the most important components in diagnostics and laboratory kits. Fig. 6.2 shows the structure of biotin and its hydrogen bonding interactions with streptavidin.
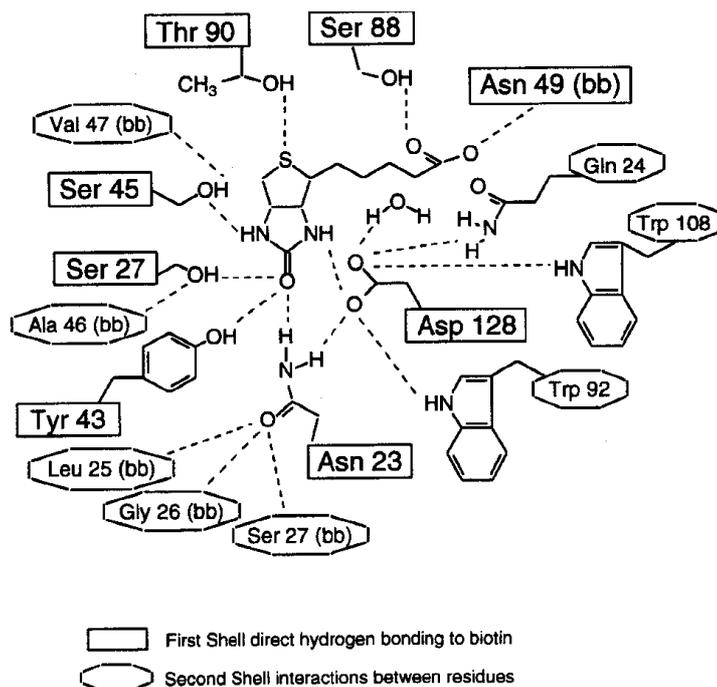
Fig. 6.2.   Hydrogen bonding network between streptavidin and biotin (vitamin H); first shell interactions are direct hydrogen bonds between protein side chains and biotin, second shell interactions are between protein backbone (bb) or side chains and first shell protein side chains.[21]

Streptavidin exhibits an isoelectric point pI = 6.5. The native protein has a relatively high mass (66-75 kDa) and can be converted to a lower-mass form (i.e. 60 kDa) by proteolytic digestion at both the *N* and *C* termini.[22]   The truncated protein is called "core streptavidin" and has a molecular size of 5.4x5.8x4.8 nm[17] while retaining full binding activity.

Site-directed mutagenesis allows replacement of amino acids within proteins. Using this powerful tool, Stayton et al. have studied the functions of individual amino acids on the high binding affinity of biotin and streptavidin.[21,23]

Similarly to streptavidin, the glycoprotein avidin contains four identical subunits with each subunit having one binding site for biotin. The corresponding binding constant is of the same magnitude as that of the streptavidin-biotin interaction, i.e. $K_a \approx 10^{15}$ L/mol, and binding is as insensitive to variations in pH or temperature as streptavidin-biotin binding is. The subunits of 16.4 kDa give an intact molecular weight of approximately 66 kDa. The primary structure of avidin is considerably different from that of streptavidin despite the fact that both proteins bind to biotin with a very high affinity. The variation in amino acid sequence results in a much higher isoelectric point for avidin, which is highly basic with a pI of 10.[15] This, along with its carbohydrate content, makes avidin disadvantageous with respect to streptavidin as there is a tendency to bind non-specifically to components other than protein. The strong positive charge on the protein causes ionic interactions with more

negatively charged molecules, especially cell surfaces. In addition, carbohydrate binding proteins on cells can interact with the polysaccharide portions on the avidin molecule to bind them in regions that are devoid of targeted biotinylated molecules.[14]

6.1.3   Strategies for polymer-protein conjugation

The presence of reactive functional groups in both polymer and protein allows for selective, site-specific conjugation of the two components.

In the following sections, conjugation of polymers to streptavidin or model compounds is described using amine-reactive polymers, cross-linkers, or direct linkage via disulfide bonds. In the case of streptavidin, conjugates were also obtained by non-covalent attachment of biotinylated polymers to the biotin binding pockets of wild-type streptavidin.

6.2   Conjugation to model compounds

6.2.1   Amine-reactive polymer conjugates with a model peptide

The active ester polymers poly(*N*-hydroxysuccinimide methacrylate) PNHSM and poly(2-vinyl-4,4-dimethyl-5-oxazolone) PVO as well as the multifunctional polymer poly(diacetone acrylamide) PDAA were reacted with the dipeptide glycine-leucine (GlyLeu, structure see Fig. 6.3) as a model compound. The primary amino group of the peptide is a common functionality found in proteins and reacts in a nucleophilic manner with the above-mentioned polymers.

$$H_3C-\underset{\underset{COOH}{|}}{\overset{\overset{\displaystyle CH_3}{|}}{CH}}-CH_2-\underset{|}{CH}\qquad \overset{NHCO-CH_2-NH_2}{}$$
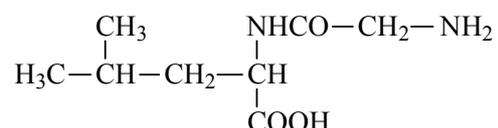
Fig. 6.3.   Structure of the dipeptide GlyLeu.

Short oligo(active ester) blocks incorporated into a block copolymer are especially interesting for conjugation as the active ester provides the binding sites for the protein and the major component provides the desired physical properties. For example, active ester units combined with PNIPAAm result in a hydrophilic and thermoresponsive system. It has to be kept in mind that the block copolymers contain more than one active ester unit so that peptides may conjugate several times to the block copolymer, therefore leading to a broadening of molecular weight distribution due to different numbers of conjugated peptides. However, steric factors will minimize the conjugation of several peptides to the active ester blocks or, in the case of proteins, will prevent multiple conjugation of large molecules.

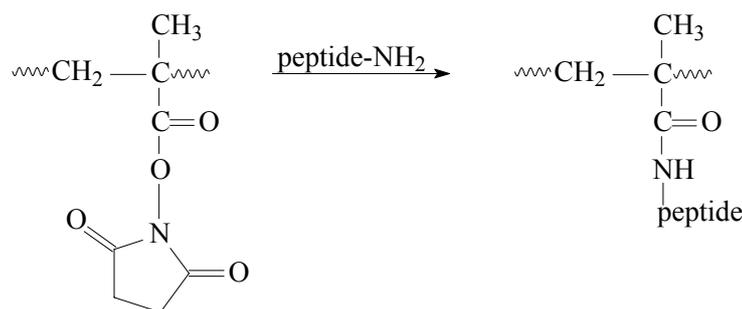PNHSM forms an amide bond with the primary amino group of GlyLeu (Fig. 6.4).

Fig. 6.4.   Reaction of PNHSM with primary amino group of a peptide.

The *N*-hydroxysuccinimide unit is inert towards hydrolysis and reacts readily with amines to amides, even at 0 °C, in neutral or slightly basic aqueous solution.[1] The conjugation of GlyLeu to PNHSM was performed in a mixture of DMSO and phosphate buffer pH 7.4 at room temperature. Conjugation was proven by ^{1}H-NMR spectroscopy (Fig. 6.5).
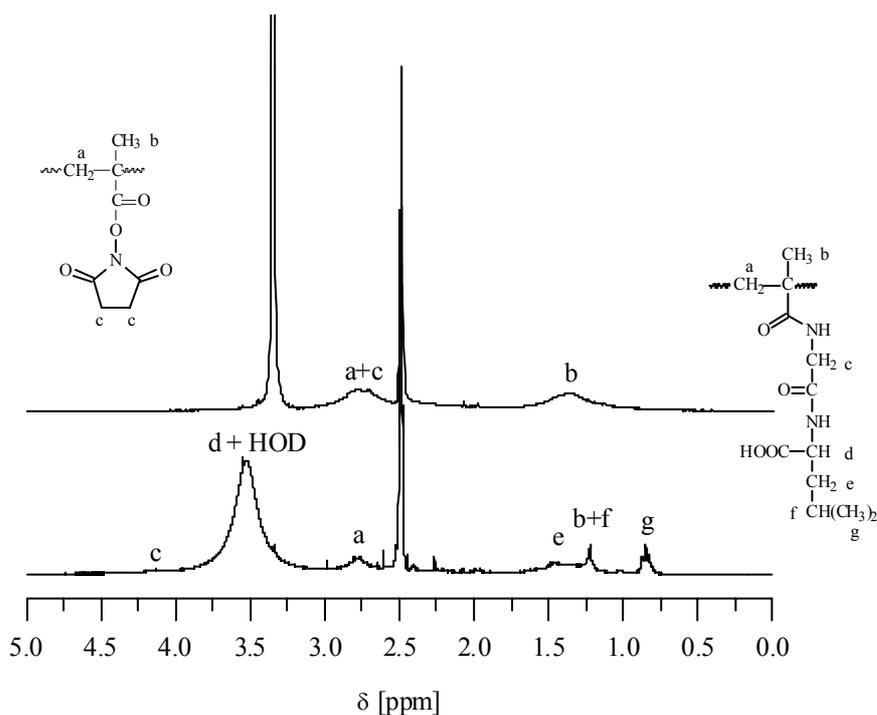

Fig. 6.5. ^{1}H-NMR spectra of PNHSM (top) and PHNSM-GlyLeu conjugate (bottom) in d$_6$-DMSO.

Conjugation of GlyLeu to PNHSM has a relatively small effect on the NMR signals. A narrowing of the proton signal at 2.5-3.0 ppm is observed as the succinimide methylene protons (**c**) disappear. The small upfield shift of the methyl protons (**b**) in the conjugate is ascribed to the amide group that is slightly less electron-withdrawing than the ester group.

PVO undergoes ring opening on addition of the peptide (Fig. 6.6).
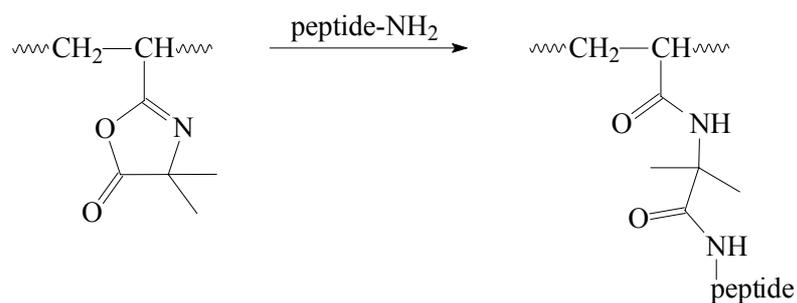
Fig. 6.6.   *Reaction of PVO with amino functionality.*

The azlactone ring is very reactive towards compounds containing active hydrogen atoms so that the reaction has to be carried out in the absence of water to avoid hydrolysis. Azlactone ring opening is especially easy with primary amines.[24,25] The conjugation of GlyLeu to PVO was carried out in dry DMF and under reflux. Unconjugated GlyLeu remained undissolved and could easily be separated from the product by filtration. Conjugation was confirmed by ^{1}H-NMR spectroscopy. Fig. 6.7 shows the ^{1}H-NMR spectra of PVO and the PVO-GlyLeu conjugate.
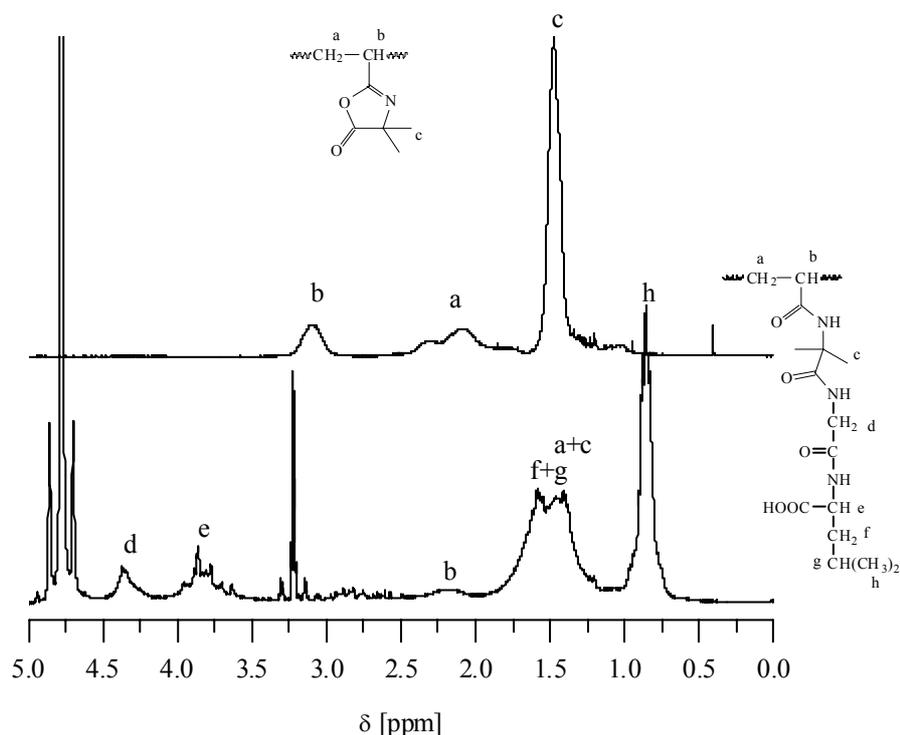
Fig. 6.7.   *^{1}H-NMR spectra of PVO (top) and PVO-GlyLeu conjugate (bottom) in C_6D_6 and CD_3OD, respectively.*

Successful conjugation is most evident by the strong upfield shift of the methine proton (**b**) as compared to the unconjugated polymer, which is due to the less electron-withdrawing nature of the amide group as compared to the azlactone functionality.

PDAA possesses the reactivity of an activated double bond, an *N*-substituted amide and a methyl ketone. It reacts with the primary amino group of GlyLeu to form an imine (Fig. 6.8).
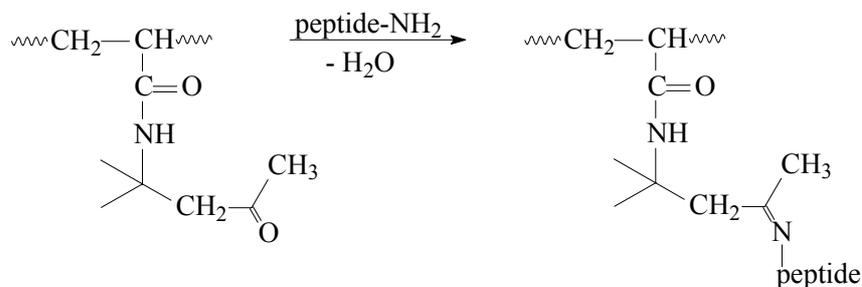
Fig. 6.8.   *Reaction of PDAA with peptide amino group.*

Even though being a water-insoluble polymer, PDAA is not only interesting as a component of a block copolymer but also as a homopolymer as it might render proteins or drugs more hydrophobic upon conjugation, enabling their use for wound-healing purposes.
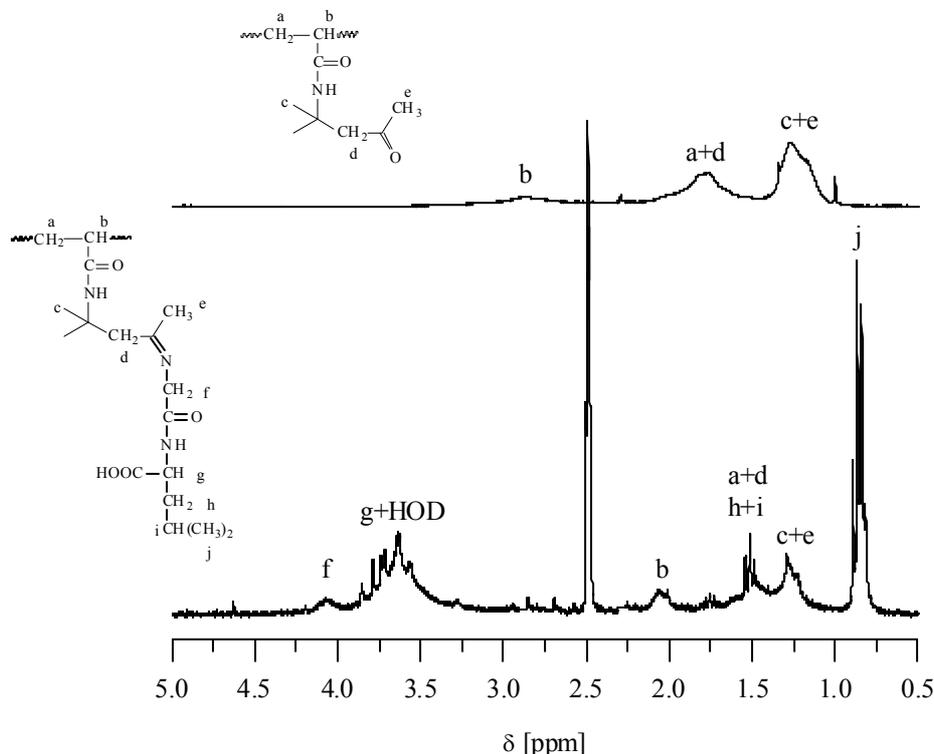
Fig. 6.9.   *^{1}H-NMR spectra of PDAA (top) and PDAA-GlyLeu conjugate (bottom) in C_6D_6 and CD_3OD, respectively.*

The conjugation of PDAA with GlyLeu was performed in dry DMF using *p*-toluenesulfonic acid as a catalyst and in the presence of molecular sieve to absorb formed water and shift the reaction equilibrium towards the conjugate. Conjugate formation was checked by NMR spectroscopy (Fig. 6.9). The product spectrum clearly shows the protons of the GlyLeu part (**f-j**). Little influence of conjugation on the shift of the PDAA protons **d** and **e** is found as the imine and carbonyl structures have similar electron densities.

6.2.2   Sulfhydryl conjugates with model compounds

6.2.2.1   Hydrolysis of the dithiocarbamate endgroup

Reversible addition-fragmentation chain transfer (RAFT) polymerization of *N*-isopropylacrylamide, NIPAAm, with cumyl/benzyl 1-pyrrolecarbodithioate as chain transfer agent yields polymers with dithiocarbamate chain ends. Due to the reactivity of the dithiocarbamate moiety, this group can easily be hydrolyzed to the corresponding thiol under alkaline conditions using either primary/secondary amines or inorganic bases, such as sodium hydroxide.[26] Hydrolysis on the PNIPAAm samples was performed under inert atmosphere in order to prevent oxidation of thiol to disulfide or to species of higher oxidation states, such as sulfonic acids, which is catalyzed by bases.[27] The course of the hydrolytic process can be followed by UV spectroscopy. The characteristic dithiocarbamate absorption band at a wavelength of 296.2 nm disappears upon complete hydrolysis (Fig. 6.10).
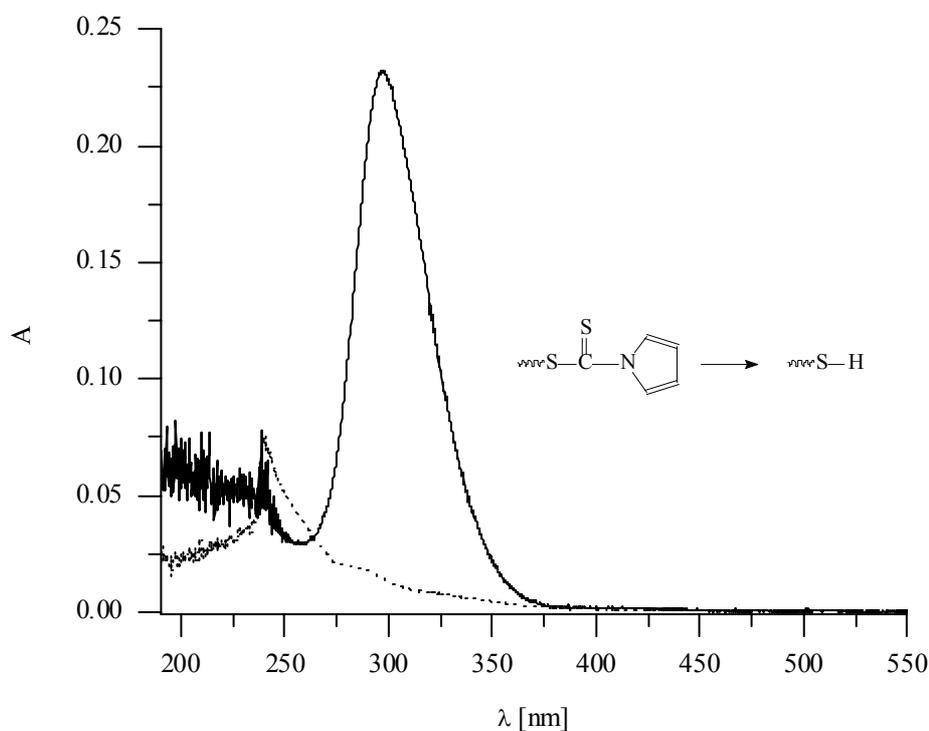

Fig. 6.10.   *UV spectra of dithiocarbamate- (▬) and thiol-terminated (- -) PNIPAAm in methanol.*

Several approaches were made to characterize the synthesized polymeric thiols. One approach that is widespread in biochemistry is the so-called Ellman's assay. Protein sulfhydryl groups are detected with Ellman's reagent, 5,5'-dithiobis-[2-nitrobenzoic acid] (DTNB). The compound is a disulfide that shows practically no absorbance in the UV-vis region but, under mild alkaline conditions (pH 7-8), it reacts with thiols to the corresponding mixed disulfide and 2-nitro-5-thiobenzoate (Fig. 6.11). The anion shows a strong absorption in UV with a wavelength at maximal absorbance of λ_{max} = 412 nm and a molar extinction coefficient of ε_{max} = 14,140 cm^2/mmol (in phosphate buffer pH 8.0).
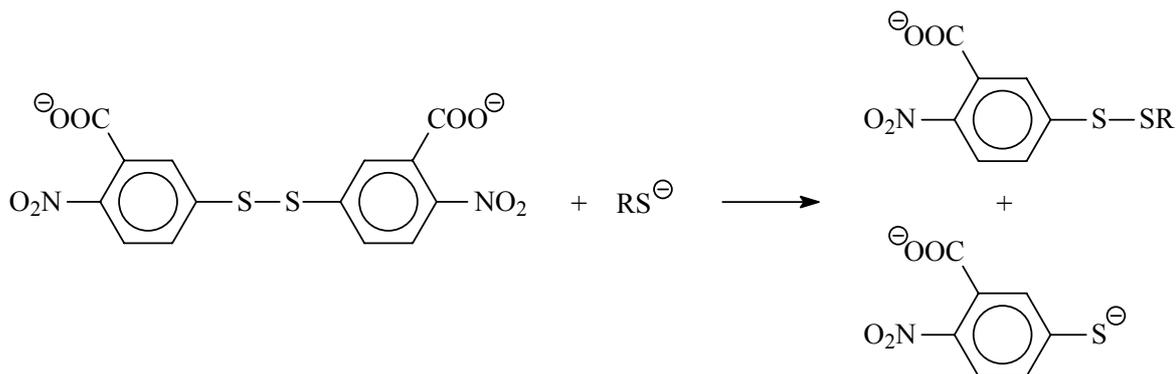
Fig. 6.11.   Reaction of 5,5'-dithiobis-[2-nitrobenzoic acid] with thiols (Ellman's assay).

Consequently, every thiol equivalent releases one equivalent of 2-nitro-5-thiobenzoate. The increase in absorbance at 412 nm is directly proportional to the concentration of sulfhydryls in solution. From the known extinction coefficient, the amount of sulfhydryl groups present in the protein can be calculated.[28,29] For Ellman's assay on hydrolyzed PNIPAAm, the polymer was dissolved in phosphate buffer and Ellman's solution was used as a reference. The reaction was followed over a time period of several hours as the thiol-disulfide exchange is reported to be relatively slow.[30]

The assay clearly shows the presence of a thiol but quantification results in much lower values than expected ($A_{theor} \approx 1$, Fig. 6.12). It has been described in the literature that evaluation of the data derived from Ellman's assay for sulfhydryl-containing proteins can be complicated by pH-induced disulfide disruption, reoxidation of thiol groups and thermochromic effects. Furthermore, sulfhydryl groups exhibit variable reactivity toward DTNB owing to steric factors. Different reactivities will therefore influence the rate of reaction. Compared to Ellman's assay on proteins, the reaction with PNIPAAm is even slower; an assay on proteins can take up to 60 min, but in the present case, a reaction time of almost 180 min is observed. It has also been shown that only thiolate anions react with DTNB but not undissociated thiols.[30] Besides, one has to take into account that Ellman's assay is designed for proteins and not for polymers. Proteins usually have to be denatured in order to expose all sulfhydryl groups. The abovementioned difficulties are all factors

that can contribute to the lower thiol concentration observed for PNIPAAm. Due to the coiled structure of the polymers in solution, thiol groups might not be accessible easily so that not all groups are detected. In summary, in this work, it was demonstrated that Ellman's assay can be used as a qualitative, but not as a quantitative, proof of thiol groups in PNIPAAm.
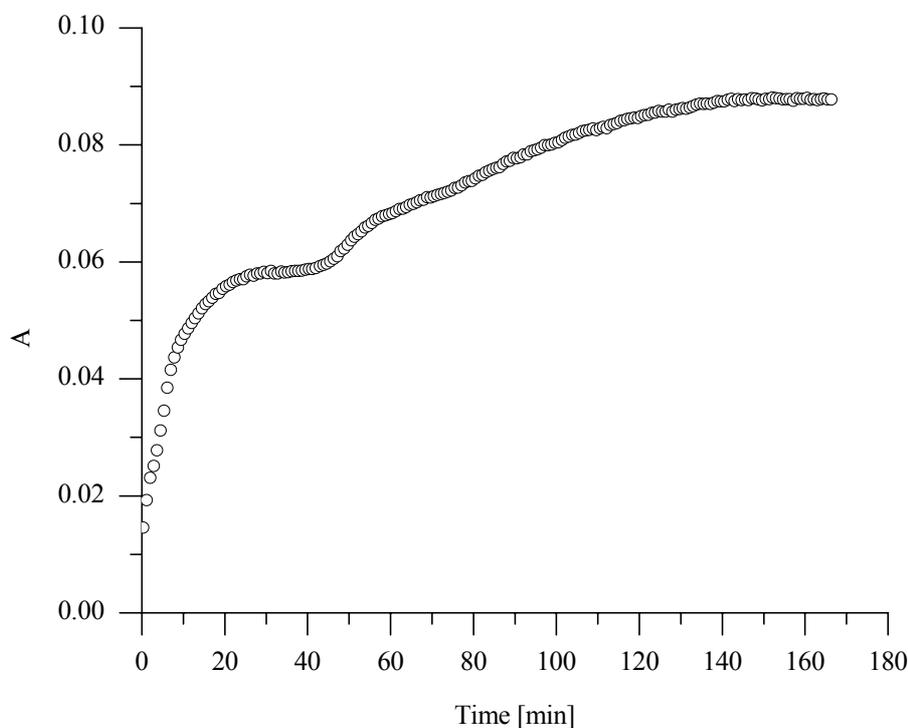

Fig. 6.12.   *UV absorption with time at* $\lambda = 412$ *nm for the reaction of thiol-terminated PNIPAAm with Ellman's reagent.*

Due to the problematic Ellman's assay, another proof of formation of polymeric thiol was desirable. An alternative is the reaction with 2-naphthoylchloride. The compound shows UV absorption in the region from 240 to 350 nm. Addition of a polymeric thiol leads to a blue shift of the absorption bands (cf. Fig. 6.13).

Another very reliable proof of thiol formation is MALDI-TOF analysis. Evaluation of the peaks allows determination of chain end structures and clearly shows the presence of sulfhydryl groups. Results have already been discussed in chapter 4.
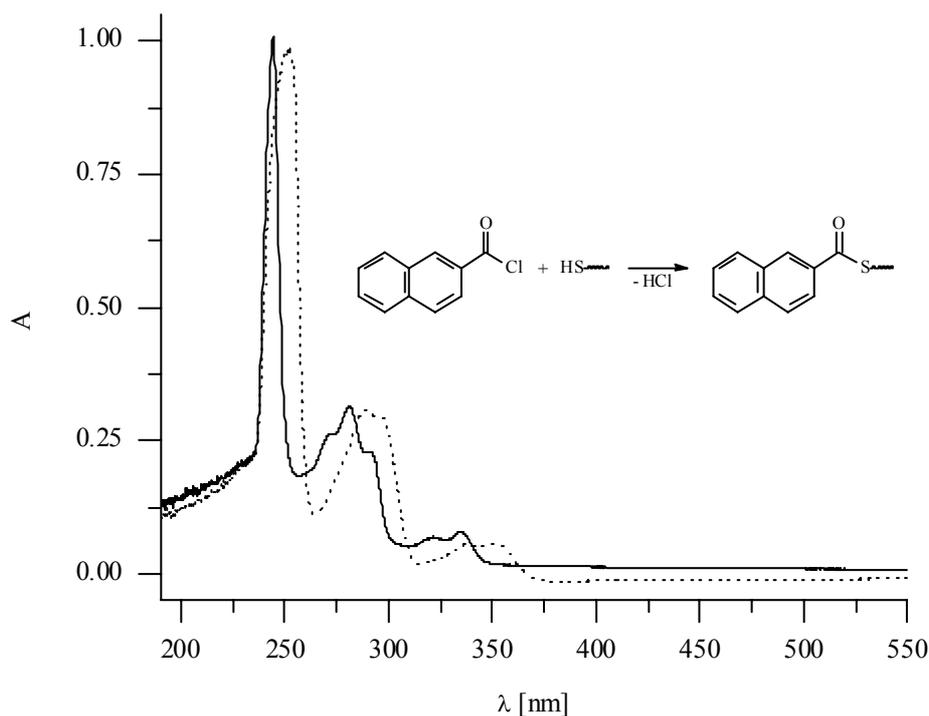
Fig. 6.13. *UV spectra of 2-naphthoylchloride (dashed line) and of its adduct with polymeric thiol (solid line) in chloroform.*

6.2.2.2 Conjugation to model compounds

Three approaches for conjugating thiol-terminated polymers to thiol-functionalized proteins were made with model compounds: (a) mixed disulfide formation via a diethyl azodicarboxylate (DEAD) adduct, (b) reaction of a thiol with a pyridyl disulfide reagent, (c) nucleophilic addition of a thiol to a maleimide compound.

Diethyl azodicarboxylate (**1**) (DEAD) is a strong hydrogen acceptor and adds to one equivalent of sulfhydryl under formation of diethyl *N*-sulfenylhydrazodicarboxylate (**2**). This adduct forms a mixed disulfide upon addition of another sulfhydryl compound, releasing reduced DEAD as diethyl hydrazodicarboxylate (**3**), which is the main driving force for formation of unsymmetrical disulfides (Fig. 6.14). The reaction is reported to proceed under mild and neutral conditions.[31] Major drawbacks of the reagent are its sensitivity towards water and other functionalities, such as alcohols, which requires the use of anhydrous, aprotic organic solvents.[32]
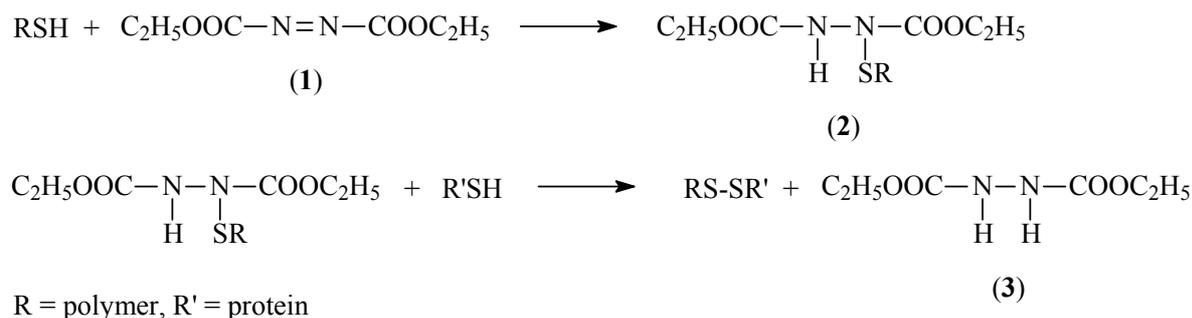
$$RSH + C_2H_5OOC{-}N{=}N{-}COOC_2H_5 \longrightarrow C_2H_5OOC\underset{\overset{|}{H}}{-}N{-}\underset{\overset{|}{SR}}{N}{-}COOC_2H_5$$

(1)

(2)

$$C_2H_5OOC\underset{\overset{|}{H}}{-}N{-}\underset{\overset{|}{SR}}{N}{-}COOC_2H_5 + R'SH \longrightarrow RS\text{-}SR' + C_2H_5OOC\underset{\overset{|}{H}}{-}N{-}\underset{\overset{|}{H}}{N}{-}COOC_2H_5$$

(3)

R = polymer, R' = protein

Fig. 6.14.   Formation of mixed disulfides using DEAD.

Like diethyl azodicarboxylate, pyridyl disulfides belong to the group of thiol disulfide exchange reagents. The compounds readily undergo interchange reaction with free sulfhydryl to yield a single mixed disulfide product (Fig. 6.15). The exclusive formation of the latter results from the leaving group that is transformed into a compound (pyridine-2-thione) that does not participate in further mixed disulfide formation.[33,34]

Fig. 6.15.   Reaction of sulfhydryls with pyridyl disulfide.

The reaction of sulfhydryl groups with maleimides (Michael addition) results in stable thioether bonds (Fig. 6.16). Maleimide reactions are specific for sulfhydryls at pH 6.5-7.5. At pH 7, the reaction with thiols is a thousand times faster than that with amines.[14,35,36]
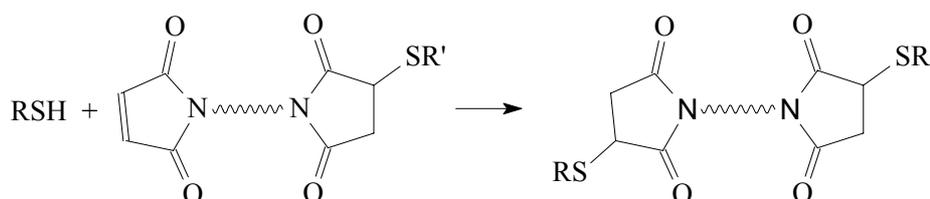
Fig. 6.16.   Reaction of sulfhydryls with bismaleimide.

The above-mentioned approaches were used with thiol-terminated PNIPAAm obtained from hydrolysis of RAFT-polymerized, dithiocarbamate-terminated PNIPAAm. Weighing advantages and disadvantages of the different methods, bismaleimide cross-linkers seem to be the system of choice as they give rather high yields, involve mild reaction conditions and display high selectivity towards sulfhydryls. The DEAD approach appears inappropriate, especially in the case of proteins, as non-aqueous conditions are required for the reaction. Pyridyl disulfides gave lower yields than maleimides and conjugates are labile due to disulfide cleavage in the presence of reducing agents.

The formation of bismaleimide-functionalized PNIPAAm was even possible by radical addition of dithiocarbamate-terminated PNIPAAm to the respective maleimide, which circumvents the hydrolysis step. The reaction proceeds via fragmentation of the C-S bond of the dithiocarbamate-functionalized PNIPAAm and addition to the maleimide double bond in a manner similar to copolymerization of a macromolecular chain transfer agent with additional monomer, the difference being that the maleimide does not polymerize.[37] The addition was performed at 60 °C in 1,4-dioxane using AIBN as initiator with an excess of bismaleimide in order to prevent twofold addition of PNIPAAm. The PNIPAAm-maleimide conjugate was obtained in high yield and may be used for protein conjugation after purification. Fig. 6.17 shows an exemplary reaction using *N,N*-(1,4-phenylene)bismaleimide. Successful conjugation was checked by ^{1}H-NMR spectroscopy, where the aromatic protons give characteristic signals at 6.8-7.7 ppm and the unreacted part of the bismaleimide is evident from the olefinic methine protons at ca. 6.2 ppm.
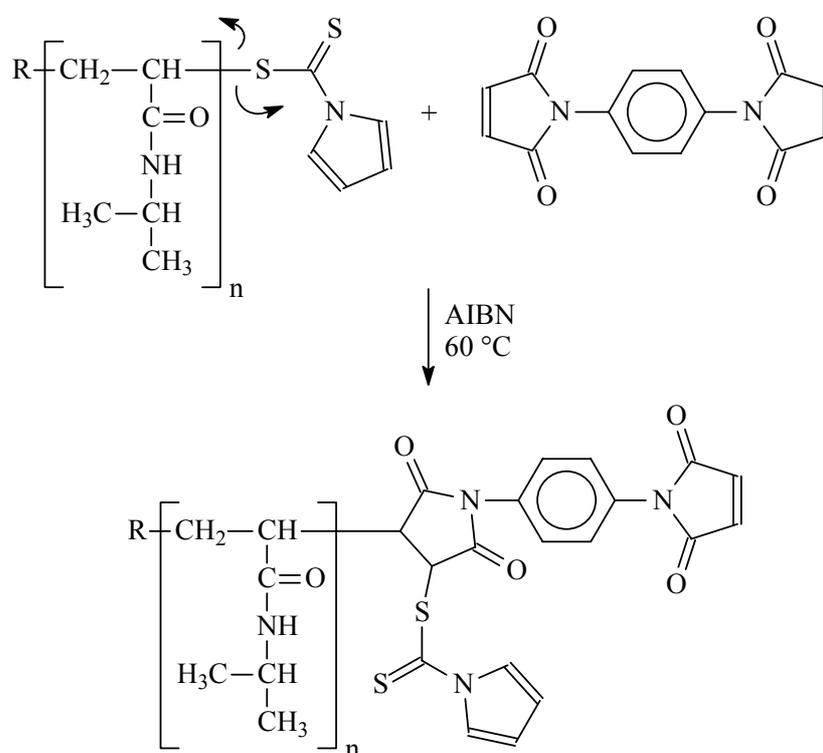
Fig. 6.17. *Conjugation of dithiocarbamate-terminated PNIPAAm to* N,N-*(1,4-phenylene)bismaleimide via radical addition.*

6.3   Conjugation to streptavidin

In previous works dealing with polymer-streptavidin conjugates, polymers with broad molecular weight distributions and only an approximate number of functional groups have been used in the conjugation assays.[7,38,39] Attempted fractionations of the polymers for more narrowly distributed molecular weights was usually not very effective and appropriate polymerization techniques were not at hand. Besides, only thiol-reactive but not thiol-functionalized polymers had been used in earlier studies. With the use of RAFT polymers, well-defined conjugates can be synthesized with respect to both endgroup functionality and polydispersity. The sulfhydryls obtained from endgroup hydrolysis of the RAFT polymers display very specific reactivity towards common cross-linkers.

Both sulfhydryl-terminated PNIPAAm and PNIPAAm-*b*-PAA with a sulfhydryl-terminated PNIPAAm block were used for the conjugation reactions. PNIPAAm exhibits an LCST of 32 °C in aqueous solutions. With the conjugation to streptavidin, a thermoresponsive system is created. Poly(acrylic acid) enables response to pH and ionic strength. Streptavidin conjugated to PNIPAAm-*b*-PAA is expected to exhibit response to the combined external stimuli, i.e. pH, temperature and ionic strength.

The polymers were conjugated to both wild-type streptavidin and the bioengineered type S139C, in which the amino acid serine (S) at position 139 is replaced by the amino acid cysteine (C) at the *C*-terminal end of the polypeptide subunit. The streptavidin mutant S139C can be genetically engineered by site-directed cassette mutagenesis using a synthetic "core" streptavidin gene designed and constructed for protein expression in *Escherichia coli*.[38,40] Site-specific conjugation to S139C takes place at a location in the molecule that is not adjacent to the biotin binding pockets so that interference of conjugations with biotin binding is not very likely but it is possible in the case of large biotinylated molecules. In contrast to that, the streptavidin mutant E116C (substitution of glutamic acid with cysteine) has its conjugation site near the tryptophan-120 (W-120) residue, which shows van der Waals interactions with neighboring biotin (Fig. 6.18).[38] Both mutants are composed of amino acid residues 13-139, whereas native (wild-type) streptavidin consists of amino acid residues 1-159. It has been demonstrated that sulfhydryl conjugations of small molecules as well as the absence of fragments 1-12 and 140-159 do not significantly alter the biodistribution in genetically engineered streptavidin as compared to wild-type streptavidin.[40]
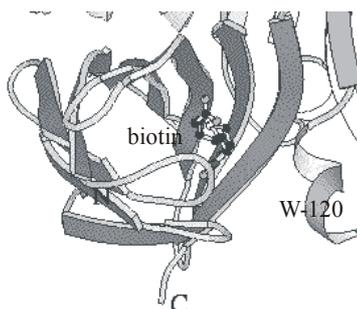
Fig. 6.18.   Interaction of biotin with tryptophan-120, W-120, of a neighboring streptavidin subunit.

Fig. 6.19 illustrates, in a simplified way, the conjugation of a biotinylated polymer to wild-type streptavidin and of a sulfhydryl-terminated polymer to the conjugation sites of S139C.
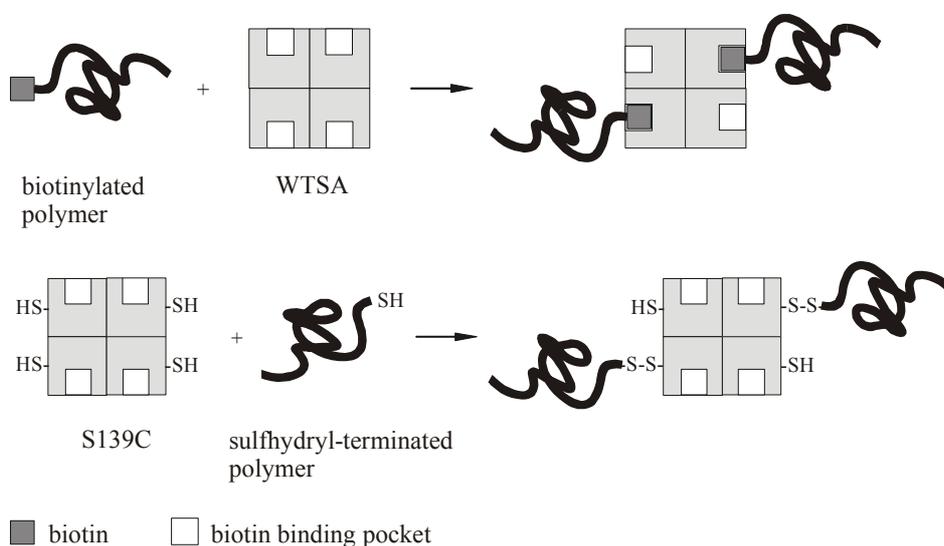

Fig. 6.19.   Binding of biotinylated polymer to biotin binding pockets in WTSA (top) and of sulfhydryl-terminated polymer to conjugation sites in S139C (bottom).

Conjugation of PNIPAAm-*b*-PAA to S139C may result in the formation of structures with active sites that are accessible or inaccessible so that binding can be switched on and off in dependence of pH and temperature. A possible influence of the block copolymer on biotin binding, which is unlikely for small molecules due to the distance of the conjugation site from the binding pocket, should not be excluded, especially in the light of possible electrostatic interactions with carboxylate groups of PNIPAAm-*b*-PAA. Besides, only two out of four sulfhydryl binding sites are expected to be occupied by the polymer due to steric crowding so that binding of smaller sulfhydryl-reactive molecules to adjacent sites may be blocked or made accessible depending on the polymer conformation (expanded or collapsed coil) and conjugate concentration (see below).

6.3.1 Conjugation to wild-type streptavidin (WTSA)

6.3.1.1 Conjugation of biotinylated PNIPAAm

Non-covalent attachment of biotinylated polymers to streptavidin is a reliable tool for the formation of conjugates due to the high affinity of biotin to streptavidin. PNIPAAm samples of molecular weights ranging from 2,900 to 25,900 g/mol were used primarily in order to investigate the influence of polymer size on a possible aggregation of PNIPAAm-streptavidin conjugates above LCST. In case of aggregate formation, vacant biotin binding pockets will not be accessible for binding. At temperatures above LCST, PNIPAAm chains collapse and aggregates will be formed if the conjugate concentration is higher than the critical aggregate concentration, cac. If the concentration is too low, no aggregates will form and the binding sites will be accessible even at $T > LCST$. This concept is demonstrated in Fig. 6.20.
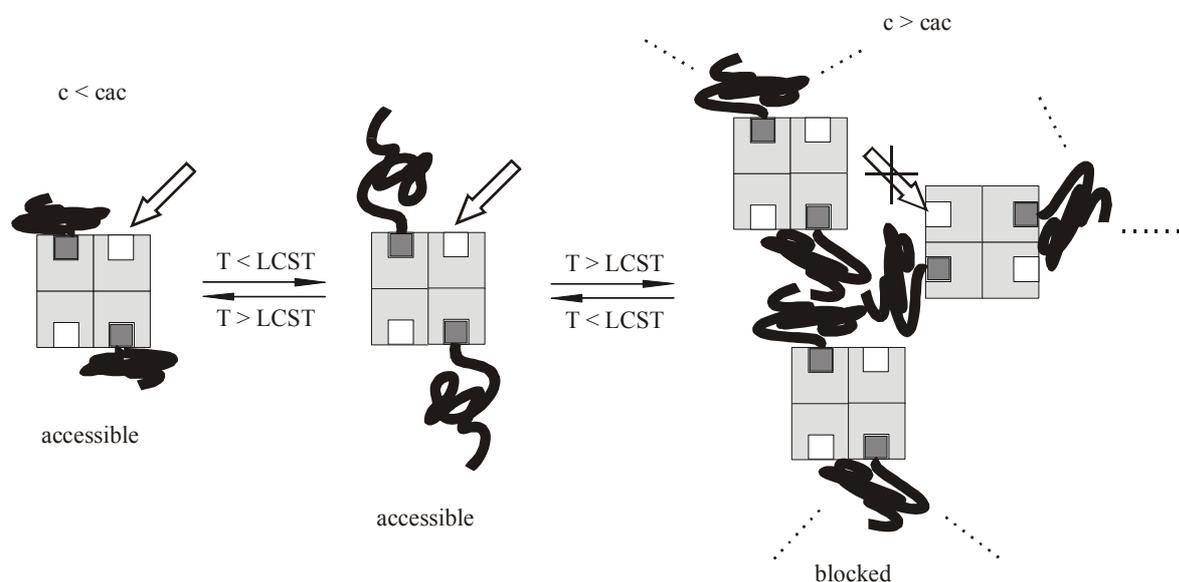
Fig. 6.20.   Concept of conjugate manipulation of biotin binding pocket access through concentration below (left) and above (right) critical aggregate concentration, cac, and temperature; (·····) continuation of aggregation.

Biotinylation of sulfhydryl-terminated PNIPAAm was performed using biotinBMCC (1-biotinamido-4-[4'-(maleimidomethyl)cyclohexane-carboxamido]butane), which is a functionalized biotin derivative containing a maleimide group at the end of an extended spacer arm (Fig. 6.21). The long spacer arm (32.6 Å) provides enough distance between the polymer functionality and the bicyclic biotin end to allow efficient binding of streptavidin or avidin.[14]
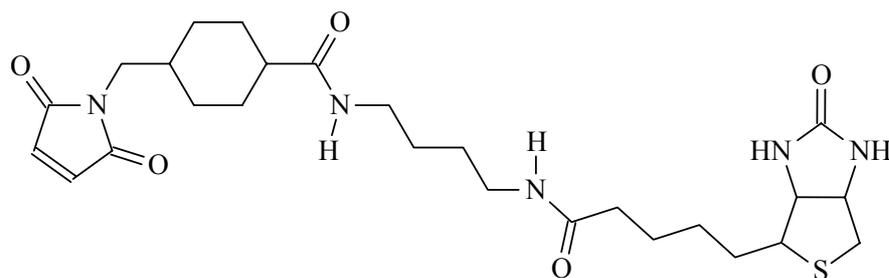
Fig. 6.21.   Structure of the biotinylation reagent biotinBMCC.

Biotinylation efficiency was checked by the so-called HABA assay, which makes use of the dye 4-hydroxyazobenzene-2-carboxylic acid (HABA). The analysis is performed in the presence of avidin, which displays a strong affinity to biotin, similar to streptavidin. In the absence of biotin, HABA forms specific non-covalent complexes with avidin at its biotin binding sites and exhibits a characteristic absorption band at 500 nm ($\varepsilon = 35,500$ $M^{-1}cm^{-1}$). The addition of biotin to an excess of this complex results in displacement of HABA from the binding site, since the affinity constant of the avidin-biotin interaction ($1.3 \cdot 10^{15}$ L/mol) is much larger than that for avidin-HABA ($6 \cdot 10^{6}$ L/mol). As HABA is displaced, the absorbance of the complex decreases proportionally. Comparison of the response of a biotinylated molecule with a standard curve of various biotin concentrations allows calculation of the molar ratio of biotin incorporation.[14,15]

The biotinylation efficiencies obtained for the PNIPAAm samples are shown in Tab. 6.1. The degree of biotinylation is virtually independent of polymer molecular weight, amounting to approximately 60 %. As it is very difficult to separate biotinylated polymer from unreacted polymer, the calculated biotinylation efficiencies were considered in the subsequent conjugation reactions and an appropriately higher amount of polymer was used to ensure equimolar amounts of reactants.

Tab. 6.1.   Biotinylation results for sulfhydryl-terminated PNIPAAm samples of various molecular weights.

entry	M_n [g/mol]	biotinylation efficiency [%]
1	2900	60
2	4800	62
3	9800	57
4	14900	57
5	25900	57

Biotinylated PNIPAAm was reacted with wild-type streptavidin in a 4:1 ratio, which corresponds to a twofold excess of polymer with respect to the number of accessible biotin binding pockets. Stayton, Hoffman et al. have claimed that biotinylated proteins occupy

only two of the four biotin-binding pockets due to steric hindrance.[41] This assumption seems also reasonable for biotinylated polymers, at least for the high-molecular weight samples (entry 3-5 in Tab. 6.1).

The synthesized conjugates can be used to allow or block binding of biotinylated ligands of appropriate size to neighboring binding pockets in dependence of polymer size and temperature.

Preliminary studies of the PNIPAAm/WTSA conjugates with dynamic light scattering (DLS) below and above the LCST of PNIPAAm give strong evidence of aggregates at temperatures above LCST, especially for the high-molecular weight samples. For example, the conjugate with PNIPAAm of molecular weight 25,900 g/mol forms uniform particles with a hydrodynamic radius of ca. 650 nm at a concentration of 9 μM, where the size of the formed mesoglobules strongly decreases with decreasing concentration. For conjugates with PNIPAAm of molecular weight 14,900 g/mol, particles with a hydrodynamic radius of 920 nm are formed at the same concentration and size also decreases with concentration.[42] By varying the parameters concentration, molecular weight and temperature, biofunctional aggregates of desired sizes can be obtained, which may be used to switch proteins on and off.

6.3.1.2   Conjugation of biotinylated PNIPAAm-b-PAA

Similar to the biotinylation of sulfhydryl-terminated PNIPAAm samples, the biotinylation of a PNIPAAm-b-PAA block copolymer of molecular weight $M_n = 17,200$ g/mol that is sulfhydryl-terminated at the PNIPAAm end was performed using biotinBMCC. Again, biotinylation efficiency was calculated from a HABA assay and amounted to 192 %. The high percentage can be explained by an interaction of the negatively charged carboxylate units of PAA with positively charged avidin (cf. section 6.1.2) that gives rise to a larger decrease in absorbance, possibly due to an increased release of HABA from avidin, and therefore leads to a biotinylation efficiency greater than 100 %.

Biotinylated PNIPAAm-b-PAA was reacted with wild-type streptavidin in a 4:1 ratio in order to have a twofold excess of polymer with respect to the number of accessible biotin binding pockets. Only two of the four binding pockets may be occupied due to steric hindrance introduced by the large size of the block copolymer.

Due to the responsiveness of PNIPAAm-b-PAA towards pH and temperature, it was of interest to investigate the behaviour of the PNIPAAm-b-PAA/WTSA conjugate in aqueous solution in dependence of temperature and pH. Fig. 6.22 shows the cloud point curves obtained for the conjugate at different pH values. It is obvious that complete precipitation of the conjugate can be achieved neither by lowering pH nor by increasing the temperature

above LCST. At pH 4.5, the initial transmission of the conjugate solution decreases to about 40 % when raising the temperature above 30 °C. It has to be noted that the initial transmission is already below 90 % and that the transmission decreases with temperature even below LCST. This is attributed to hydrogen bonding interactions between PNIPAAm and PAA units in the block copolymer, leading to the formation of small aggregates that decrease the transmission of the solution. At pH values below 4.4, the transmission of the solutions is slightly above 40 % and does not change upon temperature increase. These observations are different from those made for the block copolymer itself (cf. filled symbols in Fig. 6.22). PNIPAAm-*b*-PAA is completely precipitated from its aqueous solution at pH 4.5 when the temperature is raised above the LCST of PNIPAAm and it is insoluble at pH values below 4.5. This is due to formation of large aggregates at low pH values and at T > LCST, which might eventually lead to gel formation. Obviously, for the conjugate, the concentration is too low for the formation of large aggregates, i.e. precipitation. The decrease in transmission to 40 % might be ascribed to the formation of platelets that are transparent to light in one direction but absorb it in the other direction so that the measured transmission may be an average value. A similar phenomenon has been observed for collagen, thus platelet formation cannot be ruled out.[43]
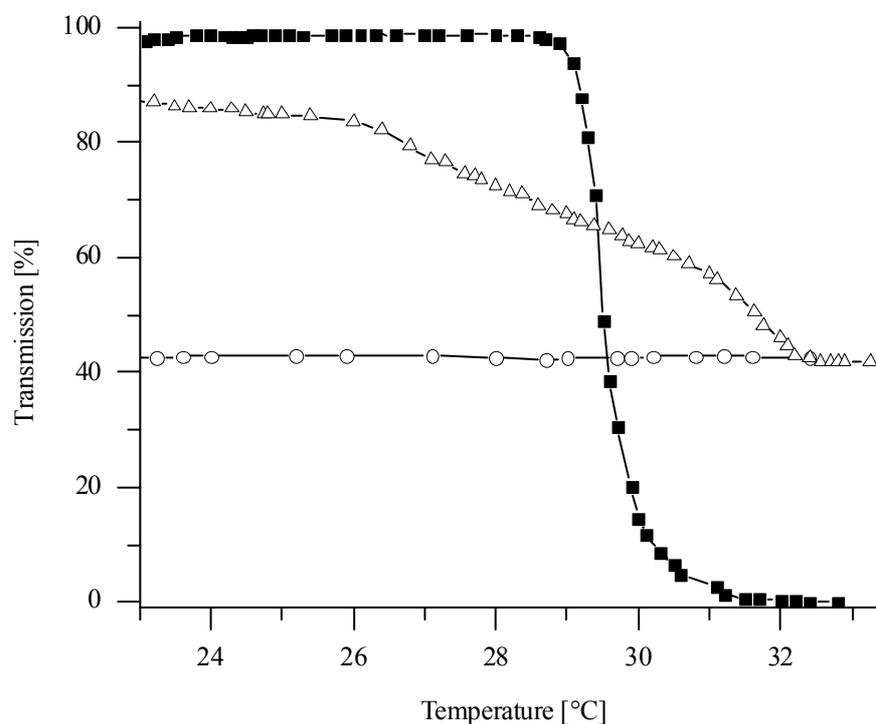
Fig. 6.22.   *Turbidimetry of 0.2 wt.-% aqueous solutions of wild-type streptavidin conjugate with biotinylated PNIPAAm-b-PAA in 0.1 M citrate buffer at pH 3.7 (○) and 4.5 (△); (■) unconjugated block copolymer at pH 4.5 for comparison.*

The results obtained with the conjugate indicate that conjugation to the relatively large streptavidin molecule leads to solubilization of the conjugate even at temperatures above 30 °C, where the pure block copolymer precipitates. The transmission of the conjugate solutions decreases to ca. 40 %, which presumably results from the formation of aggregates. This assumption is confirmed by radio-labeling experiments with ^{3}H-biotin, where conjugates were exposed to an excess of ^{3}H-biotin at 42 °C in solutions of pH 4.5 or 7.4, respectively. At pH 7.4 and T > LCST, the PNIPAAm chains are collapsed but the PAA chains should be expanded, whereas at pH 4.5, PNIPAAm and PAA chains form aggregates as a result of hydrogen bonding interactions. Therefore, it would be expected that adjacent biotin binding pockets are blocked by the aggregated chains. In fact, biotin binding is larger at pH 7.4, which again confirms aggregate formation of the PNIPAAm-*b*-PAA conjugates at pH 4.5.

6.3.2 Conjugation of thiol-terminated PNIPAAm-*b*-PAA to streptavidin mutant S139C

Sulfhydryl-terminated PNIPAAm-*b*-PAA was conjugated to the cysteine group of S139C in two manners, i.e. using a direct disulfide link and via a bismaleimide cross-linking reagent. Conjugation of molecules to cysteine in position 139 is away from the biotin binding pockets and is therefore expected to influence binding to these sites only in the case of large molecules. Depending on pH, temperature and polymer size, aggregated and non-aggregated structures may be formed with active sites that are inaccessible and accessible, respectively, so that binding can be switched on and off. This concept is similar to that illustrated in Fig. 6.20 whereas, in the case of PNIPAAm-*b*-PAA, pH represents an additional factor in the formation of aggregates.

A particular challenge of these novel conjugation approaches was not only to obtain conjugates using sulfhydryl-functionalized polymers but also to perform the conjugation assays without the aid of magnetic beads. Streptavidin can be immobilized on biotinylated or tosyl-activated magnetic beads, which makes two binding pockets inaccessible. These were used in previous experiments in order to facilitate the purification process required after conjugation reaction due to easy removal of the beads owing to their paramagnetic properties. The small diameter of the beads also permits easy suspension and mixing with reactants. Nevertheless, the use of magnetic beads suffers some drawbacks, which were the reasons why they were not used in the conjugations described in this work. The efficiency of immobilization is dependent on the molecular weight of the polymer that is conjugated to the protein and decreases with increasing molecular weight. This is ascribed to steric hindrance induced by the conjugated polymer chains which hinders the conjugate from reaching the magnetic bead surface. In covalent immobilization with tosyl-activated

magnetic beads, the sulfhydryl groups of the streptavidin mutant participate in the immobilization reaction. Therefore, a small amount of sulfhydryl groups has to be left unreacted during conjugation to obtain high immobilization efficiency.[44]

Bismaleimide cross-linking was performed using commercial BM[PEO]$_3$ (1,8-bis-maleimidotriethyleneglycol), which contains a trimeric ethylene glycol chain with maleimido functions at both ends (Fig. 6.23).
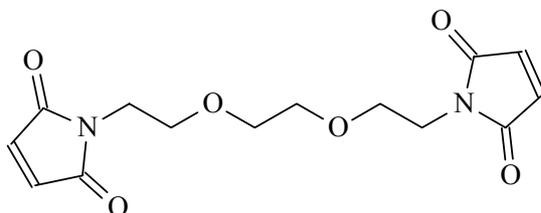

Fig. 6.23.   *Structure of the bismaleimide cross-linking reagent BM[PEO]$_3$.*

The block copolymer was first reacted with a tenfold excess of the cross-linker in order to decrease the amount of symmetrical coupling products, then the polymer-maleimide adduct was reacted with threefold excess of freshly reduced S139C. The conjugate was removed from the unconjugated protein by temperature- and pH- induced precipitation, making use of a rather high conjugate concentration (about three times as much as that used in the turbidimetry measurements). The conjugated protein becomes insoluble and aggregates with other conjugate molecules and free polymer chains at temperatures above LCST and at low pH values, whereas the unconjugated protein remains soluble. Precipitation was achieved by centrifuging the acidified reaction mixture at 15,000 rpm for 15 min at 42 °C. Unconjugated streptavidin remains in the supernatant.

The obtained fractions were subjected to gel electrophoresis using SDS-PAGE analysis (sodium dodecylsulfate polyacrylamide gel electrophoresis). For visualization, the fractions were stained with Coomassie Blue, which is a heterocyclic organic stain that binds to virtually all proteins. In order to evaluate the molecular weights of the stained lanes, kaleidoscope prestained standards ("markers") were used that contain stained proteins with specific molecular weights. Prior to loading of the solutions onto the gel, most of the solutions were heated to 90 °C, unless otherwise stated (marked "not boiled" in the figures), in order to defold the proteins. Tetrameric S139C has a molecular weight of 54,000 Da but streptavidin dissociates when heated to ca. 90 °C, which leads to monomer (13,500 Da) formation. The polymer has a molecular weight of 17,200 g/mol.

Fig. 6.24 shows the PAGE gel result for the conjugation with BM[PEO]$_3$ as cross-linker. Protein staining is observed in the precipitate lane. A higher content of streptavidin monomer is found in the "boiled precipitate" lane as compared to the "unboiled precipitate" lane due to heating dissociation, showing the presence of unconjugated

subunits in the conjugates. The tetrameric conjugate dissociates into two conjugated and two unconjugated subunits upon heating as only a maximum occupancy of two binding pockets is possible due to steric crowding. The "boiled precipitate" lane also shows staining around 30 kDa that corresponds to the conjugated subunits. Pure, boiled S139C (Fig. 6.24) was used for comparison and clearly shows that unconjugated streptavidin is primarily present in its monomer form. The supernatant displays streptavidin monomer that corresponds to unconjugated protein. (This was proven by a blind experiment, mixing polymer and protein in the absence of cross-linker. The precipitate showed no staining in gel electrophoresis, i.e. unconjugated protein remains in the supernatant.) Besides, a small portion of the conjugate seems to be left in the supernatant. This is found for many conjugations and is ascribed to incomplete precipitation.[44]
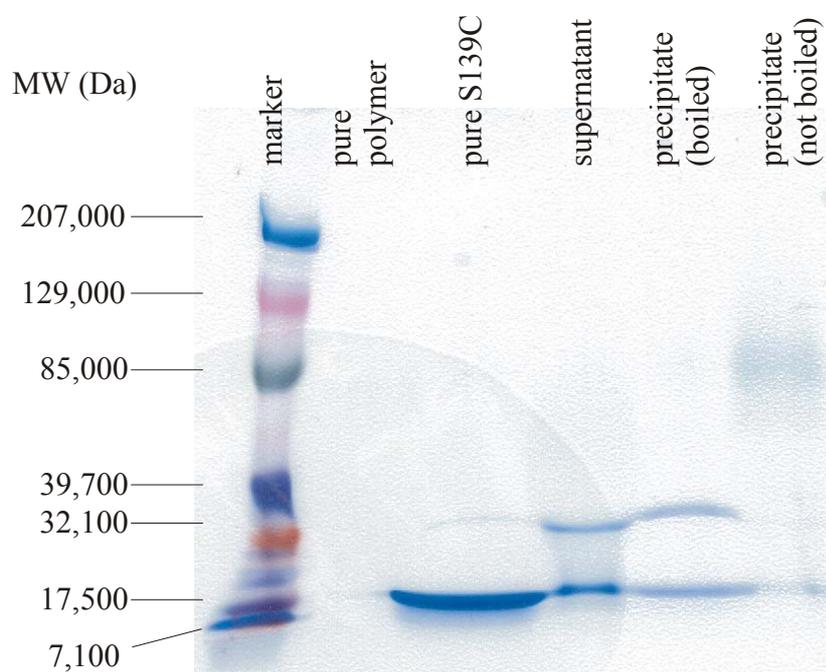
Fig. 6.24.   PAGE gel picture of PNIPAAm-b-PAA/S139C conjugate obtained with bismaleimide cross-linker.

The efficiency of conjugation was evaluated as ca. 50 % by measuring the absorbance of the initial reaction mixture and that of the supernatant after precipitation of the conjugate at 280 nm. Proteins generally show absorption at 275-280 nm due to the presence of aromatic amino acids, especially tryptophan which contributes most to the total absorption of proteins. By measuring the difference in absorbance between the initial mixture and the supernatant, the amount of reacted protein can be determined.

Conjugation via a direct disulfide link was performed by reacting polymer and S139C overnight. Precipitation of the conjugate was achieved by centrifuging the acidified

reaction mixture at 15,000 rpm for 15 min at 42 °C. Unconjugated streptavidin remains in the supernatant.

Fig. 6.25 shows the PAGE gel result for the conjugate obtained with direct disulfide conjugation. Protein staining is observed in the precipitate lane. It is obvious that the conjugation was successful. Basically, the same findings as in the case of maleimide-crosslinked conjugates were made. This time, heated and unheated S139C were used for comparison. It becomes evident from Fig. 6.25 that unheated S139C mainly exists in the monomer and tetramer form, whereas heated S139C is mainly present in its monomer form. Again, a higher content of streptavidin monomer is found in the "boiled precipitate" lane as compared to the "unboiled precipitate" lane due to heating dissociation, showing the presence of unconjugated subunits in the conjugates. Furthermore, no protein is seen in the supernatant after a second precipitation of the conjugate from its solution, i.e. there is only conjugated streptavidin present. The efficiency of conjugation was determined by absorbance measurements at 280 nm and is more than 50 %.
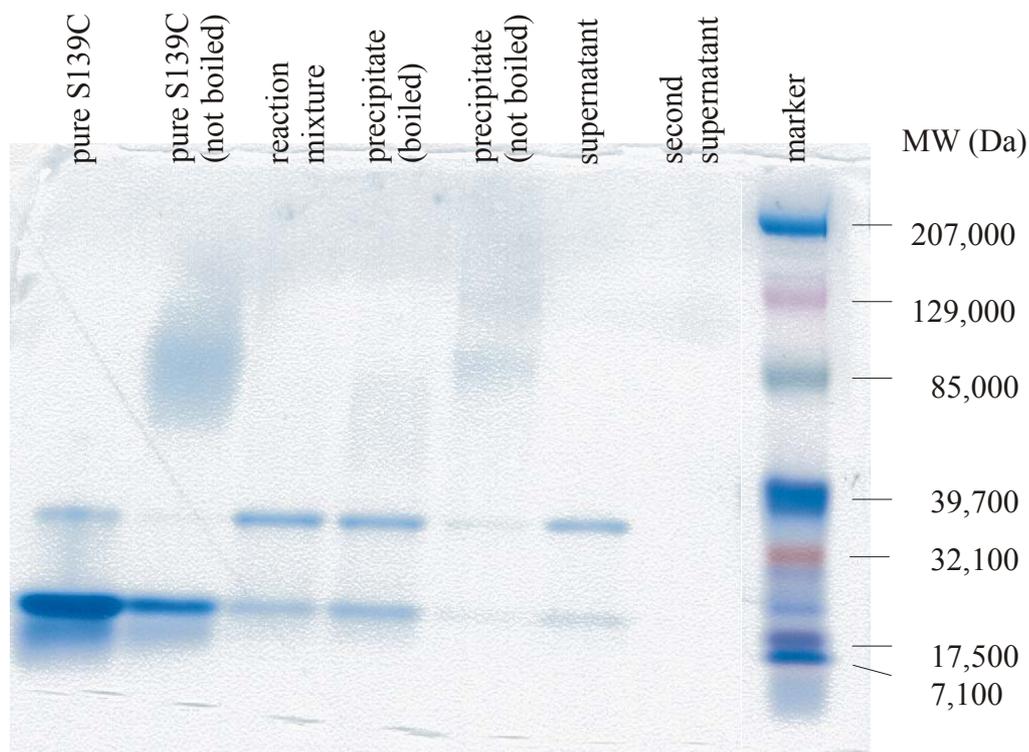
Fig. 6.25. *PAGE gel picture of PNIPAAm-*b-*PAA/S139C conjugate obtained via direct disulfide linkage; second supernatant = supernatant after second precipitation of redissolved precipitate.*

6.4   Outlook

In the present work, the model peptide glycine-leucine, GlyLeu, could be attached successfully to the active ester polymers poly(*N*-hydroxysuccinimide methacrylate), PNHSM, and poly(2-vinyl-4,4-dimethyl-5-oxazolone), PVO, and also to the multi-functional polymer poly(diacetone acrylamide), PDAA. These polymers, having binding sites for primary amino groups, may subsequently be used as constituents of stimuli-sensitive block copolymers for drug attachment.

The successful covalent conjugation of the streptavidin mutant S139C to PNIPAAm-*b*-PAA was demonstrated using a maleimide cross-linker or direct disulfide linkage. With the use of biotinylated PNIPAAm or PNIPAAm-*b*-PAA, non-covalent conjugates to wild-type streptavidin, WTSA, were obtained by interaction of biotinylated polymer with the binding pockets of the protein.

DLS measurements showed the formation of smart polymer-protein nanoparticles from biotinylated PNIPAAm and WTSA. The formation of these particles depends on the solution temperature and their sizes vary with the size of PNIPAAm and the concentration of the conjugate. The nanoparticles can be formed and disaggregated reversibly by using an external stimulus. Potential applications of these "smart" aggregates lie in chip-based chemical reactions and microfluidics, i.e. the transport of fluids and materials in an environment of reduced dimensions, where properties like diffusion, sedimentation and adhesion of biomolecules to channel walls or beads are controlled by the attached stimuli-responsive polymer. Dependent on the site of conjugation, the aggregates may also function as switches by occluding the active site in aggregate form and releasing it after reversing the temperature stimulus. It would also be of interest to investigate the aggregation behaviour of PNIPAAm-*b*-PAA/WTSA conjugates with sulfhydryl-terminated PAA as opposed to the conjugates studied with sulfhydryl-terminated PNIPAAm, which is also dependent on temperature, pH and ionic strength.

For both covalent and non-covalent conjugates, investigation of shielding/deshielding of protein binding by the attached polymers will provide some insight into the dependence of this on/off effect on the size of polymer/protein, temperature, and pH. Polymers conjugated to streptavidin are expected to influence binding of ligands to the active sites in dependence of their size and of external stimuli. Earlier studies with differently sized proteins have shown that size-dependent control of binding is achieved, while binding of very large molecules is blocked and that of very small molecules is unblocked independent of polymer conformation.[41]

The potential actions of conjugates derived from PNIPAAm-*b*-PAA are steric and electrostatic blocking of active sites by the block copolymer that can be triggered by the

external stimuli temperature, pH, and ionic strength. Promising supplementary investigations of these smart polymer-protein conjugates would be to perform binding assays with fluorescence- or radio-labeled ligands of various sizes, where oligonucleotides, such as DNA, would be especially interesting due to possible electrostatic interaction with the PAA block owing to their inherent charge.

Another interesting aspect for further studies is the triggered release of biotinylated drugs/proteins from the streptavidin conjugates.

In summary, smart polymer-protein conjugates possess unique characteristics that may find applications in various fields, ranging from drug delivery to bioseparation and even to miniaturization of chemical analysis and synthesis ("lab on a chip"[45]).

References

(1)   Batz, H.-G.; Franzmann, G.; Ringsdorf, H. *Angew. Chem.* **1972**, *84*, 1189-1190.

(2)   Godwin, A.; Hartenstein, M.; Müller, A. H. E.; Brocchini, S. *Angew. Chem. Int. Ed.* **2001**, *40*, 594.

(3)   Duncan, R. *Anti-Cancer Drugs* **1992**, *3*, 175-210.

(4)   Nucci, M. L.; Shorr, R.; Abuchowski, A. *Adv. Drug Delivery Rev.* **1991**, *6*, 133-151.

(5)   Dagani, R. *Chem. Eng. News* **1995**, *9*, 30-33.

(6)   Galaev, I. Y.; Mattiasson, B. *Trends Biotechnol.* **1999**, *17*, 335-340.

(7)   Hoffman, A. S.; Stayton, P. S.; Bulmus, V.; Chen, G.; Chen, J.; Cheung, C.; Chilkoti, A.; Ding, Z.; Dong, L.; Fong, R.; Lackey, C. A.; Long, C. J.; Miura, M.; Morris, J. E.; Murthy, N.; Nabeshima, Y.; Park, T. G.; Press, O. W.; Shimoboji, T.; Shoemaker, S.; Yang, H. J.; Monji, N.; Nowinski, R. C.; Cole, C. A.; Priest, J. H.; Harris, J. M.; Nakamae, K.; Nishino, T.; Miyata, T. *J. Biomed. Mater. Res.* **2000**, *52*, 577-586.

(8)   Hoffman, A. S. *Clin. Chem.* **2000**, *46*, 1478-1486.

(9)   Cole, C.-A.; Schreiner, S. M.; Priest, J. H.; Monji, N.; Hoffman, A. S. *ACS Symp. Ser.* **1987**, *350 (Reversible Polym. Gels Relat. Syst.)*, 245-254.

(10)   Gupta, M. N.; Mattiasson, B. *Highly Selective Separations in Biotechnology*; Blackie Academic & Professional: London, 1994.

(11)   Godbey, W. T. *J. Control. Release* **1999**, *60*, 149-160.

(12)   Godbey, W. T.; Mikos, A. G. *J. Control. Release* **2001**, *72*, 115-125.

(13)   Murthy, N.; Campbell, J.; Fausto, N.; Hoffman, A. S.; Stayton, P. S. *Bioconjugate Chem.* **2003**, *14*, 412-419.

(14)   Hermanson, G. T. *Bioconjugate Techniques*; Academic Press Inc.: San Diego, 1996.

(15)   Green, N. M. *Adv. Protein Chem.* **1975**, *29*, 85-133.

(16)   Weber, P. C.; Ohlendore, D. H.; Wendoloski, J. J.; Salemme, F. R. *Science* **1989**, *243*, 85-88.

(17)   Hendrichson, W. A.; Pahler, A.; Smith, J. L.; Satow, Y.; Merritt, E. A. *Proc. Natl. Acad. Sci. USA* **1989**, *86*, 2190-2194.

(18)   Grubmueller, H.; Heymann, B.; Tavan, P. *Science* **1996**, *271(5251)*, 997-999.

(19)   Sano, T.; Cantor, C. R. *Proc. Natl. Acad. Sci. USA* **1995**, *92(8)*, 3180-3184.

(20)   Freitag, S.; Le, T.-I.; Klumb, L.; Stayton, P. S.; Stenkamp, R. E. *Protein Science* **1997**, *6(6)*, 1157-1166.

(21)   Klumb, L. A.; Chu, V.; Stayton, P. S. *Biochemistry* **1998**, *37*, 7657 -7663.

(22) Diamandis, E. P.; Christopoulos, T. K. *Clinical Chemistry* **1991**, *37(5)*, 625-636.

(23) Chilkoti, A.; Boland, T.; Ratner, B. D.; Stayton, P. S. *Biophys. J.* **1995**, *69(5)*, 2125-2130.

(24) Zimmermann, J.; Mülhaupt, R. *Polym. Prepr. (Am. Chem. Soc., Div. Polym. Chem.)* **2000**, *41(1)*, 764-765.

(25) Guichard, B.; Noel, C.; Reyx, D.; Thomas, M.; Chevalier, S.; Senet, J.-P. *Macromol. Chem. Phys.* **1998**, *199*, 1657-1674.

(26) Mayer, R.; Scheithauer, S. *Carbonsäuren und Carbonsäure-Derivate*; Houben-Weyl: Stuttgart, 1985; Vol. E5.

(27) Schwetlick, K. *Organikum*, 19. Auflage; Barth Verlagsgesellschaft mbH: Leipzig, Berlin, Heidelberg, 1993.

(28) Ellman, G. L. *Arch. Biochem. Biophys.* **1959**, *82*, 70-77.

(29) Habeeb, A. F. S. A. *Methods Enzymol.* **1972**, *25 (Part B)*, 457-464.

(30) Wenck, H.; Schneider, F. *Experientia* **1971**, *27(1)*, 20-22.

(31) Mukaiyama, T.; Takahashi, K. *Tetrahedr. Lett.* **1968**, 5907-5908.

(32) Yoneda, F.; Suzuki, K.; Nitta, Y. *J. Org. Chem.* **1967**, *32*, 727-729.

(33) Macindoe, W. M.; van Oijen, A. H.; Boons, G.-J. *Chem. Commun. (Cambridge)* **1998**, 847-848.

(34) Rabanal, F.; DeGrado, W. F.; Dutton, P. L. *Tetrahedron Lett.* **1996**, *37*, 1347-1350.

(35) Ghosh, S. S.; Kao, P. M.; McCue, A. W.; Chappelle, H. L. *Bioconjugate Chem.* **1990**, *1*, 71-76.

(36) Partis, M. D.; Griffiths, D. G.; Roberts, G. C.; Beechey, R. B. *J. Protein Chem.* **1983**, *2*, 263-277.

(37) Feng, X.-S.; Pan, C.-Y. *Macromolecules* **2002**, *35*, 4888-4893.

(38) Ding, Z.; Long, C. J.; Hayashi, Y.; Bulmus, E. V.; Hoffman, A. S.; Stayton, P. S. *Bioconjugate Chem.* **1999**, *10*, 395-400.

(39) Stayton, P. S.; Nelson, K. E.; McDevitt, T. C.; Bulmus, V.; Shimoboji, T.; Ding, Z.; Hoffman, A. S. *Biomol. Eng.* **1999**, *16*, 93-99.

(40) Wilbur, D. S.; Stayton, P. S.; To, R.; Buhler, K. R.; Klumb, L. A.; Hamlin, D. K.; Stray, J. E.; Vessella, R. L. *Bioconjugate Chem.* **1998**, *9*, 100 -107.

(41) Ding, Z.; Fong, R. B.; Long, C. J.; Stayton, P. S.; Hoffman, A. S. *Nature* **2001**, *411*, 59-62.

(42) Kulkarni, S.; Schilli, C.; Müller, A.; Hoffman, A.; Stayton, P., to be published.

(43) Hoffman, A. H. *personal communication*.

(44) Ding, Z. *Ph.D. thesis*; University of Washington: Seattle, 2000.

(45) www.lgc.co.uk/research_labonachip.asp. LGC.

7 Experimental section

7.1 Synthesis of the chain transfer agents

All solvents of p.a. or HPLC grade were purchased from Fluka or Aldrich and were used as received unless stated otherwise. Pyrrole (Fluka, purum) was distilled over NaOH prior to use. CS_2 (purum) and benzylchloride (purum) were purchased from Fluka and used as received. NaH was used in the form of a free-flowing powder, moistened with oil (55-65 %, Fluka). Cumene was purchased from Fluka and distilled prior to use. 2-Pyrrolidone and 2-chloropropionitrile of p.a. grade were purchased from Fluka and used without further purification. *N*-Bromosuccinimide (purum, Fluka) was dried prior to use. Phenyl magnesium bromide was purchased as a 0.1 M solution in THF (Fluka) and used as received. Azobisisobutyronitrile (AIBN, Fluka, purum) was recrystallized three times from methanol and dried under vacuum prior to use. $K_3Fe(CN)_6$ and *p*-toluenesulfonic acid from Fluka (purum) were used without further purification. Mg turnings were purchased from Fluka. Styrene (BASF) was destabilized by running it on an adsorption column filled with Alumina B (ICN Biomedicals GmbH, Germany).

7.1.1 Benzyl-1-pyrrolecarbodithioate

The synthesis of this chain transfer agent was carried out according to the procedure reported in the literature.[1] A suspension of NaH (0.48 g, 20 mmol) in anhydrous DMSO (20 mL) was prepared. Pyrrole (1.34 g, 20 mmol) was added under vigorous stirring. The yellow solution was then stirred for another 30 min at room temperature. The solution was cooled to 20 °C and CS_2 (1.52 g, 20 mmol) was added dropwise. The resultant reddish brown solution was stirred for 30 min at room temperature, then benzyl chloride (2.54 g, 20 mmol) was added. After stirring for 1 h, water (20 mL) and then diethylether (20 mL) was added. The organic layer was separated and the aqueous layer was extracted three times with diethylether (40 mL). The combined extracts were dried over Na_2SO_4, filtered and the solvent was evaporated. The crude product was subjected to column chromatography (silicagel 60, mesh 70-230) with cyclohexane/ethyl acetate 95:5 (v:v) as eluent. The main fraction was yellow. The solvent was evaporated and the product dried under vacuum to yield a bright yellow oil.
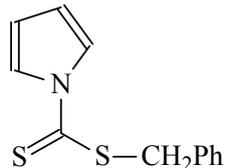
Yield: 89 %. ^{1}H NMR ($CDCl_3$): δ [ppm] 4.61 (s, 2H, CH_2), 6.31-6.34 (t, 2H, pyrrole CH), 7.30-7.43 (m, 5H, phenylic CH), 7.70-7.72 (t, 2H, pyrrole CH-N); ^{13}C NMR ($CDCl_3$):

δ [ppm] 41.72 (CH$_2$), 114.18 (pyrrole CH), 120.64 (pyrrole CH-N), 127.93 (phenylic C), 128.74 (phenylic C), 129.37 (phenylic C), 134.44 (phenylic C), 199.33 (C=S); UV (CHCl$_3$): λ$_{max}$ = 296.2 nm.

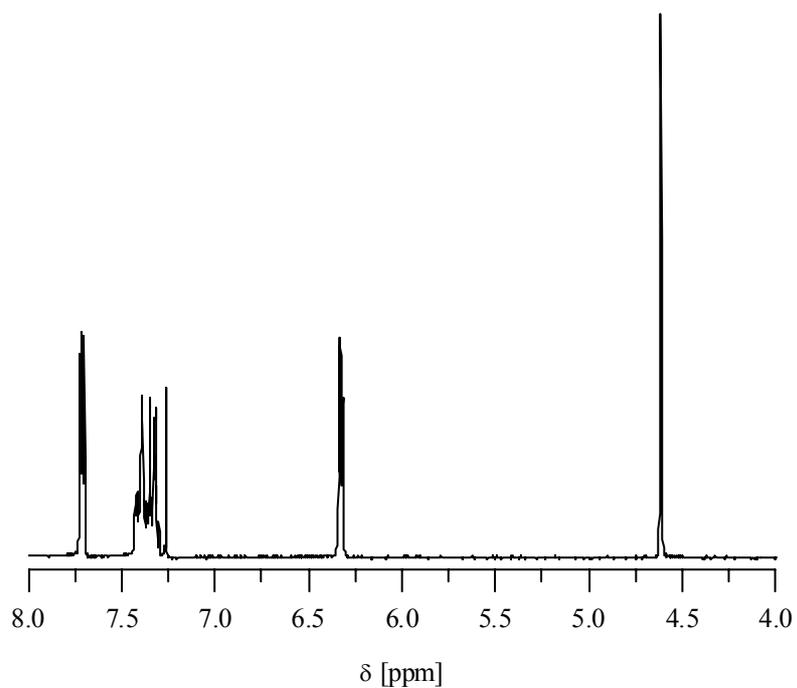Fig. 7.1 and Fig. 7.2 shows the ^{1}H-NMR and ^{13}C-NMR spectrum, respectively, of the chain transfer agent.

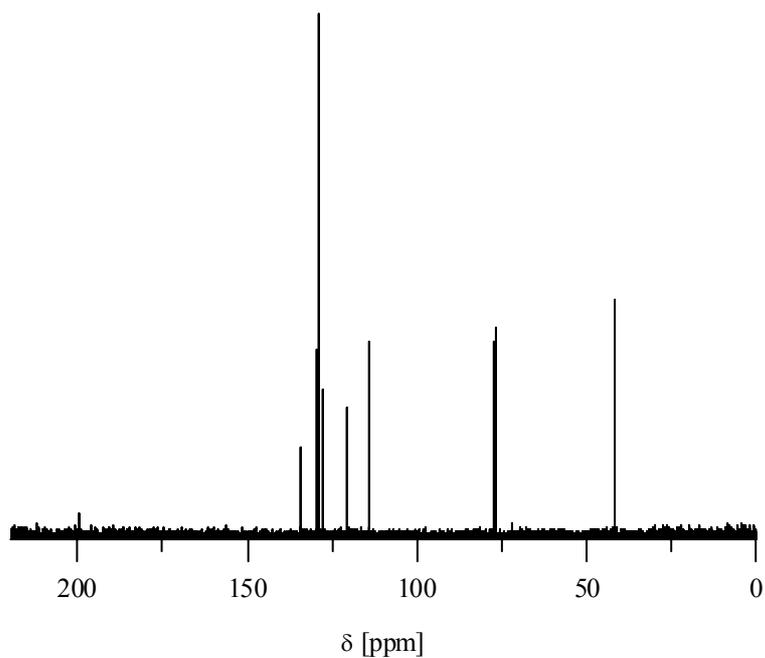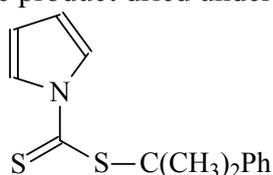*Fig. 7.1.* ^{1}*H-NMR spectrum of benzyl-1-pyrrolecarbodithioate in CDCl$_3$.*

Fig. 7.2. ^{13}*C-NMR spectrum of benzyl-1-pyrrolecarbodithioate in CDCl$_3$.*

7.1.2 Cumyl-1-pyrrolecarbodithioate

Cumyl bromide was not commercially available and thus had to be synthesized from cumene and *N*-bromosuccinimide.[2] A solution of cumene (15 mL, 12.96 g, 0.108 mol), AIBN (0.2 g, 1.22 mmol) and *N*-bromosuccinimide NBS (21.0 g, 0.118 mol) in dry CCl_4 (120 mL, distilled over CaH_2) was immersed into an oil bath at 100 °C. The mixture was stirred vigorously (very exothermic reaction) and stirring was continued until 10 min after beginning of reflux. Then the reaction mixture was cooled in an icebath and the obtained white precipitate was filtered off. The solvent was removed from the filtrate by rotary evaporation. The crude product was subjected to fractionating distillation (b.p. 63 °C at $5.3 \cdot 10^{-2}$ mbar) to give a yellowish oil.

Yield: 48 %. ^{1}H NMR (C_6D_6): δ [ppm] 1.82 (s, 6H, CH_3), 6.93-7.08 (m, 3H, aromatic CH), 7.31-7.37 (m, 2H, aromatic ortho-CH).

A suspension of NaH (0.48 g, 20 mmol) in anhydrous DMSO (20 mL) was prepared. Pyrrole (1.34 g, 20 mmol) was added under vigorous stirring. The yellow solution was then stirred for another 30 min at room temperature. The solution was cooled to 20 °C and CS_2 (1.52 g, 20 mmol) was added dropwise. The resultant reddish orange solution was stirred for 30 min at room temperature, then cumylbromide (3.98 g, 20 mmol) was added. After stirring for 2 h, water (20 mL) and then diethylether (20 mL) was added. The organic layer was separated and the aqueous layer was extracted three times with diethylether (40 mL). The combined extracts were dried over $MgSO_4$, filtered and the solvent was evaporated. The crude product was subjected to column chromatography (silicagel 60, mesh 70-230) with cyclohexane/ethyl acetate 95:5 (v:v) as eluent. The main fraction was bright orange. The solvent was evaporated and the product dried under vacuum to yield an orange oil.

Yield: 48 %. ^{1}H NMR ($CDCl_3$): δ [ppm] 1.95 (s, 6H, CH_3), 6.20 (dd, 2H, pyrrole CH), 7.15-7.28 (m, 5H, phenylic CH), 7.56 (dd, 2H, pyrrole CH-N); ^{13}C NMR ($CDCl_3$): δ [ppm] 28.89 (CH_3), 56.71 (isopropyl C), 113.45 (pyrrole CH), 119.92 (pyrrole CH-N), 126.81 (phenylic C), 128.02 (phenylic C), 143.96 (phenylic C), 197.01 (C=S); UV ($CHCl_3$): $\lambda_{max} =$ 299.0 nm.

Fig. 7.3 and Fig. 7.4 shows the ^{1}H-NMR and ^{13}C-NMR spectrum, respectively, of cumyl-1-pyrrolecarbodithioate.

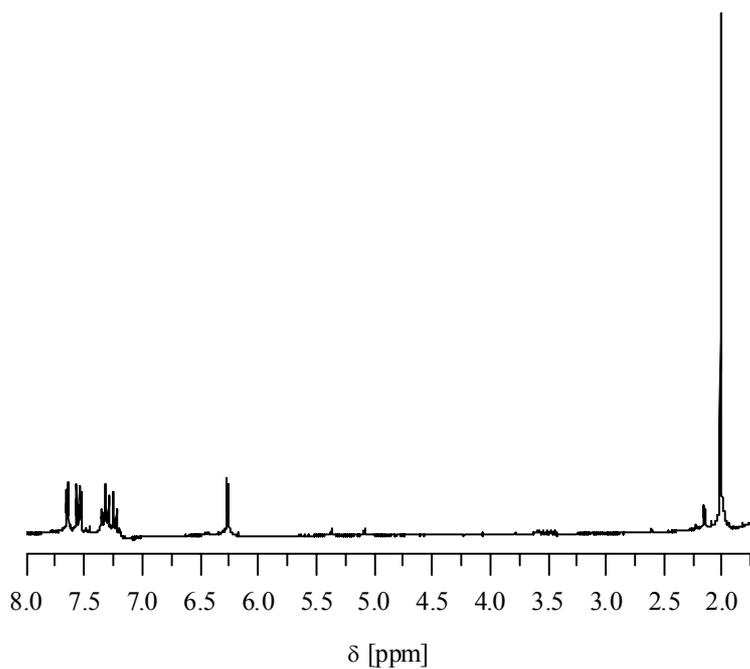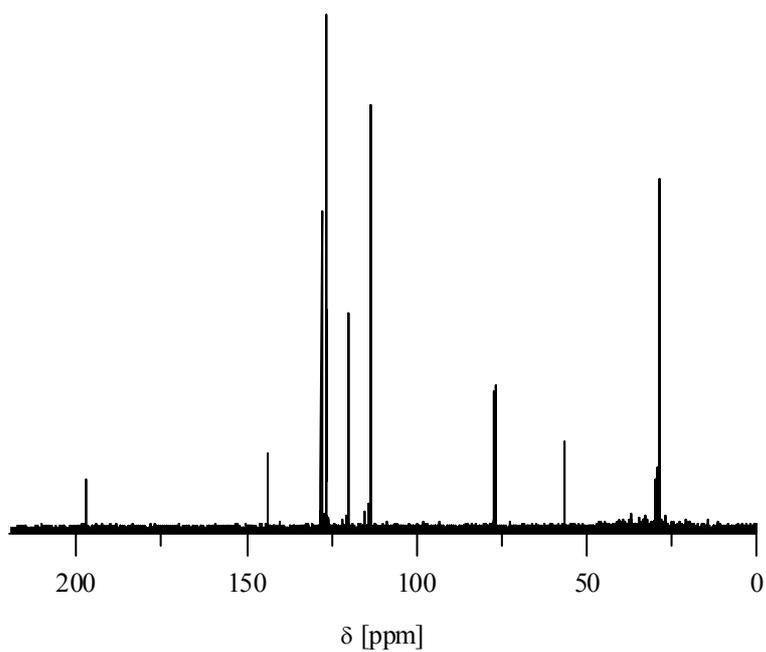*Fig. 7.3.* *¹H-NMR spectrum of cumyl-1-pyrrolecarbodithioate in CDCl₃.*

Fig. 7.4. *¹³C-NMR spectrum of cumyl-1-pyrrolecarbodithioate in CDCl₃.*

7.1.3   1-Cyanoethyl 2-pyrrolidone-1-carbodithioate

The synthesis of 1-(2-pyrrolidinone)carbodithioic acid was performed according to the procedure reported in the literature.[3] 2-Pyrrolidone (6.0 g, 70.50 mmol) was dissolved in anhydrous DMSO (30 mL) and the mixture was cooled to 15 °C. CS_2 (4.7 mL, 5.92 g, 77.78 mmol) was added dropwise to the solution. After complete addition of CS_2, 6 N aq. KOH (12 mL) was added to the yellow mixture under stirring and cooling (< 20 °C). The resultant brown mixture was stirred for 40 min at 15-20 °C. Then the mixture was poured onto a mixture of 40 mL 33% HCl, 200 mL H_2O and 200 g ice. The obtained yellow precipitate is filtered off and washed with H_2O, then with diethylether. The bright orange solid is recrystallized from acetone and vacuum-dried.

Yield: 20 %. ^{1}H NMR (CDCl$_3$): δ [ppm] 2.04-2.16 (m, 2H, CH$_2$), 2.76 (t, 2H, CH$_2$C=O), 4.23 (t, 2H, CH$_2$N), 6.52 (bs, 1H, SH); ^{13}C NMR (CDCl$_3$): δ [ppm] 16.01 (CH$_2$), 32.95 (CH$_2$C=O), 52.70 (CH$_2$N), 173.82 (C=O), 195.34 (C=S).

For the synthesis of 1-cyanoethyl 2-pyrrolidone-1-carbodithioate,[4] 2-chloropropionitrile (1.01g, 11.3 mmol) was added to a suspension of 1-(2-pyrrolidinone)carbodithioic acid (0.97 g, 6.02 mmol) and potassium carbonate (0.84g, 6.09mmol) in anhydrous acetonitrile (10 mL) at room temperature. The resulting ochre mixture was stirred at room temperature for 18 h whereupon the colour changed to brown. Water (25 mL) was added, and the aqueous layer was extracted twice with ethyl acetate (30 mL). The combined organic layers were dried over anhydrous Na$_2$SO$_4$. After removal of solvent, the residue was subjected to column chromatography (silicagel 60, 70-230 mesh) using ethyl acetate/*n*-hexane 6:19 (v:v) as eluent. The product was a light-yellow oil.
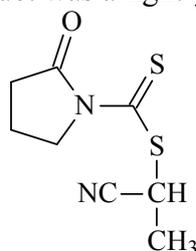
Yield: 64 %. ^{1}H NMR (C$_6$D$_6$): δ [ppm] 0.86-0.98 (m, 2H, CH$_2$), 1.14 (d, 3H, CH$_3$), 1.76-1.83 (dt, 2H, CH$_2$C=O), 3.39-3.58 (m, 2H, CH$_2$N), 4.42-4.51 (q, 1H, CH) ; ^{13}C NMR (C$_6$D$_6$): δ [ppm] 16.12 (CH$_3$), 16.41 (CH$_2$), 32.37 (CH$_2$C=O), 33.02 (S-CH), 52.94 (CH$_2$-N), 119.70 (CN), 173.14 (C=O), 195.93 (C=S).

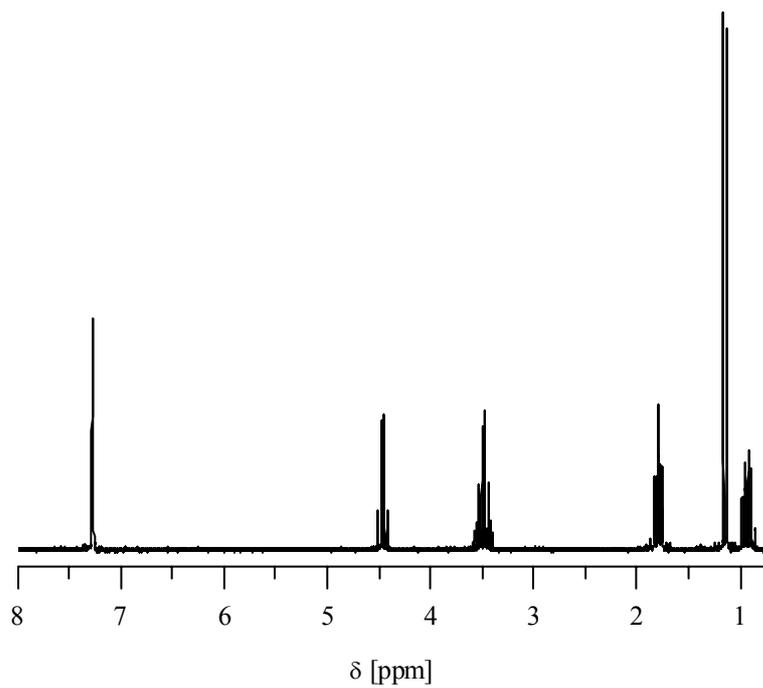Fig. 7.5 and Fig. 7.6 shows the ^{1}H-NMR and ^{13}C-NMR spectrum, respectively, of the chain transfer agent.

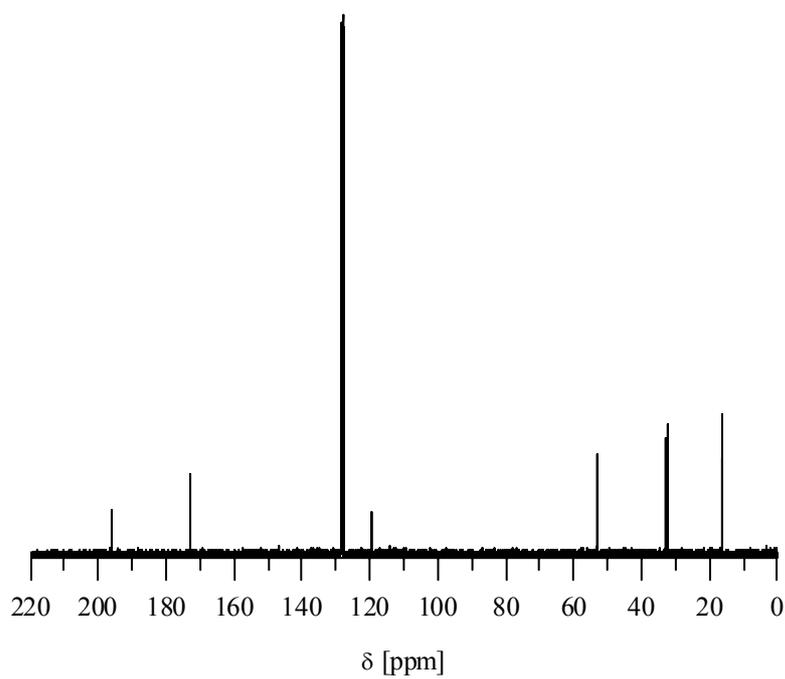*Fig. 7.5.*   *¹H-NMR spectrum of 1-cyanoethyl 2-pyrrolidone-1-carbodithioate in C₆D₆.*

Fig. 7.6.   *¹³C-NMR spectrum of 1-cyanoethyl 2-pyrrolidone-1-carbodithioate in C₆D₆.*

7.1.4   Cyanoisopropyl-1-benzylcarbodithioate

Dithiobenzoic acid was synthesized from phenyl magnesium bromide and CS_2.[5] Phenyl magnesium bromide (6.53 g, 0.036 mol) in THF (100 mL) was reacted with CS_2 (2.7 g, 0.036 mol) in dry THF (30 mL, distilled over potassium) at - 5 °C for 1h. The reaction mixture was diluted with diethyl ether (50 mL) and decomposed with icecold diluted HCl (50 mL). The organic layer was isolated and extracted three times with icecold 10 % NaOH (30 mL). The alkaline solution was washed three times with diethyl ether and acidified with icecold 10 % HCl, then extracted with diethyl ether. The ether solution was washed three times with water. After evaporation of the solvent, pure dithiobenzoic acid was obtained which was stored as an aqueous solution of sodium dithiobenzoate.

Bis(thiobenzoyl) disulfide was synthesized from sodium dithiobenzoate according to the literature procedure.[6] $K_3Fe(CN)_6$ (3.29 g, 0.01 mol) was dissolved in water (50 mL) and was added dropwise over 1h to a solution of sodium dithiobenzoate (1.76 g, 0.01 mol) in water (10 mL) while stirring vigorously. The resultant red precipitate was filtered off and washed with water until the washings were colourless. The solid was dried in vacuum overnight and recrystallized from ethanol.

The chain transfer agent was synthesized according to the literature procedure.[7,8] A solution of 2,2'-azobis(isobutyronitrile) (10.5 g, 64.02 mmol) and bis(thiobenzoyl) disulfide (13.05 g, 42.68 mmol) in ethyl acetate (250 mL) was refluxed for 18 h. After evaporation of the solvent, the crude product was subjected to column chromatography (silicagel 60, 70-230 mesh) using ethyl acetate/n-hexane 2:3 (v:v) as an eluent. The product was a purple oil that crystallized in the freezer overnight.
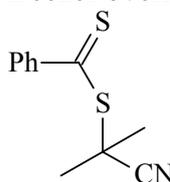
Yield: 68 %. ^{1}H NMR ($CDCl_3$): δ [ppm] 1.83 (s, 6H, CH_3), 7.25-7.31 (dt, 2H, aromatic meta-CH), 7.42-7.48 (dt, 1H, aromatic para-CH), 7.79-7.82 (dd, 2H, aromatic ortho-CH); ^{13}C NMR ($CDCl_3$): δ [ppm] 26.37 (CH_3), 41.64 (isopropyl C), 119.91 (CN), 126.57 (aromatic C), 128.47 (aromatic C), 132.86 (aromatic C), 144.44 (aromatic C).

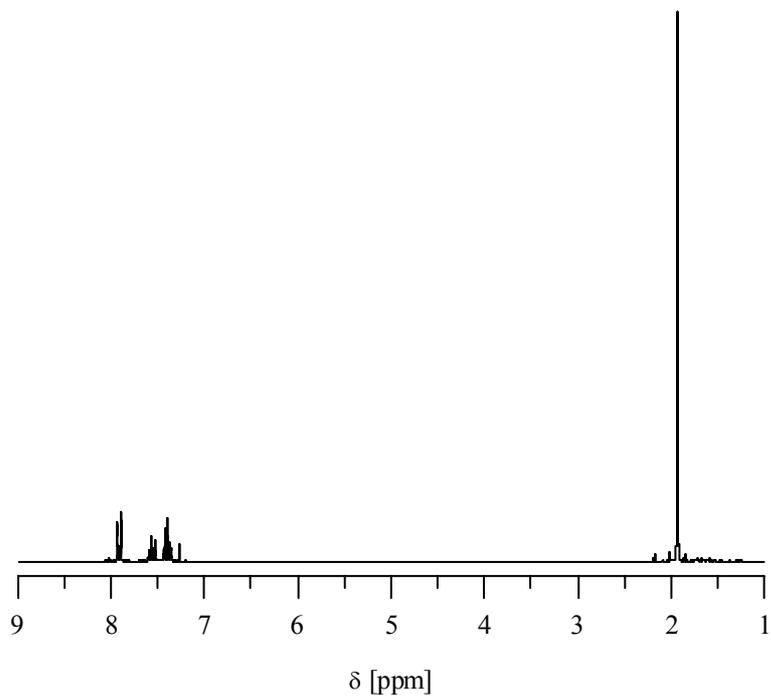Fig. 7.7 and Fig. 7.8 shows the ^{1}H-NMR and ^{13}C-NMR spectrum, respectively, of the chain transfer agent.

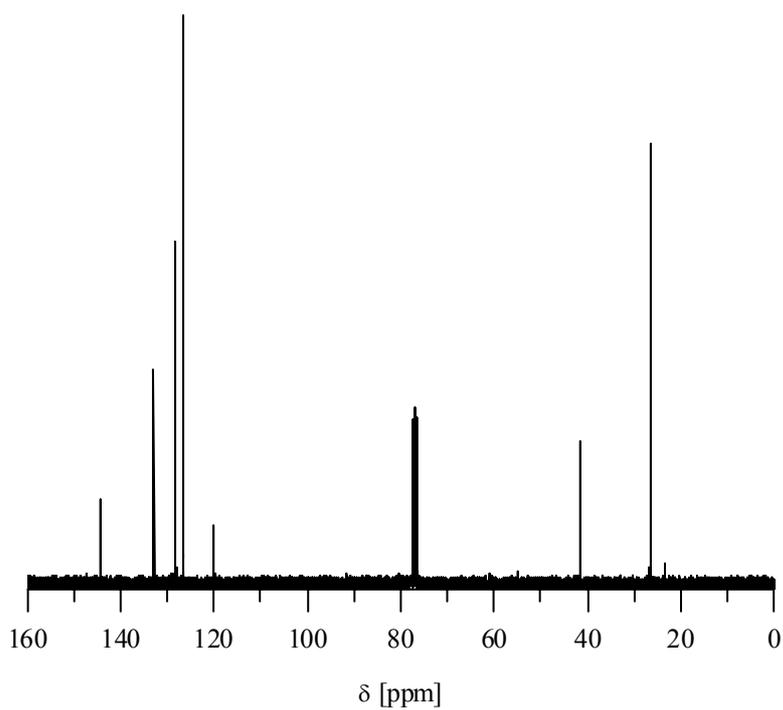*Fig. 7.7.*   *¹H-NMR spectrum of cyanoisopropyl-1-benzylcarbodithioate in CDCl₃.*

Fig. 7.8.   *¹³C-NMR spectrum of cyanoisopropyl-1-benzylcarbodithioate in CDCl₃.*

7.1.5   1-Phenylethyl phenyldithioacetate

In the first step, dithiobenzoic acid was prepared following the literature procedure[5] To a mixture of magnesium turnings (3.8 g, 0.156 mol) in dry diethyl ether (100 mL, distilled over sodium), benzyl chloride (19.8 g, 0.156 mol) was added dropwise under vigorous stirring. After complete addition of benzyl chloride, the mixture was refluxed for 3 ½ h. After cooling to − 5 °C, CS_2 (9.5 mL, 11.97 g, 0.157 mol) was added and the resultant brownish mixture was stirred at 0 °C for 2 h. A viscous yellow mixture resulted and 100 mL ice water as well as 100 mL 33 % HCl were added. The organic layer was extracted three times with icecold 10 % NaOH (120 mL). The alkaline layer was extracted three times with diethyl ether. To the residual alkaline layer, the same amount of 10 % HCl was added (i.e. 200 mL ice water and 100 mL 33 % HCl) and the aqueous phase was extracted three times with diethyl ether. All combined organic layers were then dried over 4 Å molecular sieve. After complete drying, the solvent was evaporated and a dark orange oil was recovered which was directly used for further conversion to 1-phenylethyl phenyldithioacetate in a procedure similar to the one reported in the literature.[9] To a mixture of dithiobenzoic acid (9.91 g, 58.90 mmol) and *p*-toluenesulfonic acid monohydrate (catalytic amount), CCl_4 (15 mL, distilled over CaH_2) was added. After stirring for 15 min, styrene (10 mL, 87.28 mmol) was added dropwise and the mixture was refluxed overnight. Evaporation of the solvent yielded a dark brown residue which was subjected to column chromatography (silicagel 60, 70-230 mesh) with ethyl acetate/*n*-hexane 1:9 (v:v) as an eluent. An orange liquid was obtained which crystallized to a bright orange solid upon storage in the freezer overnight.
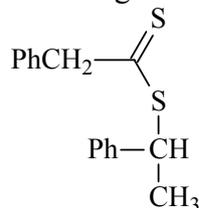
Yield: 35 %. ^{1}H NMR ($CDCl_3$): δ [ppm] 1.60 (d, 3H, CH_3), 4.19 (s, 2H, CH_2), 4.96-4.99 (q, 1H, CH), 7.18-7.25 (m, 10H, aromatic CH); ^{13}C NMR ($CDCl_3$): δ [ppm] 20.47 (CH_3), 49.81 (CH_2), 57.79 (CH), 127.16 (aromatic C), 127.65 (aromatic C), 129.05 (aromatic C), 136.82 (aromatic C), 140.93 (aromatic C).

Fig. 7.9 and Fig. 7.10 shows the ^{1}H-NMR and ^{13}C-NMR spectrum, respectively, of the chain transfer agent.
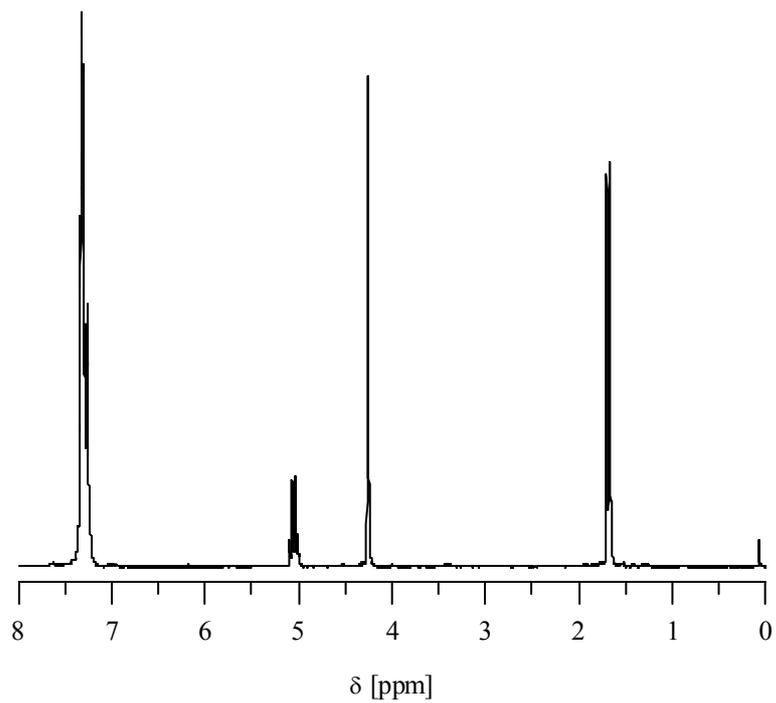
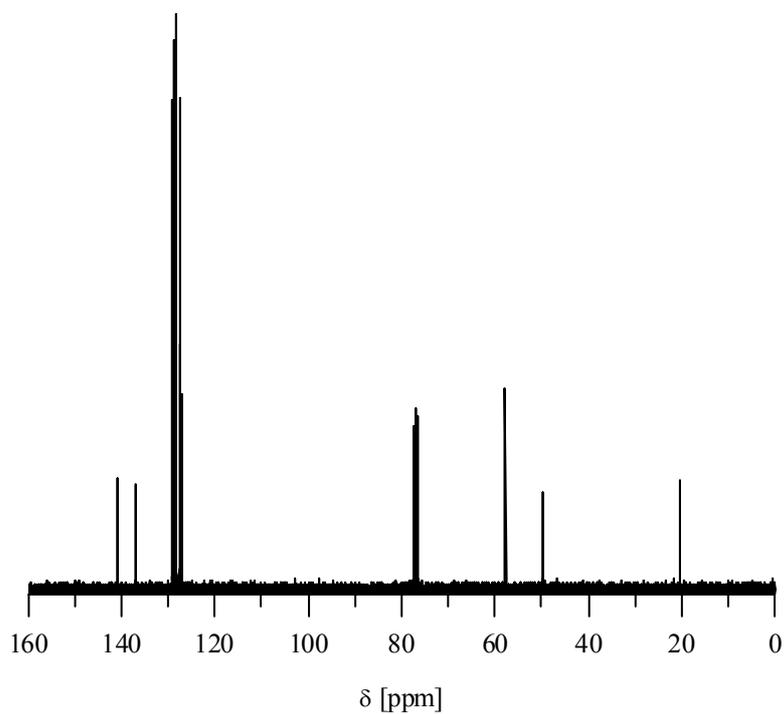*Fig. 7.9.* *¹H-NMR spectrum of 1-phenylethyl phenyldithioacetate in CDCl₃.*

*Fig. 7.10.* *¹³C-NMR spectrum of 1-phenylethyl phenyldithioacetate in CDCl₃.*

7.2   Homopolymer synthesis via RAFT

All solvents used in the RAFT polymerizations were purchased from Fluka or Aldrich and were of p.a. or HPLC quality. Unless noted otherwise, they were used without further purification. The monomers 2-vinyl-4,4-dimethyl-5-oxazolone (TCI Tokyo) and diacetone acrylamide (Lubrizol Co.) were used as received. Purification of the other monomers is described in the respective paragraphs. The initiators AIBN (Fluka) and ACP (4,4'-azobis(4-cyanopentanoic acid), Fluka) were recrystallized three times from methanol, VAZO-88 (azobis(cyclohexanecarbonitrile), DuPont) was recrystallized twice from ethanol, and V-70 (2,2'-azobis(4-methoxy-2,4-dimethyl valeronitrile), Wako Chemicals GmbH Germany) was used as received. Generally, the reagents were mixed in a vial and aliquots were transferred to either ampoules or Schlenk tubes, which were degassed by three freeze-thaw-evacuate cycles. The ampoules were flame sealed under vacuum. The polymerization vessels were immersed completely into a thermostatted oil bath at the specified temperature for the specified time. Typically, the polymerizations were terminated by cooling the ampoules or Schlenk tubes to room temperature. If not worked up immediately, the polymerization vessels were stored in the freezer (- 10 ºC) until use.

7.2.1   Poly(*N*-hydroxysuccinimide methacrylate)

7.2.1.1   *Synthesis of* N-*hydroxysuccinimide methacrylate*

The monomer was synthesized from methacrylic acid following the literature procedure.[10] Methacrylic acid (98 %, Fluka) was distilled prior to use. *N*-Hydroxysuccinimide and dicyclohexyl carbodiimide (Fluka) were used as received. 1,4-Dioxane (p.a., Fluka) was distilled over potassium for 3 d. *N*-Hydroxysuccinimide NHS (17.25 g, 0.15 mol) was dissolved in dioxane (200 mL) under nitrogen. The mixture was cooled to 0 °C and methacrylic acid (12.9 g, 0.15 mol) was added under stirring. Then, dicyclohexyl carbodiimide DCC (31.21 g, 0.15 mol) was added and the reaction mixture was stirred at 0-5 °C for 2 h. *t*-Butylcatechol (0.2 g, 1.2 mmol) was added, the mixture was warmed to room temperature and stirred overnight. The resultant white precipitate was filtered off and the solvent was evaporated. The yellowish crystalline crude product was crystallized twice from *n*-heptane to yield a white solid.
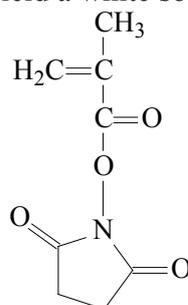
Yield: 76 %. ^{1}H NMR (d_8-THF): δ [ppm] 2.02 (dd, 3H, CH$_3$), 2.77 (t, 4H, CH$_2$), 5.89 (q, 1H, *trans*-C$\underline{H}$=C(CH$_3$)-COOR), 6.31 (q, 1H, *cis*-C$\underline{H}$=C(CH$_3$)-COOR).

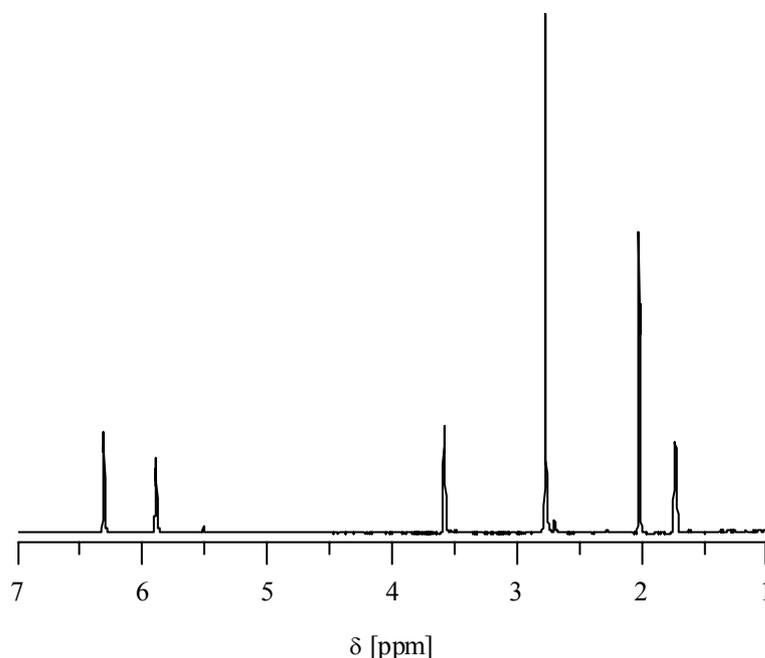Fig. 7.11 shows the ^{1}H-NMR spectrum of *N*-hydroxysuccinimide methacrylate.

Fig. 7.11. ^{1}*H-NMR spectrum of* N-*hydroxysuccinimide methacrylate in* d$_8$-*THF.*

7.2.1.2   RAFT polymerization

The solvent DMF was redistilled under nitrogen and the monomer was vacuum-dried prior to use. The polymer was precipitated from the polymerization mixture using acetone. The polymer samples were dried to constant weight under high vacuum. GPC was measured in DMF + 0.05 M LiBr.

^{1}H NMR (d_6-DMSO): δ [ppm] 1.02-1.71 (bs, 3H, CH$_3$), 2.53-3.03 (m, 6H, 3xCH$_2$).

7.2.2   Poly(*tert*-butyl acrylate)

The monomer (Fluka, purum) was washed three times with 5 % aqueous NaOH, then two times with distilled water. The organic layer was dried with CaCl$_2$ and then with Na$_2$SO$_4$. The dried monomer was condensed. The solvent ethyl acetate was distilled over CaH$_2$ prior to use. The polymer samples were obtained by evaporating the solvent of the polymerization mixture and drying to constant weight under high vacuum. GPC was measured in THF.

^{1}H NMR (C$_6$D$_6$): δ [ppm] 1.64 (bs, 9H, CH$_3$), 2.15-2.45 (m, 2H, CH$_2$), 2.61-2.92 (m, 1H, CH).

7.2.3 Poly(acrylic acid)

The monomer acrylic acid was condensed prior to polymerization. Methanol of HPLC quality was used as cosolvent along with distilled deionized water. After the respective polymerization times, the solvent was evaporated and the polymer was purified by reprecipitating its methanol solution from ethyl acetate. The polymers were dried to constant weight.

^{1}H NMR (CD$_3$OD): δ [ppm] 1.48-1.86 (m, 2H, CH$_2$), 2.28-2.59 (m, 1H, CH).

For GPC measurements in THF, the polymers were methylated to the corresponding methylesters of poly(acrylic acid). For the methylation of the samples, 100 mg PAA were dissolved in 3 mL MeOH in a Young's vessel. 0.79 mL of a 20 wt.-% Me$_4$NOH solution in MeOH were added. After mixing thoroughly, 0.14 mL MeI were added. The vessel was purged with nitrogen, closed tight and immersed into an oil bath at 80 °C for 1 h. A white precipitate formed upon heating. The reaction mixture was cooled down, the precipitate was filtered off and the solution was transferred to a flask. The solid was rinsed twice with 0.4 mL ethyl acetate and the combined solutions were evaporated to dryness. 1 mL H$_2$O was added and the aqueous phase was extracted three times with 1 mL ethyl acetate. The organic layer was washed with aqueous sodium chloride solution and then dried over MgSO$_4$. After drying, the solvent was evaporated and the sample further dried under vacuum.

^{1}H NMR (CDCl$_3$): δ [ppm] 1.48-1.78 (m, 2H, CH$_2$), 2.15-2.50 (m, 1H, CH), 3.64 (bs, 3H, OCH$_3$).

7.2.4 Poly(N-isopropylacrylamide)

7.2.4.1 RAFT polymerization

N-Isopropylacrylamide (Aldrich, 97 %) was recrystallized twice from benzene/hexane 3:2 (v:v) and dried under vacuum prior to use. 1,4-Dioxane (Merck, p.a.) was refluxed over potassium for 3 d and then distilled. Azobisisobutyronitrile (AIBN, Fluka, purum) was recrystallized from methanol and dried under vacuum prior to use.

For the polymerization series conducted at different benzyl CTA concentrations, stock solutions were prepared with a monomer concentration of 1.742 mol/L, an initiator concentration of 6.90 mmol/L and CTA concentrations of $3.92 \cdot 10^{-2}$ mol/L, $1.96 \cdot 10^{-2}$ mol/L, $9.80 \cdot 10^{-3}$ mol/L, and $4.90 \cdot 10^{-3}$ mol/L. Benzyl CTA (0.915 g to 0.114 g, 3.92 mmol to 0.49 mmol) and cumyl CTA (0.512 g, 1.96 mmol), respectively, were dissolved in 1,4-dioxane (98 mL) and the solutions were degassed by three freeze-thaw evacuation cycles. AIBN (0.115 g, 0.70 mmol) was dissolved in 1,4-dioxane (2 mL) and degassed by three freeze-thaw evacuation cycles. The monomer (20.37 g, 0.18 mol) was added via a Schlenk tube under nitrogen to the solution of the chain transfer agent in dioxane. After complete

dissolution of the monomer and heating of the mixture to 60 °C (temperature of oil bath), the initiator solution was injected with a syringe. All polymerizations were conducted under nitrogen atmosphere and samples were withdrawn at different time intervals. The samples were immediately immersed into liquid nitrogen and subsequently freeze-dried. The residues were dried under vacuum, whereby residual monomer was removed by sublimation. The dried substances were dissolved in THF + 0.25 % tetrabutyl ammoniumbromide for GPC analysis.

^{1}H NMR (d_8-THF): δ [ppm] 0.99-1.01 (d, 6H, CH_3), 1.42-1.72 (m, 2H, CH_2), 1.86-2.29 (m, 1H, CH), 3.89 (q, 1H, C$\underline{H}$(CH_3)$_2$).

7.2.4.2   Hydrolysis of dithiocarbamate endgroups

For the hydrolysis of the dithiocarbamate-terminated PNIPAAm samples, different techniques were employed which provide some advantages and some disadvantages over the other techniques. Some methods lead to high yields but incomplete hydrolysis, whereas other techniques result in pure hydrolysis products but give poor yields.

7.2.4.2.1   Dioxane / 5 % aq. NaOH[11-13]

PNIPAAm (1.0 g, 8.84 mmol) was dissolved in 1,4-dioxane (10 mL) whereupon a yellow solution was obtained. To this solution, 5 % aq. NaOH (10 mL) was added and the resulting emulsion was stirred under nitrogen at room temperature for 7 d. An orange solution with some precipitate was obtained. To this solution, 88 % formic acid was added for neutralization and a clear solution resulted. Dioxane was evaporated and acetone was added to the residual liquid giving rise to a white precipitate which was filtered off. The solvent of the residual solution was evaporated to give a slightly yellow sticky solid. The crude product was redissolved in dioxane along with a small amount of acetone and reprecipitated from petroleum ether (b.p. 40-60 °C) at 50 °C. The fine, pale yellow precipitate was filtered off while warm and dried under vacuum.

Yield: 63 %. ^{1}H NMR (d_8-THF): δ [ppm] 0.99-1.02 (d, 6H, CH_3), 1.51-1.63 (m, 2H, CH_2), 2.11 (m, 1H, CH), 3.89 (q, 1H, C$\underline{H}$(CH_3)$_2$), 6.60-7.56 (m, NH + aromatic CH of chain end); UV (CHCl$_3$): λ_{max} = 240.6 nm (SH).

7.2.4.2.2   Methanol / 5 % aq. NaOH

PNIPAAm (2.0 g, 17.67 mmol) was dissolved in methanol (20 mL). To the yellow solution, 5 % aq. NaOH (20 mL) was added and an orange solution was obtained. The mixture was stirred at room temperature under nitrogen for 5 d. Afterwards, the reaction mixture was directly subjected to ultrafiltration using a polyethersulfone membrane with an exclusion volume of 4 kDa (UF-PES-004H, Celgard Germany) at 3.5 bar and methanol as

an eluent. The solvent was evaporated and an ochre solid was obtained. UV spectroscopy in chloroform indicated some residual unhydrolyzed dithiocarbamate groups. A significant loss of polymer was observed due to the ultrafiltration procedure.

In a modification of this method, small amounts of 0.1 M Na$_2$EDTA solution and mercaptoethanol were added in order to prevent oxidation of the formed thiol groups. However, no oxidation could be proven in the former case.

Yield: 30 %. ^{1}H NMR (d_8-THF): δ [ppm] 1.01 (m, 6H, CH$_3$), 1.51-1.62 (m, 2H, CH$_2$), 2.07 (m, 1H, CH), 3.89 (m, 1H, C$\underline{H}$(CH$_3$)$_2$), 6.70-7.53 (m, NH + aromatic CH of chain end); UV (CHCl$_3$): λ$_{max}$ = 240.4 nm (SH), λ$_{shoulder}$ = 282.4 nm (dithio).

7.2.4.2.3 Methanol / ammonia

PNIPAAm (1.0 g, 8.84 mmol) was dissolved in methanol (25 mL). To this solution, 0.1 M Na$_2$EDTA solution (4 mL), β-mercaptoethanol (4 mL) and 25 % ammonia solution (5 mL) was added under nitrogen in the stated order. The clear yellow solution was stirred at room temperature for 6 d. The pale yellow reaction mixture was then neutralized with 88 % formic acid and subjected to ultrafiltration using a polyethersulfone membrane (PES-004H, cutoff 4 kDa, Celgard Germany) and methanol as an eluent. The solvent was evaporated and the obtained white solid dried under vacuum. NMR and UV spectroscopy revealed some residual unhydrolyzed polymer (peaks in aromatic region and shoulder around 280 nm, respectively).

In a modification of this method, small amounts of 0.1 M Na$_2$EDTA solution and mercaptoethanol were added in order to prevent oxidation of the formed thiol groups. However, no oxidation could be proven in the absence of these reagents.

Yield: 69 %. ^{1}H NMR (CD$_3$OD): δ [ppm] 1.19 (d, 6H, CH$_3$), 1.62-1.68 (m, 2H, CH$_2$), 2.14 (m, 1H, CH), 4.02 (q, 1H, C$\underline{H}$(CH$_3$)$_2$), 7.18-7.29 (dd, 2H, pyrrole-CH from unhydrolyzed polymer), 7.61-7.71 (m, aromatic CH of chain end), 8.12-8.15 (dd, 2H, pyrrole-CH from unhydrolyzed polymer); UV (MeOH): λ$_{max}$ = 218.8 nm (SH), λ$_{shoulder}$ = 281.2 nm (dithio).

7.2.4.2.4 Methanol / 28 % aq. NaOH[14]

Due to incomplete hydrolysis with 5 % aq. NaOH in methanol (cf. 7.2.5.2.2), a higher concentration of NaOH was used which yielded a completely hydrolyzed product with moderate to excellent yields.

PNIPAAm (1.0 g, 8.84 mmol) was dissolved in methanol (18 mL). To the yellow polymer solution, 0.1 M Na$_2$EDTA solution (3 mL) and 28 % aq. NaOH (8 mL) were added under nitrogen. The reaction mixture was stirred at room temperature overnight. Different workup procedures were applied after hydrolysis:

a) Direct ultrafiltration of the reaction mixture using a polyethersulfone membrane in methanol; yield: 40 %.

b) Neutralization of the reaction mixture with 88 % formic acid and extraction of the product with chloroform; yield: 98 %.

c) Neutralization with 88 % formic acid and subsequent evaporation of methanol followed by freeze-drying; this product was used for MALDI-TOF analysis without further purification.

^{1}H NMR (d_8-THF): δ [ppm] 1.03 (m, 6H, CH$_3$), 1.48-1.69 (m, 2H, CH$_2$), 1.93-2.19 (m, 1H, CH), 3.89 (m, 1H, C$\underline{H}$(CH$_3$)$_2$), 6.56-7.40 (m, NH + aromatic CH of chain end); UV (MeOH): λ$_{max}$ = 218.2 nm (SH); MALDI-TOF (DHB, THF): m/z 1199.20 (cumyl-(M)$_8$-SH Na$^+$).

7.2.4.3 Reaction of hydrolyzed PNIPAAm with 2-naphthoyl chloride

Hydrolyzed PNIPAAm (0.05 g, 0.44 mmol) was dissolved in acetonitrile (3 mL) and added to a solution of potassium carbonate (0.182 g, 1.32 mmol) in acetonitrile (1 mL). To this suspension, 2-naphthoyl chloride (0.352 g, 1.85 mmol, Fluka, purum) was added and the mixture was stirred under nitrogen for 4 d. Residual undissolved reactants were filtered off. In order to destroy excess naphthoyl chloride, water was added resulting in a white precipitate which was also filtered off. The remaining solution was subjected to rotary evaporation. The crude product was dissolved in dioxane and precipitated twice from petroleum ether. A white solid was obtained which was dried under vacuum.
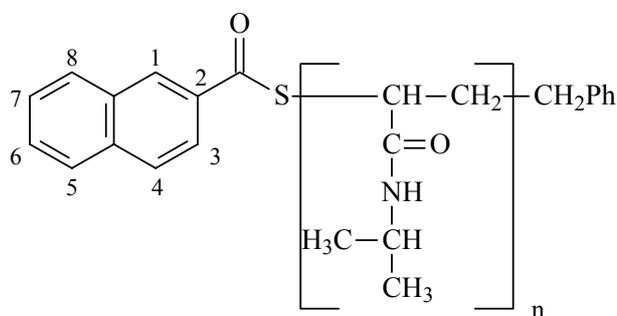
Yield: 81 %. ^{1}H NMR (CDCl$_3$): δ [ppm] 1.07 (m, 6H, CH$_3$), 1.56 (m, 2H, CH$_2$), 1.97 (m, 1H, CH), 3.94 (m, 1H, C$\underline{H}$(CH$_3$)$_2$), 7.46-7.65 (m, 2H, H-3+H-4), 7.76-8.02 (m, 4H, H-5−H-7), 8.60 (d, 1H, H-1); UV (CHCl$_3$): λ$_{max}$ = 244.4 nm, 281.4 nm.

7.2.4.4 Reaction of hydrolyzed PNIPAAm with 5,5'-dithiobis-[2-nitrobenzoic acid] (DTNB) – Ellman test for thiol groups[15-17]

0.1 M Sørensen phosphate buffer pH 8.0 was prepared according to the following method:

solution A: 2.72 g KH_2PO_4 in 100 mL H_2O

solution B: 8.90 g $Na_2HPO_4 \cdot 2H_2O$ in 250 mL H_2O

5.3 mL solution A and 94.7 mL solution B were mixed and filled up with water to a total volume of 200 mL. The solution was adjusted to pH 8.0 with either 0.1 M HCl or 0.1 M NaOH using a potentiometer.

Preparation of Ellman solution:

39.6 mg DTNB (0.1 mmol, 5,5'-dithiobis-[2-nitrobenzoic acid], Sigma, $\geq$ 98 %) was dissolved in 10 mL Sørensen phosphate buffer. The solution was used immediately due to its relative instability (5 % decomposition after 48 h at room temperature).

Preparation of polymer solution:

Hydrolyzed PNIPAAm (0.5 mg, $1.1 \cdot 10^{-4}$ mmol with respect to thiol groups present) was dissolved in 500 µL phosphate buffer.

UV measurements were performed in the time-drive mode using an absorption wavelength of 412 nm with an interval of 10 s between datapoints. The reference cell was filled with 1000 µL phosphate buffer and 20 µL Ellman solution. The measurement cell was filled with 500 µL phosphate buffer, 500 µL polymer solution, and 20 µL Ellman solution.

7.2.4.5 *Reduction of dithiocarbamate endgroups with Bu$_3$SnH[18,19]*

PNIPAAm (1.0 g, 0.08 mmol with respect to dithiocarbamate group) was dissolved in THF (10 mL) under nitrogen. To the solution, a small amount of AIBN was added and the mixture was heated to 60 °C. At this temperature, Bu_3SnH (0.9 mL, 3.4 mmol, Fluka, purum) was slowly added to the solution. The mixture was stirred at 60 °C for 20 h. The initial yellow colour of the mixture disappeared. The mixture was cooled in an icebath and icecold water (1 mL) was slowly added in order to destroy excess Bu_3SnH. The resultant mixture was filtered and added dropwise to benzene/*n*-hexane 1:1 (400 mL). A white precipitate was obtained which was washed with benzen/*n*-hexane and dried under vacuum.

Yield: 89 %. ^{1}H NMR (CD$_3$OD): δ [ppm] 1.19 (m, 6H, CH$_3$), 1.62 (m, 2H, CH$_2$), 2.12 (m, 1H, CH), 4.00 (m, 1H, C$\underline{H}$(CH$_3$)$_2$), 7.49-7.79 (m, aromatic CH of chain end); UV (MeOH): λ_{max} = 212.2 nm (benzyl group of chain end).

7.2.5   Poly(diacetone acrylamide)

For the polymerization, methanol of HPLC quality was used as a solvent. The monomer was used as received, the initiators AIBN and 4,4'-azobis(4-cyanopentanoic acid) (ACP, Fluka, $\geq$ 98 %) were recrystallized three times from methanol. The reagents were mixed

and aliquots were transferred to ampoules, which were degassed by three freeze-thaw-evacuate cycles and then flame sealed under vacuum. The ampoules were immersed completely into an oil bath at the specified temperature. The polymerization mixture was poured onto water for precipitation. The solution was decanted and the precipitate washed twice with water, then redissolved in methanol. The solvent was evaporated and the polymer dried under vacuum.

GPC on the polymer samples was performed in THF.

^{1}H NMR (C_6D_6): δ [ppm] 1.33-1.81 (bs, 9H, $(CH_3)_2C+CH_3C=O$), 1.82-2.81 (m, 4H, $2 \times CH_2$), 3.28-4.35 (m, 1H, CH).

7.2.6   Poly(2-vinyl-4,4-dimethyl-5-oxazolone)

The monomer was used as received and the solvent benzene was distilled over potassium. The reagents were mixed in a vial and aliquots were transferred to ampoules, which were degassed by three freeze-thaw-evacuate cycles and then flame sealed under vacuum. The ampoules were immersed completely into an oil bath at the specified temperature for the specified time. The ampoules were cracked open and the polymer was precipitated from anhydrous *n*-hexane. In order to prevent hydrolysis by moisture in the air, the polymer samples were stored in an exsiccator.

GPC on the polymers was performed in THF.

^{1}H NMR (C_6D_6): δ [ppm] 1.34-1.63 (bs, 6H, CH_3), 1.94-2.46 (m, 2H, CH_2), 2.96-3.24 (m, 1H, CH).

7.3   Block copolymer synthesis via RAFT

7.3.1   PNIPAAm-*b*-PAA

Poly(acrylic acid) was used as macromolecular chain transfer agent. It was obtained according to the polymerization procedure outlined in paragraph 7.2. Methanol of HPLC quality was used as a solvent. The reagents were mixed in a vial and aliquots were transferred to the polymerization vessels, which were degassed by three freeze-thaw-evacuate cycles. The vessels were immersed into an oil bath at 60 °C. A glassy, pale yellow polymer was obtained after evaporation of the solvent. Residual NIPAAm was removed by rinsing the product mixture with ethyl acetate, which dissolves the monomer.

GPC on the polymer samples was performed using DMF as an eluent.

^{1}H NMR (d_7-DMF): δ [ppm] 1.29-1.31 (d, 6H, CH_3(PNIPAAm)), 1.64-1.96 (m, 2H, CH_2(PNIPAAm)), 2.24-2.51 (m, 1H, CH(PNIPAAm)), 2.59-2.70 (m, 2H, CH_2(PAA)), 3.72 (m, 1H, CH(PAA)), 4.14 (m, 1H, C$\underline{H}$(CH$_3$)$_2$(PNIPAAm)).

7.3.2   PNIPAAm-*b*-PVO

Poly(2-vinyl-4,4-dimethyl-5-oxazolone) was used as a macromolecular chain transfer agent. Its polymerization procedure is described in paragraph 7.2. The solvent benzene was distilled over sodium prior to use. All reagents were mixed in a vial and aliquots were transferred to ampoules which were degassed by three freeze-thaw-evacuate cycles. The ampoules were immersed into an oil bath at a temperature of 65 °C. A glassy, pale pink polymer was obtained after evaporation of the solvent. In order to sublime off residual NIPAAm, the polymer/monomer mixture was subjected to high vacuum for several days.

GPC on the polymers was performed in THF.

^{1}H NMR (C$_6$D$_6$): δ [ppm] 0.65 (d, 6H, CH$_3$(PNIPAAm)), 1.02 (bs, 6H, CH$_3$(PVO)), 1.23-1.65 (m, 6H, 2xCH$_2$+2xCH), 4.57 (m, 1H, C$\underline{H}$(CH$_3$)$_2$(PNIPAAm)).

7.4   Conjugation of polymers to proteins/peptides

7.4.1   Conjugation to PNIPAAm
7.4.1.1   Coupling to hydrolyzed PNIPAAm – model reactions
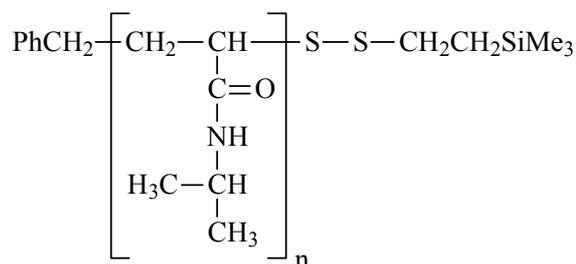##### *7.4.1.1.1   Coupling of 2-(trimethylsilyl)ethanethiol to PNIPAAm[20,21]*

In a first step, diethyl azodicarboxylate (DEAD, Fluka, ≥ 97 %) was coupled to 2-(trimethylsilyl)ethanethiol (Aldrich, p.a.) to form an active ester that reacts with the thiol group of the hydrolyzed PNIPAAm. For this purpose, DEAD (0.6 mL, 3.81 mmol) and the ethanethiol derivative (0.6 mL, 3.87 mmol) were reacted at room temperature for 44 h under exclusion of moisture and air. The initial orange mixture turned yellow after this time. Unreacted thiol was removed by evaporation under high vacuum. The product was a yellow oil.

$$EtOOC-\underset{\underset{H}{|}}{N}-\underset{\underset{SCH_2CH_2SiMe_3}{|}}{N}-COOEt$$
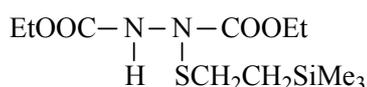
Yield: 92 %. ^{1}H NMR (C$_6$D$_6$): δ [ppm] 0.00-0.05 (s, 9H, Si(CH$_3$)$_3$), 0.78-0.95 (t, 2H, SiCH$_2$), 1.01-1.15 (t, 6H, CH$_2$C$\underline{H}$$_3$), 2.80-2.87 (t, 2H, SiCH$_2$C$\underline{H}$$_2$), 4.00-4.18 (q, 4H, C$\underline{H}$$_2CH_3$), 7.53 (bs, 1H, NH).

In the second step, the thiol-DEAD adduct was reacted with hydrolyzed PNIPAAm. A solution of thiol-DEAD adduct (0.159 g, 0.52 mmol) in 1,4-dioxane (15 mL) was added to hydrolyzed PNIPAAm (0.106 g, 0.05 mmol thiol equivalents) under nitrogen. The solution was heated to 80 °C for 24 h. After complete reaction, the dioxane solution was poured into petroleum ether (b.p. 40-60 °C) at 50 °C whereupon a yellowish precipitate formed,
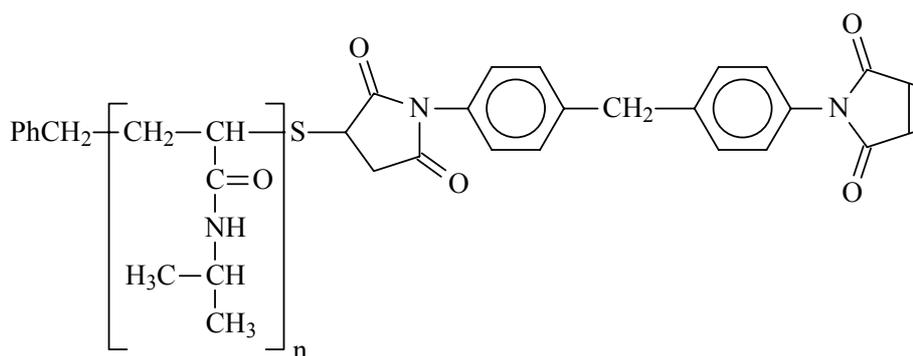
which was filtered off while warm. After reprecipitating the crude product's dioxane solution twice from petroleum ether, a white powder was obtained.

$$PhCH_2 \left[CH_2-CH \right]_n S-S-CH_2CH_2SiMe_3$$

where the repeat unit bears a side chain: $C=O$, NH, H_3C-CH, CH_3.

Yield: 46 %. ^{1}H NMR (D_2O): δ [ppm] 0.00-0.03 (s, 9H, Si(CH$_3$)$_3$), 0.81 (t, 2H, SiCH$_2$), 1.13 (d, 6H, CH$_3$(PNIPAAm)), 1.39-1.78 (m, 2H, CH$_2$(PNIPAAm)), 1.89-2.21 (m, 1H, CH(PNIPAAm)), 2.55 (t, 2H, SiCH$_2$C$\underline{H}_2$), 3.78-3.97 (q, 1H, C$\underline{H}$(CH$_3$)$_2$(PNIPAAm)), 7.20-7.41 (m, aromatic CH of PNIPAAm chain end).

7.4.1.1.2 Coupling to 1,1'-(methylenedi-4,1-phenylene)bismaleimide[22-25]

Hydrolyzed PNIPAAm (0.5 g, 0.11 mmol thiol equivalents) was dissolved in 0.1 M phosphate buffer pH 7.5 / methanol 1:1 (25 mL) and a small amount of triethylamine was added as a catalyst. A suspension of the bismaleimide BM (0.158 g, 0.44 mmol, Aldrich, ≥ 98 %) in methanol (5 mL) was prepared and added to the polymer/catalyst mixture. The yellow polymer solution turned slightly pink on addition of the bismaleimide. The reaction mixture was stirred at room temperature and under nitrogen overnight. The greenish yellow mixture contained some pink precipitate which dissolved upon addition of methanol (50 mL). The obtained solution was directly subjected to ultrafiltration using a polyethersulfone membrane (PES-004H, cutoff 4 kDa, Celgard Germany) and methanol as an eluent. The solvent was evaporated and the obtained white solid dried under vacuum.
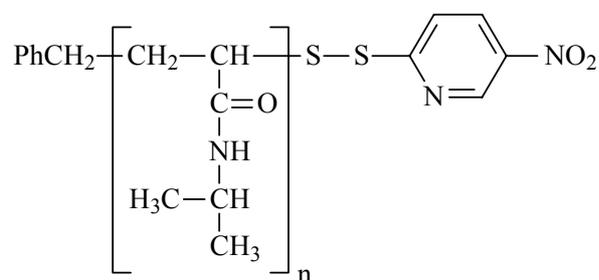
$$PhCH_2 \left[CH_2-CH \right]_n S-\text{(succinimide)}-N-C_6H_4-CH_2-C_6H_4-N-\text{(maleimide)}$$

Yield: 69 %. ^{1}H NMR (d_8-THF): δ [ppm] 0.97-1.09 (d, 6H, CH$_3$(PNIPAAm)), 1.36 (m, 2H, CH$_2$(PNIPAAm)), 1.89 (m, 1H, CH(PNIPAAm)), 2.67-2.69 (d, 2H, CH$_2$C=O(BM)), 3.76 (m, 2H, C$_6$H$_4$-C$\underline{H}_2$-C$_6$H$_4$(BM)), 3.79 (t, 1H, CH-S(BM)), 3.88 (m, 1H,

C$\underline{H}$(CH$_3$)$_2$(PNIPAAm)), 6.10 (d, 2H, olefinic CH (BM)), 6.98-7.02 (dd, 8H, phenylene-CH(BM)), 7.47-7.50 (m, aromatic chain end).

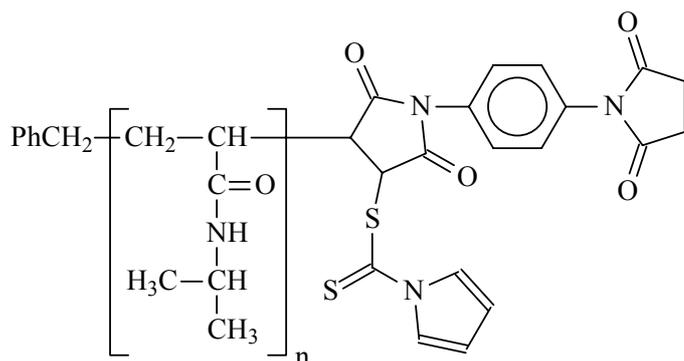### 7.4.1.1.3 Coupling to 2,2'-dithiobis(5-nitropyridine)[25-27]

Hydrolyzed PNIPAAm (0.5 g, 0.11 mmol thiol equivalents) was dissolved in 0.1 M phosphate buffer pH 7.0 / methanol 1:1 (25 mL). A suspension of 2,2'-dithiobis(5-nitropyridine) (0.679 g, 2.188 mmol, Aldrich, ≥ 98 %) was prepared in acetic acid/water (3:1) (15 mL) and added to the polymer solution. The pale yellow solution turned bright yellow upon addition of the nitropyridine compound. The reaction mixture was stirred overnight at room temperature and under nitrogen. The solution was filtered from undissolved reactants and subjected to ultrafiltration using a polyethersulfone membrane (PES-004H, cutoff 4 kDa, Celgard Germany) and methanol as an eluent. The solvent was evaporated and the obtained white solid dried under vacuum.

Yield: 51 %. ^{1}H NMR (d_8-THF): δ [ppm] 1.01 (d, 6H, CH$_3$(PNIPAAm)), 1.35 (m, 2H, CH$_2$(PNIPAAm)), 1.89-2.22 (m, 1H, CH(PNIPAAm)), 3.89 (m, 1H, C$\underline{H}$(CH$_3$)$_2$(PNIPAAm)), 6.96-7.15 (m, aromatic CH (PNIPAAm)), 7.42-7.46 (m, aromatic CH (pyridine)), 7.56-7.60 (m, aromatic CH (pyridine)).

7.4.1.2 Addition of dithiocarbamate-terminated PNIPAAm to bismaleimide[28]

PNIPAAm (0.2 g, 0.05 mmol with respect to dithiocarbamate group), N,N-(1,4-phenylene)bismaleimide (0.27 g, 0.94 mmol, Aldrich, p.a.), and AIBN (1 mg, 6 μmol) were mixed with 1,4-dioxane (8 mL) in an ampoule under nitrogen. The ampoule was immersed into an oil bath at 60 °C and the reaction mixture was stirred for 18 h. Undissolved bismaleimide was filtered off and the residual solution was added dropwise to petroleum ether (b.p. 40-60 °C) at 50 °C in order to precipitate the polymer. A yellow solid was obtained that was purified by reprecipating its dioxane solution from petroleum ether.

Yield: 70 %. ^{1}H NMR (d_8-THF): δ [ppm] 1.01 (d, 6H, CH$_3$(PNIPAAm)), 1.40-1.66 (m, 2H, CH$_2$(PNIPAAm)), 1.93-2.11 (m, 1H, CH(PNIPAAm)), 3.06-3.17 (d, 1H, CH(BM)), 3.88 (m, 1H, C$\underline{H}$(CH$_3$)$_2$(PNIPAAm)), 3.63 (d, 1H, CH-S(BM)), 6.22 (d, 2H, olefinic CH (BM)), 6.80-7.68 (m, aromatic CH).

7.4.1.3 Conjugation of biotinylated PNIPAAm to wild-type streptavidin

The biotinylation agent 1-biotinamido-4-[4'-(maleimidomethyl)cyclohexane-carbox-amido]butane (biotin-BMCC) was purchased from Pierce Chemical Co., Rockford, Illinois. Wild-type streptavidin was obtained from Boehringer Mannheim, Indianapolis, Indiana. HABA (4-hydroxyazobenzene-2-carboxylic acid), avidin, and D-biotin were purchased from Pierce Chemical Co., Rockford, Illinois. PD-10 desalting columns (molecular weight cutoff 10 kDa, material Sephadex G-25) were purchased from Amersham Biosciences, England.

7.4.1.3.1 Biotinylation of hydrolyzed PNIPAAm with biotinBMCC

A stock solution of biotinBMCC in DMSO was prepared (24 mg in 1.5 mL). The polymer samples were dissolved in 0.1 M phosphate buffer pH 6.57 (e.g. 10 mg of polymer with MW 9,800 in 2300 μL) and 200 μL biotinBMCC solution was added. The mixtures were incubated at r.t. for 20-22 h. The reaction mixtures were desalted (after centrifuging insoluble biotinBMCC residue) on a PD-10 column using deionized, distilled water. Of the 3.5 mL eluents, 50 μL were taken for HABA assays and the residual amounts were freeze-dried immediately.

The reagents for the HABA assay were prepared as follows:

10 mM HABA solution: 24.2 mg HABA in 9.9 mL H$_2$O + 0.1 mL 1 N NaOH

Phosphate-buffered saline (PBS): 100 mM Na phosphate, 150 mM NaCl, pH 7.2

Avidin-HABA reagent: 10 mg of avidin and 600 μL of HABA solution was added to 19.4 mL PBS

Biotin: 0.5 mM D-biotin in PBS pH 6.7

50 µL of the solution of biotinylated polymer obtained after desalting on PD-10 column was used for the assay.

7.4.1.3.2 Conjugation of biotinylated PNIPAAm to wild-type streptavidin

0.5 mg of wild-type streptavidin (WTSA) was used for conjugation of each of the PNIPAAm polymers used. The conjugation was done using a 4:1 ratio of polymer to protein. The final concentration of the conjugate was 45 µM. It was assumed that the biotinylated polymer binds to two of the four biotin binding pockets of WTSA.

7.4.2   Conjugation to PNIPAAm-*b*-PAA

The biotinylation agent 1-biotinamido-4-[4'-(maleimidomethyl)cyclohexane-carbox-amido]butane (biotin-BMCC) was purchased from Pierce Chemical Co., Rockford, Illinois. Wild-type streptavidin was obtained from Boehringer Mannheim, Indianapolis, Indiana. The streptavidin mutant S139C (substitution of serine at position 139 with cysteine) was genetically engineered in the working groups of profs. Pat Stayton and Allan Hoffman at the University of Washington/Seattle by site-directed cassette mutagenesis using a synthetic "core" streptavidin gene designed and constructed for protein expression in *Escherichia coli*.[29,30] HABA (4-hydroxyazobenzene-2-carboxylic acid), avidin, and D-biotin for the HABA assay were purchased from Pierce Chemical Co., Rockford, Illinois. PD-10 desalting columns (molecular weight cutoff 10 kDa, material Sephadex G-25) were purchased from Amersham Biosciences, England. The slide-a-lyzer® cassettes used for dialysis of the polymer solutions were purchased from Pierce Chemical Co., Rockford, Illinois. Millipore ultrafree centrifugal filter devices were used for microconcentration. The bismaleimide linker BM[PEO]₃ (1,8-bis-maleimidotriethyleneglycol) and dithiothreitol (DTT) were purchased from Pierce Chemical Co. SDS-PAGE gel used for analysis of the conjugates was obtained from BioRad Laboratories. Reagents for gel-load buffer, gel-run buffer, staining solution, and destaining solution were obtained either from BioRad Laboratories or from Pierce Chemical Co. Kaleidoscope prestained standards were obtained from BioRad Laboratories, Philadelphia.

7.4.2.1 Biotinylation with biotinBMCC

Hydrolyzed PNIPAAm-*b*-PAA was obtained in a procedure similar to the one used for hydrolysis of the homopolymer PNIPAAm. The reaction was performed under nitrogen at room temperature for 3 d. After complete hydrolysis, the mixture was acidified with 88 % formic acid and then dialyzed against 0.1 M phosphate buffer pH 7.2 using a slide-a-lyzer® cassette (Pierce Chemical Co.) with a molecular weight cutoff of 3,500 Da.

A stock solution of biotinBMCC in DMSO was prepared (24 mg in 1.5 mL). The polymer (4 mg, molecular weight 17,200 g/mol) was dissolved in 850 μL phosphate buffer pH 6.57. 75 μL biotinBMCC solution was added. The mixture was incubated at room temperature for 39 h. The reaction mixture was then desalted on a PD-10 column (after centrifuging residual undissolved biotinBMCC) using deionized, distilled water. 50 μL of the 3.5 mL eluent were taken for the HABA assay, the rest was freeze-dried immediately. Biotinylation efficiency was checked using the above-described (cf. 7.4.1.3.1) HABA assay.

7.4.2.2 Conjugation to S139C via BM[PEO]$_3$

Hydrolyzed PNIPAAm-*b*-PAA (0.58 mM) was reacted with 5 eq dithiothreitol (DTT) in phosphate buffer pH 7.2 (100 mM) for 1 h to reduce any oxidized thiol. The polymer was then purified from excess DTT using a PD-10 desalting column with deionized, distilled water as an eluent. The reduced polymer was freeze-dried overnight. The polymer (0.3 μmol) was redissolved in 250 μL phosphate buffer and reacted with 10 eq BM[PEO]$_3$ linker for 2 h. The polymer/BM[PEO]$_3$ mixture was then desalted on a PD-10 column using phosphate buffer pH 6.7 as an eluent.

S139C streptavidin protein (1 mg in 200 μL phosphate buffer pH 6.7) was reduced with 10 mM DTT for 1 h. The reduced protein was then separated from excess DTT using a PD-10 column and phosphate buffer pH 6.7.

The protein and polymer solutions obtained after desalting were mixed and microconcentrated (2000 rpm, 5kDa cutoff) from 7 mL to 1 mL. The concentrated solution was reacted overnight at room temperature. The conjugate was purified by precipitating the polymer by acidification.

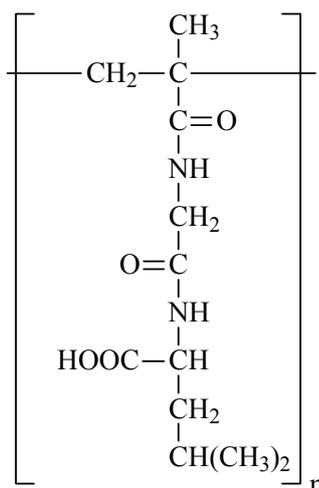### 7.4.2.3 Conjugation to S139C via direct disulfide

PNIPAAm-*b*-PAA (0.58 mM) was reacted with 5 eq DTT in phosphate buffer pH 7.2 (100 mM) for 1 h. The polymer was then purified from DTT using a PD-10 desalting column and deionized, distilled water. The reduced polymer was freeze-dried overnight.

S139C Streptavidin protein (1 mg in 200 μl buffer) was reduced with 30 mM DTT for 1 h. The reduced protein was separated from DTT using two consecutive PD-10 desalting columns and phosphate buffer pH 8.1. The polymer (0.3 μmol) was dissolved in the protein solution and the mixture was microconcentrated (2000 rpm, 5kDa cutoff) from 3.5 mL to 0.5 mL. The concentrated solution was reacted at room temperature for 2 d. The conjugate was purified by precipitating the polymer by acidification.

7.4.3 Conjugation to amine-reactive polymers

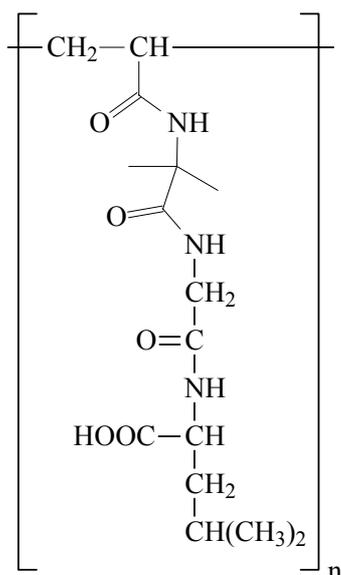### *7.4.3.1 Conjugation of PNHSM to model peptide GlyLeu*

PNHSM (31.4 mg, 0.17 mmol) was dissolved in DMSO (2 mL) and GlyLeu (48.0 mg, 0.255 mmol, Sigma, 98 %) was dissolved in phosphate buffer pH 7.4 (0.75 mL). The solutions were mixed and stirred at room temperature overnight. The reaction mixture was poured into acetone and the resulting white precipitate was separated from the solution by centrifugation. The product was obtained as a white powder by lyophilizing the filtered solution.

$$
\left[-CH_2-\underset{\underset{\underset{\underset{\underset{\underset{\underset{\underset{CH(CH_3)_2}{|}}{CH_2}}{|}}{HOOC-CH}}{|}}{\overset{\overset{\overset{\overset{\overset{\overset{\overset{CH_3}{|}}{C}}{|}}{C=O}}{|}}{NH}}{\underset{O=C}{\underset{|}{NH}}}}{}}{}} - \right]_n
$$

Yield: 89 %. ^{1}H NMR (d_6-DMSO): δ [ppm] 0.83-0.88 (d, 6H, (C$\underline{H}_3$)$_2$CH(GlyLeu)), 1.22-1.51 (bs, 3H, CH$_3$(PNHSM)), 1.99 (dd, 2H, CH$_2$(GlyLeu)), 2.49-2.57 (C$\underline{H}_2$-NHCO(GlyLeu)), 2.80 (bs, 2H, CH$_2$(PNHSM)), 3.53 (m, 2H, 2xCH(GlyLeu)).

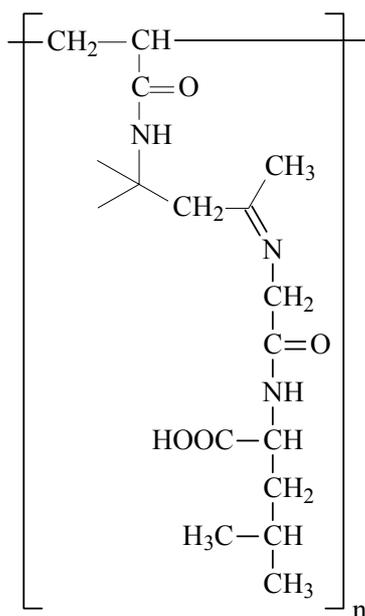### *7.4.3.2 Conjugation of PVO to model peptide GlyLeu*

PVO (0.11 g, 0.79 mmol) was dissolved in dry DMF (15 mL) and GlyLeu (0.29 g, 1.54 mmol) was added, whereupon a suspension was obtained. The reaction mixture was heated to 70 °C overnight. GlyLeu was dissolved almost completely after this time, and the color of the reaction mixture changed from pink to yellow, which was ascribed to hydrolysis of the chain transfer agent moieties at the end of the polymer by primary amine groups. Residual undissolved peptide was filtered off and the conjugate was isolated by repeated precipitation from acetone in order to recover unreacted GlyLeu.

Yield: 78 %. ^{1}H NMR (CD$_3$OD): δ [ppm] 0.83-0.88 (m, 6H, CH$_3$(GlyLeu)), 1.39-1.59 (m, 11H, CH$_2$+CH$_3$(PVO), C<u>H</u>(CH$_3$)$_2$, C<u>H$_2$</u>CH(CH$_3$)$_2$), 2.20 (m, 1H, CH(PVO)), 3.63-3.96 (t, 1H, C<u>H</u>-COOH), 4.35 (bs, 2H, C<u>H$_2$</u>C=O), 7.73-8.15 (m, 4H, NH+COOH).

7.4.3.3 Conjugation of PDAA to model peptide GlyLeu

PDAA (0.10 g, 0.59 mmol) was dissolved in dry DMF (15 mL). 4 Å molar sieve for water absorption, a small amount of *p*-toluenesulfonic acid, and GlyLeu (0.27 g, 1.43 mmol) was added. A suspension was obtained that was heated to 80 °C for 2 d. GlyLeu dissolved upon reaction and residual reactant was filtered off. Unreacted GlyLeu was precipitated from acetone and separated from the product solution by centrifugation.

Yield: 84 %. ^{1}H NMR (d_6-DMSO): δ [ppm] 0.84-0.87 (d, 6H, CH$_3$(GlyLeu)), 1.29 (m, 6H, CH$_3$(PDAA)), 1.49-1.55 (8 H, m, C$\underline{H}$(CH$_3$)$_2$, CH$_3$C=N, C$\underline{H}_2$CH(CH$_3$)$_2$, CH$_2$(PDAA)), 2.00 (m, 1H, CH(PDAA)), 3.47-4.20 (m, 5H, C$\underline{H}$-COOH, CH$_2$N=C, CH$_2$C=O), 7.72-8.06 (m, 3H, NH+COOH).

7.5   Characterization methods

In the following, characterization methods that are not of common use in the laboratory are described in more detail. For the other methods, only a brief description of the instrument's characteristics is given.

7.5.1   MALDI-TOF mass spectrometry

Laser desorption mass spectrometry (LDMS) is a technique that focuses high-power laser beams on surfaces and analyzes the mass of the ablated species. MALDI (matrix-assisted laser desorption/ionization) is a special case of LDMS. MALDI uses low-fluence laser desorption to create the analyte ions. Since its introduction by Tanaka and Hillenkamp,[31,32] this method has rapidly grown in applications ranging from sequencing peptides to measuring the average molecular weights of complex synthetic polymer materials.

Some of the advantages of MALDI-TOF mass spectrometry are a very low sample consumption and short analysis time. In matrix-assisted laser desorption, the analyte is embedded homogeneously into the matrix material that absorbs the laser energy and is responsible for the transfer of the analyte into the gas phase. There is no general rule for matrix selection for a given polymer. It has to be found on a trial and error basis.[33,34] Typical MALDI matrices are aromatic organic acids, examples can be found in Tab. 7.1. Usually, a dilute solution of the polymer sample is mixed with a more concentrated matrix solution. A small aliquot of the mixture is applied to the MALDI target and crystallized as the solvent evaporates. After the target is placed in the source of the mass spectrometer, a pulsed UV laser irradiates the target, vaporizing the matrix, and desorbing polymer oligomers into the gas phase. Neutral gas-phase oligomers are cationized by protons or metal cations that originate from impurities, the polymerization process or from added salts (Fig. 7.12). The ions are extracted into the mass spectrometer, where they are mass analyzed and detected.
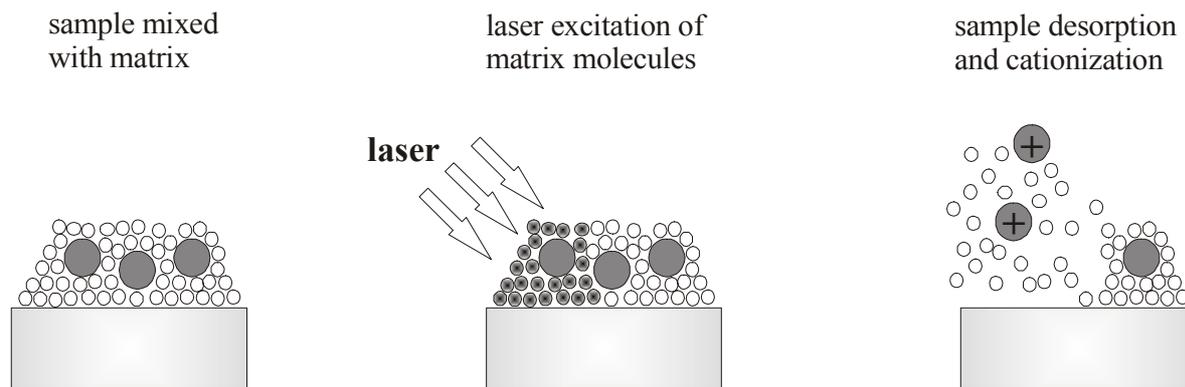
Fig. 7.12. *Process of laser desorption ionization.*

A typical setup of a MALDI-TOF mass spectrometer is shown in Fig. 7.13. The intensity of the laser beam is adjusted by a variable attenuator to a value slightly above the threshold for ion production. Once ions are formed after a laser pulse, they are accelerated simultaneously by a static electric field. Depending on the mass-to-charge ratio, the ions have different velocities when leaving the acceleration zone and pass the following field-free drift tube with different flight times. The time of flight for each ion is measured by the time difference between the start signal, given by the laser pulse, and the stop signal, caused by ions impinging on the detector.
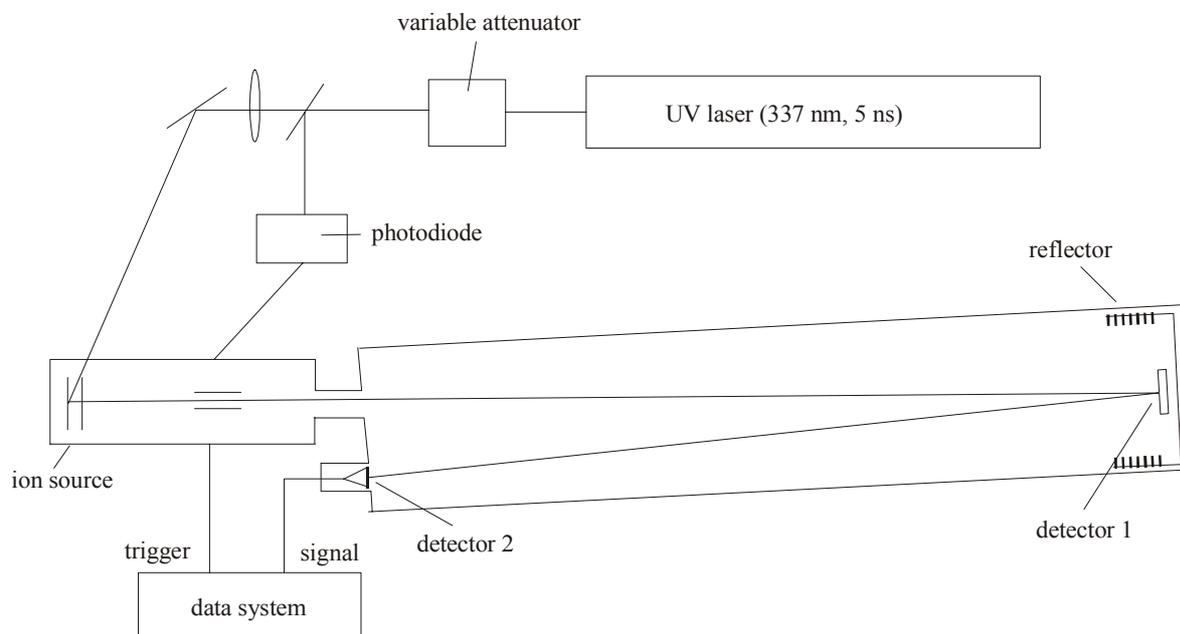

Fig. 7.13. *Typical setup of an instrument equipped with a matrix-assisted laser desorption ion source.[33]*

The square of the flight time is proportional to the mass-to-charge ratio:

$$\frac{m}{z} = \frac{2 \cdot U \cdot t^2}{s^2}$$ Eq. 7.1

where m = ion mass, z = number of charges, U = accelerating voltage, t = ion flight time, and s = flight distance. As the accelerating voltage and the flight distance are known, the mass-to-charge ratio can be calculated from the flight time using Eq. 7.1. Nevertheless, in practice, there are some uncertainties in the flight time. These arise from a short delay in ion formation after the laser pulse so that the real starting time of ions is not identical with the time of the laser pulse, which provides the starting signal for flight time measurement. Therefore, more exact mass-to-charge values are obtained from the empirical equation Eq. 7.2:

$$\frac{m}{z} = a \cdot t^2 + b$$ Eq. 7.2

The constants a and b are measured through the flight times of two ions with known masses, which are used for calibration.[33]

The accelerated ions can be detected in two different ways, i.e. either in the linear or in the reflection mode. The main difference between the two modes is that the reflection mode provides higher resolution, whereas the linear mode has a higher sensitivity for larger molecules. The higher resolution in the reflection mode is achieved by a reflecting field at the end of the flight tube that possesses a slightly higher potential and the same polarity as the accelerating voltage. This means that ions with the same mass-to-charge ratio but different velocities, which cause a peak broadening in the linear detection mode, can be time-focused with the reflector because faster ions penetrate deeper into the reflection field and travel a longer flight path. It has to be noted that the resolution of MALDI-TOF MS is mainly restricted by the ionization process, not by instrumental parameters, because the ions possess a certain time span of formation, a spatial distribution, and a kinetic energy spread. The linear mode has a high sensitivity and requires only a very short ion lifetime of about 1 µs acceleration time for detection of molecular ions. In the linear mode, fragments of molecules that decompose after the acceleration zone have still almost the same velocity as the respective intact molecular ions and cause signals at the same flight time with a slight increase in peak width. Since high-molecular weight molecules tend to decompose during the flight time due to the higher energy required for their desorption, the linear mode enables measurement of high molecular weights.[35]

MALDI-TOF mass spectrometry is a reliable method for end group determination in polymers and for the determination of weight-average and number-average molecular weights as well as molecular weight distributions. For the latter purpose, a quantitative evaluation of the complete polymer distribution is necessary. Quantitative analysis by mass spectrometry is not straightforward. MALDI-TOF mass spectrometry is an absolute

method only for molecular weight distributions with low polydispersities (≤ 1.1). At polydispersities PDI > 1.1, MALDI-TOF results show increasing deviations from values obtained by conventional methods, such as size-exclusion chromatography (SEC). In order to obtain absolute values for broad polymer distributions, MALDI-TOF mass spectrometry has to be combined with SEC fractionation.[33]

Each peak in the polymer spectrum represents a different degree of polymerization, and the peak-to-peak distance reflects the mass of the monomer repeating unit. With the absolute mass of each signal, end groups can be identified. Knowledge of the ionization process is a prerequisite for spectrum interpretation, e.g. for cationization with sodium each signal has to be corrected by the mass of sodium. Ionization and detection mechanisms influence the mass range detectable and the shape of the distribution curve so that preparation conditions, matrices, salt addition, type of analyzer, and acceleration voltage are of prime importance. Different cations added to the matrix solution do also have an influence on the spectra. As a rule of thumb and based on the principle of hard and soft acids and bases, soft bases are compatible with soft acids, e.g. polystyrene is preferentially cationized with silver; on the other hand, polar molecules with hard base sites (oxygen, nitrogen), such as PMMA, should complex more readily with hard acids like sodium or potassium.[33]

Furthermore, the influence of laser power on the spectra should not be underestimated. A too high laser power shifts the maximum of distribution to lower mass values, most probably due to increased fragmentation processes. This makes higher-molecular weight polymers detectable but decreases mass resolution.

The signal-to-noise ratio decreases with increasing number of different mass-to-charge ratios in polydisperse polymers. It is assumed that ion distribution in the gas phase is representative of the number of ions in the condensed phase. Therefore, polydispersity involves the problem of discrimination effects, which may lead to a false shape of polymer distribution and causes incorrect results for calculation of average molecular weight values. Thus, care must be taken to avoid loss of sample fractions during sample preparation.

The MALDI process is capable of producing ions over the entire molar mass distribution but high-mass tails cannot be detected when lower mass ions are allowed to reach the detector. Consequently, one reason for high-mass discrimination in high-polydispersity samples is detector saturation.[33]

MALDI-TOF mass spectrometry was performed on a Bruker Reflex III equipped with a 337 nm N_2 laser in the reflector mode and 20 kV acceleration voltage. Dithranol, 2,5-dihydroxybenzoic acid (DHB), or sinapinic acid (SA) (Aldrich, 97 %) was used as matrix. Sodium or potassium trifluoroacetate was added for ion formation. Usually, samples were prepared from THF or ethanol solution by mixing matrix (20 mg/mL), sample (10 mg/mL)

and salt (10 mg/mL) in a ratio of 10:1:1. The number-average molecular weights, M_n, of the polymer samples were determined in the linear mode.

Tab. 7.1 gives an overview of the different conditions used for the respective polymers:

Tab. 7.1.   *Conditions used for preparation of polymer samples for MALDI-TOF analysis; SA=sinapic acid, DHB=2,5-dihydroxybenzoic acid.*

polymer	matrix	solvent	ratio matrix:sample:salt
PNIPAAm	dithranol	THF	10:1:1
PNIPAAm-*b*-PAA	SA	EtOH	10:1 (no salt)
PAA	SA	EtOH	10:1 (no salt)
PNHSM	DHB	none	10:1 (no salt)
PVO	DHB	THF	10:1 (no salt)

7.5.2   In-situ FT-NIR spectroscopy

Fourier-transform near-infrared (FT-NIR) spectroscopy in combination with a fiber optic probe can be used for monitoring reactions online. This so-called in-situ FT-NIR spectroscopy provides real-time structural and kinetic information in the near-infrared range (4,000-10,000 cm^{-1}). It allows, for example, the continuous determination of monomer conversion in controlled/living polymerization processes without time-consuming sampling and post-processing.[36] One of the prerequisites for the applicability of this technique is that the monomer shows absorbances in the near-infrared region and that these absorption bands do not overlap significantly with other bands, such as those of the polymer or the solvent. An immersion transmission probe is connected to the FT-NIR instrument by fiber-optical cables. The fiber optic probe is immersed into the reaction mixture, which allows remote monitoring that does not interfere with the polymerization system. The probe consists of a prism and a window that are permeable to light (Fig. 7.14). The light beam is only transmitted once through the sample. Thus, the principle is the same as that of a cuvette.

Most NIR absorbances are overtone or combination bands of fundamental bands and are typically weaker than their corresponding fundamental transitions. Consequently, NIR might not be suitable for minor component analysis but lower extinction coefficients simplify sample preparation as it is easier to obtain a linear Beer's law at higher concentrations. NIR also permits facile subtraction of the polymerization solvent background.
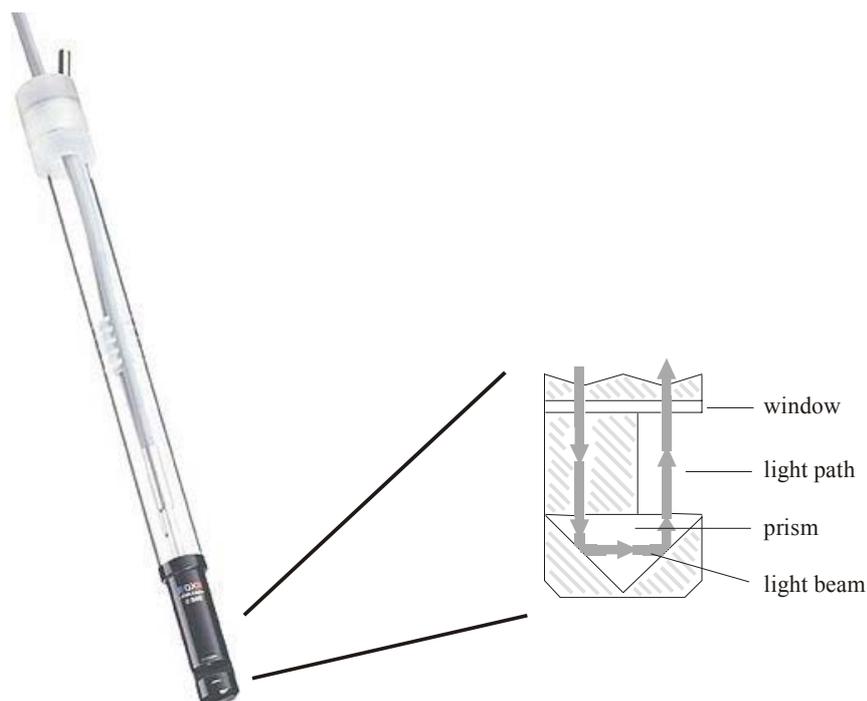
Fig. 7.14.   Fiber-optic deep-temperature immersion probe used for online FT-NIR monitoring.[37]

Fourier-transform near infrared (FT-NIR) spectroscopy was performed using a Nicolet Magna 560 FT-IR optical bench equipped with a white-light source and a PbS detector. The fiber-optic deep-temperature immersion probe (Hellma, quartz glass Suprasil® 300) with an optical path length of 10 mm was connected to the FT-NIR instrument by 2 m fiber-optical cables. Data processing was performed with Nicolet's OMNIC Series software. Each spectrum was constructed from 32 scans with a resolution of 4 cm⁻¹. The total collection time per spectrum was approximately 22 s. Prior to the measurements, a blank spectrum was recorded with the solution of the corresponding chain transfer agent in 1,4-dioxane at 60 °C. After addition of the monomer, the measurement was started and the initiator solution was injected shortly after. The baseline for signal height determination was drawn from 7000 to 5035 cm⁻¹.

For evaluation of the kinetic data of NIPAAm polymerization, monomer conversions x_p were calculated using the following equation:

$$x_p = \frac{A_0 - A_t}{A_0 - A_\infty}$$
Eq. 7.3

where A_t is the absorbance at time t, A_0 is the initial absorbance and A_∞ is the absorbance at full conversion.

7.5.3   Dynamic light scattering (DLS)

Light scattering on molecules results from incidental fluctuations in density or concentration, respectively. These fluctuations can be investigated by dynamic light scattering (DLS). They result from Brownian movement and are on a time scale in the nano- and millisecond range. Molecules in solution move in all directions with the same probability and they have a continuous rate distribution. Consequently, the frequency of the scattered light is shifted to higher or lower values depending on the velocity and direction of the molecules relative to the detector (Doppler effect). Thus, a broadening of the spectrum is observed with respect to the frequency line of the stimulating radiation (v_0). Therefore, light scattering is rather quasi-elastic than elastic.[38] The spectral broadening is too small to be detected by conventional spectrometers working in the frequency domain (interferometers). For this reason, measurements are performed in the time domain, and fluctuation of the scattered light with time is measured. Generally, this is done according to the Homodyn method, i.e. the scattering light is directed to the photo detector. The detector's output signal is proportional to the intensity of light $I(t)$ and, thus, also proportional to the mean square of the electric field $|E(t)|^2$. The output signal of the detector is auto-correlated with time according to the following equation:[39,40]

$$g_2(t) = \frac{\langle I(0) \cdot I(t) \rangle}{\langle I(0) \rangle^2} \qquad \text{Eq. 7.4}$$

where $g_2(t)$ is the normalized intensity autocorrelation function. The field autocorrelation function $g_1(t)$ can be deduced from $g_2(t)$ using the Siegert relation:[41]

$$g_1(t) = \sqrt{\frac{g_2(t) - A}{B}} \qquad \text{Eq. 7.5}$$

where A and B are usually equal to unity. A is determined by an experimental baseline. The function $g_1(t)$ describes the fluctuations of the electric field of the scattered light:

$$g_1(t) = \frac{\langle E(0) \cdot E(t) \rangle}{\langle E(0) \rangle^2} \qquad \text{Eq. 7.6}$$

In the case of hard spheres, the function $g_1(t)$ is described by an exponential function:

$$g_1(t) = \exp(-\Gamma \cdot t) \qquad \text{Eq. 7.7}$$

where Γ is the fluctuation rate with $\Gamma = Dq^2$ and q = scattering vector. The translational diffusion coefficient D is inversely proportional to the hydrodynamic radius R_h.[39,42] D describes an auto-diffusion process, where the system is in a chemical equilibrium.

For a system of polydisperse spheres, the following equation holds:

$$g_1(q,t) = \sum_j a_j(q) \exp(-\Gamma_j t) \qquad \text{Eq. 7.8}$$

with $a_j(q)$ = relative amplitudes:

$$a_j(q) = \frac{c_j M_j P_j(q)}{\sum\limits_j c_j M_j P_j(q)}$$

Eq. 7.9

where M_j and $P_j(q)$ are the molecular weight and particle form factor, respectively, of particle j. In the case of large spheres (diameter $> \lambda/20$ and $P_j(q) > 1$), the field autocorrelation function becomes dependent on q. Change from hard spheres to polymers in solution involves rotational diffusion and internal modes in addition to translational diffusion. Rotational diffusion is of particular importance in rod-like molecules, whereas internal modes are significant in large coil-like molecules.[42] From a mathematical point of view, these factors involve additional additive and multiplicative terms. The terms can be eliminated by angle-dependent measurements as the amplitudes approach zero for $q^2 \rightarrow 0$.[39]

The determination of the mean diffusion coefficient and standard deviation for polydisperse systems is best accomplished by the CONTIN method.[43,44] The function $g_1(t)$ is described by a continuous distribution:

$$g_1(t) = \int\limits_{\Gamma_{min}}^{\Gamma_{max}} G(\Gamma) \exp(-\Gamma \cdot t) d\Gamma$$

Eq. 7.10

which can be inverted by a Laplace transformation. This inversion is problematic as there is basically an unlimited number of solutions that describe the data within experimental error. In order to minimize these solutions, the CONTIN analysis uses the following regularization:

$$R_n(G(\Gamma)) = \int\limits_{\Gamma_{min}}^{\Gamma_{max}} \left(\frac{\partial^n G(\Gamma)}{\partial \Gamma^n} \right) d\Gamma$$

Eq. 7.11

n is the order of regularization. Regularization of 0th order represents minimization of the integration area of function $G(\Gamma)$; regularization of 2nd order corresponds to smoothing of function $G(\Gamma)$. The original CONTIN routine calculates a rate distribution (logΓ scale), whereas the CONTIN routine of the ALV software calculates a time distribution (log(t) scale) that is proportional to the distribution of radii. The ALV software also enables a direct fit of $g_2(t)$-1 via a special algorithm (see below). This usually yields a smoother distribution function with less artifacts as compared to $g_1(t)$.

Care must be exerted on interpreting results so as to avoid artifacts, especially in the case of a low signal-to-noise ratio, an inappropriate baseline or inappropriate choice of Γ_{max} and Γ_{min}. Thus, the signal-to-noise ratio should always be high. For evaluation of the results, it should be considered that two different distributions can only be distinguished with the CONTIN program if the respective hydrodynamic radii differ from each other by a minimal factor of two.

The mean radii or rather diffusion coefficients obtained by the CONTIN method are z values. In order to eliminate the influence of form factors for large molecules, the D and R_h values, respectively, measured at different angles have to be extrapolated for $q^2 \rightarrow 0$.

DLS was performed on an ALV DLS/SLS-SP 5022F compact goniometer system with an ALV 5000/E correlator and a He-Ne laser ($\lambda = 632.8$ nm). The polymer solutions were those used for tensiometry with $c \approx 10$ mg/mL. The solutions were filtered twice through Millipore Teflon filters (pore size 0.45 μm). The normalized intensity autocorrelation function $g_2(t)$ was measured experimentally. The CONTIN method was used for data analysis of $g_2(t)$. The following nonlinear fit model was used:

$$g_2(t) - 1 = \left(\int_{t_{min}}^{t_{max}} e^{-t} G(t) dt \right)^2 \qquad \text{Eq. 7.12}$$

where G(t) denotes the decay rate distribution function. This analysis results in a discrete, intensity-average distribution function of logarithmically equidistant-spaced decay time. The hydrodynamic radii were calculated from the corresponding decay time applying the Stokes-Einstein equation. Based on the assumption that the scattering particles behave as hard spheres in dilute solution and according to the Rayleigh-Debye theory, the particle radii were calculated from the decay time distribution.

7.5.4   Tensiometry

Substances that decrease the surface tension upon addition to a liquid are called surfactants. The surface tension as a function of surfactant concentration can be measured using a tensiometer. From these results, critical micelle concentration can be determined.

The work needed to change the surface area γ of a sample by an infinitesimal amount dγ is proportional to dγ:

$$dw = \sigma \cdot d\gamma \qquad \text{Eq. 7.13}$$

the coefficient σ is called the surface tension.

One of the most common techniques for measuring surface tension is the platinum ring method (Du-Noüy ring method). In the ring method, a horizontally positioned platinum ring of known radius is immersed into the solution to be investigated. The wetted ring is moved upward and pulls the surface with it until the pending liquid lamella breaks off (Fig. 7.15). The ring experiences the hydrostatic weight of the pending lamella and the counterforce resulting from surface tension. The deformation of the liquid surface requires a force that is maximal when the tangent on the wetting point is directed perpendicular to it, i.e. when the lamella breaks off. This force maximum is determined by a torsion balance. The following relation between surface tension σ and maximum force F_{max} applies:

$$\sigma = \frac{F_{max}}{4\pi \cdot r \cdot f_{HJ}} \qquad\qquad \text{Eq. 7.14}$$

where r = ring radius and f_{HJ} = Harkins-Jordan correction factor. The correction factor is a function of the density of both the liquid and gas phase and of the ring radius.
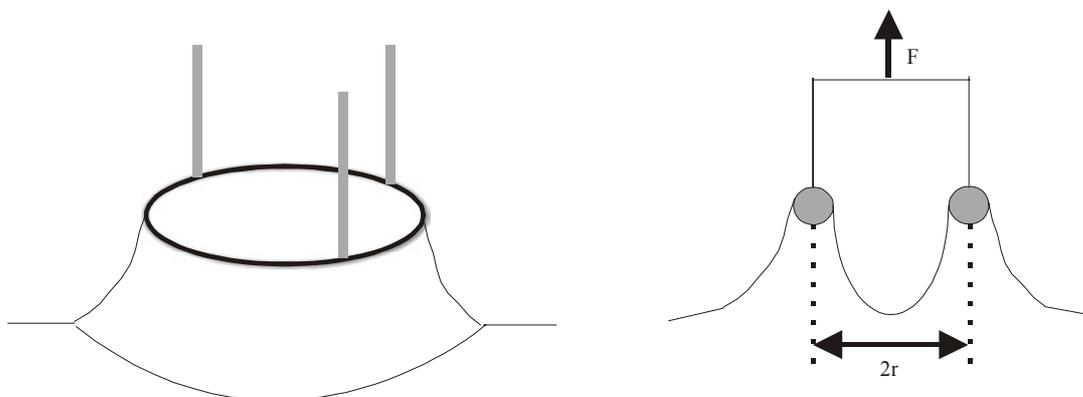

Fig. 7.15.   Measurement of surface tension using the Du-Noüy ring method; the right image shows the cross-section of the ring (shaded grey) and the force F that is applied to pull it out of the liquid.

The presence of a surfactant in water decreases the surface tension. This is described by Gibbs' adsorption isotherm:

$$d\sigma = \Gamma \cdot d\mu \qquad\qquad \text{Eq. 7.15}$$

where Γ = surface concentration (surface excess) of surfactant, and μ = chemical potential of surfactant. From Eq. 7.7, the surface concentration of the surfactant can be calculated, assuming an ideal solution with very dilute surfactant concentration and $d\mu = RT \cdot d\ln c$:

$$\Gamma = -\frac{1}{RT} \cdot \left[\frac{d\sigma}{d\ln c} \right] \qquad\qquad \text{Eq. 7.16}$$

where R = gas constant, T = solution temperature, and c = surfactant concentration.

The plot of σ versus ln$c$ shows two different curves around the critical micelle concentration (cmc). The left curve (c < cmc) is approximated by a tangent fitted to the steepest part, and the right curve (c > cmc) is approximated by a straight line. The point of intersection of the two fittings is the critical micelle concentration.

Surface tension was measured on a Lauda tensiometer (platinum ring method). The platinum ring was annealed with a Bunsen burner prior to each measurement in order to ensure wetting by the aqueous solutions. The block copolymers were dissolved in 0.1 M citrate buffer pH 5.6 and directly used for measurement or dialyzed against 0.1 M citrate buffer pH 4.5 for measurements at lower pH. All solutions were kept at room temperature for 48 h prior to measurement. Each sample was measured three times and the deviation of each measurement ranged within 0.2 mN/m.

7.5.5 Commonly used methods

7.5.5.1 NMR spectroscopy

^{1}H- and ^{13}C-NMR spectra were obtained on a Bruker AC 250 at an operating frequency of 250 MHz and 62.5 MHz, respectively. Various deuterated solvents (Deutero GmbH) were used depending on the solubility of the samples. As an internal standard, either tetramethylsilane or the residual proton signal of the deuterated solvent was used.

Temperature-sweep measurements on PNIPAAm-*b*-PAA were performed in d_6-DMF + 0.05 M LiBr using a polymer concentration of 10 mg/mL. NMR spectra were recorded from 25 °C to 125 °C with a temperature interval of 10 °C, leaving the sample solution for 30 min prior to measurement at each temperature for equilibration.

7.5.5.2 UV spectroscopy

UV spectra were recorded on a Perkin-Elmer Lambda15 UV-vis spectrophotometer in the wavelength range from 190 to 550 nm. Measurements were carried out in solution.

7.5.5.3 IR spectroscopy

IR spectra were recorded on a Bruker Equinox 55/S FT-IR spectrometer. The measurements were performed either on a film on KBr or CaF_2 plates (for aqueous solutions) cast from a suitable solvent or on a KBr pellet (approx. 1.5 mg sample per 150 mg KBr).

7.5.5.4 Raman spectroscopy

Raman spectra were recorded using a confocal optical setup consisting of a He-Ne laser (λ=632.8 nm), objectives of numerical aperture 0.45 and 0.20, and a 50 μm pinhole replacing the entrance slit of the monochromator. A CCD line detector in the exit focal plane of the monochromator was used for recording the spectra.

7.5.5.5 Gel permeation chromatography (GPC)

Gel permeation chromatography (GPC) of the THF-soluble polymers (poly(methacrylate), poly(2-vinyl-4,4-dimethyl-5-oxazolone), poly(diacetone acrylamide), and PNIPAAm-*b*-PVO) was performed on PSS SDVgel columns (30 x 8 mm, 5 μm particle size) with 10^2, 10^3, 10^4, and 10^5 Å pore sizes using RI and UV detection (λ=254 nm). THF was used as an eluent (flow rate 0.5 mL/min) at a temperature of 25 °C. For the polyNIPAAm samples, GPC was performed using THF + 0.25 wt.-% of tetrabutylammonium bromide as an eluent (flow rate 0.5 mL/min). The injection volume was 100 μL. As an internal standard, *o*-dichlorobenzene was used. Polystyrene standards were used for calibration.

For GPC measurements on the poly(N-isopropylacrylamide) samples in THF, 0.25 wt.-% tetrabutylammonium bromide (TBAB) had to be added in order to prevent polymer adsorption to the columns. GPC was performed on a Waters Associates liquid chromatograph equipped with an RI detector and a UV detector (λ=254 nm) at a temperature of 25 °C. PSS SDVgel columns (30 x 8 mm, 5 µm particle size) with 10^2, 10^3, 10^4, and 10^5 Å pore sizes were used. THF + 0.25 wt.-% of tetrabutylammonium bromide was used as an eluent (flow rate 0.5 mL/min). The injection volume was 100 µL and a Spectra Physics P 100 pump was used. As an internal standard, o-dichlorobenzene was used. Polystyrene standards were used for calibration.

GPC on the DMF-soluble polymers (poly(N-hydroxysuccinimide methacrylate), poly(N-acryloxysuccinimide), and PNIPAAm-b-PAA) was performed using a series of four Styragel columns HT2, HT3, HT4, and HT5 and an oven temperature of 80 °C. The solvent was DMF + 0.05 M LiBr at a flow rate of 1.0 mL/min. A Dawn EOS light scattering detector with Optilab DSP refractometer (both set at 690 nm) was used.

GPC using water + 0.05 M sodium azide was conducted on PSS Suprema columns (300 x 8 mm, 10 µm particle size) with 10^2, 10^3, and 10^4 Å pore sizes. Poly(methacrylic acid) standards were used for calibration. The measurements were carried out at a flow rate of 1 mL/min at 25 °C or 60 °C, respectively, using RI and UV detection (λ=254 nm).

7.5.5.6   *Cloud point measurements*

Cloud point measurements were performed in 0.2 wt.-% (buffered) aqueous polymer solutions on a Hewlett Packard HP 8453 UV-visible chem station at a wavelength λ = 500 nm using a thermostatted cell with a heating rate of 0.5 K/min. Spectra were recorded in transmission and cloud points were determined as the inflection points of the transmission versus temperature plots.

7.5.5.7   *Differential scanning calorimetry (DSC)*

DSC measurements were performed on a Perkin-Elmer DSC 7 instrument at a heating/cooling rate of 10 K/min. Calibration was done using two of the calibration samples indium, naphthalin, chloroform, and tin so that their melting temperatures were in the lower and upper part of the used temperature range. In a first heating/cooling cycle, all samples were heated in the respective temperature range in order to exclude any influence of thermal history on the measurement.

7.5.5.8   *Cryogenic transmission electron microscopy (cryoTEM)*

TEM measurements were performed at Uppsala University, Sweden, on a Zeiss EM 902A instrument with operation in the zero-loss bright-field mode and an acceleration

voltage of 80 kV. Digital images were recorded with a BioVision Pro-SM Slow Scan CCD camera system. A climate chamber was used for sample preparation in order to control temperature and relative humidity. The temperature was set to 25 °C and the relative humidity to 99 %. Samples were prepared by placing a drop of the aqueous solution on the grid, thinning by blotting and vitrifying in liquid ethane. Holey polymer films were used as supports. The polymer film was transferred to a copper grid, and a carbon layer was evaporated onto both sides of the grid.

References

(1)   Chiefari, J.; Mayadunne, R. T. A.; Moad, G.; Rizzardo, E.; Thang, S. H. In *WO 99/31144*; E.I. DuPont de Nemours and Company: Australia, 1999.

(2)   Rizzardo, E.; Serelis, A. K.; Solomon, D. H. *Aust. J. Chem.* **1982**, *35*, 2013-2024.

(3)   Takeshima, T.; Ikeda, M.; Yokoyama, M.; Fukada, N.; Muraoka, M. *J. Chem. Soc., Perkin Trans. 1* **1979**, 692-695.

(4)   Thang, S. H. *personal communication*.

(5)   Bai, R.-K.; You, Y.-Z.; Pan, C.-Y. *Polym. Int.* **2000**, *49*, 898-902.

(6)   Mitsukami, Y.; Donovan, M. S.; Lowe, A. B.; McCormick, C. L. *Macromolecules* **2001**, *34(7)*, 2248-2256.

(7)   Le, T. P.; Moad, G.; Rizzardo, E.; Thang, S. H. In *WO 98/01478*; E.I. Du Pont De Nemours and Co., USA; Le, Tam Phuong; Moad, Graeme; Rizzardo, Ezio; Thang, San Hoa: Australia, 1998.

(8)   Thang, S. H.; Chong, B. Y. K.; Mayadunne, R. T. A. *Tetrahedr. Lett.* **1999**, *40*, 2435-2438.

(9)   Quinn, J. F.; Rizzardo, E.; Davis, T. P. *Chem. Commun.* **2001**, 1044-1045.

(10)   Ferruti, P.; Bettelli, A.; Fere, A. *Polymer* **1972**, *13*, 462-464.

(11)   Mindl, J.; Sulzer, J.; Vecera, M. *Collect. Czech. Chem. Commun.* **1981**, *46*, 1970-1975.

(12)   Tsai, L.; Miwa, T.; Newman, M. S. *J. Am. Chem. Soc.* **1957**, *79*, 2530-2533.

(13)   Webster, F. X.; Millar, J. G.; Silverstein, R. M. *Tetrahedron Lett.* **1986**, *27*, 4941-4944.

(14)   Nakayama, Y.; Nakamata, K.; Hirano, Y.; Goto, K.; Matsuda, T. *Langmuir* **1998**, *14*, 3909-3915.

(15)   Ellman, G. L. *Arch. Biochem. Biophys.* **1959**, *82*, 70-77.

(16)   Habeeb, A. F. S. A. *Methods Enzymol.* **1972**, *25 (Part B)*, 457-464.

(17)   Wenck, H.; Schneider, F. *Experientia* **1971**, *27(1)*, 20-22.

(18)   Marcos, I.; Redero, E.; Bermejo, F. *Tetrahedron Lett.* **2000**, *41*, 8451-8455.

(19)   Burke, S. D.; Fobare, W. F.; Armistead, D. M. *J. Org. Chem.* **1982**, *47*, 3348-3350.

(20)   Mukaiyama, T.; Takahashi, K. *Tetrahedr. Lett.* **1968**, 5907-5908.

(21)   Diels, O.; Wulff, C. *Ann.* **1924**, *437*, 309-318.

(22)   Pastor, S. D.; Hessell, E. T.; Odorisio, P. A.; Spivack, J. D. *J. Heterocycl. Chem.* **1985**, *22*, 1195-1197.

(23)   Ghosh, S. S.; Kao, P. M.; McCue, A. W.; Chappelle, H. L. *Bioconjugate Chem.* **1990**, *1*, 71-76.

(24)   Lio, R. G.; Thiem, J. *Carbohydrate Research* **1999**, *317*, 180-190.

(25)   Hermanson, G. T. *Bioconjugate Techniques*; Academic Press Inc.: San Diego, 1996.

(26)   Macindoe, W. M.; van Oijen, A. H.; Boons, G.-J. *Chem. Commun. (Cambridge)* **1998**, 847-848.

(27)   Rabanal, F.; DeGrado, W. F.; Dutton, P. L. *Tetrahedron Lett.* **1996**, *37*, 1347-1350.

(28)   Feng, X.-S.; Pan, C.-Y. *Macromolecules* **2002**, *35*, 4888-4893.

(29)   Wilbur, D. S.; Stayton, P. S.; To, R.; Buhler, K. R.; Klumb, L. A.; Hamlin, D. K.; Stray, J. E.; Vessella, R. L. *Bioconjugate Chem.* **1998**, *9*, 100 -107.

(30)   Ding, Z.; Long, C. J.; Hayashi, Y.; Bulmus, E. V.; Hoffman, A. S.; Stayton, P. S. *Bioconjugate Chem.* **1999**, *10*, 395-400.

(31)   Tanaka, K.; Waki, H.; Ido, Y.; Akita, S.; Yoshida, Y.; Yoshida, T. *Rapid Commun. Mass Spectrom.* **1988**, *2*, 151.

(32)   Karas, M.; Hillenkamp, F. *Anal. Chem.* **1988**, *60*, 2299-2301.

(33)   Räder, H. J.; Schrepp, W. *Acta Polym.* **1998**, *49*, 272-293.

(34)   Nielen, M. W. F. *Mass Spectrom. Rev.* **1999**, *18*, 309-344.

(35)   Montaudo, G. *Mass Spectrometry of Polymers*; CRC Press: Boca Raton, 2002.

(36)   Long, T. E.; Liu, H. Y.; Schell, B. A.; Teegarden, D. M.; Uerz, D. S. *Macromolecules* **1993**, *26*, 6237-6242.

(37)   www.hellma-worldwide.de/tauch/infofr.htm. HELLMA.

(38)   Santos, N. C.; Castanho, M. A. R. B. *Biophys. J.* **1996**, *71*, 1641.

(39)   Berne, B. J.; Pecora, R. *Dynamic Light Scattering*; John Wiley & Sons: New York, 1976.

(40)   Schmitz, K. S. *An Introduction to Dynamic Light Scattering by Macromolecules*; Academic Press, Inc.: Boston, 1990.

(41)   Siegert, A. J. F. *MIT Rad. Lab. Report* **1943**, *465*.

(42)   Burchard, W.; Richterling, W. *Progr. Colloid & Polymer Sci.* **1989**, *80*, 151.

(43)   Provencher, S. W. *Makromol. Chem.* **1979**, *180*, 201.

(44)   Provencher, S. W. *Computer Phys. Commun.* **1982**, *27*, 229.

8   Summary

Polymeric precursors for the synthesis of polymer-protein conjugates were prepared by reversible addition-fragmentation chain transfer (RAFT) polymerization. These precursors include the stimuli-responsive polymers poly(N-isopropylacrylamide) and poly(acrylic acid) as well as amine-reactive polymers, such as poly(2-vinyl-4,4-dimethyl-5-oxazolone). Chain transfer agent structures had to be adjusted to the individual monomers and new transfer agents were synthesized for polymerization in a controlled manner.

The polymers obtained by RAFT polymerization represent macromolecular chain transfer agents that can be used to synthesize block copolymers by further monomer addition. Stimuli-responsive block copolymers consisting of poly(N-isopropylacrylamide) and poly(acrylic acid) or poly(2-vinyl-4,4-dimethyl-5-oxazolone) blocks, respectively, were synthesized by RAFT for the first time for use in protein/drug conjugation.

The presence of dithiocarbonyl endgroups in the polymers enabled their hydrolysis to sulfhydryl-terminated polymers. Sulfhydryl-terminated poly(N-isopropylacrylamide), PNIPAAm, and poly(N-isopropylacrylamide)-*block*-poly(acrylic acid), PNIPAAm-*b*-PAA, were used for conjugation to the protein streptavidin.

The RAFT polymerization of N-isopropylacrylamide with two different chain transfer agents, namely benzyl 1-pyrrolecarbodithioate and cumyl 1-pyrrolecarbodithioate, yielded polymers with narrow molecular weight distributions as well as M_n values that were in good agreement with the calculated ones. A comparison between the M_n values determined from gel permeation chromatography, GPC, and the values from MALDI-TOF mass spectrometry showed that the molecular weights obtained from GPC using polystyrene standards were considerably higher. A relation between log $M_{n,MALDI}$ and log $M_{n,GPC}$ was established, which permitted construction of a calibration curve for PNIPAAm polymers.

In-situ Fourier-transform near-infrared spectroscopy was applied for the reliable determination of monomer conversions and it indicated living characteristics. Both polymerization processes showed an induction period that seems to be correlated with a retardation in rate, where the induction time is higher for the cumyl chain transfer agent as compared to the benzyl chain transfer agent of the same concentration. The induction periods decrease with decreasing transfer agent concentration and were explained in terms of the different stabilities of the respective radicals that add to monomer in the reinitiation step. The more stable cumyl radical adds slower than the benzyl radical.

Both UV spectroscopy and MALDI-TOF mass spectrometry confirm the presence of the expected dithiocarbamate endgroups. MALDI-TOF characterization of the polymer samples showed the transfer agent endgroups together with some initiator-derived

polymers. Endgroups that seemed to originate from disproportionation or transfer were the result of fragmentation under MALDI conditions as was shown by a post source decay analysis and MALDI-TOF characterization of the hydrolyzed polymer.

Poly(*N*-isopropylacrylamide), PNIPAAm, was further investigated in terms of its lower critical solution temperature, LCST, and it was shown that its cloud point increases with increasing molecular weight as the hydrophobic endgroups lower the LCST until it reaches 32 °C for high-molecular weight PNIPAAm.

Dithiocarbamate-terminated PNIPAAm obtained from RAFT polymerization with cumyl and benzyl chain transfer agent, respectively, was hydrolyzed under basic conditions in order to obtain sulfhydryl-terminated PNIPAAm for subsequent conjugation to model compounds and streptavidin. Formation of these endgroups was probed using several techniques, including MALDI-TOF analysis.

With amine-reactive diacetone acrylamide, 2-vinyl-4,4-dimethyl-5-oxazolone and *N*-hydroxysuccinimide methacrylate, new monomers were polymerized via RAFT in a controlled manner. Poly(diacetone acrylamide) and poly(2-vinyl-4,4-dimethyl-5-oxazolone) showed low polydispersities and good control over molecular weight, where poly(*N*-hydroxysuccinimide methacrylate) displayed relatively high polydispersities despite the controlled polymerization evident from the monomodal GPC traces. These amine-reactive polymers were subsequently used for successful conjugation to the primary amino group of the model peptide glycine-leucine.

The RAFT polymerization of *tert*-butyl acrylate and acrylic acid gave polymers with low polydispersities when using suitable chain transfer agents. Successful, direct polymerization of acrylic acid without protection group chemistry demonstrated the potential of this technique, tolerating virtually any monomer functionality.

For poly(*N*-isopropylacrylamide)-*block*-poly(acrylic acid), PNIPAAm-*b*-PAA, it was demonstrated that hydrogen bonding between *N*-isopropylacrylamide and acrylic acid units influences strongly its behavior in both the solid state and in solution. The block copolymers form micelles in aqueous solutions in dependence of pH and temperature. Cloud point measurements indicated the formation of larger aggregates at pH 4.5 and temperatures above LCST, whereas micelles formed at pH 5-7 and temperatures above LCST. At pH 5.6 and 50 °C, only micelles were found, whereas, at lower temperatures, larger aggregates and micelles coexist. Formation of larger aggregates by hydrogen

bonding interactions was revealed by IR and Raman spectroscopy as well as by cryogenic transmission electron microscopy and dynamic light scattering.

Differential scanning calorimetry yielded glass transition temperatures of PNIPAAm-*b*-PAA that were well above the transition temperatures of the homopolymers, demonstrating molecular interactions between the acrylic acid and the *N*-isopropylacrylamide blocks.

For poly(*N*-isopropylacrylamide)-*block*-poly(2-vinyl-4,4-dimethyl-5-oxazolone), PNIPAAm-*b*-PVO, an increase of LCST with respect to the homopolymer poly(*N*-isopropylacrylamide) was found that was ascribed to the hydrophilic poly(2-vinyl-4,4-dimethyl-5-oxazolone) block. Differential scanning calorimetry showed complete mixing of the two blocks in the solid phase.

Conjugation of sulfhydryl-terminated PNIPAAm to thiol disulfide exchange reagents and maleimides was probed for later conjugation to proteins. Evaluation of the different cross-linking systems resulted in the choice of maleimides as cross-linkers for subsequent conjugation to the protein streptavidin.

Sulfhydryl-terminated PNIPAAm-*b*-PAA was conjugated to the streptavidin mutant S139C using a bismaleimide cross-linker and also direct conjugation via disulfide linkage. Both conjugations were successful and proceeded with more than 50 % conversion.

Conjugation of PNIPAAm and PNIPAAm-*b*-PAA was also achieved by non-covalent attachment of the biotinylated polymers to wild-type streptavidin. Conjugates of wild-type streptavidin with biotinylated PNIPAAm-*b*-PAA were found to remain dissolved at temperatures above LCST even at very low pH values, which was in contrast to the observed precipitation of the unconjugated block copolymer at pH ≤ 4.5. Conjugates of wild-type streptavidin with biotinylated PNIPAAm of different molecular weights formed aggregates in aqueous solutions above LCST and a dependence of aggregate size on the size of the polymer was found.

9 **Zusammenfassung**

Über reversible Additions-Fragmentierungs-Transfer (RAFT)-Polymerisation wurden polymere Vorstufen zur Synthese von Polymer-Protein-Konjugaten hergestellt. Die reizempfindlichen Polymere Poly(*N*-Isopropylacrylamid) und Polyacrylsäure sowie amin-reaktive Polymere wie Poly(2-Vinyl-4,4-dimethyl-5-oxazolon) wurden synthetisiert. Die Kettenüberträger-Strukturen wurden an die entsprechenden Monomere angepasst, und neue Kettenüberträger wurden dargestellt, um kontrollierte Polymerisationen zu ermöglichen.

Die durch RAFT-Polymerisation erhaltenen Polymere stellen makromolekulare Kettenüberträger dar, die zur Blockcopolymer-Synthese benutzt werden können, indem weiteres Monomer zugegeben wird. Reizempfindliche Polymere aus Poly(*N*-Isopropylacrylamid) und Polyacrylsäure bzw. Poly(2-Vinyl-4,4-dimethyl-5-oxazolon) wurden erstmals über RAFT hergestellt zur Konjugation an Proteine/Therapeutika.

Die Dithiocarbonyl-Endgruppen der Polymere konnten zu sulfhydryl-terminierten Polymeren hydrolysiert werden. Sulfhydryl-terminiertes Poly(*N*-Isopropylacrylamid), PNIPAAm, und Poly(*N*-Isopropylacrylamid)-*block*-Polyacrylsäure, PNIPAAm-*b*-PAA, wurden an das Protein Streptavidin konjugiert.

Die RAFT-Polymerisation von *N*-Isopropylacrylamid wurde mit den Kettenüberträgern Benzyl-1-pyrrolcarbodithioat und Cumyl-1-pyrrolcarbodithioat durchgeführt und Polymere mit enger Molekulargewichtsverteilung sowie M_n-Werten, die gut mit den berechneten übereinstimmten, konnten erhalten werden. Ein Vergleich der M_n-Werte aus Gelpermeationschromatographie, GPC, und MALDI-TOF-Massenspektrometrie zeigte, dass die Molekulargewichte aus der GPC unter Benutzung von Polystyrol-Standards viel höher waren. Es wurde eine mathematische Beziehung zwischen $\log M_{n,MALDI}$ und $\log M_{n,GPC}$ abgeleitet, die es ermöglichte, eine Eichkurve für die PNIPAAm-Polymere zu erstellen.

In-situ Fourier-Transform-Spektroskopie im nahen Infrarot wurde zur Bestimmung der Monomerumsätze benutzt. Beide Polymerisationen zeigten eine Induktionsperiode, die scheinbar mit einer Verlangsamung der Polymerisationsgeschwindigkeit zusammenhängt, wobei die Induktionszeit bei gleicher Konzentration für den Cumyl-Kettenüberträger größer ist als die des Benzyl-Kettenüberträgers. Die Induktionsperioden nehmen mit abnehmender Kettenüberträger-Konzentration ab und scheinen auf unterschiedlichen Stabilitäten der entsprechenden Radikale zu gründen, die an das Monomer im Reinitierungsschritt addieren. Das stabilere Cumyl-Radikal addiert langsamer als das Benzyl-Radikal.

Sowohl UV-Spektroskopie als auch MALDI-TOF-Massenspektrometrie bestätigen die erwarteten Dithiocarbamat-Endgruppen. Eine Untersuchung der Polymerproben mit MALDI-TOF zeigte die erwarteten Kettenüberträger-Endgruppen und Initiator-abgeleitete Polymere. Endgruppen, die durch Disproportionierung oder Übertragung entstanden schienen, erwiesen sich als Produkte von Fragmentierungsreaktionen, die während der MALDI-Messungen stattfanden. Dies wurde mit einer "Post Source Decay"-Analyse und MALDI-TOF-Charakterisierung des hydrolysierten Polymers nachgewiesen.

Die untere kritische Lösungstemperatur von Poly(*N*-Isopropylacrylamid), PNIPAAm, wurde gemessen, und es konnte gezeigt werden, dass der Trübungspunkt mit zunehmendem Molekulargewicht ansteigt, da die hydrophoben Endgruppen die untere kritische Lösungstemperatur erniedrigen, so dass nur für hochmolekulares PNIPAAm der Literaturwert von 32 °C erreicht wird.

Dithiocarbamat-terminiertes PNIPAAm aus der RAFT-Polymerisation mit Cumyl- bzw. Benzyl-Kettenüberträger wurde unter basischen Bedingungen hydrolysiert, um sulfhydryl-terminiertes PNIPAAm für eine anschließende Konjugation an Modellverbindungen und Streptavidin zu erhalten. Die Bildung dieser Endgruppen wurde mit unterschiedlichen Methoden nachgewiesen, unter anderem auch MALDI-TOF-Massenspektrometrie.

Die aminreaktiven Monomere Diacetonacrylamid, 2-Vinyl-4,4-dimethyl-5-oxazolon und *N*-Hydroxysuccinimidmethacrylat wurden erstmals über RAFT kontrolliert polymerisiert. Poly(Diacetonacrylamid) und Poly(2-Vinyl-4,4-dimethyl-5-oxazolon) zeigten niedrige Polydispersitäten und eine gute Kontrolle über das Molekulargewicht, während Poly(*N*-Hydroxysuccinimidmethacrylat) relativ hohe Polydispersitäten aufwies trotz einer kontrollierten Polymerisation. Die aminreaktiven Polymere wurden erfolgreich an die primäre Aminogruppe des Modellpeptids Glycin-Leucin konjugiert.

RAFT-polymerisiertes Poly(*tert*-Butylacrylat) und Polyacrylsäure zeigten bei Verwendung geeigneter Kettenüberträger niedrige Polydispersitäten. Die Polymerisation von Acrylsäure konnte ohne Schutzgruppen erfolgreich durchgeführt werden und demonstriert das große Potential dieser Technik, die praktisch jede funktionelle Gruppe toleriert.

Im Fall von Poly(*N*-isopropylacrylamid)-*block*-Polyacrylsäure, PNIPAAm-*b*-PAA, konnte gezeigt werden, dass Wasserstoffbrücken-Bildung zwischen *N*-Isopropylacrylamid- und Acrylsäure-Einheiten das Verhalten im festen Zustand und in Lösung stark beeinflusst. Die Blockcopolymere bilden Micellen in wässrigen Lösungen in Abhängigkeit von pH und Temperatur. Trübungsmessungen wiesen auf die Bildung größerer Aggregate bei pH 4.5

und Temperaturen oberhalb der unteren kritischen Lösungstemperatur hin, während sich bei pH 5-7 und Temperaturen oberhalb der unteren kritischen Lösungstemperatur Micellen bildeten. Bei pH 5.6 und 50 °C findet man nur Micellen, wohingegen bei niedrigeren Temperaturen sowohl größere Aggregate als auch Micellen vorliegen. Die Bildung größerer Aggregate durch Wasserstoffbrücken-Wechselwirkungen wurde mittels IR- und Raman-Spektroskopie sowie Tieftemperatur-Transmissionelektronenmikroskopie und dynamischer Lichtstreuung nachgewiesen.

Die Glasübergangstemperaturen von PNIPAAm-*b*-PAA wurden mittels dynamischer Differenzkalorimetrie bestimmt und lagen oberhalb der Glasübergangstemperaturen der Homopolymere, was wiederum auf molekulare Wechselwirkungen zwischen Acrylsäure- und *N*-Isopropylacrylamid-Blöcken schließen lässt.

Im Fall von Poly(*N*-Isopropylacrylamid)-*block*-Poly(2-Vinyl-4,4-dimethyl-5-oxazolon), PNIPAAm-*b*-PVO, wurde eine Zunahme der unteren kritischen Lösungstemperatur im Vergleich zum Homopolymer Poly(*N*-Isopropylacrylamid) beobachtet, die auf den hydrophilen Poly(2-Vinyl-4,4-dimethyl-5-oxazolon)-Block zurückgeführt wurde. Eine Vermessung der Proben mit dynamischer Differenzkalorimetrie ergab, dass sich die beiden Blöcke im festen Zustand vollständig mischen.

Die Konjugation von sulfhydryl-terminiertem PNIPAAm an Thiol-Disulfid-Austausch-Reagenzien und Maleimide wurde für eine spätere Konjugation an Proteine getestet. Eine experimentelle Abwägung der unterschiedlichen Verknüpfungssysteme ergab, dass Maleimide am besten als Verknüpfungsreagenzien für eine Konjugation an das Protein Streptavidin geeignet sind.

Sulfhydryl-terminiertes PNIPAAm-*b*-PAA wurde an den Streptavidin-Mutanten S139C konjugiert mithilfe eines Bismaleimid-Verknüpfers und auch mittels direkter Konjugation über Disulfid-Brücken. Beide Konjugationen waren erfolgreich mit einem Umsatz von über 50 %.

Eine Konjugation von PNIPAAm und PNIPAAm-*b*-PAA wurde auch über nicht-kovalente Anbindung biotinylierter Polymere an natürliches Streptavidin erreicht. Konjugate von natürlichem Streptavidin mit biotinyliertem PNIPAAm-*b*-PAA blieben selbst oberhalb der unteren kritischen Lösungstemperatur und bei niedrigen pH-Werten in Lösung, was im Gegensatz zu Beobachtungen am unkonjugierten Blockcopolymeren steht, das bei pH-Werten unterhalb 4.5 ausfällt. Konjugate von natürlichem Streptavidin mit biotinylierten PNIPAAm-Proben unterschiedlichen Molekulargewichts bildeten oberhalb der unteren kritischen Lösungstemperatur Aggregate in wässriger Lösung, und es wurde eine Abhängigkeit der Aggregatgröße von der Polymergröße gefunden.

Danksagung

Die vorliegende Arbeit wurde von mir selbständig verfasst und ich habe keine anderen als die angegebenen Quellen und Hilfsmittel benutzt.

Ferner habe ich nicht versucht, anderweitig mit oder ohne Erfolg eine Dissertation einzureichen oder mich der Doktorprüfung zu unterziehen.

Bayreuth, 16.04.03

(Christine Schilli)